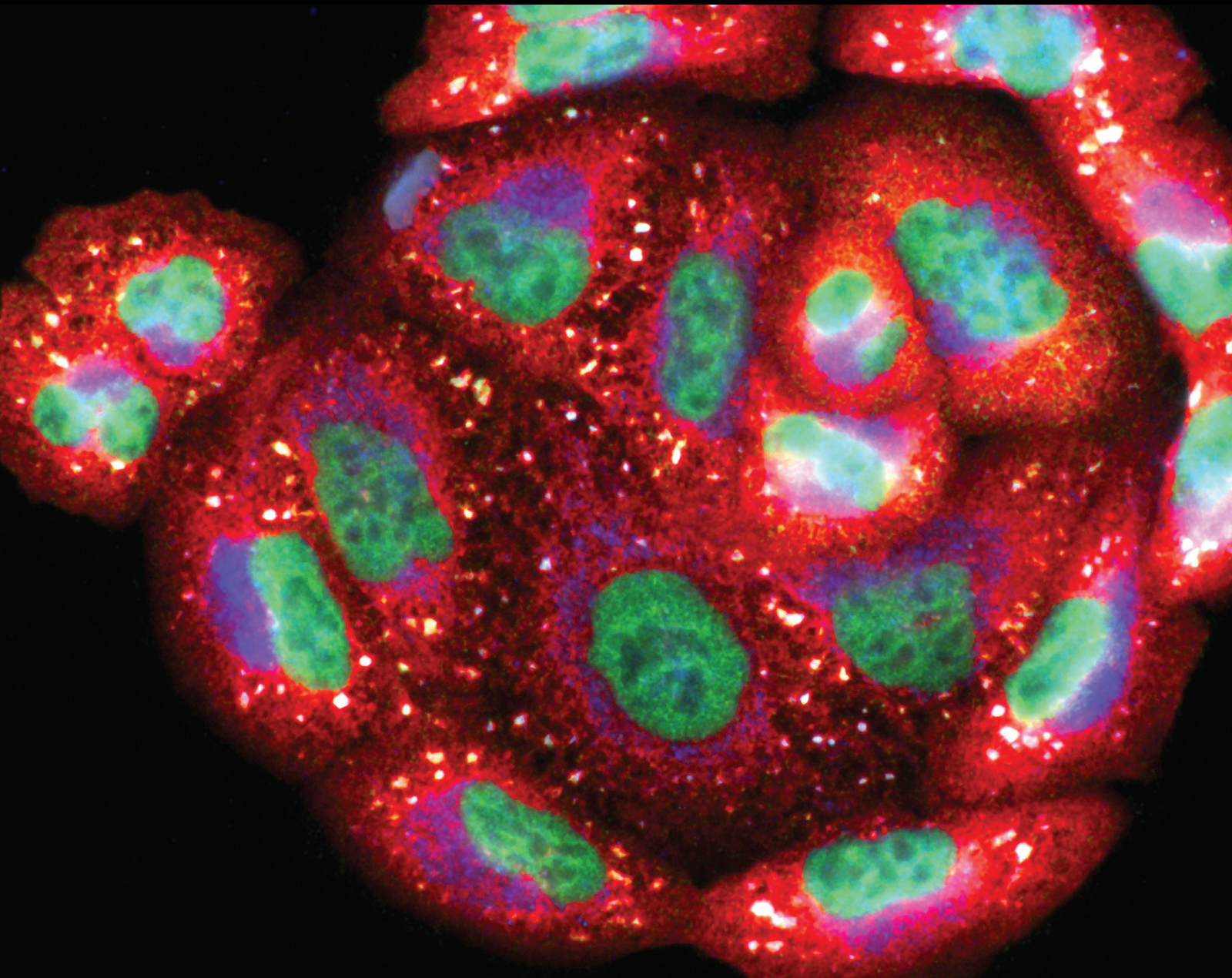# Oxidative Stress and Mitochondria in Ischemia-Reperfusion Injury and Vascular Diseases

Lead Guest Editor: Ding-Sheng Jiang
Guest Editors: Jinwei Tian, Xin Tu, Xin Yi, and Yuxuan Luo

Oxidative Stress and Mitochondria in Ischemia-Reperfusion Injury and Vascular Diseases

Oxidative Stress and Mitochondria in Ischemia-Reperfusion Injury and Vascular Diseases

Lead Guest Editor: Ding-Sheng Jiang
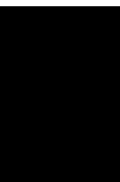Guest Editors: Jinwei Tian, Xin Tu, Xin Yi, and Yuxuan Luo

Tim Hofer, Norway
John D. Horowitz, Australia
Silvana Hrelia, Italy
Dragan Hrncic, Serbia
Zebo Huang, China
Zhao Huang, China
Tarique Hussain, Pakistan
Stephan Immenschuh, Germany
Norsharina Ismail, Malaysia
Franco J. L, Brazil
Sedat Kacar, USA
Andleeb Khan, Saudi Arabia
Kum Kum Khanna, Australia
Neelam Khaper, Canada
Ramoji Kosuru, USA
Demetrios Kouretas, Greece
Andrey V. Kozlov, Austria
Chan-Yen Kuo, Taiwan
Gaocai Li, China
Guoping Li, USA
Jin-Long Li, China
Qiangqiang Li, China
Xin-Feng Li, China
Jialiang Liang, China
Adam Lightfoot, United Kingdom
Christopher Horst Lillig, Germany
Paloma B. Liton, USA
Ana Lloret, Spain
Lorenzo Loffredo, Italy
Camilo López-Alarcón, Chile
Daniel Lopez-Malo, Spain
Massimo Lucarini, Italy
Hai-Chun Ma, China
Nageswara Madamanchi, USA
Kenneth Maiese, USA
Marco Malaguti, Italy
Steven McAnulty, USA
Antonio Desmond McCarthy, Argentina
Sonia Medina-Escudero, Spain
Pedro Mena, Italy
Víctor M. Mendoza-Núñez, Mexico
Lidija Milkovic, Croatia
Alexandra Miller, USA
Sara Missaglia, Italy

Premysl Mladenka, Czech Republic
Sandra Moreno, Italy
Trevor A. Mori, Australia
Fabiana Morroni, Italy
Ange Mouithys-Mickalad, Belgium
Iordanis Mourouzis, Greece
Ryoji Nagai, Japan
Amit Kumar Nayak, India
Abderrahim Nemmar, United Arab
Emirates
Xing Niu, China
Cristina Nocella, Italy
Susana Novella, Spain
Hassan Obied, Australia
Pál Pacher, USA
Pasquale Pagliaro, Italy
Dilipkumar Pal, India
Valentina Pallottini, Italy
Swapnil Pandey, USA
Mayur Parmar, USA
Vassilis Paschalis, Greece
Keshav Raj Paudel, Australia
Ilaria Peluso, Italy
Tiziana Persichini, Italy
Shazib Pervaiz, Singapore
Abdul Rehman Phull, Republic of Korea
Vincent Pialoux, France
Alessandro Poggi, Italy
Zsolt Radak, Hungary
Dario C. Ramirez, Argentina
Erika Ramos-Tovar, Mexico
Sid D. Ray, USA
Muneeb Rehman, Saudi Arabia
Hamid Reza Rezvani, France
Alessandra Ricelli, Italy
Francisco J. Romero, Spain
Joan Roselló-Catafau, Spain
Subhadeep Roy, India
Josep V. Rubert, The Netherlands
Sumbal Saba, Brazil
Kunihiro Sakuma, Japan
Gabriele Saretzki, United Kingdom
Luciano Saso, Italy
Nadja Schroder, Brazil

Anwen Shao (iD), China
Iman Sherif, Egypt
Salah A Sheweita, Saudi Arabia
Xiaolei Shi, China
Manjari Singh, India
Giulia Sita (iD), Italy
Ramachandran Srinivasan (iD), India
Adrian Sturza (iD), Romania
Kuo-hui Su (iD), United Kingdom
Eisa Tahmasbpour Marzouni (iD), Iran
Hailiang Tang, China
Carla Tatone (iD), Italy
Shane Thomas (iD), Australia
Carlo Gabriele Tocchetti (iD), Italy
Angela Trovato Salinaro, Italy
Rosa Tundis (iD), Italy
Kai Wang (iD), China
Min-qi Wang (iD), China
Natalie Ward (iD), Australia
Grzegorz Wegrzyn, Poland
Philip Wenzel (iD), Germany
Guangzhen Wu (iD), China
Jianbo Xiao (iD), Spain
Qiongming Xu (iD), China
Liang-Jun Yan (iD), USA
Guillermo Zalba (iD), Spain
Jia Zhang (iD), China
Junmin Zhang (iD), China
Junli Zhao (iD), USA
Chen-he Zhou (iD), China
Yong Zhou (iD), China
Mario Zoratti (iD), Italy

Contents

Research Article

Hypothermia Prevents Cardiac Dysfunction during Acute Ischemia Reperfusion by Maintaining Mitochondrial Bioenergetics and by Promoting Hexokinase II Binding to Mitochondria

Jie Sun,[1,2] **Jyotsna Mishra** [iD](ORCID)**,**[1] **Meiying Yang,**[1] **David F. Stowe,**[1,3,4,5] **James S. Heisner,**[1] **Jianzhong An,**[2] **Wai-Meng Kwok,**[1,5,6,7] **and Amadou K. S. Camara** [iD](ORCID) [1,3,5,7]

[1]*Department of Anesthesiology, Research Division, Medical College of Wisconsin, USA*
[2]*Institute of Clinical Medicine Research, Department of Gastroenterology and Hepatology, Suzhou Science and Technology Town Hospital, Suzhou, Jiangsu, China*
[3]*Department of Physiology, Medical College of Wisconsin, Milwaukee, WI, USA*
[4]*Department of Biomedical Engineering, Medical College of Wisconsin and Marquette University, Milwaukee, WI, USA*
[5]*Cardiovascular Center, Medical College of Wisconsin, Milwaukee, WI, USA*
[6]*Department of Pharmacology and Toxicology, Medical College of Wisconsin, Milwaukee, WI, USA*
[7]*Cancer Center, Medical College of Wisconsin, Milwaukee, WI, USA*

Correspondence should be addressed to Amadou K. S. Camara; aksc@mcw.edu

Background. Hypothermia (H), cardioplegia (CP), and both combined (HCP) are known to be protective against myocardial ischemia reperfusion (IR) injury. Mitochondria have molecular signaling mechanisms that are associated with both cell survival and cell death. In this study, we investigated the dynamic changes in proapoptotic and prosurvival signaling pathways mediating H, CP, or HCP-induced protection of mitochondrial function after acute myocardial IR injury. *Methods.* Rats were divided into five groups. Each group consists of 3 subgroups based on a specific reperfusion time (5, 20, or 60 min) after a 25-min global ischemia. The time control (TC) groups were not subjected to IR but were perfused with 37 °C Krebs-Ringer's (KR) buffer, containing 4.5 mM K$^+$, in a specific perfusion protocol that corresponded with the duration of each IR protocol. The IR group (control) was perfused for 20 min with KR, followed by 25-min global ischemia, and then KR reperfusion for 5, 20, or 60 min. The treatment groups were exposed to 17 °C H, 37 °C CP (16 mM K$^+$), or HCP (17 °C + CP) for 5 min before ischemia and for 2 min on reperfusion before switching to 37 °C KR perfusion for the remainder of each of the reperfusion times. Cardiac function and mitochondrial redox state (NADH/FAD) were monitored online in the *ex vivo* hearts before, during, and after ischemia. Mitochondria were isolated at the end of each specified reperfusion time, and changes in O$_2$ consumption, membrane potential ($\Delta\Psi_m$), and Ca^{2+} retention capacity (CRC) were assessed using complex I and complex II substrates. In another set of hearts, mitochondrial and cytosolic fractions were isolated after a specified reperfusion time to conduct western blot assays to determine hexokinase II (HKII) and Bax binding/translocation to mitochondria, cytosolic pAkt levels, and cytochrome *c* (Cyto-*c*) release into the cytosol. *Results.* H and HCP were more protective of mitochondrial integrity and, concomitantly, cardiac function than CP alone; H and HCP improved post-ischemic cardiac function by (1) maintaining mitochondrial bioenergetics, (2) maintaining HKII binding to mitochondria with an increase in pAkt levels, (3) increasing CRC, and (4) decreasing Cyto-*c* release during reperfusion. Bax translocation/binding to mitochondria was unaffected by any treatment, regardless of cardiac functional recovery. *Conclusions.* Hypothermia preserved mitochondrial function and cardiac function, in part, by maintaining mitochondrial bioenergetics, by retaining HKII binding to mitochondria via upstream pAkt, and by reducing Cyto-*c* release independently of Bax binding to mitochondria.

1. Introduction

Cardiac ischemia reperfusion (IR) injury results when a disease-induced blockage of blood flow in a major coronary vessel is relieved by reperfusion. IR injury can also occur during coronary angioplasty, cardiac valve replacement, or coronary bypass grafting [1]. Following cardiac ischemia, the most effective strategy for mitigating injury and limiting infarction is early restoration (reperfusion) of coronary blood flow to the ischemic myocardium [2–5]. However, this approach, while essential, is often associated with functional and structural damage to the myocardium because of the reperfusion damage that occurs the longer the ischemia [2, 6, 7]. Hence, timely reperfusion during acute ischemia is crucial for salvage of the ischemic myocardium. Unfortunately, reperfusion leads to the activation of many signaling pathways that contribute independently to both apoptotic and necrotic tissue injury and thus decreases the amount of viable myocardium. Reperfusion mediated mitochondrial damage is usually characterized by increased reactive oxygen species (ROS) production, cytosolic-induced mitochondrial Ca^{2+} overload, a decreased NADH/FAD redox ratio, and formation and opening of the deleterious mitochondria permeability transition pore (mPTP) [7].

Mitochondria are key regulators of cellular metabolism in the heart; but their dysfunction during cardiac IR injury can lead to cardiac dysfunction and myocyte demise [8]. The importance of mitochondria as both targets and mediators of IR injury is now well recognized. Pharmacological and nonpharmacological interventions to mitigate mitochondrial damage during IR have proven to be somewhat beneficial in rescuing the myocardium from IR injury, particularly if the intervention is applied before or during the ischemia. For example, we have reported that amobarbital, a drug that attenuates respiration at complex I [9], and ranolazine, a clinical antianginal drug that reduces cell and mitochondrial Ca^{2+} overload, and indirectly reduces ROS production with IR injury [7], are both cardioprotective in part by preserving mitochondrial function. We also reported previously that nonpharmacological interventions, like hypothermia (H), cardioplegia (CP), and HCP, provide varying degrees of protection against IR injury by attenuating excess mitochondrial and cytosolic Ca^{2+} and by reducing deleterious mitochondrial ROS production [10–13]. The mitochondrial mechanisms underlying protection against acute IR injury by H and CP have not been investigated during early and late reperfusion. A better understanding of the mitochondrial mechanisms that provide protection by H, CP, or HCP may enhance the organelle's therapeutic potential and the timing for improving cardioprotection after IR injury.

Clinically, both H and CP are utilized as effective interventions to protect the heart against ischemic injury during cardiac surgery. CP provides a motionless field by arresting the heart and H reduces cardiac metabolism even while the heart is not contracting; switching from cold CP perfusate to warm blood reperfusion allows for effective post-ischemic myocardial resuscitation [14]. Even though the effect of cooling on reducing overall metabolism is well known, the mitochondrial mechanisms by which H attenu-

ates IR injury remain to be elucidated. Hypothermic-induced protection during reperfusion may be linked to a myriad of effects, including diminished ROS production and decreased cytosolic and mitochondrial Ca^{2+} overload [15], lower lactate levels from anaerobic metabolism, decreased cellular acidosis [4], and decreased energy utilization during ischemia that preserves essential mechanisms for rapid regeneration of ATP on reperfusion. Hypothermia has also been reported to modulate cell survival signaling pathways such as the Akt pathway [16]. CP generally entails the use of a hyperkalemic perfusate to depolarize all heart cells in synchrony, which provides diastolic cessation of all electromechanical activity and reduced myocardial O_2 consumption.

In a previous report, we showed that normothermic CP decreased ROS generation during IR and better maintained a reduced mitochondrial redox state (NADH and $FADH_2$) [11]. Hypothermic CP (HCP) [10] is widely used for coronary artery bypass grafting because it not only abruptly stops the heart but also reduces the cardiac energy demand. The central roles of H, CP, and HCP on altering mitochondrial function as both a target and initiator of signaling cascades that lead to cardiac protection during IR injury are not well described. A better understanding of changes in signaling pathways induced by H, CP, and HCP that mediate mitochondrial adaptation to IR injury could lead to new therapeutic approaches that specifically target mitochondria to protect the heart from IR injury.

We hypothesized that perfusion of CP, H, or HCP just before and after ischemia attenuates myocardial IR injury by initiating key antiapoptotic proteins/signaling molecules that are important in promoting mitochondrial-mediated cell survival on reperfusion. In addition, we postulated that activation of these signaling molecules is dependent on the duration of the reperfusion time at which protection is elicited. In planning our approach, we sought to define the chronological order of signaling events that promote or mitigate damage to mitochondria and confer cardiac dysfunction or protection, respectively. Factors that we looked at were as follows: (1) the comparative protective effects of H, CP, and HCP on hexokinase II (HKII) binding to mitochondria over time during reperfusion mediated by an Akt mechanism; (2) the role of the proapoptotic protein Bax translocation/binding to mitochondria; and (3) cytochrome *c* (Cyto-*c*) release, a marker of apoptosis. We found that H, rather than CP, is the most important intervention in maintaining HKII binding to mitochondria likely via a pAkt mechanism [16] and in attenuating Cyto-*c* release. Bax translocation/binding to mitochondria was not affected. These mitochondrial events appear to be important contributing factors to the protection afforded by hypothermia.

2. Materials and Methods

2.1. Isolated Heart Preparation and Measurements. All experiments conformed to the NIH "Guide for the Care and Use of Laboratory Animals" (NIH Publication N0. 85-23, Revised in 1996) for humane care and was approved by the Institutional Animal Care Committee of the Medical College of Wisconsin (MCW). Male Sprague-Dawley rats

(weight: 250 to 300 g; $n = 81$), aged 10-12 weeks, were housed at the MCW animal facility in rooms set at 25 °C with 60% humidity under a 12-h light-dark cycle. Rats were allowed access to food and water *ad libitum*.

The methods described here have been detailed in our previous studies [7, 10, 12, 13, 17–22]. In brief, rats were injected intraperitoneally with a combination of ketamine (50 mg/kg) for anesthesia, and 1000 units heparin to prevent blood coagulation. Rats were decapitated only when unresponsive to a noxious stimulus to the hind limb. Following decapitation and thoracotomy, the heart was rapidly excised, and the aorta was cannulated and immediately perfused retrograde, with chilled oxygenated Krebs Ringer's (KR) buffer. After proper placement of the aortic cannula, the heart was immediately transferred to a Langendorff apparatus for further perfusion under a constant pressure with a KR solution (37 °C) that contained in mM, 138 Na^+, 4.5 K^+, 1.2 Mg^{2+}, 2.5 Ca^{2+}, 134 Cl^-, 15 HCO_3^-, 1.2 $H_2PO_4^-$, 11.5 glucose, 2 pyruvate, 16 mannitol, 0.1 probenecid, 0.05 EDTA, and 5 U/L insulin, and maintained at pH 7.4 and gassed with a 3% CO_2+97% O_2.

A physiological saline-filled latex balloon attached to a transducer was inserted into the left ventricle, via the left atrium, to measure left ventricular systolic and diastolic pressures (LVP). At the start of each experiment, the balloon volume was adjusted to set the diastolic LVP to 0 mmHg so that any subsequent changes in diastolic LVP represents an index of left ventricular contracture attributable to IR damage. The systolic and diastolic LVPs were monitored continuously online. Developed LVP (dLVP) was derived from the difference between systolic LVP and diastolic LVP. The rate of contractility ($dLVP/dt_{max}$) and relaxation ($dLVP/dt_{min}$) were derived from the systolic LVP. Coronary flow (CF) was measured by an ultrasonic flowmeter (model T106X; Transonic Systems, Ithaca, NY) placed directly into the aortic inflow line. Spontaneous heart rate (HR) was monitored with bipolar electrodes placed in the right atrial and ventricular free-walls. The rate pressure product (RPP), an index of cardiac work, was calculated as the product of the dLVP and HR (RPP = $dLVP \times HR$) [23, 24]. Coronary inflow and outflow ionic conditions (Na^+, K^+, and Ca^{2+}), pH, partial pressures of O_2, and CO_2 were measured offline with an intermittently self-calibrating analyzer system (Radiometer Copenhagen ABL 505; Copenhagen, Denmark) [12].

Indices of mitochondrial redox state, i.e., NADH and FAD derived from tissue autofluorescence signals [12, 13], were measured online by fluorescence spectrophotometry (Qm-8, Photon Technology Instrument; HORIBA Scientific, Piscataway, NJ) in a light-proofed Faraday cage. A trifurcated fiberoptic probe (3.8 mm^2/bundle) was placed gently against the left ventricular free-wall, as described previously [12, 13, 25]. In the cardiomyocyte, the majority of the NADH is generated from mitochondria, with negligible amount emanating from glycolysis. FAD is primarily from mitochondria.

2.2. Experimental Groups and Protocols. Rats were divided into five groups. Each group has three subgroups based on the reperfusion times of 5, 20, or 60 min after the global ischemia. The five groups were as follows: time control (TC), IR (normothermic ischemia, no treatment), hypother-

mia (H), cardioplegia (CP), and H + CP. In the TC groups, hearts were perfused with KR for the duration of an IR protocol (Figure 1) without ischemia (n = 3 in each subgroup). The relative constancy of the functional variables during the TC perfusions validated the functional stability of our *ex vivo* perfused heart model. In the IR group (no treatment; control), after 20 min KR perfusion for stabilization, the hearts underwent 25-min global ischemia, followed by warm (37 °C) KR (4.5 mM K^+) reperfusion for 5, 20, or 60 min (n = 6 hearts/subgroup). In the H group (n = 6 hearts/subgroup), the hearts were subjected to similar KR perfusion for stabilization followed by 5 min cold KR (17 °C) perfusion before initiating cold global ischemia for 25 min. In the CP group (n = 6 hearts/subgroup), the hearts were perfused with high [K^+] KR solution at 37 °C (CP; KR with 16 mM K^+) for 5 min before 25-min global warm ischemia. In the HCP (17 °C) group (N= 6 hearts/subgroup), the hearts were perfused with HCP for 5 min before the 25-min HCP global ischemia. During reperfusion, hearts were perfused with their respective treatments for 2 min before switching back to normal warm (37 °C) KR perfusion for the remaining 5, 20, or 60-min reperfusion periods. At the end of each specified reperfusion time (5, 20, or 60 min), the hearts were immediately removed from the perfusion apparatus, and mitochondria were isolated for assessment of mitochondrial bioenergetics, Ca^{2+} retention capacity (CRC), and molecular markers associated with anti- and proapoptotic pathways, as described in our previous studies [7, 26, 27].

2.3. Mitochondrial Isolation. Mitochondria were isolated as described in our previous studies [17, 28, 29]. All procedures were performed at 4 °C. Hearts were rapidly excised and minced in 4 °C isolation buffer containing in mM: 200 mannitol, 50 sucrose, 5 KH_2PO_4, 5 MOPS, 1 EGTA, 0.1% fatty acid free BSA, and protease inhibitors, at pH 7.15 (adjusted with KOH). The tissue suspension was homogenized in a 50 mL centrifuge tube at low speed in cold isolation buffer. The suspension was centrifuged at 8000 g for 10 min. The supernatant was collected and centrifuged again at 50,000 g for 30 min. After centrifugation, the supernatant was removed and stored for determination of cytosolic proteins. The pellet was resuspended in cold isolation buffer and spun at 850 g for 10 min. The supernatant was again collected and re-centrifuged at 8000 g for 10 min. Two different types of mitochondria, crude and purified, were isolated. At the end of this last spin (crude), mitochondria were stored in ice and used to assess bioenergetics and CRC. For the purified mitochondria, the supernatant from the last spin was discarded, and the final mitochondrial pellet resuspended. The mitochondria were then purified using 30% percoll in the isolation buffer and then spun at 95,000 g for 30 min [26]. The purified mitochondria were kept on ice for western blot experiments. All mitochondrial functional studies were performed at room temperature.

2.4. Mitochondrial O_2 Consumption, Membrane Potential ($\Delta\Psi_m$), and Ca^{2+} Retention Capacity (CRC). Mitochondria isolated at the end of each specified reperfusion time from each experimental group were used to assess the impact of
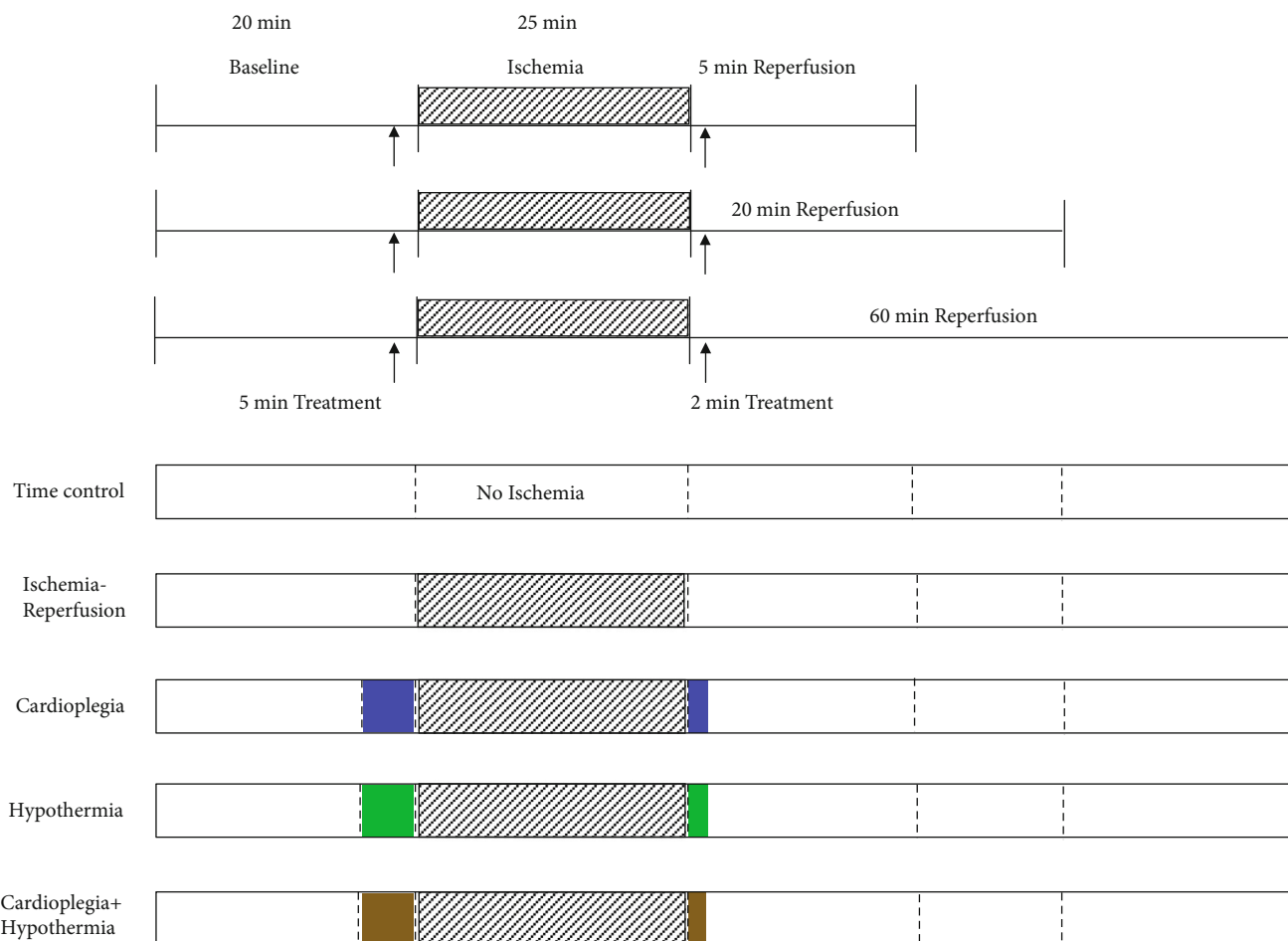
FIGURE 1: Timeline protocols for the time control (no ischemia), ischemia reperfusion (grey patterned box) ± cardioplegia (blue box), hypothermia (green box), or cardioplegia + hypothermia (brown box) treatment groups with 5, 20, or 60 min reperfusion after 25 min of global ischemia.

IR with and without treatment on bioenergetics and CRC. The mitochondrial protein content was determined by the Bradford method [7, 26]. Mitochondrial O_2 consumption was measured using a Clark electrode respirometer (System S200A, Strathkelvin Instruments). The protocol is described in our previous studies [21, 30, 31]. Mitochondria, 0.275 mg from each group, were added into 0.5 mL respiration buffer (in mM: 130 KCl, 5 K_2HPO_4, 20 MOPS, 0.1% BSA, pH 7.15) to measure the O_2 consumption rate during states 2, 3, and 4 respirations. To initiate state 2 respiration, the mitochondrial suspension was energized with 10 mM complex I substrate, Na^+-pyruvate, and Na^+-malate mixture (PM; 1 : 1), or the complex II substrate, Na^+-succinate. State 3 respiration was initiated by adding 250 μM ADP, and state 4 respiration ensued when the added ADP was completely phosphorylated to ATP via oxidative phosphorylation. The respiratory control index (RCI) was calculated as the rate of state 3/state 4 respiration. This value reflects the viability of mitochondria and the tightness of the coupling of oxidative phosphorylation for the different treatment groups during different reperfusion times.

To monitor $\Delta\Psi_m$, the cationic fluorescent dye tetramethyl-rhodamine methyl ester (1 μM) (TMRM;

Molecular Probes, Eugene, OR) was added to the mitochondrial suspension in respiration buffer as we reported previously [27, 29, 32]. Fluorescence detection representing changes in $\Delta\Psi_m$ was monitored using two excitations λ_{ex}546 and 573 nm and a single emission λ_{em}590 nm, as described previously [31, 33]. A suspension of 500 μg of mitochondria was added to 1 mL of respiration buffer and energized with 10 mM PM mixture (1 : 1) or with 10 mM succinate. After establishing $\Delta\Psi_m$, ADP (250 μM) was added to the mitochondrial suspension to transiently depolarize $\Delta\Psi_m$, which reflects state 3 respiration. The $\Delta\Psi_m$ repolarizes to baseline after the added ADP is phosphorylated to ATP (state 4 respiration). The time to repolarize was measured for all five groups. At the end of each experiment, 4 μM carbonyl cyanide m-chlorophenyl hydrazone (CCCP), a mitochondrial uncoupling agent, was added to the mitochondrial suspension to fully depolarize $\Delta\Psi_m$. The magnitude of the ADP depolarization was compared to the maximal depolarization when CCCP was added.

Our previous studies showed that acute IR leads to increased cytosolic and mitochondrial Ca^{2+} overload and that these effects were mitigated by hypothermia, but not by CP [11, 12]. Ca^{2+} overload could weaken mitochondria

and lower their threshold for mPTP opening under stress. To test the vulnerability of mitochondria after IR injury, we monitored isolated mitochondrial tolerance to excess $CaCl_2$ pulse challenges after IR $\pm$ treatments and in TC. CRC was measured by fluorescence spectrophotometry (Qm-8, Photon Technology Instrument; HORIBA Scientific, Piscataway, NJ). Isolated mitochondria (500 μg) were suspended in a cuvette containing 1 mL of respiration buffer with 0.1 μM calcium fluorescent dye Fura-4F K^+-salt with dual excitation wavelengths (λ_{ex}) at 340/380 nm and a single emission wavelength (λ_{em}) at 510 nm [27, 29]. The mitochondrial suspension in the cuvette was under continuous stirring and was energized with 10 mM PM mixture (1 : 1) or with 10 mM Na^+-succinate after 60 s at room temperature. Afterwards, mitochondria were challenged with repeated boluses of $CaCl_2$ (20 μM) every 90 s, in the presence of approximately 40 μM EGTA (carried over from the isolation buffer), until mitochondria were not able to take up and sequester the added Ca^{2+} or the mPTP opens. The opening of mPTP is indicated by a sharp increase in the extra-matrix-dye fluorescent intensity due to increase Ca^{2+} release into the medium. Mitochondrial Ca^{2+} uptake was determined by the decay of the extra-matrix fluorescent dye (Fura-4F) intensity signal towards baseline, after the addition of boluses of $CaCl_2$. A steady-state Ca^{2+} uptake was achieved by the flat response in the curve as mitochondria take up and sequester the added Ca^{2+} [27]. After mPTP opening or no additional Ca^{2+} uptake, CCCP (4 μM) was added to obtain the maximal fluorescence signal based on the total release of the sequestered Ca^{2+}.

2.5. Western Blot Assays for Hexokinase II (HKII), Phospho-Akt, Bax, and Cytochrome c (Cyt-c) in Cytosolic and Mitochondrial Fractions. At specified reperfusion times, the cytosolic fraction was separated from the mitochondrial fraction by differential centrifugation as described before [7, 17]. Both the cytosolic and mitochondrial fractions were stored at $-80\,°C$ until the time of experimentation. We used standard western blotting procedures to assess the levels of targeted anti- and proapoptotic proteins following the determination of the protein content. To verify the purity of the mitochondrial and cytosolic fractions, COX IV was used as the internal housekeeping protein for the mitochondrial fractions, and β-tubulin was used as internal housekeeping protein for the cytosolic fractions.

The cytosolic and mitochondrial protein lysates were resolved by SDS-polyacrylamide gel electrophoresis (SDS-PAGE) using a 4%-20% slab gel. After the gel electrophoresis, proteins were transferred onto a polyvinylidene difluoride (PVDF) membrane using the Transblot system (Bio-Rad, Richmond, CA). Membranes were incubated with specific primary antibodies: anti-HKII (rabbit monoclonal, 1 : 1000, Cell Signaling Technology); anti-Bax (1 : 1000 dilution; Cell Signaling); anti-Akt (1 : 1000 dilution; Cell Signaling); anti-pAkt at serine 473 (Ser473; 1 : 1000 dilution; Cell Signaling); anti-Cyt-c (mouse monoclonal, 1 : 1000, Invitrogen); anti-β tubulin (rabbit monoclonal, 1 : 1000, Cell Signaling Technology); and anti-COX IV (rabbit monoclonal, 1 : 1000, Cell Signaling Technology) overnight at $4\,°C$. After washing 3 times, the membranes were incubated with the appropriate secondary antibody conjugated to HRP and then immersed in an enhanced chemiluminescence detection solution (GE Healthcare), and images were taken using the ChemiDoc imaging system (Bio-Rad).

2.6. Statistical Analysis. Data are expressed as means ± standard error of the means (SEM). Student-Newman-Keuls' test was used to differentiate the differences within or between groups. If p values were significant ($p < 0.05$), one-way ANOVA was selected to analyze the statistically significant differences among the groups. Differences among the means were considered significant when $p < 0.05$ (two-tailed).

3. Results

3.1. Hypothermia and Cardioplegia Protected Cardiac Mechanical Function and Redox State during IR Injury. The timeline of the experimental protocol is shown in Figure 1. Cardiac functional data were assessed before, during, and at each specified reperfusion time (5, 20, and 60 min) to correlate with mitochondrial function and translocation of signaling molecules to and from mitochondria associated with promotion of cell survival *vs.* cell death, respectively. Baseline functional measurements of coronary flow (CF), diastolic left ventricular pressure (LVP), developed LVP (dLVP), and rate pressure product (RPP), were not significantly different among all five groups (Figure 2). The time control (TC) group showed relative constancy of each variable monitored during a specified perfusion protocol. At reperfusion 60 min, all the functional variables were significantly worsened in the IR alone group. IR + CP did not improve recovery of CF but showed a modest but significant recovery of all LVP indices and RPP when compared to the IR alone group. H and HCP treatments with IR led to almost full recovery of all functional variables after ischemia, as they were not significantly different from the TC at 60 min reperfusion. In this acute IR injury model, adding CP to the 17 °C perfusate did not provide any additional protection against the acute IR injury. The marked increase in diastolic LVP, an index of left ventricular contracture, in the IR group, is likely due to impaired cytosolic Ca^{2+} homeostasis, which would contribute to the diminished recovery of dLVP and RPP (Figure 2). The functional recovery of the four variables at 5 and 20 min reperfusion in the IR + H, CP, and HCP (Supplementary Figure S1) groups is comparable to that found after 60-min reperfusion. Values for dLVP/dt_{max} and dLVP/dt_{min}, i.e., rates of contractility and relaxation, complemented the data displayed in Figure 2 (Table 1). The IR group had the lowest dLVP/dt_{max} and dLVP/dt_{min} (Table 1). IR + H, CP, and HCP groups improved recovery of dLVP/dt_{max} and dLVP/dt_{min} at 60 min reperfusion. Moreover, recovery of contractility and relaxation after IR in the H and HCP groups were significantly better than in the IR + CP group. The recovery of dLVP/dt_{max} and dLVP/dt_{min} during 5 and 20 min reperfusion were again significantly better in the H and HCP treated hearts (Supplementary Table S1).

(a)

(b)

(c)

(d)
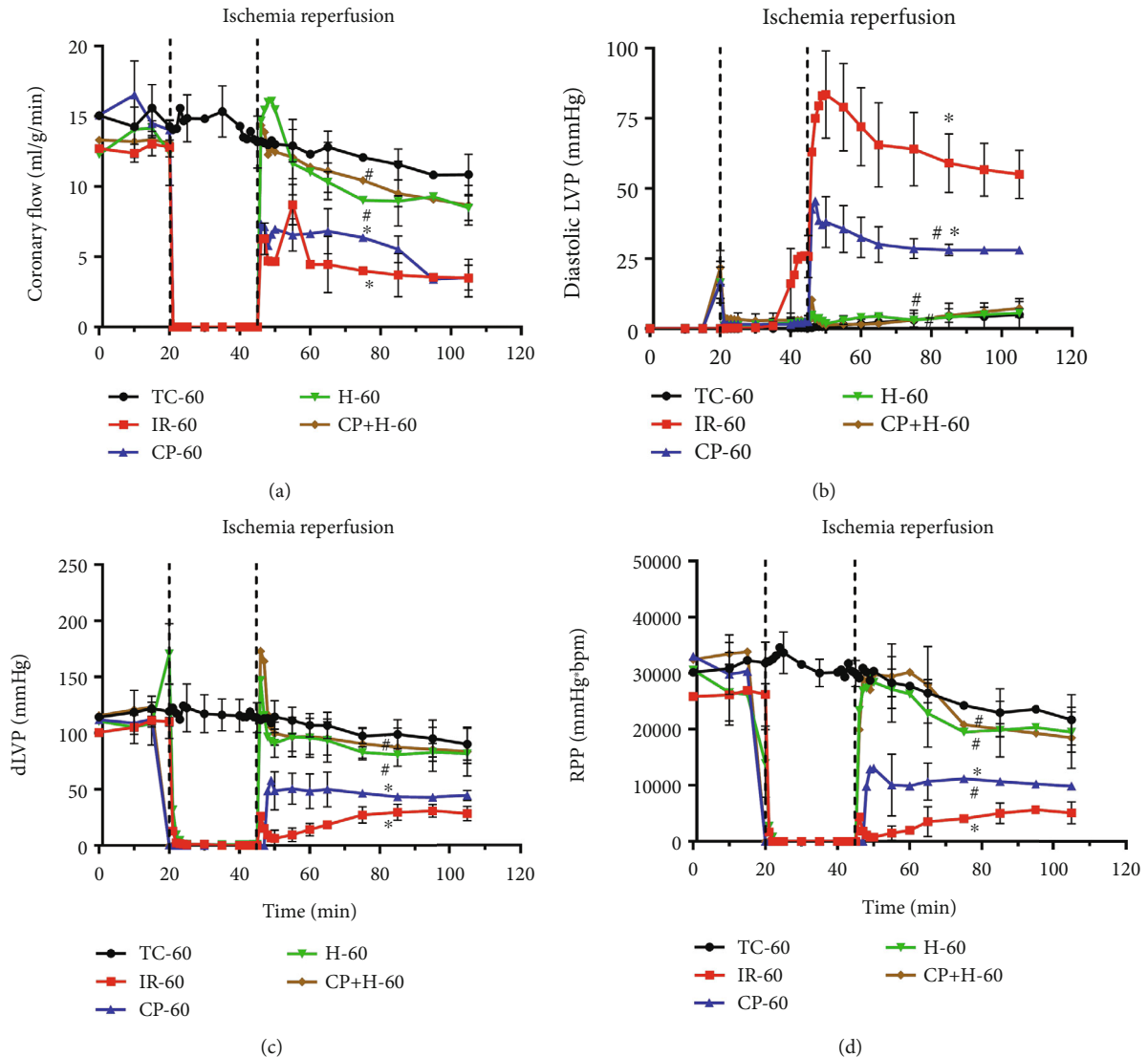
FIGURE 2: Coronary flow (CF), diastolic LVP (DiaLVP), developed LVP (dLVP), rate pressure product (RPP) at 60 min reperfusion in time control (TC), ischemia reperfusion (IR), cardioplegia (CP), hypothermia (H), and cardioplegia + hypothermia (CP + H) groups. $N = 6$ hearts in each group. Values are mean ± SE. $^*p < 0.05$, compared to TC group; $^\#p < 0.05$ compared to IR group.

NADH and FAD autofluorescence, markers of the mito-chondrial redox state, were monitored before, during, and after acute IR. NADH fluorescence signal increased, and FAD fluorescence signal did not change significantly during ischemia when compared to the TC group (Table 2). The increase in NADH signal is likely due to inhibited electron flow along the electron transfer chain (ETC) as we have reported before [12, 13]. The increase in NADH was signif-icantly more pronounced in the H and HCP groups during ischemia than in the IR alone (control) and CP groups. However, redox state was not different among all groups at 20 min reperfusion (Table 2). This indicated that H and HCP treatments elicited a higher (reduced) redox state during ischemia so that reducing equivalents were readily available on reperfusion for oxidative phosphorylation to restore ATP levels. Overall, these results indicated that in this acute IR model, hypothermia-conferred protection, just

before ischemia and in early reperfusion, largely by protect-ing mitochondria function during the period of reperfusion.

3.2. Hypothermia and Cardioplegia Improved Respiratory Control Index (RCI), Mitochondrial Membrane Potential ($\Delta\Psi_m$), and Ca^{2+} Retention Capacity (CRC) after IR Injury. Changes in bioenergetics, including the state 3 over state 4 respiration ratio, i.e., RCI (Figures 3(a) and 3(b)) and $\Delta\Psi_m$ (Figures 3(c) and 3(d)), and the ability of mitochondria to take up and retain added Ca^{2+} (CRC) (Figure 4) were assessed in TC, IR alone, and IR + H, CP, or HCP treated hearts after isolating mitochondria at the specified reperfu-sion times of 5 and 20 min. We examined mitochondrial function at these specified times based on our previous reports that showed deleterious effects that contribute to later reperfusion injury that occurs during early reperfusion [17, 25]. Mitochondrial O_2 consumption and RCI were

TABLE 1: Baseline and post-treatment variables dP/dt_{max} and dP/dt_{min} at 60-min reperfusion in time control (TC), ischemia reperfusion (IR), cardioplegia (CP), hypothermia (H), and cardioplegia + hypothermia (HCP) groups. $N = 6$ hearts in each group. Values are mean $\pm$ SE. $^*p < 0.05$, compared to TC group; $^\#p < 0.05$ compared to IR group; $^\$p < 0.05$ compared to IR + CP group.

Time (60-min REP)	TC	IR	IR + CP	IR + H	IR + HCP
dP/dt_{max} (mmHg/min)	3549 ± 49	$503 \pm 93^*$	$1610 \pm 45^{*\#}$	$2860 \pm 20^{*\#\$}$	$3507 \pm 73^{\#\$}$
dP/dt_{min} (mmHg/min)	-2916 ± 130	$-359 \pm 38^*$	$-1484 \pm 76^{*\#}$	$-2206 \pm 72^{*\#\$}$	$-2799 \pm 51^{\#\$}$

TABLE 2: Mitochondrial redox state (NADH/FAD) at 25-min ischemia (ISC) and 20-min reperfusion (REP). TC: time control; IR: ischemia and reperfusion without intervention; IR + CP: IR plus cardioplegia treatment; IR + H: IR plus hypothermia treatment; HCP: and hypothermia plus cardioplegia treatment + IR. $N = 6$ hearts in each group. Values represent mean $\pm$ SE. $^*p < 0.05$ compared to TC group; $^\#p < 0.05$ compared to IR group; $^\$p < 0.05$ compared to IR + CP group.

Time (min)	TC	IR	IR + CP	IR + H	IR + HCP
NADH (AFU)					
25-min ISC	1.30 ± 0.04	$1.45 \pm 0.03^*$	$1.50 \pm 0.03^*$	$1.92 \pm 0.07^{*\#\$}$	$1.83 \pm 0.06^{*\#\$}$
20-min REP	1.30 ± 0.06	1.26 ± 0.04	1.27 ± 0.11	1.41 ± 0.10	1.40 ± 0.11
FAD (AFU)					
25-min ISC	0.24 ± 0.01	0.26 ± 0.04	0.21 ± 0.02	0.21 ± 0.01	0.21 ± 0.02
20-min REP	0.24 ± 0.02	0.24 ± 0.04	0.25 ± 0.03	0.24 ± 0.02	0.23 ± 0.02

monitored in mitochondria energized with the complex I substrate PM or the complex II substrate succinate. In mitochondria energized with PM, O_2 consumption was significantly depressed in the IR group at 5 and 20 min reperfusion; H, CP, and HCP treatments each restored states 3 and 4 O_2 consumption rates and RCI to values not significantly different from the TC group. However, states 3 and 4 O_2 consumption rates and RCIs were not altered significantly in mitochondria energized with the complex II substrate in any group (Supplementary Figure S2).

The time to repolarize $\Delta\Psi_m$ (state 4 respiration) following ADP-induced depolarization (state 3 respiration) was assessed by TMRM fluorescence at 5 and 20 min reperfusion (Figures 3(c) and 3(d)). State 2 and state 4 $\Delta\Psi_m$ were similar for both substrates in all groups. After adding ADP, there was a rapid, partial, and reversible $\Delta\Psi_m$ depolarization in each group. IR-5 (Figure 3(c)) and IR-20 (reperfusion at 5 and at 20 min) (Figure 3(d)) groups showed a significant delay in $\Delta\Psi_m$ repolarization compared to the treatments and their respective TC groups, with both substrates (Figures 3(c) and 3(d) and Supplementary Figures S2(c) and S2(d)). The times for $\Delta\Psi_m$ repolarization following ADP-mediated $\Delta\Psi_m$ depolarization were not significantly different among IR + H, CP or HCP groups from the TC groups at the 5 and 20 min reperfusion with PM as the substrate. The duration of $\Delta\Psi_m$ depolarization was longer for the complex II substrate succinate than for the complex I substrate PM after IR-5 and IR-20 (Figures 3(c) and 3(d) and Supplementary Figure S2). Recovery of $\Delta\Psi_m$ after ADP-induced depolarization was impaired in the IR only group. H, CP, and HCP treatments with IR exhibited $\Delta\Psi_m$ repolarization like that in the TC groups.

Mitochondrial CRC was assessed by uptake and release of Ca^{2+} into the respiratory buffer containing 40 μM EGTA using Fura-4 fluorescence after 5 min (Figure 4(a)) and 20-

min (Figure 4(b)) reperfusion. The inset in each panel is an expanded view of the Ca^{2+} uptake and retention profiles for the last several $CaCl_2$ pulses just before mPTP opened, i.e., when mitochondria stop taking up Ca^{2+}. Note that with PM as substrate, isolated mitochondria from the IR + H and IR + HCP hearts took up and retained Ca^{2+} better than mitochondria isolated from the IR only hearts (inset, Figures 4(a) and 4(b)). There was no significant difference in CRC between IR + H and IR + HCP groups, which is consistent with the results on the cardiac functional recovery. Although CP alone provided a modest improvement of cardiac function and mitochondrial bioenergetics, it did not significantly improve CRC compared to the IR only group. This effect of CP is consistent with our previous study [11], which showed that in the ex vivo heart, CP-induced protection against acute IR injury did not reduce mitochondrial Ca^{2+} overload despite the modest recovery of function. Our results show that hypothermia after reperfusion better preserved mitochondria Ca^{2+} handling during excess $CaCl_2$ challenges, which agrees with its mitigating effect on mitochondrial Ca^{2+} overload in the acute ex vivo IR model [13]. There was no difference among the groups in the CRC when mitochondria were energized with the complex II substrate, succinate (Supplementary Figure S3). Overall, these results indicated that hypothermia is more protective with PM used as the substrate.

3.3. Hypothermia Promoted HKII Binding to Mitochondria after IR Injury.

We tested next whether cardioprotection against acute IR injury afforded by IR + H, CP, and HCP is mediated, in part, by increased HKII translocation/binding to mitochondria at 5, 20, and 60 min reperfusion. Western blotting of HKII bound to mitochondria and HKII expression levels in the cytosolic fraction after IR alone showed significant dissociation of HKII binding from mitochondria,
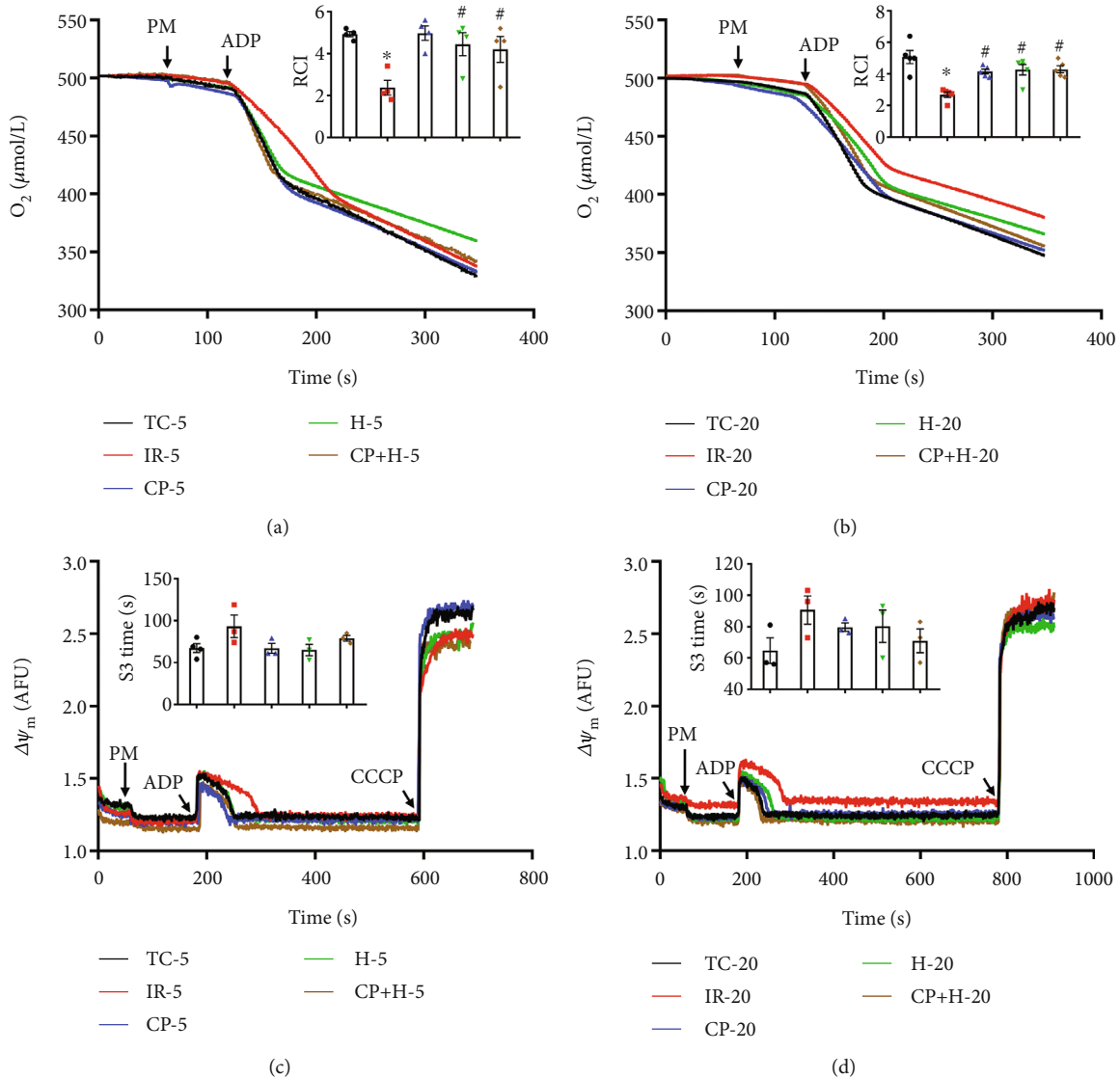
FIGURE 3: Representative traces of O_2 consumption rates (insets: average respiratory control index (RCI)) at 5 (a) and 20 min (b) reperfusion periods in time control (TC), ischemia reperfusion (IR), cardioplegia (CP), hypothermia (H), and cardioplegia + hypothermia (CP + H) groups. Change in membrane potential ($\Delta\Psi_m$) (insets: average time (S3 time (sec)) for repolarization after ADP-induced depolarization (state 3)) at 5 (c) and 20 min (d) reperfusion periods in experimental groups. Mitochondria were energized with Na^+-pyruvate and Na^+-malate (PM; complex I substrate). N = mitochondria from 3 to 4 hearts in each group. The bar graphs show mean ± SE. $^*p < 0.05$ compared to TC group; $^\#p < 0.05$ compared to IR group.

while showing increased levels of HKII in the cytosolic fraction (Figure 5). IR + H and IR + HCP groups showed significant binding of HKII to mitochondria and, correspondingly, decreased HKII levels in the cytosolic fraction at 5, 20, and 60 min reperfusion when compared to IR alone (control) hearts. There was no significant difference in mitochondrial HKII binding between H and HCP groups at 5, 20, and 60 min. Of note, the binding of HKII to mitochondria in the HCP group at 60 min reperfusion was significantly greater than in the TC group (Figure 5(c)). The data suggested that H and HCP maintained mitochondria-HKII association and improved mitochondria function as contributing factors in the robust recovery of cardiac function after IR. Just as CP alone provided only modest protection

of cardiac function against IR injury, there was no significant HKII binding to mitochondria or altered HKII levels in the cytosolic fraction at 5, 20, or 60 min reperfusion in the CP group.

3.4. Hypothermia Increased Akt (Protein Kinase B) Phosphorylation (pAkt) at Ser473 after IR Injury.

Because we observed that H and HCP treatments markedly maintained HKII binding to mitochondria (Figure 5), we determined next whether phosphorylated (p) Akt levels correspondingly increased in the IR + H, CP, and HCP groups. Since HKII binding to mitochondria was sustained for up to 60-min reperfusion in H and HCP treated hearts, we examined the phosphorylation of Akt at Ser473, which
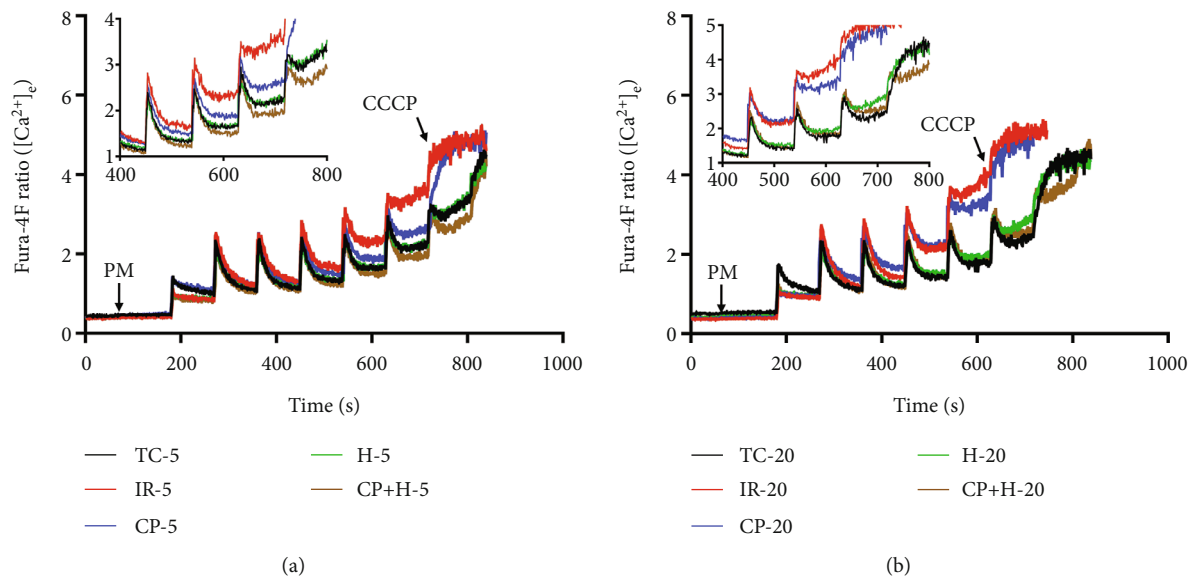
FIGURE 4: Representative traces of mitochondrial calcium retention capacity (CRC) at 5 (a) and 20 min (b) reperfusion periods in time control (TC), ischemia reperfusion (IR), cardioplegia (CP), hypothermia (H), and cardioplegia + hypothermia (CP + H) groups. The insets are representative traces at later time points that show in greater details the differences in the kinetics of mitochondrial Ca^{2+} uptake during the $CaCl_2$ pulse challenges until mitochondria stopped taking Ca^{2+}. CCCP, the mitochondrial uncoupler, was given after mitochondria stopped taking the added Ca^{2+} to unload all the Ca^{2+} sequestered during bolus additions. Mitochondria were energized with Na^+-pyruvate and Na^+-malate (PM; complex I substrate).

is associated with Akt activation an upstream activator of HKII [34, 35] in the cytosolic fraction after 60-min reperfusion (Figure 6). CP treatment did not increase cytosolic pAkt levels compared to the IR group. The diminished levels of pAkt in the IR group are consistent with the reduced HKII binding to mitochondria; in the CP group, there was a modest increase in pAkt, but this increase was not associated with increased HKII-mitochondria binding. In the H and HCP groups, there was a marked increase in pAkt, which is consistent with maintained HKII binding to mitochondria. There was a significant decrease in total (t) Akt (tAkt) expression in the IR and CP groups, compared to the TC group, indicating that IR itself reduces the levels of Akt leading to a decline in the tAkt level. H and HCP preserved tAkt levels when compared to the TC group. Altogether, these results indicated that cardioprotection afforded by H and HCP was mediated, in part, by increased levels of cytosolic pAkt, which could contribute to the maintenance of HKII binding to mitochondria. In contrast, the modest cardioprotection afforded by CP treatment was independent of the Akt-HKII signaling pathway.

3.5. Bax Binding Was Not Altered by Hypothermia or Cardioplegia after IR Injury.

We next monitored Bax, a proapoptotic protein, in mitochondrial and cytosolic fractions to assess whether H, CP, or HCP treatment alters Bax binding to mitochondria to confer protection. We found that the levels of Bax in the mitochondrial and cytosolic fractions were not significantly different among the five groups, regardless of the reperfusion time (Supplementary Figure S4). Interestingly, the H and HCP-induced increases in HKII binding to

mitochondria did not preclude Bax binding to mitochondria, as has been reported during ischemic stress [36].

3.6. Hypothermia Decreased mitochondrial Cytochrome c (Cyto-c) Release after IR Injury.

We then correlated the timing of HKII bound to mitochondria with Cyto-c release in the cytosol, a marker of mPTP opening or mPTP-independent OMM permeability, after IR injury. At 5 min reperfusion, there was no significant difference in cytosolic Cyto-c content among the groups (Figure 7(a)). However, at 20 and 60 min reperfusion, there was a significant increase in Cyto-c release in the IR group. H and HCP treatments significantly reduced the IR-induced cytosolic Cyto-c levels to levels not significantly different from TC hearts (Figure 7(b) and 7(c)). The sustained increase in HKII binding at 20 and 60 min reperfusion was associated with reduced Cyto-c release into the cytosol and improved cardiac function after IR. Since HKII translocation to mitochondria was already detected at 5-min reperfusion, these data appear to confirm that HKII binding to mitochondria before Cyto-c release is a time-dependent signaling event preceding release of the apoptotic agent. CP did not significantly reduce Cyto-c release induced by IR when compared to the IR group, suggesting that the modest CP-mediated protection is independent of these signaling molecules that converge on (HKII) or emanate (Cyto-c) from mitochondria. Together, these experiments show hypothermia as preserving mitochondria integrity and function, in part, by conserving HKII-binding to mitochondria and by reducing apoptotic signaling, culminating in the full recovery of cardiac function after acute IR.
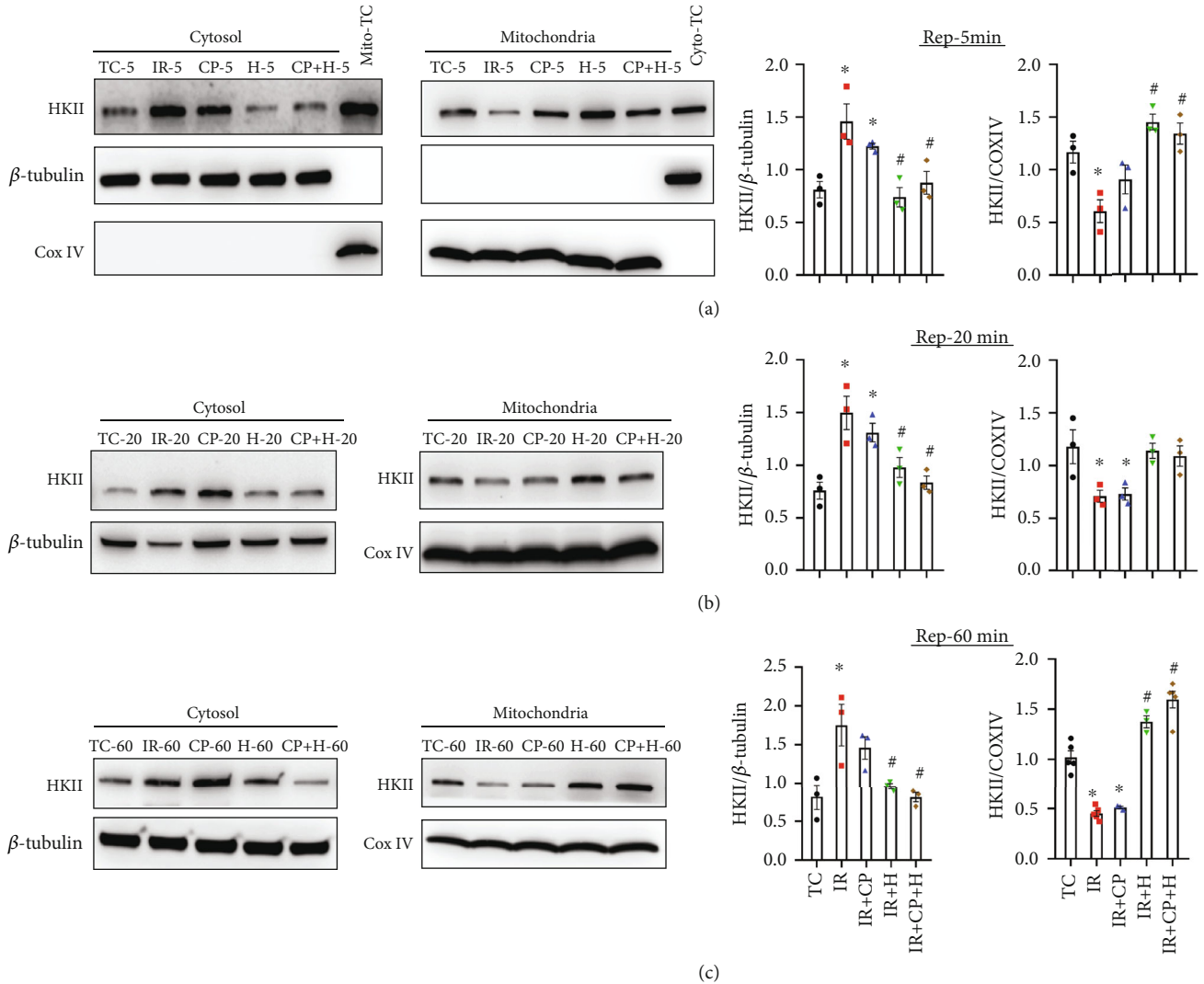
FIGURE 5: Western blot analysis of hexokinase II at 5, 20, and 60 min reperfusion periods in time control (TC), ischemia reperfusion (IR), cardioplegia (CP), hypothermia (H), and cardioplegia + hypothermia (CP + H) groups. N = mitochondria from 3 to 4 hearts in each group. Values are mean ± SE. $^*p < 0.05$ compared to TC group; $^{\#}p < 0.05$ compared to IR group.

4. Discussion

Hypothermia with and without CP has been widely used in animal models of IR and in clinical procedures to provide cardioprotection [3, 6, 37]. We have previously reported that hypothermia and CP preserve cardiac function and protect against tissue infarction [10–13, 38, 39]. However, there remains a lack of knowledge on time-dependent changes in mitochondrial functions controlled by signaling molecules during the early and later reperfusion periods in acute IR injury. In the present study, our goal was to determine how hypothermia and CP modulate signaling molecules to protect the myocardium during increasing post-ischemic times of reperfusion and to unravel the role of signaling mechanisms that converge at the mitochondria in providing protection.

Our findings are that (a) acute IR injury is independent of Bax because there was no difference in Bax translocation in the IR group compared to the treatment groups; (b) the modest CP-mediated cardioprotection against acute cardiac

IR injury is independent of HKII binding to mitochondria; (c) the robust H- and HCP-mediated cardioprotection are mediated, at least in part, by promoting HKII, a pro-survival signaling molecule, binding to mitochondria, likely, via increased pAkt, an upstream signaling molecule; (d) release of the proapoptotic protein Cyto-c, which was first observed after 20 min reperfusion and persisted during later reperfusion, was blunted by H and HCP, but not by CP; (e) H, CP, and HCP treatments improved mitochondrial respiration and $\Delta\Psi_m$, but only H and HCP better maintained the capacity of mitochondria to take up and retain Ca^{2+} during pulse application of exogenous $CaCl_2$; and (f) NADH was more reduced during ischemia by H and HCP. This latter effect may reflect less damage to complex I of the ETC as suggested using modulators of complex I [7, 18, 40]. Overall, our study demonstrates that molecular mechanisms that converge on mitochondria underlie hypothermia-mediated cardioprotection, whereas CP-induced protection appears to be less dependent on mitochondria because it did not
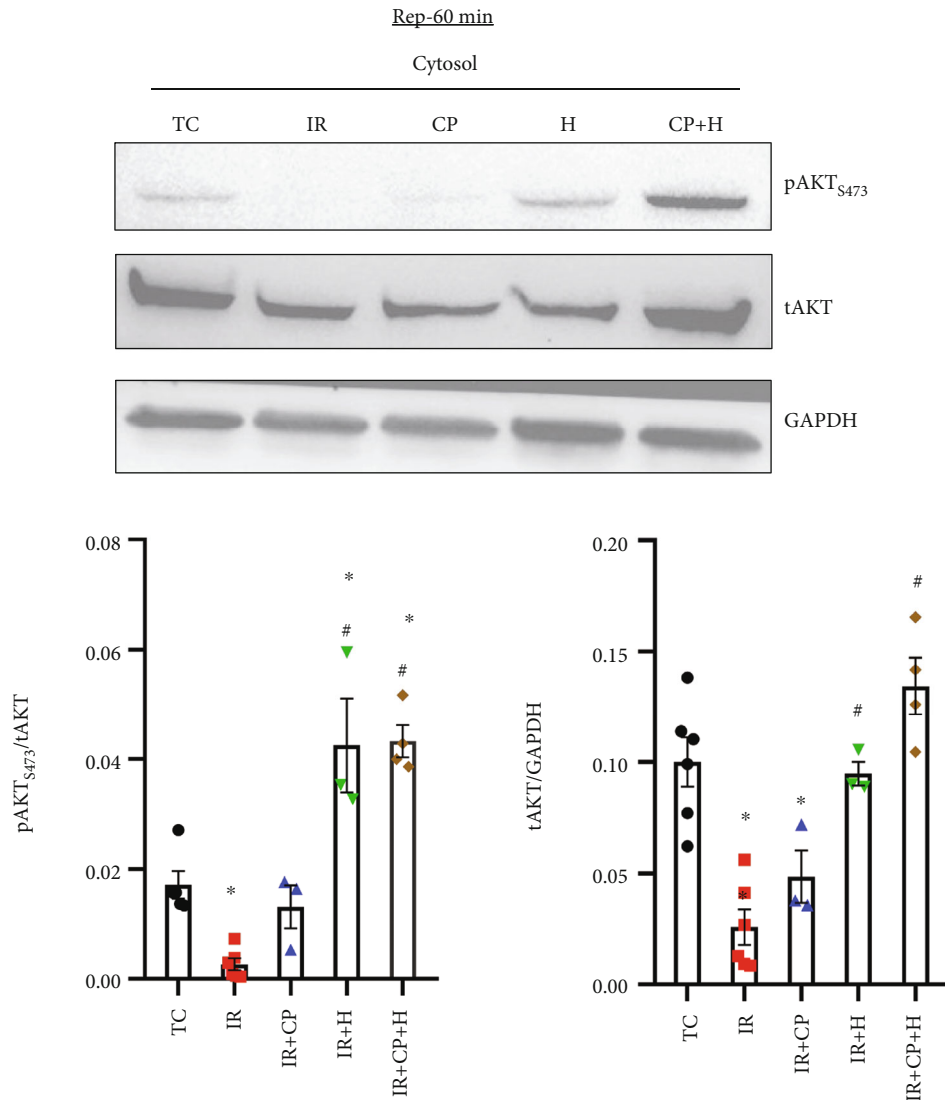
FIGURE 6: Western blot analysis of total Akt (tAkt) and phosphor-Akt at Ser 473 (pAkt) at 60-min reperfusion in time control (TC), ischemia reperfusion (IR), cardioplegia (CP), hypothermia (H), and cardioplegia + hypothermia (CP + H) groups. N = mitochondria from 3 to 5 hearts in each group. Values are mean ± SE. $^{*}p < 0.05$ compared to TC group; $^{#}p < 0.05$ compared to IR group.

prevent Cyto-c release in a HKII-dependent manner. These differences in evoking mitochondrial signaling mechanisms appear to parallel the more effective protection afforded by H and HCP compared to CP alone.

4.1. Hypothermia, Cardioplegia, and Cardioplegia + Hypothermia Differentially Protects the Myocardium from Acute IR Injury. Myocardial reperfusion injury increases as the duration of ischemia increases [5]. Reperfusion injury is a process that causes metabolic alterations like Ca^{2+} overload, lactic acidosis, and reduced ATP synthesis, which lead to activation of signaling pathways and promote mPTP opening to ultimately cause apoptotic and necrotic cell death [1, 3, 15]. Reperfusion is a double-edged sword; on the one hand, it activates endogenous events that salvage viable myocytes, while on the other hand, it exacerbates the ischemic injury, manifested as reperfusion injury.

Hypothermia is a highly effective cytoprotective approach because it can be utilized temporarily and because the reduction in myocardial metabolism is reversible with rewarming. The basic mechanisms underlying hypothermic cardiac protection are the overall reduction in enzymatic activity, most importantly those reactions that require ATP consumption [41]. During cold ischemia, hypothermia protects by attenuating the mitochondrial ATP consuming processes, thus increasing ATP reserve; in this way, on warm reperfusion, mitochondrial respiration becomes less dysfunctional, and ATP becomes more readily regenerated for restoring ionic homeostasis and cardiac contractile and relaxant function. However, prolonged hypothermia, per se, can induce ROS production by slowing the activity of antioxidant enzymes, which could lead to impaired functional recovery because of greater ROS emission [12, 41].

A depolarizing, cold CP solution remains the standard-of care for inducing diastolic arrest during extracorporeal
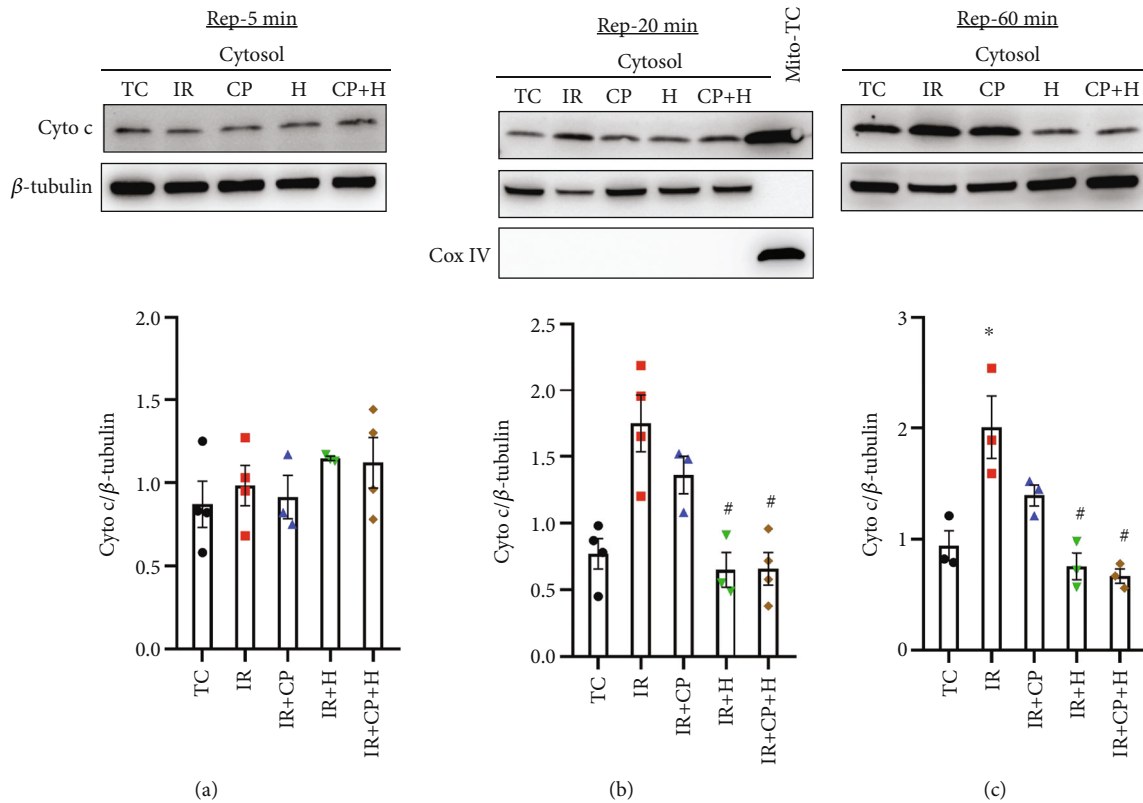
FIGURE 7: Western blot analysis of cytosolic cytochrome c (Cyto-c) release into the cytosol at 5 (a), 20 (b), and 60 (c) min reperfusion periods in time control (TC), ischemia reperfusion (IR), cardioplegia (CP), hypothermia (H), and cardioplegia + hypothermia (CP + H) groups. N = mitochondria from 3 to 4 hearts in each group. Values are mean ± SE. $^*p < 0.05$ compared to TC group; $^\#p < 0.05$ compared to IR group.

heart perfusion to facilitate cardiac surgery [42]. CP is designed to rapidly cease cardiac contractions and so reduce the metabolic rate and decrease O_2 demand [43]. But warm CP itself has little protective effect other than to induce cardiac arrest to facilitate surgical repairs [44]. Moreover, CP can contribute to post-cardioplegic injury by inducing dysrhythmias during reperfusion [45]. Although both CP and H individually have limitations, the combination HCP appears a better approach to mitigate their individual shortcomings [46].

We proposed to determine whether H, CP, and HCP protection involved signaling pathways during earlier and later reperfusion that would underlie improved mitochondrial bioenergetics and provide protection against acute IR injury. As expected, normothermic acute IR injury led to a predictable decrease in cardiac function during reperfusion (Figure 2 and Supplementary Figure S1) with no further improvement after the initial 5 min of reperfusion. This observation bolsters our previous findings that early events at reperfusion, e.g., cytosolic and mitochondrial Ca^{2+} overload, are critical determinants of cardiac functional recovery during later reperfusion. The protection by H and HCP support this notion because these interventions given for only 5 min before and for 2 min immediately after reperfusion (Figure 1) largely enhanced protective mediators or suppressed deleterious factors that improved

or compromised cardiac function, respectively, on reperfusion. We observed that the increase in diastolic contracture, which correlates with cytosolic and mitochondrial Ca^{2+} dysregulation [7, 9, 11, 12], possibly due to diminished mitochondrial ATP production, begins during ischemia and continues throughout reperfusion. In the IR group, diastolic contracture was markedly enhanced during later ischemia and during the entire reperfusion period; in the CP group, the diastolic contracture was significantly reduced when compared to the IR group, but remained higher than the TC group. This suggests that CP when compared to the IR group promoted a greater supply and utilization of ATP to restore cellular ionic homeostasis.

In contrast, H and HCP treatments completely prevented the diastolic contractures seen during ischemia and reperfusion to levels not significantly different from the TC group. The decrease in diastolic contracture likely reflects even better restoration of ATP production and better phasic Ca^{2+} handling in the H and HCP groups vs. the CP group. The lack of diastolic contracture was associated with marked improvements in cardiac contraction and relaxation that was equivalent to that found in the TCs (Figure 2 and Supplementary Figure S1; Table 1 and Supplementary Table S1). In our previous studies with acute ischemia and longer reperfusion time, we reported that CP and H provided varying degree of protection [11, 13]. In a cold,

2 h ischemia model, we found that HCP was more effective than H alone [10]. This is because hypothermia, even at increasingly lower temperatures, does not provide complete protection as the time of ischemia is extended [13]. For our current study, we then investigated several molecular mechanisms that might underlie the differences in H and CP protection following acute ischemia followed by various reperfusion times at 5, 20, and 60 min.

4.2. Hypothermia Best Maintains Mitochondrial Bioenergetics and Ca^{2+} Retention Capacity (CRC) during Reperfusion. Mitochondrial dysfunction in acute IR injury is a critical determinant of cell death because mitochondria are crucial regulators of cell life and death [8]. Mitochondria generate most of the ATP in cardiomyocytes to maintain cellular and mitochondrial ionic homeostasis. In cardiomyocytes, mitochondria produce the reducing equivalents NADH and $FADH_2$ in the TCA cycle, required for oxidative phosphorylation. NADH and $FADH_2$ are oxidized by complex I and complex II enzymes, respectively. Because the redox state (NADH/FAD) is dependent on the transfer of electrons (oxidation), monitoring NADH (reduced) and FAD (oxidized) online in the ex vivo perfused heart is a useful method to assess the state of mitochondrial redox state before, during, and after ischemia.

During ischemia, due to the decrease in O_2 delivery, an increase in NADH and a corresponding decrease in FAD represent a more reduced mitochondrial redox state [9]. In this study, the increase in NADH during ischemia (Table 2) is consistent with our previous observations [10, 13]. Our results here demonstrate that at the end of ischemia (25 min), H and HCP treatments increased NADH more than did the CP treatment or IR alone, but there was no significant change in FAD; this likely indicates that complex II was less impacted than complex I during the acute ischemia. These observations also suggest that H and HCP preserve mitochondrial function in part by protecting complex I, which would be energetically beneficial for the myocardium on reperfusion. Therefore, the decline in NADH during ischemia in the IR group compared to the H and HCP groups could be attributed to damage to complex I [7, 18, 40].

This notion is consistent with our previous findings [18] in which we reported that acute, warm IR led to a decrease in complex I activity, in part, because of oxidative damage to cardiolipin, a major inner mitochondrial membrane (IMM). This damage impairs mitochondria ability to maintain $\Delta\Psi_m$ and to provide a sustained energy supply on reperfusion [18]. By maintaining a robust redox state during ischemia, H and HCP preserved ETC function, which is necessary for ATP production, to maintain cellular ionic homeostasis during reperfusion, and so to abrogate diastolic contracture (Figure 2). Our mitochondrial functional results are consistent with an in vivo report showing that hypothermia attenuates oxidative stress by protecting the respiratory enzymes in a pig cardiac arrest model [47].

To further verify the observed improvement in bioenergetics at the intact organ level by H and HCP after IR, we isolated mitochondria at 5 and 20 min reperfusion times and monitored the rate of O_2 consumption, RCI and $\Delta\Psi_m$.

We focused on these reperfusion times because our previous studies showed that the most deleterious consequences of IR (cytosolic and mitochondrial Ca^{2+} overload and mitochondrial ROS production) are greatest during early reperfusion [7, 9, 11]. The mitochondrial suspension was energized with complex I or complex II substrates. Unlike IR alone, H, CP, and HCP treatments maintained states 3 and 4 respiration and restored RCI near to that of the TC group at 5 and 20 min reperfusion. These results confirm that H and HCP directly modulate bioenergetics to preserve mitochondrial function very early in reperfusion (Figure 2 and Supplementary Figure S1). The improved RCI by H and HCP corresponds to the improved repolarization of $\Delta\Psi_m$ (fast state 3 respiration), which suggests a more coupled oxidative phosphorylation. Interestingly, CP also improved RCI and $\Delta\Psi_m$ repolarization in isolated mitochondria; however, unlike H and HCP, the protection did not contribute to a significant improvement in cardiac function. This suggests that the modest CP-mediated cardioprotection is dependent on more than just restoration of mitochondrial function.

Mitochondrial Ca^{2+} is vital to the regulation of mitochondrial bioenergetics; but in excess, it is a key instigator of cell death. One of the driving forces for mitochondrial Ca^{2+} uptake is a fully charged $\Delta\Psi_m$. During acute IR, hypothermia reduces mitochondrial Ca^{2+} overload and improves bioenergetics [13]. Ca^{2+} uptake, along with decreased Ca^{2+} egress, during IR tends to depolarize $\Delta\Psi_m$ by diminishing the charge gradient and limiting matrix Ca^{2+} sequestration. Unlike hypothermia, we reported that CP-mediated cardioprotection during acute ischemia did not limit mitochondrial Ca^{2+} overload [11], possibly making mitochondria more susceptible to mPTP opening compared to hearts treated with H or HCP. The monitoring of CRC, an in vitro surrogate for assessing mitochondrial Ca^{2+} handling, was used to determine the susceptibility of mitochondria to mPTP opening following acute IR stress, as previously reported [48]. We found that in cardiac mitochondria isolated after reperfusion, IR + H and IR + HCP treatment allowed for a more robust uptake and sequestration of Ca^{2+} after adding exogenous $CaCl_2$ boluses than did IR and IR + CP (Figure 4). These isolated mitochondrial studies indicate that hypothermia is more protective in preserving mitochondrial Ca^{2+} handling and thereby lowering matrix free Ca^{2+} overload during IR stress, as we have reported in the ex vivo perfused heart [11, 13].

Interestingly, all treatments showed a similar CRC with the complex II substrate succinate, again confirming that impaired complex I during IR contributes in part to the impaired mitochondrial bioenergetics ($\Delta\Psi_m$) and increases the susceptibility to $\Delta\Psi_m$ dissipation during exogenous $CaCl_2$ pulse challenges. Under physiological conditions, it is the NADH derived from pyruvate (complex I) oxidation that establishes most of the proton motive force. This is because unlike complex I, complex II does not pump protons with the electron transfer. Therefore, our results suggest that H and HCP preserve complex I function, maintain a polarized $\Delta\Psi_m$, enhance tolerance to excess Ca^{2+}, and improve mitochondrial respiration during reperfusion. Thus, enhanced capacity of mitochondria to take up and

sequester the excess Ca^{2+} accounts, at least partially, for the improved function in the H and HCP groups.

4.3. Hypothermia Promotes HKII Binding to Mitochondria and Protects Against Acute Ischemia and Reperfusion Injury.

As mentioned above, a profound decrease in cellular metabolism is an important way by which H and CP protect the cell from IR stress. However, the molecular mechanisms and timing by which hypothermia and CP provide protection are not well established. As mediators of the first enzymatic step in glucose metabolism, hexokinases (HKs) orchestrate a variety of metabolic events and modulate cell death processes by directly interacting with mitochondria [6, 49–54], in part, via the voltage dependent anion channel 1 (VDAC), a putative regulatory component of the mPTP [6, 55]. HKII, a cardiac isoform of HK, binds to mitochondria with high affinity at the OMM "contact site" where it interacts with VDAC1. HKII bound to mitochondria is antiapoptotic [54], and a decrease in HKII binding to mitochondria makes cells sensitive to apoptotic stimuli [49]. HKII binding to heart mitochondria has also been implicated in resistance to reperfusion injury by inhibiting or desensitizing mitochondria to early mPTP opening [37]. HKII dissociation from heart mitochondria during ischemia, and the extent of this dissociation, correlates with the infarct size on reperfusion [56]. Thus, we investigated whether acute IR injury leads to decreased HKII binding to mitochondria and if H, CP, or HCP modulates this binding to mitigate cardiac dysfunction following acute IR injury.

Our previous study demonstrated that HKII dissociation from mitochondria worsened IR injury and that interventions that maintain its binding to mitochondria improved cardiac function on reperfusion [26]. HKII binding to mitochondria has also been shown to improve apposition at contact sites between the IMM and outer mitochondrial membrane (OMM) and to maintain the cristae structure [52]. In support of the notion of improved contact between IMM and OMM, we reported recently that HKII binding to mitochondria increased the interaction between VDAC1 in the OMM and adenine nucleotide translocator (ANT) in the IMM [26]. Stabilization of the contact site has been reported to reduce OMM permeabilization and to improve the transfer of ADP/ATP and metabolites across the membranes, which is critical for mitochondrial homeostasis and function [53].

In the current study, we showed that H and HCP treatments maintained HKII binding to mitochondria at 5min reperfusion and that the binding persisted for up to 60-min reperfusion. The early translocation of HKII to mitochondria, or its lack of dissociation during hypothermia, suggests that HKII binding could impede the destabilization of mitochondrial membranes and Cyto-c release and protect against vulnerability to cell death [35, 37, 52, 57]. It is also possible that the sustained HKII binding maintains the contact sites between OMM and IMM to enhance bioenergetic activity [26]. Increased HKII binding to mitochondria by H and HCP facilitates glucose entry into the glycolytic process [52], thereby increasing pyruvate production and oxidative phosphorylation. With improved bioenergetics

(i.e., reduced redox state, improved RCI, and normalized $\Delta\Psi_m$), the increased ATP production in the H and HCP groups leads to better ionic homeostasis and abrogation of diastolic contracture. Overall, promoting the association of HK with mitochondria, as in hypothermia, tends to protect mitochondria against IR injury, while preventing association of HK to mitochondria leads to greater IR injury and cell death [35].

The CP treatment did not reverse the effect of IR-induced dissociation of HKII from mitochondria; we posit that this could impede glycolysis, concomitantly affecting bioenergetics, and contribute only modest protection against the diastolic contracture and contractile effort (e.g., RPP) compared to H and HCP treatment (Figure 2 and Supplementary Figure S1; Table 1). This suggests that, at least in our model, CP does not offer as adequate a protection during IR as does hypothermia because CP did not maintain binding of HKII to mitochondria that would lead to a robust protection.

4.4. Hypothermia Increases Cytosolic pAkt Levels during Reperfusion.

Akt is a pro-survival kinase that mediates mitochondrial protection, and its phosphorylation (pAkt) results in its activation and rapid translocation to cellular compartments where it phosphorylates pro- (inactivates) or anti-apoptotic (activates) proteins, like HKII [6, 37]. Indeed, cells that are devoid of the gene for Akt are impaired in their ability to bind HKII to mitochondria [53]. Increased association of HKII with mitochondria as mediated by Akt has been implicated in conferring cardioprotection [50, 54]. The Akt pathway is reported to be involved in protection by hypothermia against cardiac arrest and hemorrhagic shock [16, 58].

The role and interaction of pAkt-HKII during hypothermia in mediating protection during IR has not been well explored. Since HKII is a substrate for Akt and H and HCP increased HKII binding to mitochondria during reperfusion, we sought to know whether total Akt and active Akt, i.e., pAkt expression, are associated with the increase in HKII bound to mitochondria. We found that IR injury caused marked decreases in the levels of total Akt and pAkt proteins, potentially contributing to the decline in Akt-HKII signaling. Reperfusion with H and HCP treatment prevented IR-induced Akt loss and resulted in an overall increase in pAkt, which was associated with an increase in HKII binding to mitochondria. In the IR group, and to a lesser extent the CP group, the compromised RCI, poor CRC, and impaired recovery of cardiac function could be attributed, in part, to the decrease in tAKT and pAkt levels, as they are signaling molecules upstream of HKII.

4.5. Bax Binding to Mitochondria Is Unaltered by Hypothermia and Cardioplegia during Acute Ischemia and Reperfusion Injury.

The translocation of the proapoptotic protein Bax to mitochondria, which leads to its oligomerization during cardiac stress, including IR, contributes to cell damage via OMM permeabilization [59]. HKII bound to mitochondria prevents Bax translocation and confers protection against OMM permeabilization [59]. Unexpectedly,
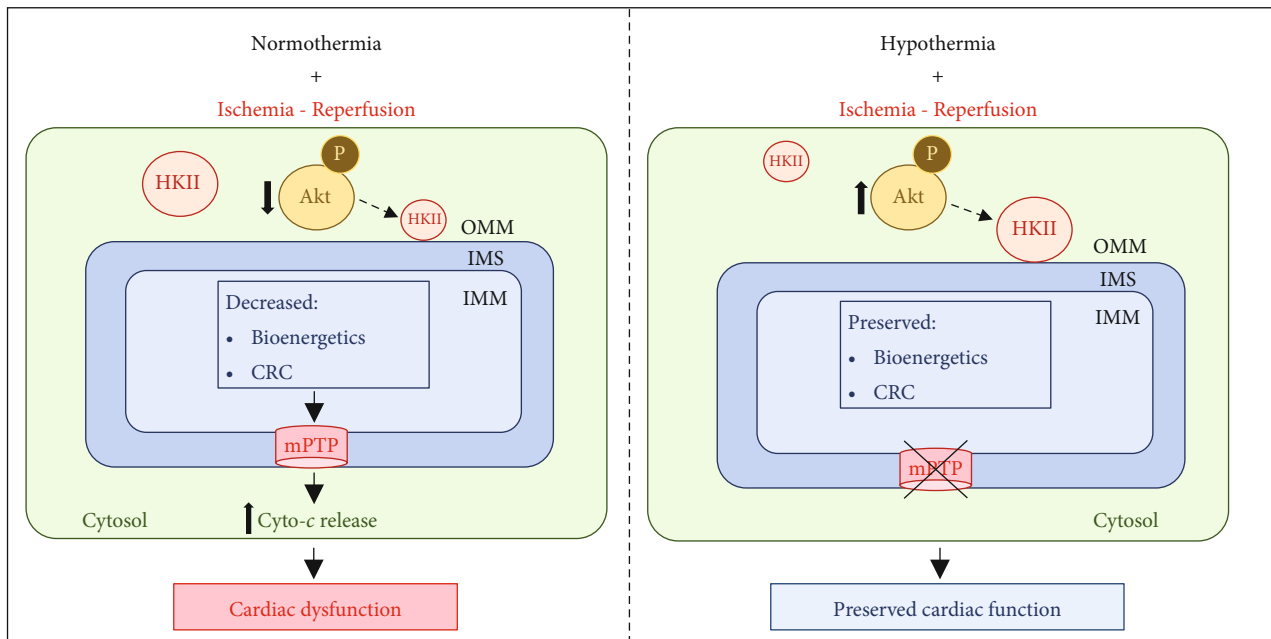
FIGURE 8: A schematic representation of the proposed molecular events associated with hypothermia mediated cardioprotection against ischemia reperfusion (IR) injury. Hypothermia exerts the cardioprotection by maintaining HKII binding to mitochondria through Akt signaling and, subsequently, delays mitochondrial permeability transition pore (mPTP) opening and decrease the cytochrome c (Cyto-c) release to preserve mitochondrial bioenergetics and calcium retention capacity (CRC), and hence contributes to cardiac survival and function improvement. OMM, outer mitochondrial membrane; IMS, intermembrane space; IMM, inner mitochondrial membrane.

the increase binding of HKII to mitochondria by H and HCP did not preclude Bax binding to mitochondria after the acute IR. Bax has been shown to be essential for OMM permeabilization [60] independent of mPTP opening. A plausible mechanism for this permeabilization is the binding of Bax to mitochondria during oxidative stress and/or Ca^{2+} overload [37, 61]. Bax can permeabilize the OMM, in part, by homo-oligomerization or hetero-oligomerization with VDAC1 or other proapoptotic proteins [6, 8, 37], which could lead to Cyto-c release to the cytosol and the trigger of cell death. In our study, we observed similar Bax binding to mitochondria on reperfusion in all treatment groups (Supplementary Figure S4) regardless of Cyto-c release (Figure 7). This indicates that in our model of acute IR injury, Cyto-c release in the IR alone and IR + CP group was not mediated via Bax permeabilization of the OMM. After H and HCP treatment, the total abrogation of Cyto-c release and the full recovery of mitochondrial bioenergetics and cardiac function (Figures 2, 3, and 4) ascertain that Bax binding to mitochondria had no effect in our acute IR model. This observation is consistent with a recent study, in which Lahnwong et al. [62] reported that Bax levels following an acute IR in rats were not significantly different between the treatment groups and the IR group. Moreover, we reported recently [57] that oxidative stress-induced cell death, due to exposure to rotenone, a complex I inhibitor, in VDAC1$^{-/-}$ H9c2 cells vs. WT H9c2 cells, was not mediated via a Bax signaling pathway. Yenari et al. [63] reported similarly that mild hypothermia did not alter Bax expression and translocation to mitochondria in protecting the brain from ischemic injury.

Taken together, these observations suggest that Bax translocation to mitochondria may not be a requisite for OMM permeabilization in our acute IR model or that it may require association with other proapoptotic proteins/activators (e.g., Bak and tBid) to induce OMM permeabilization [53, 64]. It is plausible that in our acute IR model, these activator proteins were not recruited to mitochondria to engender Bax-mediated OMM permeabilization. Consistent with this idea, it was suggested that Bax is not necessary for OMM permeabilization and that other mechanisms may be involved [53].

We further postulate that Cyto-c release in the IR and CP groups independent of Bax could be attributed to mPTP opening or destabilization of mitochondrial membranes [64], which could be due to oxidative stress and or Ca^{2+} overload, as we reported previously [7, 11–13, 25, 32, 33]. Thus, H and HCP-induced increase in HKII binding to mitochondria may prevent mPTP opening or stabilize the OMM/IMM contact sites. In this way, apoptosis is attenuated because of more normalized $\Delta\Psi_{m}$, better Ca^{2+} handling, a more tightly coupled RCI, and overall, a more efficient mitochondrial function.

4.6. Hypothermia Blunts Cytochrome c Release from Mitochondria during Reperfusion after Ischemia. Cyto-c is a labile protein in the mitochondrial intermembrane space. It is critical in the shuttle of electrons in the ETC, and it is also a key scavenger of mitochondrial ROS [19, 37]. In a previous study, we reported that Cyto-c release following acute IR was time dependent, with the greatest release into the cytosol at 60 min reperfusion [7]. These results are congruent with

our current observations, which show more Cyto-*c* release in the IR group at 20 and 60 min reperfusion (Figure 7). As discussed above, Cyto-*c* release has been associated with increased permeabilization of the OMM. This could be by translocation of proapoptotic proteins (Bax/Bak), VDAC homo-oligomerization, or mPTP opening [37, 55]. Furthermore, undocking of HKII from mitochondria leads to Cyto-*c* release [51] consistent with our results. Cyto-*c* release into the cytosol could contribute to mitochondrial dysfunction that triggers apoptosis and cell death and poor cardiac function during reperfusion.

We monitored Cyto-*c* levels in the cytosol to determine if CP- or H-mediated protection is caused by inhibiting or reducing mitochondrial Cyto-*c* release in a time dependent manner on reperfusion. H and HCP blocked Cyto-*c* release and preserved mitochondrial membrane integrity and bioenergetics and led to improved cardiac function on reperfusion. The blocking of Cyto-*c* release was preceded by enhanced HKII binding to mitochondria in H and HCP groups. Overall, these biochemical and metabolic changes that occurred within the first few minutes of reperfusion were determinants of mitochondrial and cardiac functional outcomes throughout the reperfusion period.

5. Conclusions

Hypothermia (H), and to a lesser extent cardioplegia (CP), has been shown to be cardioprotective against IR injury. Our study offers some new mechanistic insights for this by demonstrating the following: (a) H affords better protection of the heart than CP by preserving mitochondrial functional integrity via signaling pathways that converge on mitochondria; (b) H-induced protection is associated with preservation of Akt and increased levels of activated cytosolic pAkt and its substrate HKII binding to mitochondria; (c) the modest cardioprotection afforded by CP is not mediated by the pAkt-HKII signaling pathway; (d) in this acute IR model, HCP mediated protection is not distinct from hypothermia alone, which suggests that the mechanisms examined are similar and hypothermia-mediated protection with or without CP was mostly targeted to mitochondria; (e) the acute IR injury model is independent of Bax binding to mitochondria; (f) H, but not CP, attenuates/inhibits Cyto-c release and thereby preserves $\Delta\Psi_m$ and mitochondrial capacity to sequester Ca^{2+} after $CaCl_2$ pulse challenges. Collectively, activating the Akt-HKII pathway on reperfusion and the convergence of this signaling mechanism on mitochondria may be, at least in part, an underlying factor that makes hypothermia more efficacious in protecting the heart against the acute IR injury. This protection maintains the integrity of mitochondria by preserving complex I and Cyto-*c*, independent of Bax binding to mitochondria. In closing, this study shows that the robust protection against acute IR injury by hypothermia is mediated, in part, via mitochondria specific events, including Akt-HKII signaling and, concomitantly, decreased Cyto-*c* release from mitochondria into cytosol (Figure 8). In contrast, the modest protection by CP was less mitochondria-targeted and did not involve the Akt-HKII protective signaling and the blunting of mito-

chondrial Cyto-*c* release. Thus, cardioprotective therapeutic interventions aimed mainly at mitochondria could portend a better protection against myocardial ischemic injury.

Data Availability

All data supporting the conclusions of this study are provided in the article.

Ethical Approval

This study was conducted according to the guidelines of the Declaration of Helsinki and was approved by the Institutional Animal Care Committee of the Medical College of Wisconsin, certificate AUA00005236; July 6, 2017.

Conflicts of Interest

The authors declare no conflict of interest.

Authors' Contributions

Conceptualization was completed by AKSC and WMK. Methodology was completed by JS, JM, and MY. Validation was completed by JS, JM, MY, DFS, WMK, and AKSC. Formal analysis was completed by JS, JM, MY, and JSH. Investigation was completed by JS, JM, and JSH. Resources was provided by WMK and AKSC. Data curation was completed by JS, JM, and JSH. Writing-original draft preparation was completed by JS and JA. Writing-review and editing were made by JM, AKSC, DFS, and WMK. Supervision was completed by JA and AKSC. Project administration was completed by JA, AKSC, and WMK. Funding acquisition was assigned to WMK and AKSC. All authors have read and agreed to the published version of the manuscript.

Acknowledgments

Supplementary Materials

Supplementary 1. Supplementary Table 1. Baseline and posttreatment parameters of $d\mathrm{P}/dt_{max}$ and $d\mathrm{P}/dt_{min}$ at 5 and 20 min reperfusion in time control (TC), ischemia reperfusion (IR), cardioplegia (CP), hypothermia (H), and hypothermia + cardioplegia (CP + H) groups. Values are mean ± SE. $^*p < 0.05$ compared to TC group; $^\#p < 0.05$ compared to IR group; $^\$p < 0.05$ compared to IR + CP group.

Supplementary 2. Supplementary Figure S1. Coronary flow (CF), diastolic LVP (DiaLVP), developed LVP (dLVP), and rate pressure product (RPP) at 5 (a, b, c, and d) and 20 (e, f, g, and h) min reperfusion in time control (TC), ischemia reperfusion (IR), cardioplegia (CP), hypothermia (H), and cardioplegia + hypothermia (CP + H) groups. Values are mean ± SE. $^*p < 0.05$ compared to TC group; $^\#p < 0.05$ compared to IR group.

Supplementary 3. Supplementary Figure S2. Representative traces of O_2 consumption rates (insets: average respiratory control index (RCI)) at 5 (a) and 20 (b) min reperfusion periods in time control (TC), ischemia reperfusion (IR), cardioplegia (CP), hypothermia (H), and cardioplegia + hypothermia (CP + H) groups. Change in membrane potential ($\Delta\Psi_m$) (insets: average time (S3 time (sec) for repolarization after ADP-induced depolarization (state 3)) at 5 (c) and 20(d) min reperfusion periods Mitochondria were energized with Na^+-Succinate (complex II substrate). The bar graphs show mean ± SE. $^*p < 0.05$ compared to TC group; $^\#p < 0.05$ compared to IR.

Supplementary 4. Supplementary Figure S3. Representative traces of mitochondrial calcium retention capacity (CRC) at 5 (a) and 20 (b) min reperfusion periods in time control (TC), ischemia reperfusion (IR), cardioplegia (CP), hypothermia (H), and cardioplegia + hypothermia (CP + H) groups. The insets are representative traces at later time points that show in greater details the differences in the kinetics of mitochondrial Ca^{2+} uptake during the $CaCl_2$ pulse challenges until mitochondria stopped taking Ca^{2+}. CCCP, the mitochondrial uncoupler, was given after mitochondria stopped taking the added Ca^{2+} to unload all the Ca^{2+} sequestered during bolus additions. Mitochondria were energized with Na^+-Succinate (complex II substrate).

Supplementary 5. Supplementary Figure S4. Western blot analysis of Bax at 5 (a), 20 (b), and 60 (c) min reperfusion periods in time control (TC), ischemia reperfusion (IR), cardioplegia (CP), hypothermia (H), and cardioplegia + hypothermia (CP + H) groups. N = mitochondria from 3 to 4 hearts in each group. There was no significant difference in Bax level in cytosolic and mitochondrial fractions between the groups at any reperfusion time.

References

[1] C. J. A. Ramachandra, S. Hernandez-Resendiz, G. E. Crespo-Avilan, Y. H. Lin, and D. J. Hausenloy, "Mitochondria in acute myocardial infarction and cardioprotection," *eBioMedicine*, vol. 57, article 102884, 2020.

[2] D. J. Hausenloy and D. M. Yellon, "Myocardial ischemia-reperfusion injury: a neglected therapeutic target," *The Journal of Clinical Investigation*, vol. 123, no. 1, pp. 92–100, 2013.

[3] B. Ibanez, G. Heusch, M. Ovize, and F. Van de Werf, "Evolving therapies for myocardial ischemia/reperfusion injury," *Journal of the American College of Cardiology*, vol. 65, no. 14, pp. 1454–1471, 2015.

[4] T. Kalogeris, C. P. Baines, M. Krenz, and R. J. Korthuis, "Cell biology of ischemia/reperfusion injury," *International Review of Cell and Molecular Biology*, vol. 298, pp. 229–317, 2012.

[5] G. Simonis, R. H. Strasser, and B. Ebner, "Reperfusion injury in acute myocardial infarction," *Critical Care*, vol. 16, no. S2, p. A22, 2012.

[6] A. K. Camara, M. Bienengraeber, and D. F. Stowe, "Mitochondrial approaches to protect against cardiac ischemia and reperfusion injury," *Frontiers in Physiology*, vol. 2, p. 13, 2011.

[7] M. Aldakkak, A. K. Camara, J. S. Heisner, M. Yang, and D. F. Stowe, "Ranolazine reduces Ca^{2+} overload and oxidative stress and improves mitochondrial integrity to protect against ischemia reperfusion injury in isolated hearts," *Pharmacological Research*, vol. 64, no. 4, pp. 381–392, 2011.

[8] S. Javadov, A. V. Kozlov, and A. K. S. Camara, "Mitochondria in health and diseases," *Cell*, vol. 9, no. 5, p. 1177, 2020.

[9] M. Aldakkak, D. F. Stowe, Q. Chen, E. J. Lesnefsky, and A. K. Camara, "Inhibited mitochondrial respiration by amobarbital during cardiac ischaemia improves redox state and reduces matrix Ca^{2+} overload and ROS release," *Cardiovascular Research*, vol. 77, no. 2, pp. 406–415, 2008.

[10] M. Aldakkak, D. F. Stowe, J. S. Heisner, M. L. Riess, and A. K. Camara, "Adding ROS quenchers to cold K+ cardioplegia reduces superoxide emission during 2-hour global cold cardiac ischemia," *Journal of Cardiovascular Pharmacology and Therapeutics*, vol. 17, no. 1, pp. 93–101, 2012.

[11] M. Aldakkak, D. F. Stowe, E. J. Lesnefsky, J. S. Heisner, Q. Chen, and A. K. Camara, "Modulation of mitochondrial bioenergetics in the isolated Guinea pig beating heart by potassium and lidocaine cardioplegia: implications for cardioprotection," *Journal of Cardiovascular Pharmacology*, vol. 54, no. 4, pp. 298–309, 2009.

[12] A. K. Camara, M. Aldakkak, J. S. Heisner et al., "ROS scavenging before 27 degrees C ischemia protects hearts and reduces mitochondrial ROS, Ca^{2+} overload, and changes in redox state," *American Journal of Physiology. Cell Physiology*, vol. 292, no. 6, pp. C2021–C2031, 2007.

[13] M. L. Riess, A. K. Camara, L. G. Kevin, J. An, and D. F. Stowe, "Reduced reactive O_2 species formation and preserved mitochondrial NADH and $[Ca^{2+}]$ levels during short-term 17 degrees C ischemia in intact hearts," *Cardiovascular Research*, vol. 61, no. 3, pp. 580–590, 2004.

[14] C. Drescher, A. Diestel, S. Wollersheim, F. Berger, and K. R. Schmitt, "How does hypothermia protect cardiomyocytes during cardioplegic ischemia?," *European Journal of Cardio-Thoracic Surgery*, vol. 40, no. 2, pp. 352–359, 2011.

[15] I. B. Slimen, T. Najar, A. Ghram, H. Dabbebi, M. Ben Mrad, and M. Abdrabbah, "Reactive oxygen species, heat stress and oxidative-induced mitochondrial damage. A review," *International Journal of Hyperthermia*, vol. 30, no. 7, pp. 513–523, 2014.

[16] D. G. Beiser, K. R. Wojcik, D. Zhao, G. A. Orbelyan, K. J. Hamann, and T. L. Vanden Hoek, "Akt1 genetic deficiency limits hypothermia cardioprotection following murine cardiac arrest," *American Journal of Physiology. Heart and Circulatory Physiology*, vol. 298, no. 6, pp. H1761–H1768, 2010.

[17] M. Yang, A. K. Camara, B. T. Wakim et al., "Tyrosine nitration of voltage-dependent anion channels in cardiac ischemia-reperfusion: reduction by peroxynitrite scavenging," *Biochimica et Biophysica Acta*, vol. 1817, no. 11, pp. 2049–2059, 2012.

[18] A. K. Gadicherla, D. F. Stowe, W. E. Antholine, M. Yang, and A. K. Camara, "Damage to mitochondrial complex I during cardiac ischemia reperfusion injury is reduced indirectly by anti-anginal drug ranolazine," *Biochimica et Biophysica Acta*, vol. 1817, no. 3, pp. 419–429, 2012.

[19] M. Yang, D. F. Stowe, K. B. Udoh, J. S. Heisner, and A. K. Camara, "Reversible blockade of complex I or inhibition of PKCbeta reduces activation and mitochondria translocation of p66Shc to preserve cardiac function after ischemia," *PLoS One*, vol. 9, no. 12, article e113534, 2014.

[20] J. An, Z. J. Bosnjak, and M. T. Jiang, "Myocardial protection by isoflurane preconditioning preserves Ca2+ cycling proteins independent of sarcolemmal and mitochondrial K_{ATP}

channels," *Anesthesia and Analgesia*, vol. 105, no. 5, pp. 1207–1213, 2007, table of contents.

[21] M. Yang, A. K. S. Camara, M. Aldakkak, W. M. Kwok, and D. F. Stowe, "Identity and function of a cardiac mitochondrial small conductance Ca(2+)-activated K(+) channel splice variant," *Biochimica et Biophysica Acta, Bioenergetics*, vol. 1858, no. 6, pp. 442–458, 2017.

[22] S. S. Rhodes, A. K. Camara, J. S. Heisner, M. L. Riess, M. Aldakkak, and D. F. Stowe, "Reduced mitochondrial Ca^{2+} loading and improved functional recovery after ischemia-reperfusion injury in old vs. young guinea pig hearts," *American Journal of Physiology. Heart and Circulatory Physiology*, vol. 302, no. 3, pp. H855–H863, 2012.

[23] M. F. la Cour, S. Mehrvar, J. S. Heisner et al., "Optical metabolic imaging of irradiated rat heart exposed to ischemia-reperfusion injury," *Journal of Biomedical Optics*, vol. 23, no. 1, pp. 1–9, 2018.

[24] K. Ait-Aissa, J. S. Heisner, L. E. Norwood Toro et al., "Telomerase deficiency predisposes to heart failure and ischemia-reperfusion injury," *Frontiers in Cardiovascular Medicine*, vol. 6, p. 31, 2019.

[25] L. G. Kevin, A. K. Camara, M. L. Riess, E. Novalija, and D. F. Stowe, "Ischemic preconditioning alters real-time measure of O_2 radicals in intact hearts with ischemia and reperfusion," *Heart and Circulatory Physiology*, vol. 284, no. 2, pp. H566–H574, 2003.

[26] M. Yang, Y. Xu, J. S. Heisner et al., "Peroxynitrite nitrates adenine nucleotide translocase and voltage-dependent anion channel 1 and alters their interactions and association with hexokinase II in mitochondria," *Mitochondrion*, vol. 46, pp. 380–392, 2019.

[27] J. Mishra, A. J. Davani, G. K. Natarajan, W. M. Kwok, D. F. Stowe, and A. K. S. Camara, "Cyclosporin A increases mitochondrial buffering of calcium: an additional mechanism in delaying mitochondrial permeability transition pore opening," *Cell*, vol. 8, no. 9, p. 1052, 2019.

[28] B. Agarwal, D. F. Stowe, R. K. Dash, Z. J. Bosnjak, and A. K. Camara, "Mitochondrial targets for volatile anesthetics against cardiac ischemia-reperfusion injury," *Frontiers in Physiology*, vol. 5, p. 341, 2014.

[29] C. A. Blomeyer, J. N. Bazil, D. F. Stowe, R. K. Dash, and A. K. Camara, "Mg(2+) differentially regulates two modes of mitochondrial Ca(2+) uptake in isolated cardiac mitochondria: implications for mitochondrial Ca(2+) sequestration," *Journal of Bioenergetics and Biomembranes*, vol. 48, no. 3, pp. 175–188, 2016.

[30] D. F. Stowe, M. Yang, J. S. Heisner, and A. K. S. Camara, "Endogenous and agonist-induced opening of mitochondrial big versus small Ca^{2+}-sensitive K^+ channels on cardiac cell and mitochondrial protection," *Journal of Cardiovascular Pharmacology*, vol. 70, no. 5, pp. 314–328, 2017.

[31] C. A. Blomeyer, J. N. Bazil, D. F. Stowe, R. K. Pradhan, R. K. Dash, and A. K. Camara, "Dynamic buffering of mitochondrial Ca^{2+} during Ca^{2+} uptake and Na^+-induced Ca^{2+} release," *Journal of Bioenergetics and Biomembranes*, vol. 45, no. 3, pp. 189–202, 2013.

[32] D. P. Lindsay, A. K. Camara, D. F. Stowe, R. Lubbe, and M. Aldakkak, "Differential effects of buffer pH on Ca(2+)-induced ROS emission with inhibited mitochondrial complexes I and III," *Frontiers in Physiology*, vol. 6, p. 58, 2015.

[33] M. Aldakkak, D. F. Stowe, R. K. Dash, and A. K. Camara, "Mitochondrial handling of excess Ca^{2+} is substrate-

dependent with implications for reactive oxygen species generation," *Free Radical Biology and Medicine*, vol. 56, pp. 193–203, 2013.

[34] S. Miyamoto, A. N. Murphy, and J. H. Brown, "Akt mediates mitochondrial protection in cardiomyocytes through phosphorylation of mitochondrial hexokinase-II," *Cell Death and Differentiation*, vol. 15, no. 3, pp. 521–529, 2008.

[35] D. J. Roberts, V. P. Tan-Sah, J. M. Smith, and S. Miyamoto, "Akt phosphorylates HK-II at Thr-473 and increases mitochondrial HK-II association to protect cardiomyocytes," *The Journal of Biological Chemistry*, vol. 288, no. 33, pp. 23798–23806, 2013.

[36] J. M. Gall, V. Wong, D. R. Pimental et al., "Hexokinase regulates Bax-mediated mitochondrial membrane injury following ischemic stress," *Kidney International*, vol. 79, no. 11, pp. 1207–1216, 2011.

[37] A. K. Camara, E. J. Lesnefsky, and D. F. Stowe, "Potential therapeutic benefits of strategies directed to mitochondria," *Antioxidants and Redox Signaling*, vol. 13, no. 3, pp. 279–347, 2010.

[38] J. An, A. K. Camara, S. S. Rhodes, M. L. Riess, and D. F. Stowe, "Warm ischemic preconditioning improves mitochondrial redox balance during and after mild hypothermic ischemia in guinea pig isolated hearts," *American Journal of Physiology. Heart and Circulatory Physiology*, vol. 288, no. 6, pp. H2620–H2627, 2005.

[39] Q. Chen, A. K. Camara, J. An, M. L. Riess, E. Novalija, and D. F. Stowe, "Cardiac preconditioning with 4-h, 17 degrees C ischemia reduces [Ca(2+)](i) load and damage in part via K(ATP) channel opening," *American Journal of Physiology. Heart and Circulatory Physiology*, vol. 282, no. 6, pp. H1961–H1969, 2002.

[40] E. J. Lesnefsky, Q. Chen, B. Tandler, and C. L. Hoppel, "Mitochondrial dysfunction and myocardial ischemia-reperfusion: implications for novel therapies," *Annual Review of Pharmacology and Toxicology*, vol. 57, no. 1, pp. 535–565, 2017.

[41] A. K. Camara, M. L. Riess, L. G. Kevin, E. Novalija, and D. F. Stowe, "Hypothermia augments reactive oxygen species detected in the guinea pig isolated perfused heart," *Heart and Circulatory Physiology*, vol. 286, no. 4, pp. H1289–H1299, 2004.

[42] G. P. Dobson, G. Faggian, F. Onorati, and J. Vinten-Johansen, "Hyperkalemic cardioplegia for adult and pediatric surgery: end of an era?," *Frontiers in Physiology*, vol. 4, p. 228, 2013.

[43] H. B. Fallouh, J. C. Kentish, and D. J. Chambers, "Targeting for cardioplegia: arresting agents and their safety," *Current Opinion in Pharmacology*, vol. 9, no. 2, pp. 220–226, 2009.

[44] A. Ghimire, E. S. Bisset, and S. E. Howlett, "Ischemia and reperfusion injury following cardioplegic arrest is attenuated by age and testosterone deficiency in male but not female mice," *Biology of Sex Differences*, vol. 10, no. 1, p. 42, 2019.

[45] K. Kinoshita, A. Mitani, Y. Tsuruhara, Y. Kanegae, and K. Tokunaga, "Analysis of determinants of ventricular fibrillation induced by reperfusion: dissociation between electrical instability and myocardial damage," *The Annals of Thoracic Surgery*, vol. 53, no. 6, pp. 999–1005, 1992.

[46] J. C. Cleveland Jr., D. R. Meldrum, R. T. Rowland, A. Banerjee, and A. H. Harken, "Optimal myocardial preservation: cooling, cardioplegia, and conditioning," *The Annals of Thoracic Surgery*, vol. 61, no. 2, pp. 760–768, 1996.

[47] P. Gong, C. S. Li, R. Hua et al., "Mild hypothermia attenuates mitochondrial oxidative stress by protecting respiratory

enzymes and upregulating MnSOD in a pig model of cardiac arrest," *PLoS One*, vol. 7, no. 4, article e35313, 2012.

[48] R. Harisseh, M. Abrial, P. Chiari, R. Al-Mawla, C. Villedieu, and N. Tessier, "External and reticular Ca²⁺ stores in mPTP opening," *The Journal of Biological Chemistry*, vol. 294, no. 42, pp. 15282–15292, 2019.

[49] D. J. Roberts and S. Miyamoto, "Hexokinase II integrates energy metabolism and cellular protection: Akting on mitochondria and TORCing to autophagy," *Cell Death and Differentiation*, vol. 22, no. 2, p. 364, 2015.

[50] J. G. Pastorino and J. B. Hoek, "Regulation of hexokinase binding to VDAC," *Journal of Bioenergetics and Biomembranes*, vol. 40, no. 3, pp. 171–182, 2008.

[51] R. Nederlof, E. Gurel-Gurevin, O. Eerbeek, C. Xie, G. S. Deijs, and M. Konkel, "Reducing mitochondrial bound hexokinase II mediates transition from non-injurious into injurious ischemia/reperfusion of the intact heart," *Journal of Biochemistry and Physiology*, vol. 73, no. 3, pp. 323–333, 2016.

[52] R. Nederlof, O. Eerbeek, M. W. Hollmann, R. Southworth, and C. J. Zuurbier, "Targeting hexokinase II to mitochondria to modulate energy metabolism and reduce ischaemia-reperfusion injury in heart," *British Journal of Pharmacology*, vol. 171, no. 8, pp. 2067–2079, 2014.

[53] N. Majewski, V. Nogueira, P. Bhaskar et al., "Hexokinase-mitochondria interaction mediated by Akt is required to inhibit apoptosis in the presence or absence of Bax and Bak," *Molecular Cell*, vol. 16, no. 5, pp. 819–830, 2004.

[54] G. Calmettes, B. Ribalet, S. John, P. Korge, P. Ping, and J. N. Weiss, "Hexokinases and cardioprotection," *Journal of Molecular and Cellular Cardiology*, vol. 78, pp. 107–115, 2015.

[55] A. K. S. Camara, Y. Zhou, P. C. Wen, E. Tajkhorshid, and W. M. Kwok, "Mitochondrial VDAC1: a key gatekeeper as potential therapeutic target," *Frontiers in Physiology*, vol. 8, p. 460, 2017.

[56] A. P. Halestrap, G. C. Pereira, and P. Pasdois, "The role of hexokinase in cardioprotection - mechanism and potential for translation," *British Journal of Pharmacology*, vol. 172, no. 8, pp. 2085–2100, 2015.

[57] M. Yang, J. Sun, D. F. Stowe, E. Tajkhorshid, W. M. Kwok, and A. K. S. Camara, "Knockout of VDAC1 in H9c2 cells promotes oxidative stress-induced cell apoptosis through decreased mitochondrial hexokinase II binding and enhanced glycolytic stress," *Cellular Physiology and Biochemistry*, vol. 54, no. 5, pp. 853–874, 2020.

[58] H. Zhao, T. Shimohata, J. Q. Wang et al., "Akt contributes to neuroprotection by hypothermia against cerebral ischemia in rats," *Journal of Neuroscience*, vol. 25, no. 42, pp. 9794–9806, 2005.

[59] V. Shoshan-Barmatz, E. N. Maldonado, and Y. Krelin, "VDAC1 at the crossroads of cell metabolism, apoptosis and cell stress," *Cell Stress*, vol. 1, no. 1, pp. 11–36, 2017.

[60] G. Dewson and R. M. Kluck, "Mechanisms by which Bak and Bax permeabilise mitochondria during apoptosis," *Journal of Cell Science*, vol. 122, no. 16, pp. 2801–2808, 2009.

[61] A. B. Gustafsson and R. A. Gottlieb, "Bcl-2 family members and apoptosis, taken to heart," *American Journal of Physiology. Cell Physiology*, vol. 292, no. 1, pp. C45–C51, 2007.

[62] S. Lahnwong, S. Palee, N. Apaijai et al., "Acute dapagliflozin administration exerts cardioprotective effects in rats with cardiac ischemia/reperfusion injury," *Cardiovascular Diabetology*, vol. 19, no. 1, p. 91, 2020.

[63] M. A. Yenari, S. Iwayama, D. Cheng et al., "Mild hypothermia attenuates cytochrome c release but does not alter Bcl-2 expression or caspase activation after experimental stroke," *Journal of Cerebral Blood Flow and Metabolism*, vol. 22, no. 1, pp. 29–38, 2002.

[64] G. Kroemer, L. Galluzzi, and C. Brenner, "Mitochondrial membrane permeabilization in cell death," *Physiological Reviews*, vol. 87, no. 1, pp. 99–163, 2007.

Research Article

The Preventive Effect of Cardiac Sympathetic Denervation Induced by 6-OHDA on Myocardial Ischemia–Reperfusion Injury: The Changes of lncRNA/circRNAs-miRNA-mRNA Network of the Upper Thoracic Spinal Cord in Rats

Zhixiao Li,[1] Yujuan Li,[1] Zhigang He,[1] Zhen Li,[1] Weiguo Xu [ID],[2] and HongBing Xiang [ID][1]

[1]*Department of Anesthesiology and Pain Medicine, Tongji Hospital of Tongji Medical College, Huazhong University of Science and Technology, Wuhan, 430030 Hubei, China*
[2]*Department of Orthopedics, Tongji Hospital of Tongji Medical College, Huazhong University of Science and Technology, Wuhan 430030, China*

Correspondence should be addressed to Weiguo Xu; 354818938@qq.com and HongBing Xiang; xhbtj2004@163.com

In this study, we investigated whether chemical 6-hydroxydopamine (6-OHDA) stimuli caused cardiac sympathetic denervation (SD), and we analyzed gene expression profiles to determine the changes in the lncRNA/circRNAs-miRNA-mRNA network in the affected spinal cord segments to identify putative target genes and molecular pathways in rats with myocardial ischemia–reperfusion injury (MIRI). Our results showed that cardiac sympathetic denervation induced by 6-OHDA alleviated MIRI. Compared with the ischemia reperfusion (IR, MIRI model) group, there were 148 upregulated and 51 downregulated mRNAs, 165 upregulated and 168 downregulated lncRNAs, 70 upregulated and 52 downregulated circRNAs, and 12 upregulated and 11 downregulated miRNAs in the upper thoracic spinal cord of the SD-IR group. Furthermore, we found that the differential genes related to cellular components were mainly enriched in extracellular and cortical cytoskeleton, and molecular functions were mainly enriched in chemokine activity. Pathway analysis showed that the differentially expressed genes were mainly related to the interaction of cytokines and cytokine receptors, sodium ion reabsorption, cysteine and methionine metabolism, mucoglycan biosynthesis, cGMP-PKG signaling pathway, and MAPK signaling pathway. In conclusion, the lncRNA/circRNAs-miRNA-mRNA networks in the upper thoracic spinal cord play an important role in the preventive effect of cardiac sympathetic denervation induced by 6-OHDA on MIRI, which offers new insights into the pathogenesis of MIRI and provides new targets for MIRI.

1. Introduction

Myocardial ischemia/reperfusion injury (MIRI) accounts for a large proportion of the total incidence of heart diseases, and it seriously affects human quality of life [1–3]. Previous studies have reported the cellular and molecular mechanisms of neural–cardiac interactions [4, 5] during pathological remodeling after MIRI [6]. However, to date, no effective methods have been found to prevent MIRI.

Cardiac nerves, comprising both the sensory nerves and the autonomic nerves, transmit the information from the heart to the spinal cord and brain, which then results in an appropriate sympathetic neural outflow [7]. The role of sympathetic activity in the development of cardiac electrical activity has been well known for decades [8, 9]. Neural regulation is involved in an imbalance between the sympathetic and parasympathetic nervous systems within the ischemic myocardial tissues. Experimental studies have shown that cardiac innervation abnormality is an important cause of the sympathetic nervous system overactivity. Several studies have reported the vital role of the sympathetic nerves in MIRI progression, and sympathetic nerves have been shown

to infiltrate the myocardial microenvironment thereby accelerating cardiac injury [10, 11]. In this study, we examined the preventive effect of cardiac sympathetic denervation induced by 6-OHDA, a catecholamine-specific toxin [12], on MIRI rats.

Myocardial ischemia/reperfusion injury is a complex process, and further understanding of the related biological processes and their regulation is necessary [13, 14]. Several lines of evidence have revealed a close correspondence between the spinal cord and cardiovascular system [15–17]; indeed, the spinal cord and cardiovascular system develop in concert and are functionally interconnected in heart disease. It is an accepted fact that noncoding RNAs (ncRNAs) of the spinal cord are vital components of the regulation and cross-talk among MIRI-related signaling pathways [16]. In recent years, a strong consensus has been reached that ncRNAs, including long noncoding RNAs (lncRNAs) and circular RNAs (circRNAs), play an important role in many cellular processes and occurrence of diseases [18–23]. However, the underlying mechanisms based on the function of lncRNAs, circRNAs, and mRNAs in the spinal cord following MIRI remain unclear. Thus, it is necessary to analyze the lncRNAs and circRNAs comprehensively and explore the role of the lncRNA/circRNAs-miRNA-mRNA network in MIRI.

In this study, we first investigated whether cardiac sympathetic denervation induced by 6-OHDA alleviates MIRI. Next, we performed high-throughput sequencing on the spinal cord tissues for the first time to describe and analyze the expression profiles of ncRNAs, including lncRNA and circRNA. Furthermore, we performed Gene Ontology (GO) and Kyoto Encyclopedia of Genes and Genomes (KEGG) analysis of differentially expressed lncRNAs and circRNAs. We also constructed lncRNA/circRNA-miRNA-mRNA networks to further explore their underlying mechanism and possible relationships in the preventive effect of cardiac sympathetic denervation induced by 6-OHDA on MIRI.

2. Materials and Methods

2.1. Animals.
Adult male Sprague–Dawley rats (weighing 250–300 g) were used, and two animals were placed in each cage. The animals had free access to food and water and were housed in a light- and temperature-controlled room. The experiment started following the approval of the Institutional Animal Care and Use Committee in Tongji Hospital, Huazhong University of Science and Technology (approval No. TJ-A0804).

2.2. Groups and Chemical Sympathetic Denervation.
The rats were randomly assigned to the following two groups: MIRI model (IR) group and sympathetic denervation (SD) + IR (SD-IR) group (n = 9 for each group). In the SD-IR group, intraperitoneal (i.p.) injections of 50 mg/kg 6-hydroxydopamine (6-OHDA, Sigma), containing 0.1% ascorbic acid in the saline solution of 6-OHDA, were administered for 3 consecutive days [1, 24, 25], whereas MIRI rats received i.p. injections of the same volume of saline. One day after the last injection, rats (n = 6 for each group) were

Table 1: Primer sequences for reverse transcriptase-quantitative polymerase chain reaction.

Primer name	Primer sequences (5′ to 3′)
LncRNA	
NONRATT012797.2-F	CTGGGGTGAGAAGGGCTGAC
NONRATT012797.2-R	AAGGTGTTTTCCCGGAGGGC
NONRATT029190.2-F	ACTGGGGTGGCACTTAGAGG
NONRATT029190.2-R	TGTCCACCGTAACATCCCCT
NONRATT000247.2-F	CAGGGCCTTGTGCTTGCTA
NONRATT000247.2-R	ATGTTTTCCCTCCGCTGCTT
NONRATT004098.2-F	ACCTCTTCCCCTCAGCCTACAG
NONRATT004098.2-R	TCACTGCCATGAATCACATTCCA
NONRATT025664.2-F	ATGCCAACCTTACTATACGTTTCC
NONRATT025664.2-R	TGACTCTCCCACCAACTTCAG
mRNA	
Ubd-F	GGTGAAGCCCAGTGATGAAGAGC
Ubd-R	GGGAGGCACAGCAGTCACATTC
Ccl12-F	CTGCTCATAGCTGCCGCCATC
Ccl12-R	GCCTCCGAATGTGGATCTTCTGC
Cxcl10-F	GTTCTCTGCCTCGTGCTGCTG
Cxcl10-R	AACATGCGGACAGGATAGACTTGC
LOC100912599-F	GCAGTTCAAGCAGCAGCATCAC
LOC100912599-R	AACAAGGGACACCATTCACAGAGC
Dpep1-F	CATCGCATGTGCCAGCTCTATCC
Dpep1-R	GCCACCTTCCACGCCAATCAG
GAPDH-F	GACATGCCGCCTGGAGAAAC
GAPDH-R	AGCCCAGGATGCCCTTTAGT

deeply anesthetized, and left ventricular tissues were harvested for further laboratory study, whereas other rats received the establishment of MIRI model.

2.3. Establishment of the MIRI Model.
The MIRI model was modified from a previous study [3, 15, 16, 26, 27]. In brief, after routine disinfection, anesthesia, and tracheal intubation, surgical thoracotomy was conducted. In both groups (n = 9 for each group), the left anterior descending coronary artery (LAD) was ligated 2 mm below the left atrial appendage for 30 minutes and then reperfused for 2 hours. The core temperature was maintained throughout the protocol. The rats were monitored to confirm ischemic ST segment elevation during LAD occlusion by an electrocardiogram. Serum troponin cTnI of the two groups was measured 2 hours after reperfusion as an index of myocardial necrosis. Hearts were harvested for hematoxylin and eosin (H&E) staining and 2,3,5-triphenyl tetrazolium chloride (TTC) staining.

2.4. Determination of Norepinephrine Content.
The norepinephrine (NE) content of myocardial tissue from the left ventricle was measured using a high-performance liquid chromatography (HPLC) method [28–31]. In brief, cardiac tissue of the left ventricle was weighed (about 100 mg) and homogenized in 500 μL of precooled methanol/water (V:V = 2/1). The homogenate mixture was sonicated
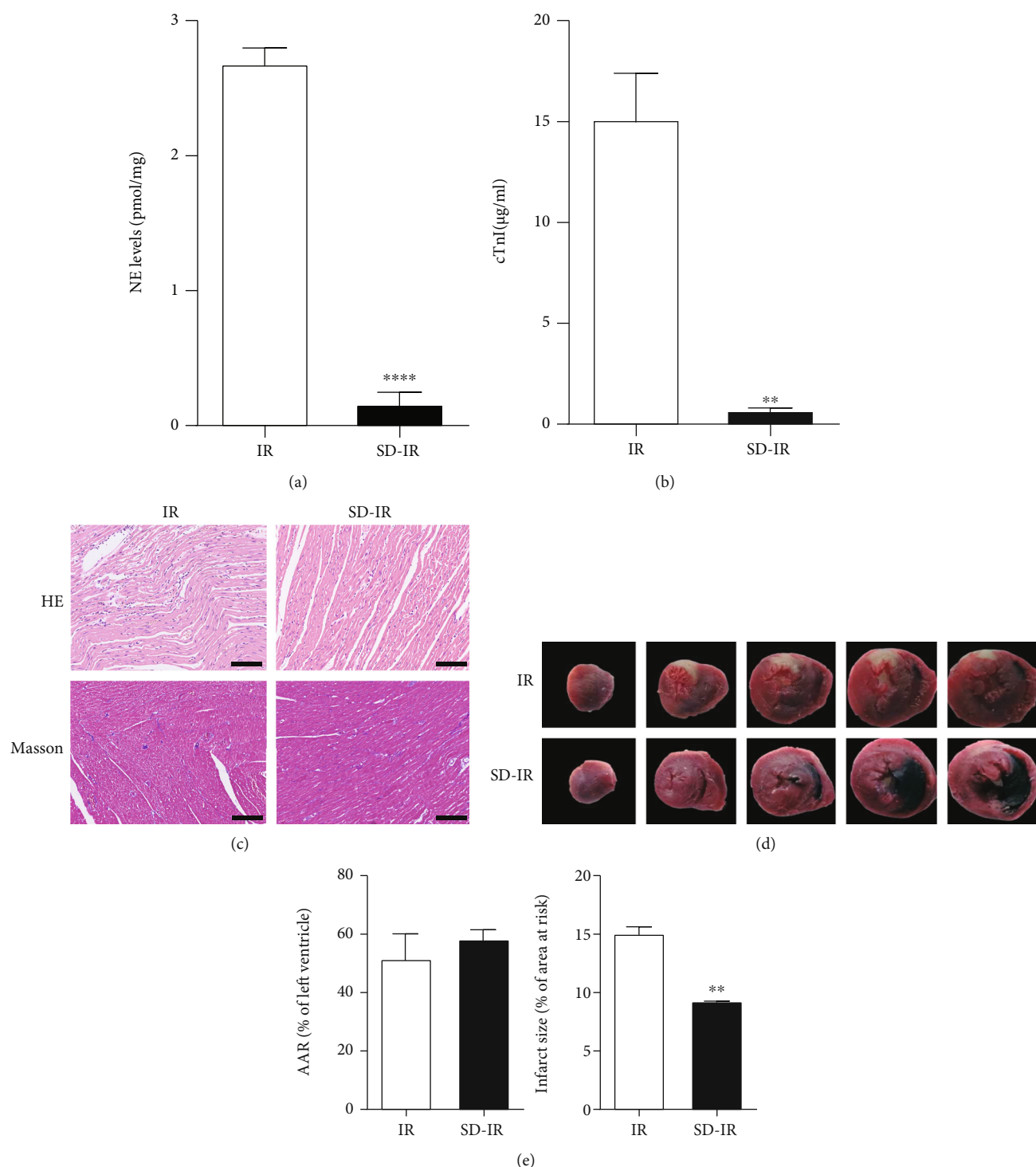
FIGURE 1: Chemical sympathetic denervation attenuates myocardial ischemia–reperfusion injury. (a) Serum NE and (b) serum cTnI concentrations in rats with IR or SD-IR. (c) Representative images of hematoxylin and eosin staining and Masson trichrome staining of rat hearts 24 h after IR injury. Scale bar = 100 μm. (d) Representative photographs of TTC-Evan blue staining in hearts subjected to IR and SD-IR surgery. (e) Quantification of AAR and infarct area vs. AAR in rat hearts in IR group and SD-IR group. Data are expressed as mean ± SEM. $**p < 0.01$, $****p < 0.0001$ vs. IR group. NE: norepinephrine; IR: ischemia reperfusion; AAR: area at risk.

(12000 rpm, 10 minutes, 4°C) and the supernatant was collected, while the remaining pellets were repeatedly treated twice. Three supernatants were combined and dried, and then redissolved in 100 μL formic acid solution (0.1%). Next, the following chemicals were added in turn to the supernatant (10 μL): NEM solution (2.5 mM, 80 μL), tBBT solution (1 M in DMSO, 10 μL), borate buffer (0.2 M, pH 8.8, 700 μL), 5-AIQC solution (200 μL), formic acid (10 μL).

Statistic of differentially expressed RNAs
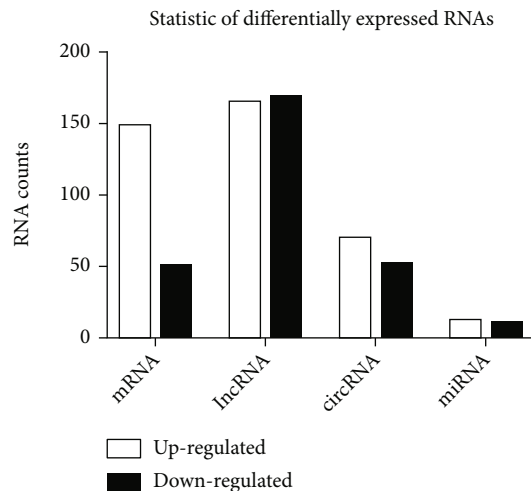
FIGURE 2: Differentially expressed RNAs. Through high-throughput RNA sequencing, we found that 148 mRNAs were upregulated and 51 mRNAs were downregulated; 165 lncRNAs were upregulated and 168 lncRNAs were downregulated; 70 circRNAs were upregulated and 52 circRNAs downregulated; and 12 miRNAs were upregulated and 11 miRNAs were downregulated.

The solution was sonicated (12000 rpm, 10 minutes, 4°C) and the supernatant was filtered by a $0.22\,\mu m$ membrane filter before HPLC analysis. HPLC analyses were conducted on the 1290-6470 UPLC-MS/MS system (Agilent, USA). Data preprocessing was performed using Mass Hunter Workstation software (Agilent, Version B.08.00).

2.5. Myocardial Tissue Staining. Myocardial tissue staining was performed as described previously [15]. In brief, each myocardial tissue sample was cut transversely. Hematoxylin and eosin (H&E) staining was used to observe myocardial pathology. After deparaffinization, 4-μm-thick sections were immersed in hematoxylin (cat. no. H9627; Sigma-Aldrich; Merck KGaA) for 5–7 min at room temperature, differentiated in 1% acid alcohol for 2–5 seconds, and stained with 0.5% eosin (cat. no. 71014544; Sinopharm Chemical Reagent Co., Ltd.) for 2 minutes at room temperature.

After rinsing with distilled water for 30 seconds, the sections were dehydrated with graded alcohols and cleared in xylene. Infarct size was assessed by TTC staining 2 hours after reperfusion. After surgery, the hearts were removed and frozen for 20 minutes at −20°C, and then transversally cut into sections with a thickness of 1–2 mm. The tissue sections were incubated for 10 minutes in 2% TTC in dark conditions at 37°C and then fixed overnight in 10% formaldehyde at 4°C. The infarct area was white, while the normal tissues were red.

Infarct size and area at risk (AAR) in TTC-stained cardiac sections of the left ventricle were determined as previously described [32]. Briefly, Pale regions were regarded as the areas of necrosis (AON). AON and AAR were calculated as the average percent area per slice from both sides of each section. Then, they were normalized to slice weight as follows: weight of total AAR = (weight of slice 1 × % AAR of slice 1) + (weight of slice 2 × % AAR of slice 2) + (weight

of slice 3 × % AAR of slice 3) + (weight of slice 4 × % AAR of slice4) + (weight of slice 5 × % AAR of slice 5). AON weight was calculated in the same manner.

Finally, infarct size was expressed as the percentage of the weight of AON to the weight of AAR [33]. If the AAR was >90%, this animal was excluded.

2.6. RNA Sequencing for lncRNA-circRNA-mRNA. Two hours after reperfusion, the animals were quickly sacrificed to limit their suffering. The upper thoracic (T1–T4) spinal cord segments were immediately cut and frozen with liquid nitrogen and sent to Oebiotech Corporation (Shanghai, China) for RNA sequencing. The extraction of total RNA from T1–T4 spinal tissues was conducted by using the mirVana™ PARIS™ Kit (Ambion-1556, USA) in accordance with the user manual. We assessed total RNA integrity using Agilent Bioanalyzer 2100 (Agilent Technologies). The spinal samples from the two groups were selected for microarray analysis. We used the Affymetrix® GeneChip® Whole Transcript Expression Arrays to analyze lncRNA and mRNA expression profiles, and we applied Agilent circRNA Microarray 8x60K to analyze circRNA expression profiles in the T1–T4 spinal cord segments [34]. Microarray data were obtained and analyzed by Oebiotech Corporation (Shanghai, China). The RNA-sequencing results were used to prioritize the heart-related spinal genes.

2.7. Identifying Differentially Expressed Genes and Gene Ontology (GO) Analysis. The differentially expressed mRNAs, lncRNAs, and circRNAs from the RNA-seq data were identified by using the edgeR algorithm. The mRNAs, lncRNAs, and circRNAs were deemed differentially expressed if they showed a false-discovery rate (FDR) < 5% and fold change (FC) > 2. The molecular functions, cellular components, and biological processes of differentially expressed lncRNAs and circRNAs were described by using GO analysis (http://www.geneontology.org).

2.8. Kyoto Encyclopedia of Genes and Genomes (KEGG) Pathway Analysis. The gene set scores were calculated by using the FAIME algorithm based on the rank-weighted gene expression levels of individual samples (from the T1–T4 segments of the spinal cord), which converts each sample's transcriptomic profile to molecular mechanisms. KEGG analysis was applied to determine the biologic pathway roles of these differentially expressed lncRNAs and circRNAs based on the latest KEGG data (http://www.genome.jp/kegg/). Student's t test was used to identify the differentially expressed KEGG pathways between IR and SD-IR samples. The KEGG pathways with adjusted $p < 0.05$ by Benjamini–Hochberg procedure were considered differentially expressed.

2.9. RT-qPCR Analysis for the Upper Thoracic Spinal Cord. The total RNA extracted from the T1–T4 segments of the spinal cord using the TRIzol® reagent (Invitrogen; Thermo Fisher Scientific, Inc.) in line with the manufacturer's instructions was used for the generation of cDNA. The primers were designed using the Primer Express 3.0 software (Applied Biosystems; Thermo Fisher Scientific,

(a)

Figure 3: Continued.

(b)

Figure 3: Continued.

Type
Antisense_genic_exonic (6.8%)
Antisense_genic_intronic (6.6%)
Antisense_intergenic_downstream (4.8%)
Antisense_intergenic_upstream (7.1%)
Sense_genic_exonic (51.1%)
Sense_genic_intronic (9.8%)
Sense_intergenic_downstream (8.5%)
Sense_intergenic_upstream (5.3%)

(c)

Type
Antisense_genic_exonic (0.7%)
Antisense_genic_intronic (0.2%)
Antisense_intergenic_downstream (0.4%)
Antisense_intergenic_upstream (1.5%)
Sense_genic_exonic (94.4%)
Sense_genic_intronic (1%)
Sense_intergenic_downstream (0.8%)
Sense_intergenic_upstream (1%)

(d)

FIGURE 3: Comparison of the characteristics of lncRNAs, circRNAs, and mRNAs expression profiles in IR group and SD-IR group. (a) The distribution of lncRNAs and circRNAs on chromosomes. (b) LncRNAs and mRNAs on chromosomes. (c, d) Classification of lncRNAs and circRNAs.

Inc.); the specific forward and reverse primer sequences are listed in Table 1. RNA samples were quantified using a spectrophotometer (BioPhotometer; Eppendorf AG) and then synthesized to cDNA by reverse transcription using the PrimeScript™ RT reagent kit (Takara Bio, Inc.). The temperature protocol was conducted using the following protocol: 15 minutes at 37°C, 5 seconds at 85°C, and held at 4°C. cDNA was quantitated via RT-qPCR using a TB green® Premix Ex Taq (cat. no. RR420A; Takara Bio, Inc.). The thermocycling conditions for PCR were as follows: Initial denaturation for 30 seconds at 95°C, followed by 40 cycles of 15 seconds at 95°C, 15 seconds at 60°C, and 45 seconds at 72°C. The threshold cycle (Cq) was used to estimate the amount of target mRNA. The comparative Cq method with a formula for relative FC ($2^{-\Delta\Delta Cq}$) was used to quantify the amplified transcripts. The relative gene expression levels were determined via normalization to GAPDH. Experiments were evaluated in triplicate and repeated ≥3 times.

2.10. Construction of lncRNA/circRNA-miRNA-mRNA Network. The TargetScan (Release 7.2) and Miranda (version 0.10.80) software were used to predict the relationship among lncRNA/circRNA, miRNAs, and mRNAs through base pairing. These predicted results were integrated to build the potential lncRNA/circRNA-miRNA-mRNA network. The Cytoscape software (version 3.7.2) was used to visualize the above data so as to explore the role of lncRNA/circRNA-miRNA-mRNA ceRNA network in the pathogenesis of MIRI after cardiac sympathetic denervation.

2.11. Computational Prediction of Protein–Protein Interaction (PPI) Analysis. The STRING database (ver. 10.5; https://string-db.org/) is an online database tool for searching known or predicted information on PPIs. The minimum PPI interaction score was set at 0.900 (highest confidence), and the wide disconnected node in the network was observed to obtain a complex PPI network of differentially expressed mRNAs. The Cytoscape software (version 3.7.2) was used to visualize the PPI network, and Cytohubba (a plug-in of Cytoscape) was used to identify the most relevant nodes by setting the degree. The PPI analysis was limited to an interaction threshold of 0.4 (medium confidence).

2.12. Statistical Analysis. Data were presented as the mean ± SEM and were analyzed using GraphPad Prism software v5.0 (GraphPad Software, Inc.). Based on Gene Ontology

(a)

(b)

(c)
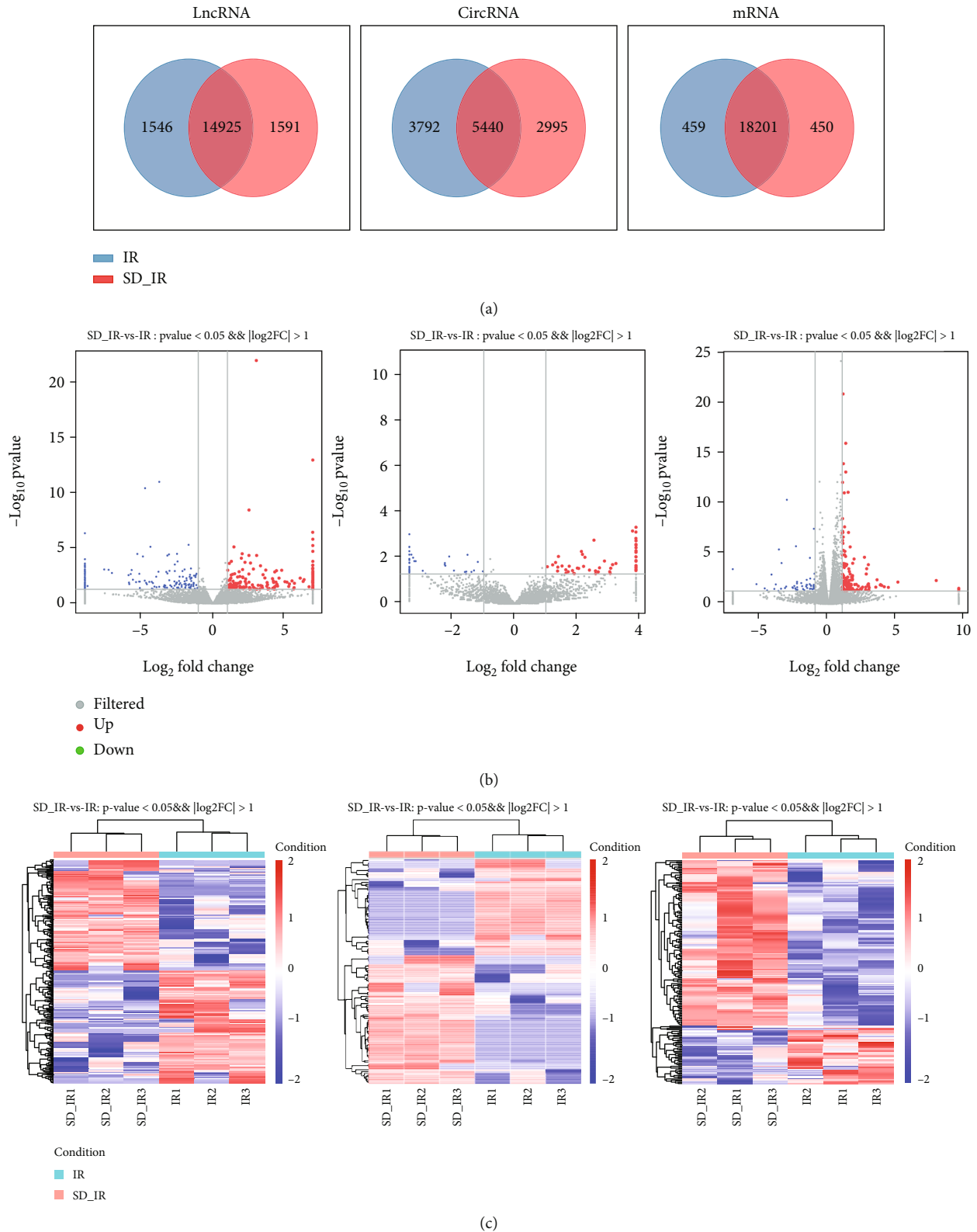
FIGURE 4: Differential expression patterns of lncRNAs, circRNAs, and mRNAs. (a) The specific lncRNAs, circRNAs, and mRNAs shared between IR group and SD-IR group. (b) The volcano plot of lncRNAs, circRNAs, and mRNAs expression. Red color is indicative of upregulated and blue color is indicative of downregulated genes, where $p < 0.05$ and $|FC| > 2$ are considered statistically significant; grey color is indicative of nonsignificantly different genes. (c) The hierarchical heat map shows the deregulated lncRNAs, circRNAs, and mRNAs in the T1–T4 spinal cord segments between IR group and SD-IR group; up- and downregulated genes are colored in red and green, respectively ($p < 0.05$ and $\log_2|FC| > 1$).

TABLE 2: The detail information of the top 30 up-regulated mRNAs in the T1-4 spinal cord between SD-IR group and IR group.

Gene ID	log$_2$FC (SD-IR/IR)	Pvalue	Description
LOC102553010	4.40	0.021887	Leukocyte elastase inhibitor A-like
RGD1359290	4.10	0.019123	Ribosomal_L22 domain containing protein RGD1359290
LOC108348083	3.91	0.014045	Delta-1-pyrroline-5-carboxylate synthase
RGD1305184	3.83	0.011827	Similar to CDNA sequence BC023105
Gns	3.81	0.012511	Glucosamine (N-acetyl)-6-sulfatase
Prf1	3.57	0.003838	Perforin 1
LOC100911034	3.47	0.020641	Cysteine desulfurase, mitochondrial-like
Ubd	2.99	0.024065	Ubiquitin D
Mcpt9	2.96	0.016414	Mast cell protease 9
LOC100910446	2.95	0.039393	Syntaxin-7-like
Sctr	2.94	0.009767	Secretin receptor
Ccl12	2.92	0.000115	Chemokine (C-C motif) ligand 12
Cxcl10	2.89	0.011969	C-X-C motif chemokine ligand 10
Ngp	2.81	0.000296	Neutrophilic granule protein
Rhag	2.78	0.001015	Rh-associated glycoprotein
Cxcl11	2.74	0.020485	C-X-C motif chemokine ligand 11
Car1	2.64	2.06E-05	Carbonic anhydrase I
Padi3	2.50	0.02082	Peptidyl arginine deiminase 3
S100a5	2.43	0.031729	S100 calcium binding protein A5
Unc45b	2.19	0.016491	Unc-45 myosin chaperone B
Cd5l	2.10	0.034827	Cd5 molecule-like
Ermap	2.03	0.010957	Erythroblast membrane-associated protein
Capn13	1.94	0.046362	Calpain 13
Clec5a	1.87	3.08E-05	C-type lectin domain family 5, member A
Gbp1	1.84	0.040079	Guanylate binding protein 1
Hemgn	1.77	8.40E-05	Hemogen
Cxcl13	1.76	0.00143	C-X-C motif chemokine ligand 13
Kel	1.76	0.00334	Kell blood group, metallo-endopeptidase
LOC680322	1.75	0.028182	Similar to histone H2A type 1
Ms4a3	1.75	0.003821	Membrane spanning 4-domains A3

|log 2FC| > 1; p < 0.05 by analysis of variance.

Biological Process (GOBP) definition, Fisher's exact test was applied to determine whether the proportion of differentially expressed genes in a given GOBP gene set was significantly enhanced. RT-qPCR parameters were analyzed using the unpaired t test for repeated measures, with P value less than 0.05 was considered statistically significant.

3. Results

3.1. Chemical Sympathectomy-Induced Cardiac Alterations.
The level of NE in the cardiac tissues of the SD-IR group (n = 6, 0.1650 ± 0.1057 ng/mg) was significantly lower compared with that in the IR group (n = 6, 2.687 ± 0.1349 ng/mg) (Figure 1(a)).

3.2. Characteristics of Myocardial Ischemic Tissue.
In the two groups, we observed the development of ST-segment elevation and QRS complex changes on an electrocardiogram; moreover, there was a cyanotic change in the myocardium

of the occluded area 30 minutes after cardiac ischemia. Serum cardiac troponin cTnI (0.73 ± 0.26 μg/L) in the SD-IR group was significantly lower than that in the IR group (15.14 ± 2.44 μg/L) 2 hours after reperfusion (Figure 1(b)). These results verified the successful occlusion of the LAD.

In the IR group, a structural disorder of the cardiac tissue was observed, with different degrees of vacuolar degeneration and necrosis, as well as loose stroma (Figure 1(c)). Moreover, the number of cardiomyocyte fibers was markedly increased after IR. In the SD-IR group, myocardium showed a better architecture, and the myocardial fibers and myocardial cells were relatively intact and arranged in an orderly manner (Figure 1(c)).

The results from TTC staining clearly exhibited a reduced myocardial infarction—indicated by the pale color region in the transverse section of heart—in the IR group (Figure 1(d)). To ensure that the difference in the infarct size was not caused by different myocardium injuries, we measured the area at risk (AAR) and found no difference

TABLE 3: The detail information of the top 30 down-regulated mRNAs in the T1-4 spinal cord between SD-IR group and IR group.

Gene ID	log$_2$FC (SD-IR/IR)	Pvalue	Description
LOC100912599	-5.31	0.010395	NADH dehydrogenase [ubiquinone] iron-sulfur protein 6, mitochondrial-like
LOC100911994	-3.89	0.01095	Coiled-coil domain-containing protein 132-like
Clcn2	-3.51	0.029527	Chloride channel, voltage-sensitive 2
LOC100910308	-3.47	7.97E-05	Multifunctional protein ADE2-like
LOC100910207	-3.12	0.018014	Protein Dr1-like
Vwa5a	-2.62	0.02532	von Willebrand factor A domain containing 5A
Dpep1	-2.53	0.015698	Dipeptidase 1 (renal)
NEWGENE_1582994	-2.45	0.02675	DCN1, defective in cullin neddylation 1, domain containing 2
LOC103689986	-2.41	1.64E-06	Protein YIF1B
Iqcf3	-2.40	0.036362	IQ motif containing F3
Ahsg	-2.32	0.021173	Alpha-2-HS-glycoprotein
Hpgd	-2.01	0.008083	Hydroxyprostaglandin dehydrogenase 15 (NAD)
RGD1561778	-1.94	0.016898	Similar to dendritic cell-derived immunoglobulin(Ig)-like receptor 1, DIgR1 - mouse
LOC297568	-1.88	0.032025	Alpha-1-inhibitor III
Rlim	-1.78	0.042544	Ring finger protein, LIM domain interacting
Slc39a12	-1.65	0.017633	Solute carrier family 39 member 12
LOC100911865	-1.62	1.20E-02	TBC1 domain family member 12-like
Myo18b	-1.61	0.003815	Myosin XVIIIb
Tspan10	-1.59	0.012324	Tetraspanin 10
Sds	-1.57	0.025502	Serine dehydratase
Trim63	-1.39	0.010581	Tripartite motif containing 63
LOC102550588	-1.38	0.030436	Zinc finger protein 709-like
Sh2d4b	-1.37	2.44E-05	SH2 domain containing 4B
Hif3a	-1.35	0.002856	Hypoxia inducible factor 3, alpha subunit
Galnt15	-1.30	0.01374	Polypeptide N-acetylgalactosaminyltransferase 15
LOC687780	-1.30	0.029663	Similar to Finkel-Biskis-Reilly murine sarcoma virusubiquitously expressed
Trpv4	-1.29	0.015774	Transient receptor potential cation channel, subfamily V, member 4
Mt1	-1.18	0.033903	Metallothionein 1
Fbxw10	-1.11	0.016073	F-box and WD repeat domain containing 10
Dcst1	-1.10	0.024549	DC-STAMP domain containing 1

|log 2FC| > 1; $p < 0.05$ by analysis of variance.

between the two groups (Figure 1(e)). TTC staining showed a significant reduction in infarct size in the SD-IR group ($9.26 \pm 0.16\%$, $n = 6$) compared with the IR group ($15.05 \pm 0.70\%$, $n = 6$) (Figure 1(e)).

3.3. Differential Expression of lncRNAs, circRNAs, miRNA, and mRNAs. To fully understand the role of cardiac sympathetic denervation in myocardial ischemia/reperfusion injury, we simultaneously analyzed the profiles of differential expression of lncRNAs, circRNAs, miRNAs, and mRNAs through microarray analysis. Significant difference was defined as fold change ≥2 and $p < 0.05$. In this study, the SD-IR group identified 333 lncRNAs, 122 circRNAs, 23 miRNAs, and 199 mRNAs with significant differential expression (Figure 2). Through high-throughput RNA sequencing, we found that 165 lncRNAs were upregulated and 168 lncRNAs were downregulated; 70 circRNAs were

upregulated and 52 circRNAs were downregulated; 12 miR-NAs were upregulated and 11 miRNAs were downregulated; and 148 mRNAs were upregulated and 51 mRNAs were downregulated (Figure 2).

A total of 23711 lncRNAs and 12007 circRNAs (Figures 3(a) and 3(b)) were identified in all chromosomes. Among lncRNAs, most (51.1%) were sense_genic_exonic lncRNA, followed by sense_genic_intronic lncRNAs (9.8%), sense_intergenic_downstream lncRNAs (8.5%), sense_intergenic_upstream lncRNAs (5.3%), antisense_genic_exonic lncRNA (6.8%), antisense_genic_intronic lncRNAs (6.6%), antisense_intergenic_downstream lncRNAs (4.8%), and antisense_intergenic_upstream lncRNAs (7.1%) (Figure 3(c)). In circRNA, the vast majority (94.4%) were sense_genic_exonic circRNA, followed by sense_genic_intronic circRNAs (1%), sense_intergenic_downstream circRNAs (0.8%), sense_intergenic_upstream circRNAs (1%), antisense_genic_exonic

TABLE 4: The detail information of the top 30 up-regulated lncRNAs and top 30 down-regulated lncRNAs in the T1-4 spinal cord between SD-IR group and IR group.

| | Upregulation | | | Downregulation | |
LncRNA ID	log$_2$FC (SD-IR/IR)	Pvalue	LncRNA ID	log$_2$FC (SD-IR/IR)	Pvalue
NONRATT015643.2	6.61	0.030213	NONRATT002082.2	-8.80	0.003863
NONRATT003628.2	6.28	0.006736	NONRATT004821.2	-8.62	0.025764
NONRATT005973.2	6.21	0.009866	NONRATT010722.2	-7.18	0.000854
NONRATT016279.2	6.00	0.004952	NONRATT000247.2	-5.80	0.00261
NONRATT008379.2	5.61	0.014618	NONRATT027814.2	-5.77	0.012322
NONRATT013717.2	5.58	0.036523	NONRATT008629.2	-5.75	0.017423
NONRATT016674.2	5.56	0.047236	NONRATT005321.2	-5.65	0.002079
NONRATT017458.2	5.44	0.008762	NONRATT028463.2	-5.59	0.000887
NONRATT002859.2	5.27	0.016794	TCONS_00021543	-5.51	0.006752
NONRATT009760.2	5.22	0.028265	NONRATT004098.2	-5.28	0.011345
TCONS_00002734	5.09	0.011358	NONRATT007713.2	-5.20	3.10E-05
NONRATT011768.2	4.95	0.01038	NONRATT004090.2	-5.07	0.010222
NONRATT009811.2	4.73	0.000946	NONRATT018759.2	-5.06	0.001982
NONRATT026200.2	4.54	0.004819	NONRATT003447.2	-5.03	0.010344
NONRATT030638.2	4.44	0.025926	NONRATT007815.2	-5.02	0.039319
NONRATT008615.2	4.37	0.001033	NONRATT025664.2	-4.82	5.13E-05
NONRATT012797.2	4.35	0.023183	NONRATT019695.2	-4.69	0.008267
NONRATT020189.2	4.33	0.011361	NONRATT006541.2	-4.66	3.19E-11
NONRATT020809.2	4.27	0.02875	NONRATT019538.2	-4.60	0.013069
NONRATT029190.2	4.25	0.001325	NONRATT026641.2	-4.54	0.01747
NONRATT022867.2	4.24	0.031209	NONRATT024737.2	-4.38	0.010641
NONRATT000517.2	4.24	0.031431	TCONS_00013588	-4.30	6.80E-06
NONRATT003681.2	4.18	0.012182	NONRATT020675.2	-4.21	0.010623
NONRATT021791.2	4.16	0.009107	NONRATT010709.2	-4.20	0.043975
NONRATT023302.2	4.14	0.038514	NONRATT022516.2	-4.14	0.048093
NONRATT003838.2	4.12	0.043331	NONRATT020315.2	-4.13	0.01375
NONRATT018320.2	4.10	0.005454	TCONS_00002731	-4.02	0.028687
NONRATT013257.2	3.87	0.043965	NONRATT006149.2	-3.89	0.003669
NONRATT000472.2	3.79	0.048619	NONRATT011296.2	-3.87	0.033214
NONRATT005188.2	3.76	0.019322	TCONS_00007997	-3.75	0.001282

|log 2FC| > 1; p < 0.05 by analysis of variance.

circRNA (0.7%), antisense_genic_intronic circRNAs (0.2%), antisense_intergenic_downstream circRNAs (0.4%), and antisense_intergenic_upstream circRNAs (1.5%) (Figure 3(d)).

3.4. Differential Expression Patterns of mRNAs, lncRNAs, and circRNAs in MIRI. The expression patterns of mRNAs, lncRNAs, and circRNAs in the T1–T4 spinal cord 2 hours after MIRI were examined using microarray. From the volcano map and hierarchical clustering analysis results between the SD-IR group and the IR group, a landscape of the expression characteristics of the mRNAs, lncRNAs, and circRNAs was obtained (Figure 4(a)). The volcano plots demonstrated that large numbers of mRNAs, lncRNAs, and circRNAs were differentially expressed between the two groups (Figure 4(b)). Furthermore, these differential alterations of mRNA, lncRNA, and circRNA expression in the T1–T4 spinal cord were associated with cardiac sympathetic denervation.

The hierarchical heat map showed the deregulated mRNAs, lncRNAs, and circRNAs in the T1–T4 spinal cord segments between the SD-IR group and the IR group (Figure 4(c)); up- and downregulated genes are colored in red and green, respectively (p < 0.05 and log2|FC| > 1).

3.5. Analysis of mRNAs, lncRNAs, circRNAs, and miRNAs Changes in the Spinal Cord after Cardiac Sympathetic Denervation. Among the differentially expressed mRNAs, there were 199 genes exhibiting fold change (FC) higher than 1. The number of downregulated mRNAs was 51, whereas the number of upregulated mRNAs was 148. The most upregulated mRNAs were Fxyd2, Tyrp1, Il31ra, RT1-CE4, Scn11a, MGC108823, Tnc, Irf8, and MGC105567. The most downregulated mRNAs were LOC100911256, Cyp4b1, LOC103689986, LOC103693165, Sh2d4b, LOC100910308, Nfs1, Prex2, LOC103691806, and Hif3a. The detailed

TABLE 5: The detail information of the top 20 up-regulated circRNAs in the T1-4 spinal cord between SD-IR group and IR group.

CircRNA ID	$\log_2$FC (SD-IR/IR)	Pvalue
circRNA_06761|Chr3:13146571_13147147_-	3.91	0.000446
circRNA_03748|Chr15:51936366_51954838_-	3.80	0.000648
circRNA_01962|Chr10:103586432_103677527_-	3.27	0.017323
circRNA_11924|Chr9:119105074_119127222_+	3.16	0.019308
circRNA_01988|Chr10:109580083_109583063_-	3.16	0.01944
circRNA_04213|Chr16:81879800_81897683_-	3.10	0.027871
circRNA_05436|Chr2:5570780_5576549_-	3.08	0.047573
circRNA_09388|Chr6:38617368_38619590_+	3.06	0.03965
circRNA_04650|Chr17:86845723_86873000_-	2.89	0.013496
circRNA_02217|Chr11:70539679_70570814_-	2.74	0.026695
circRNA_06237|Chr2:218919131_218929338_-	2.69	0.040249
circRNA_11356|Chr8:128384378_128391077_-	2.61	0.04823
circRNA_08473|Chr5:50318351_50319000_-	2.60	0.036427
circRNA_02159|Chr11:47165426_47169764_+	2.56	0.001643
circRNA_05629|Chr2:45801786_45859187_+	2.41	0.033552
circRNA_09485|Chr6:60609626_60633969_+	2.26	0.009238
circRNA_06869|Chr3:33465220_33473531_+	2.22	0.023101
circRNA_00547|Chr1:143712491_143723739_-	2.19	0.006884
circRNA_08772|Chr5:123824724_123825786_+	2.15	0.005133
circRNA_01552|Chr10:55283300_55338553_+	2.06	0.028481

$|\log 2FC| > 1$; $p < 0.05$ by analysis of variance.

TABLE 6: The detail information of the top 20 down-regulated circRNAs in the T1-4 spinal cord between SD-IR group and IR group.

CircRNA ID	$\log_2$FC (SD-IR/IR)	Pvalue
circRNA_06863|Chr3:29584278_29597359_-	-3.41	0.004976
circRNA_11934|Chr9:119750465_119765191_-	-3.34	0.007029
circRNA_02911|Chr13:92762599_92783433_+	-3.28	0.009623
circRNA_04274|Chr17:5524117_5571375_+	-3.25	0.013595
circRNA_04457|Chr17:53489461_53499989_+	-3.20	0.013695
circRNA_11984|ChrX:13905156_13917538_+	-2.97	0.035854
circRNA_08837|Chr5:129413066_129491380_+	-2.89	0.048702
circRNA_03573|Chr15:13454469_13468631_-	-2.26	0.019466
circRNA_07224|Chr3:113195876_113197193_-	-2.26	0.016518
circRNA_07819|Chr4:64451679_64474930_-	-2.24	0.021549
circRNA_04050|Chr16:23555919_23573530_+	-2.12	0.00851
circRNA_09970|Chr7:9826042_9826424_-	-1.97	0.035185
circRNA_11137|Chr8:96067918_96073130_-	-1.61	0.040373
circRNA_07862|Chr4:66193731_66214585_+	-1.57	0.049364
circRNA_07510|Chr3:175512077_175535023_+	-1.57	0.038954
circRNA_11420|Chr9:8350080_8421978_+	-1.53	0.007153
circRNA_03499|Chr14:113838631_113857380_+	-1.40	0.04037
circRNA_09492|Chr6:64852693_64861750_+	-1.32	0.035057
circRNA_02339|Chr12:587083_591296_-	-1.19	0.014725
circRNA_04622|Chr17:84855705_84901793_+	-1.03	0.038253

$|\log 2FC| > 1$; $p < 0.05$ by analysis of variance.

TABLE 7: The detail information of differentially expressed miRNAs in the T1-4 spinal cord between SD-IR group and IR group.

miRNA_ID	log$_2$FC (SD-IR/IR)	Pvalue	Length
Upregulation			
novel21_star	3.695484	0.021677	23
Rno-miR-293-5p	2.798924	0.000538	21
novel98_mature	2.479701	0.03268	23
novel174_mature>novel176_mature>novel705_mature	2.236875	0.046924	22
Rno-miR-146a-3p	2.118125	0.026213	21
Rno-miR-96-5p	0.903083	0.005817	23
Rno-miR-183-5p	0.614791	0.003377	22
Rno-miR-493-5p	0.60771	0.007994	22
Rno-miR-363-3p	0.60157	0.019368	21
Rno-miR-3553	0.600458	0.03527	23
Downregulation			
novel190_mature	-3.63316	0.016898	23
novel275_mature>novel301_mature	-3.4838	0.045199	24
novel586_mature	-3.41968	0.000414	23
novel88_mature	-2.24793	0.005616	23
novel252_mature	-1.81632	0.044256	23
novel62_mature	-1.46827	0.03968	24
Rno-miR-206-3p	-1.07274	0.014845	22
Rno-miR-1-3p	-0.86313	0.029666	22
Rno-miR-7a-2-3p	-0.67697	0.040237	22

|log 2FC| > 1; $p < 0.05$ by analysis of variance.

information regarding the differentially expressed mRNAs is listed in Tables 2 and 3.

The results showed that 333 lncRNAs, including 165 upregulated and 168 downregulated lncRNAs, were significantly altered in the SD-IR group compared with the IR group. The most upregulated lncRNAs were NON-RATT003225.2, TCONS_00000042, NONRATT013473.2, NONRATT011603.2, NONRATT018299.2, NONRATT-001917.2, NONRATT017719.2, NONRATT004831.2, TCONS_00008547, and NONRATT025548.2. The most downregulated lncRNAs were NONRATT003165.2, NON-RATT006541.2, NONRATT031746.1, TCONS_00013588, TCONS_00009293, NONRATT007713.2, NONRATT-016595.2, NONRATT011191.2, NONRATT025664.2, and NONRATT010240.2. Additional information regarding the differentially expressed lncRNAs is presented in Table 4.

Compared with the IR group, the SD-IR group showed 70 upregulated and 52 downregulated circRNAs. The most upregulated circRNAs were circRNA_00336, circRNA_00446, circRNA_00547, circRNA_01552, circRNA_01962, circRNA_01988, circRNA_02159, circRNA_02217, circRNA_03207, and circRNA_03748. The most downregulated circRNAs were circRNA_02339, circRNA_02911, circRNA_03499, circRNA_03573, circRNA_04050, circRNA_04274, circRNA_04457, circRNA_04622, circRNA_06863, and circRNA_07224. Additional information regarding the differentially expressed circRNAs is presented in Tables 5 and 6.

Among the differentially expressed miRNAs, there were 12 upregulated and 11 downregulated miRNAs in the SD-IR group compared with the IR group. The upregulated miRNAs were rno-miR-293-5p, rno-miR-183-5p, rno-miR-96-5p, rno-miR-493-5p, novel248_mature, rno-miR-363-3p, novel21_star, rno-miR-146a-3p, novel98_mature, rno-miR-3553, novel438_mature, and novel174_mature>novel176_mature>novel705_mature. The downregulated miRNAs were novel586_mature, novel88_mature, novel342_mature, rno-miR-206-3p, novel190_mature, rno-miR-1-3p, novel655_mature, novel62_mature, rno-miR-7a-2-3p, novel252_mature, and novel275_mature>novel301_mature. Additional information regarding the differentially expressed miRNAs is shown in Table 7.

3.6. GO and KEGG Analysis of Differentially Expressed mRNAs, lncRNAs, circRNAs, and miRNAs.
To investigate the spinal molecular mechanisms of cardiac sympathetic denervation on MIRI, we performed GO and KEGG pathway analyses of the differentially expressed mRNAs (DEM), lncRNAs (DEL), circRNAs (DEC), and miRNAs in SD-MIRI vs. IR group (Tables 8 and 9).

Based on GO analysis, DEL focusing on cell components were related to the Golgi cisterna, membrane, axon, cytoplasm, and cytoplasmic microtubules, while those focusing on molecular function (MF) were related to translation initiation factor activity, protein tyrosine kinase binding, myosin binding, and SNAP receptor activity (Figure 5(a)). The GO function prediction showed that DEC focusing on cell components were related to the VCP-NPL4-UFD1 AAA ATPase complex, nuclear chromosome telomeric region, and actin cytoskeleton, whereas those focusing on molecular functions

TABLE 8: The Gene Ontology (GO) terms enriched for the differentially expressed genes.

GO ID	Term	Gene number	Pvalue
biological_process			
GO:0035458	Cellular response to interferon-beta	12	1.80E-18
GO:0006952	Defense response	11	2.39E-14
GO:0071346	Cellular response to interferon-gamma	9	2.22E-08
GO:0071222	Cellular response to lipopolysaccharide	11	2.09E-07
GO:0050832	Defense response to fungus	4	8.84E-07
GO:0070098	Chemokine-mediated signaling pathway	6	9.17E-07
GO:0031640	Killing of cells of other organism	4	2.35E-06
GO:0032496	Response to lipopolysaccharide	12	2.41E-06
GO:0042742	Defense response to bacterium	8	2.62E-06
GO:0019731	Antibacterial humoral response	4	3.59E-06
cellular_component			
GO:0005615	Extracellular space	34	8.43E-09
GO:0005623	Cell	6	4.24E-05
GO:0030863	Cortical cytoskeleton	3	0.00016
GO:0031012	Extracellular matrix	8	0.000245
GO:0000786	Nucleosome	4	0.000876
GO:0009897	External side of plasma membrane	8	0.001475
GO:0005578	Proteinaceous extracellular matrix	7	0.001944
GO:0005576	Extracellular region	13	0.003785
GO:0030018	Z disc	4	0.006991
GO:0030141	Secretory granule	4	0.010644
molecular_function			
GO:0048248	CXCR3 chemokine receptor binding	3	3.51E-08
GO:0005525	GTP binding	15	2.48E-07
GO:0003924	GTPase activity	13	3.24E-07
GO:0008009	Chemokine activity	5	1.05E-06
GO:0045236	CXCR chemokine receptor binding	3	3.30E-06
GO:0042288	MHC class I protein binding	3	6.49E-05
GO:0003779	Actin binding	9	9.09E-05
GO:0005506	Iron ion binding	7	0.00032
GO:0004867	Serine-type endopeptidase inhibitor activity	5	0.000333
GO:0051879	Hsp90 protein binding	3	0.000451

(MF) were related to retinoic acid-responsive element binding, ubiquitin binding, ATPase activity, and sequence-specific DNA activity (Figure 5(b)).

KEGG analysis revealed the potential mechanism of DEL and DEC in the SD-IR group (Figures 5(c) and 5(d)). Namely, DEL are involved in the regulation of dilated cardiomyopathy (DCM), hypertrophic cardiomyopathy (HCM), insulin signaling pathway, and mTOR signaling pathway (Figure 5(c)). The parent gene of DEC might take part in MAPK signaling pathway, cGMP-PKG signaling pathway, protein processing in endoplasmic reticulum, and adrenergic signaling in cardiomyocytes (Figure 5(d)).

3.7. Verification of Differentially Dysregulated mRNAs and lncRNAs. We focused on the differentially dysregulated mRNAs and lncRNAs with more significant changes.

Compared with the IR group, the lncRNAs selected in the SD-IR group, including NONRATT012797.2 and NON-RATT029190.2, were significantly overexpressed and consistent with the RNA-sequencing results (Figures 6(a) and 6(c)). The lncRNAs selected in the SD-IR group, including NONRATT000247.2, NONRATT004098.2 and NON-RATT025664.2, were significantly downregulated compared with the control group and were consistent with the RNA-sequencing results (Figures 6(a) and 6(c)).

For further research, we selected three upregulated mRNAs (Ubd, Ccl12, Cxcl10) and two downregulated mRNAs (LOC100912599, Dpep1) (Figures 6(b) and 6(c)) in the SD-IR group for RT-qPCR verification, p value <0.05, fold change ≥2. The primers of mRNAs and lncRNAs are listed in Table 1. Therefore, these results proved the accuracy of the microarray results.

TABLE 9: The Kyoto Encyclopedia of Genes and Genomes (KEGG) pathways enriched for the differentially expressed genes.

Pathway ID	Term	Gene number	Pvalue
rno04960	Aldosterone-regulated sodium reabsorption	4	2.24E-05
rno04978	Mineral absorption	4	4.64E-05
rno05322	Systemic lupus erythematosus	5	0.000233
rno04614	Renin-angiotensin system	3	0.000307
rno04060	Cytokine-cytokine receptor interaction	8	0.00035
rno05145	Toxoplasmosis	5	0.000464
rno04621	NOD-like receptor signaling pathway	6	0.000495
rno04657	IL-17 signaling pathway	4	0.001424
rno05144	Malaria	3	0.00156
rno04972	Pancreatic secretion	4	0.00207
rno04668	TNF signaling pathway	4	0.002791
rno04750	Inflammatory mediator regulation of TRP channels	4	0.003408
rno04976	Bile secretion	3	0.003981
rno05133	Pertussis	3	0.004186
rno05202	Transcriptional misregulation in cancers	5	0.004801
rno04062	Chemokine signaling pathway	5	0.004938
rno04970	Salivary secretion	3	0.00532
rno00830	Retinol metabolism	3	0.006364
rno04650	Natural killer cell mediated cytotoxicity	4	0.00852
rno04974	Protein digestion and absorption	3	0.008842

3.8. Construction of the mRNA-miRNA-lncRNA/circRNA Network. CircRNA participates in the regulation of biological processes in different ways. It is well known that circRNA contains multiple binding sites of miRNA and is also regulated by miRNA. Analysis of circRNA-miRNA interaction may clarify the function and mechanism of circRNA.

As shown in Figure 7(a), the network involves 30 lncRNAs, 35 mRNAs, and 13 miRNAs. At the same time, a circRNA-miRNA-mRNA ceRNA network was constructed (Figure 7(b)), involving 26 circRNAs, 44 mRNAs, and 16 miR-NAs. Each differentially expressed lncRNA can be associated with one or more miRNAs. For example, lncRNA NON-RATT016892.2 has established connections with two miR-NAs, including rno-miR-1-3p and rno-miR-206-3p. miR-1187 is connected with four circRNAs, including circRNA_02339/Chr12:587083_591296, circRNA_07789/Chr4:5866-1995_58669806, circRNA_04050/Chr16:23555919_23573530, and circRNA_07510/Chr3:175512077_175535023. Finally, circRNA_01445/Chr10:37180938_37185721 has only established a connection with miR-438 (Figure 7(b)).

The two networks have multiple common nodes (Figure 7(c)), such as lncRNA NONRATT024121.2, lncRNA NONRATT022775.2, lncRNA NONRATT022692.2, lncRNA NONRATT011191.2, and lncRNA NONRATT017402.2, which all interact with miR-493-5p.

3.9. PPI Network and Functional Analysis of the Differentially Expressed mRNAs. To further address the most significant clusters of differentially expressed mRNAs in the ceRNA network, we conducted the PPI network analysis by using the STRING database version 11.0 and visualization under the Cytohubba plug-in and the Cytoscape. The most significant hub upregulated genes in the PPI network were Cxcl10, Cxcl11, Mmp9, Gbp2, Gbp5, Irgm, Mpa21, and Igf1, while the most significant hub downregulated genes were Ahsg, Trim63, and Trpv4 (Figure 8(a)).

To clarify the role of differential genes in the preventive effect of cardiac sympathetic denervation on MIRI, we performed GO and KEGG analyses on the differentially expressed mRNAs. The results suggested that the molecular functions (MF) are mainly enriched in the CXCR3 chemokine receptor binding, MHC class I protein binding, GTP binding, GTPase activity, and chemokine activity (Figure 8(b)). In the cell components (CC), functions are highly enriched in autophagy-related processes, which are related to the cortical cytoskeleton, nucleosomes, secretory granules. KEGG analysis showed that the differentially expressed mRNAs were involved in cytokine–cytokine receptor interaction, NOD-like receptor signaling pathway, chemokine signaling pathway, and inflammatory mediator regulation of TRP channels (Figure 8(c)). These results showed that most of the hub genes play a role in the preventive effect of cardiac sympathetic denervation on MIRI.

4. Discussion

This study provides novel information on the vital role of cardiac sympathetic denervation in the process of myocardial ischemia/reperfusion injury. Our main findings are as follows: (1) Cardiac sympathetic denervation induced by 6-OHDA alleviated myocardial ischemia/reperfusion injury. (2) The expression profiles of lncRNA, circRNA, and mRNA in the upper thoracic spinal cord were identified by RNA-seq analysis. Among them, there were 148 upregulated and 51
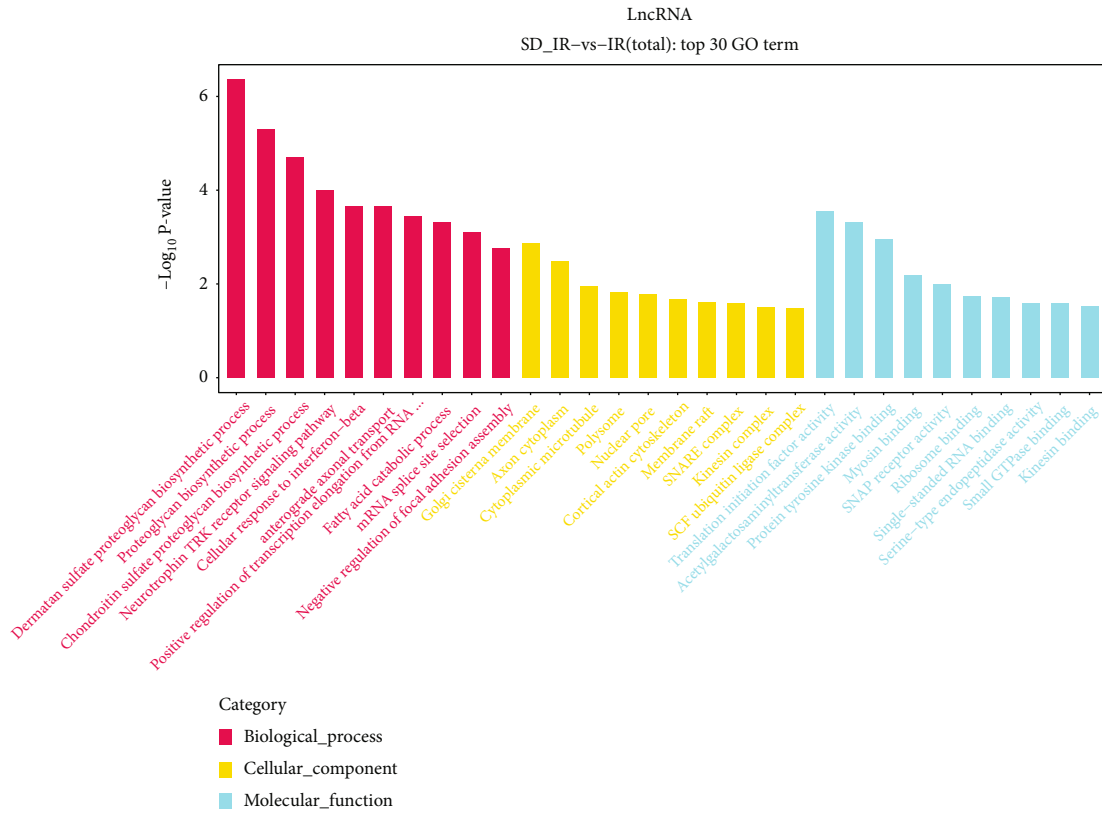
(a)
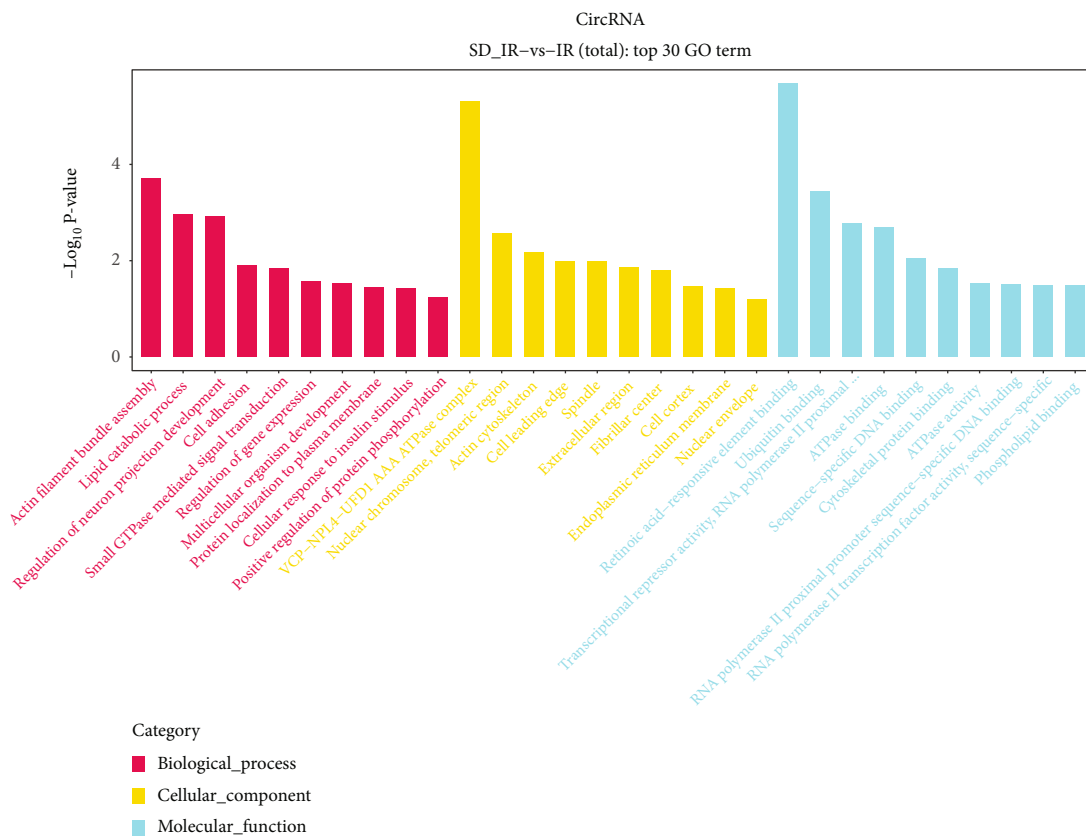
(b)

Figure 5: Continued.

(c)

(d)
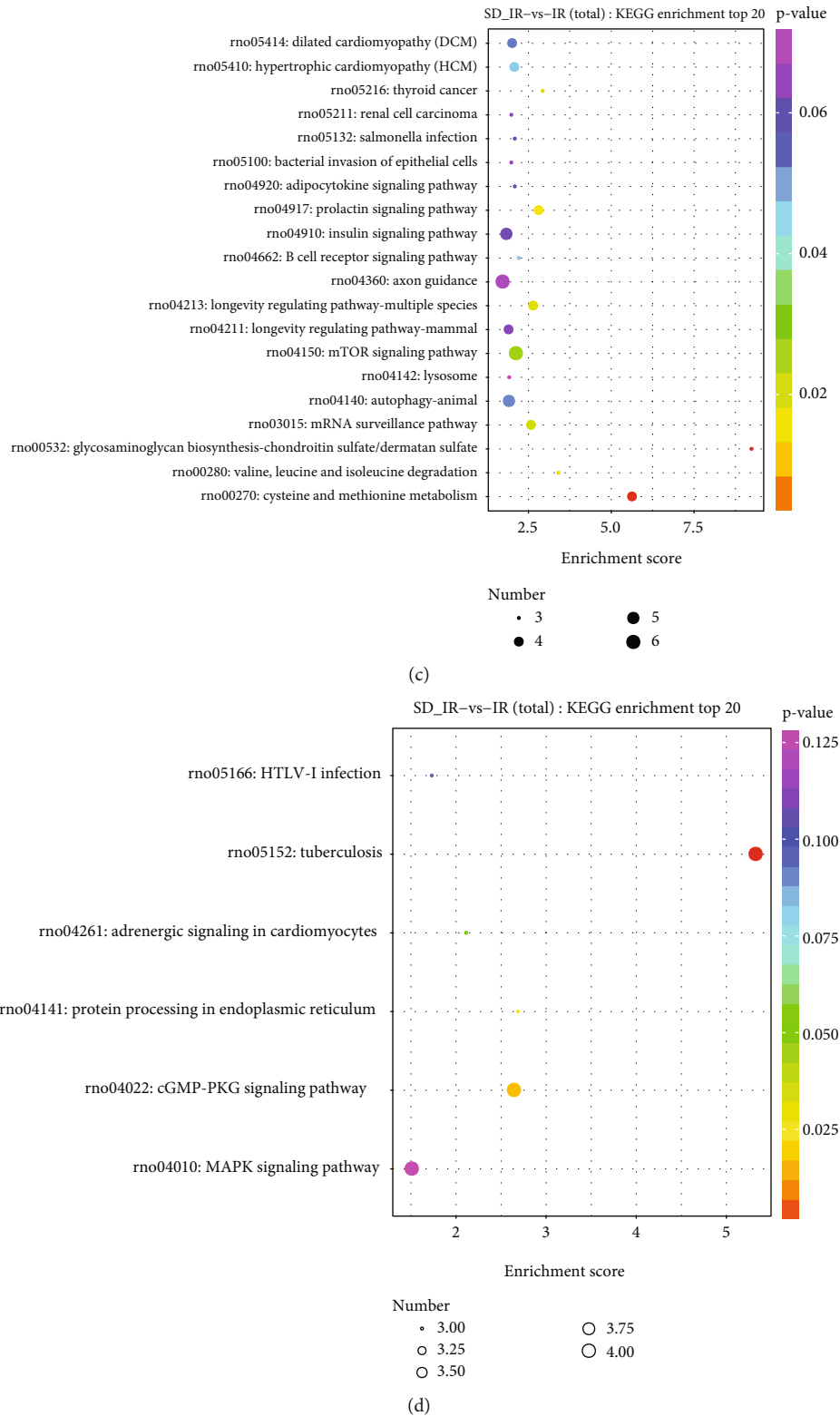
FIGURE 5: Functional analysis of the differentially expressed lncRNAs and circRNAs between IR group and SD-IR group. (a) The top 30 Gene Ontology terms of differentially expressed lncRNAs. Green color is related to biological processes; blue color is related to cellular components; and red color is related to molecular functions. (b) The top 30 Gene Ontology terms of differentially expressed circRNAs. Richly factor refers to the ratio of the number of differentially expressed genes in the KEGG pathway accounting for the total number of genes that are related to this pathway. The larger the richly factor, the higher the degree of enrichment; the size of the bubble indicates the number of genes, which is qualified by Q-value. (c) The top 20 KEGG pathway enrichment analysis of differentially expressed lncRNAs. (d) The top six KEGG pathway enrichment analysis of differentially expressed circRNAs.

(a)

(b)

(c)
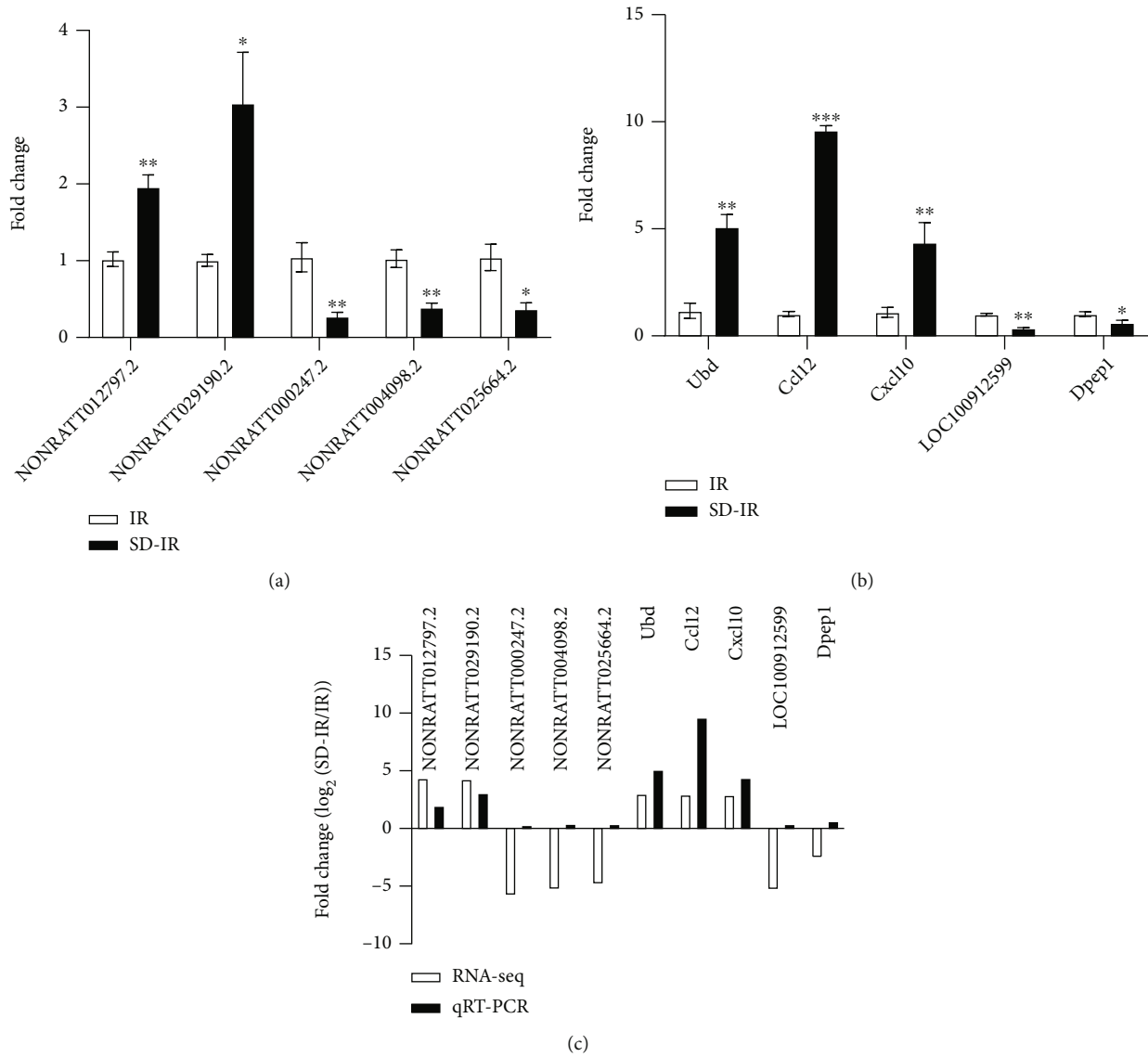
FIGURE 6: Validation of lncRNAs and mRNAs by RT-qPCR in the T1–T4 spinal cord IR group and SD-IR group. (a) The expression levels of lncRNA NONRATT012797.2 and NONRATT029190.2 were significantly upregulated in SD-IR group, whereas the expression levels of lncRNA NONRATT000247.2, NONRATT004098.2, and NONRATT025664.2 were significantly downregulated in SD-IR group. (b) The expression levels of mRNA Ubd, Ccl12, and Cxcl10 were significantly upregulated in SD-IR group, whereas the expression levels of mRNA LOC100912599 and Dpep1 were significantly downregulated in SD-IR group. (c) The expression levels of five lncRNAs and five mRNAs. Two upregulated lncRNAs, three downregulated lncRNAs, three upregulated mRNAs, and two downregulated mRNAs were validated by RT-qPCR. Data are expressed as mean ± SEM. $*P < 0.05$, $**p < 0.01$, $*** p < 0.001$ vs. IR group.

downregulated mRNAs, 165 upregulated and 168 downregulated lncRNAs, and 70 upregulated and 52 downregulated circRNAs in the SD-IR group compared with the IR group. (3) We selected three mRNAs from the most upregulated mRNAs and three lncRNAs from the most downregulated lncRNAs for RT-qPCR low-throughput verification, and the results were consistent with the sequencing results. By providing new insights into the function of lncRNA/circRNA-miRNA-mRNA networks, our results contribute to the understanding of the pathogenesis of MIRI and provide new targets for MIRI.

In recent years, a large number of studies have confirmed that cardiac sympathetic activity plays an important role in many cardiac diseases and processes [35–40]. Lu et al. reported that sympathetic hyperinnervation and/or myocardial infarction remodeled myocardial glutamate signaling and ultimately increased the severity of ventricular tachyarrhythmias [9]. It has also been shown that left stellate ganglion (LSG) suppression protects against ventricular arrhythmias. Yu et al. found that optogenetic modulation could reversibly inhibit the neural activity of LSG, thereby increasing electrophysiological stability and protecting against myocardial ischemia-induced ventricular arrhythmias [41]. These reports and our results also suggest that the presence of decreased cardiac sympathetic activity can have a cardioprotective effect, and that this depends on effective sympathetic denervation.
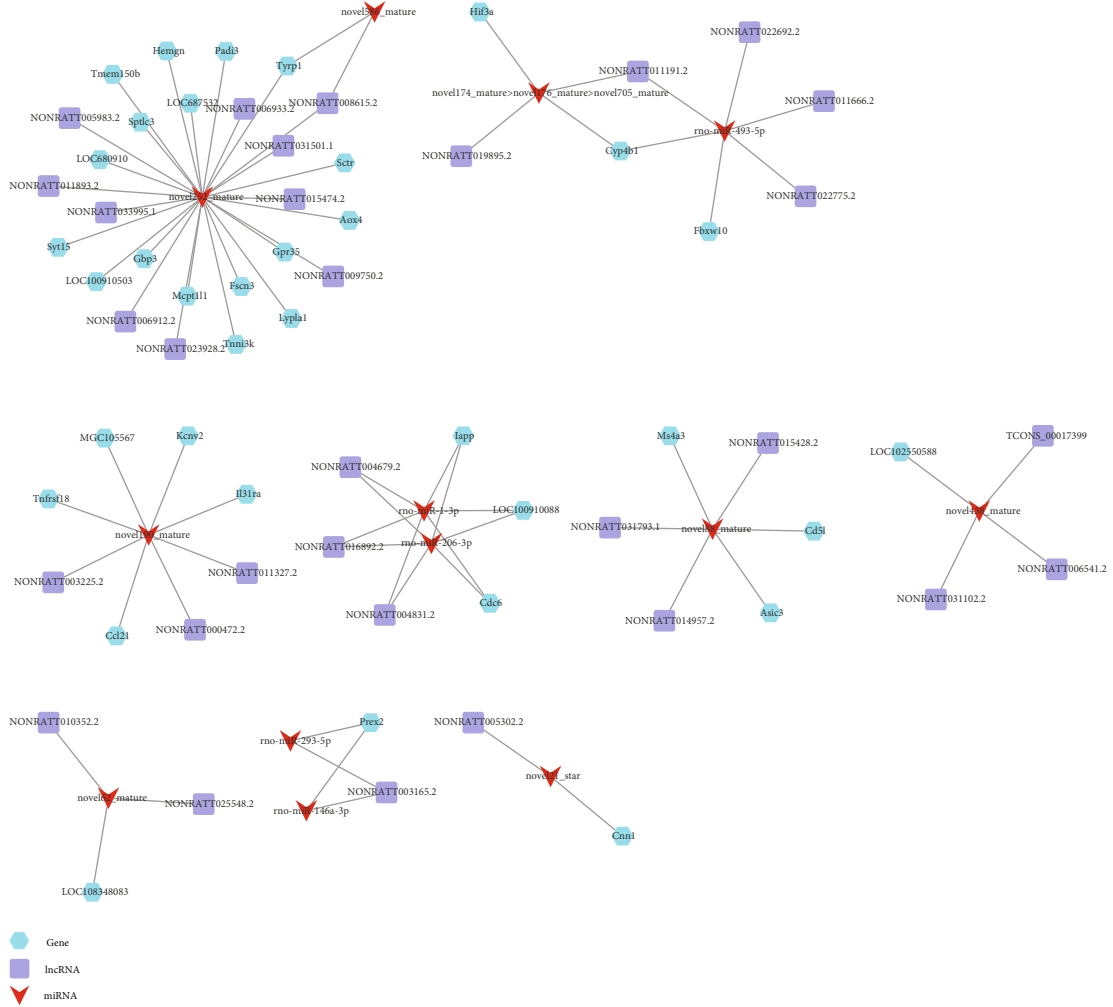
(a)

Figure 7: Continued.
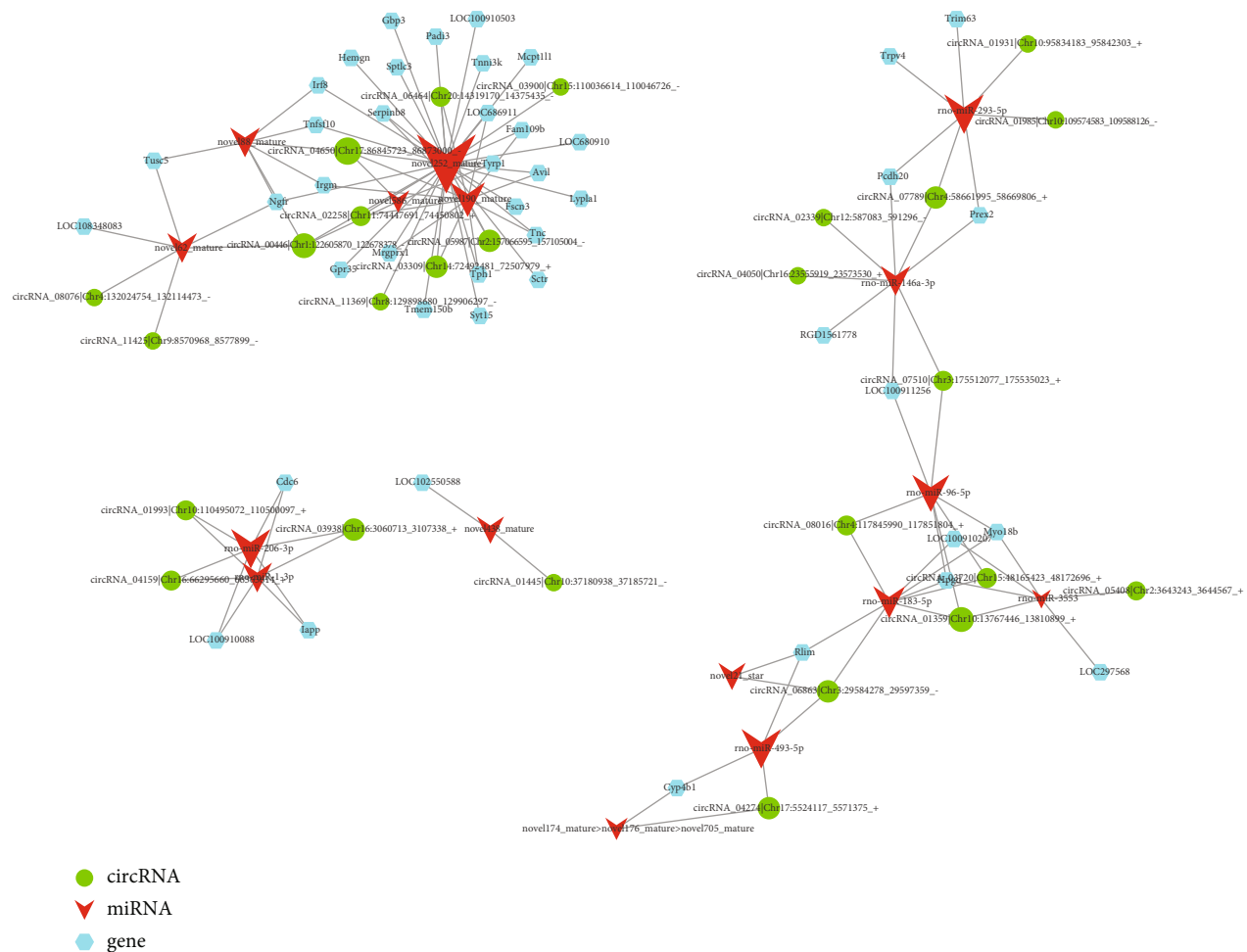
- circRNA
- miRNA
- gene

(b)

Figure 7: Continued.
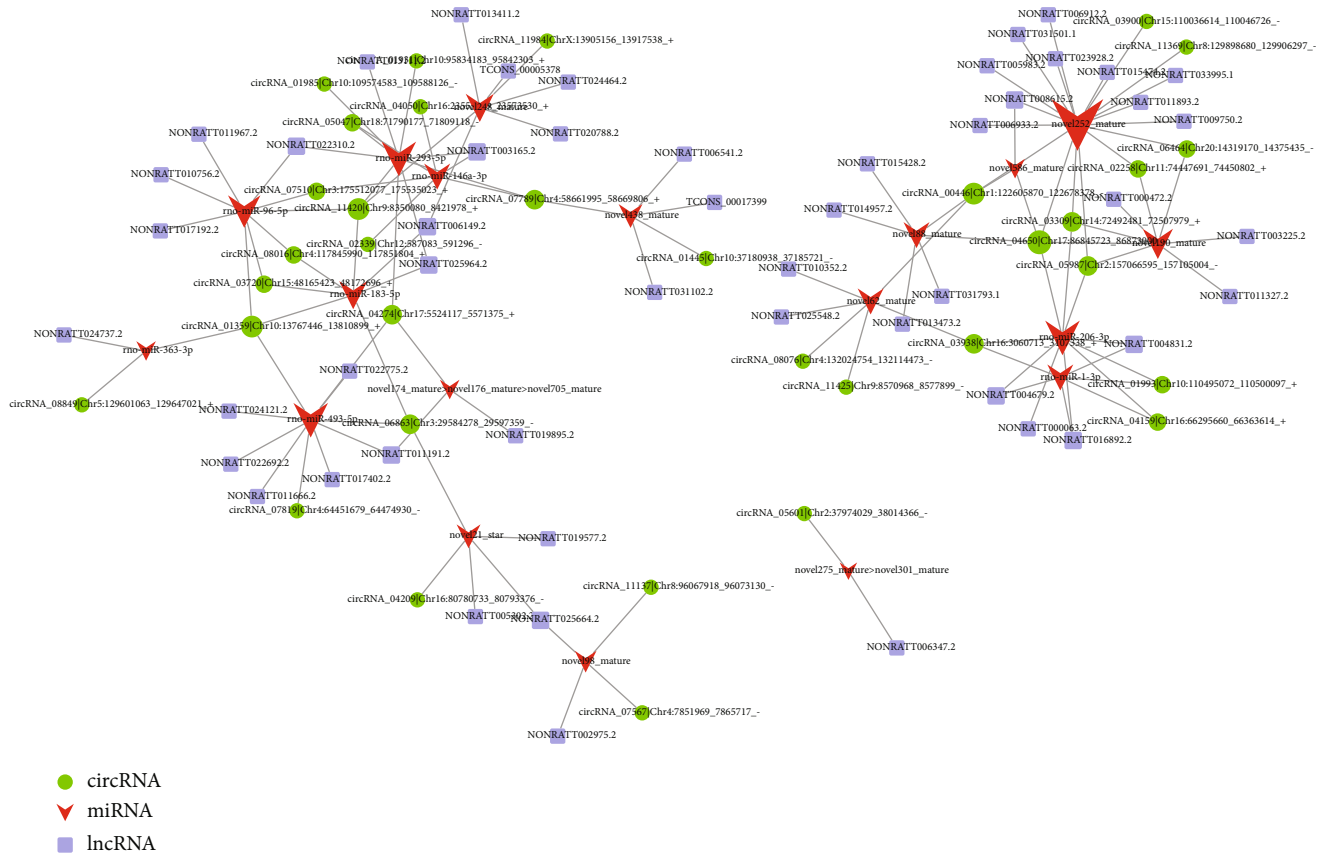
(c)

Figure 7: Construction of the mRNA-miRNA-lncRNA/circRNA network. (a) Network analysis of mRNA-miRNA-lncRNA. The blue nodes represent mRNA. The purple nodes represent lncRNA. The red nodes represent miRNA. (b) Network analysis of mRNA-miRNA-circRNA. The green nodes represent circRNA. The red nodes represent miRNA. The blue nodes represent mRNA. (c) Network analysis of lncRNA-miRNA-circRNA. The green nodes represent circRNA. The red nodes represent miRNA. The purple nodes represent lncRNA.

Recently, significant efforts have been made to understand the alterations of ncRNAs in different spinal cord segments and their contributions to specific outcomes of diseases [16, 26, 42–44]. The spinal cord is a complex and dynamic neural structure. It contains sympathetic preganglionic neurons within the intermediolateral cell column [45–47]; they are involved in the generation of sympathetic activity in many autonomic targets, including the heart and blood vessels [36, 48–50]. There is accumulating evidence of the interaction between the spinal cord and the heart [51–55]. We previously demonstrated the changes of novel lncRNAs in the upper thoracic spinal cord of rats with MIRI [42]. In recent years, there has been considerable effort to explore the relationship between cardiac sympathetic activity and cardiovascular diseases. However, the changes in spinal lncRNAs in rats with MIRI after cardiac sympathetic denervation have not been reported. Here, we aimed to understand the involvement of specific patterns of changes in the lncRNA/circRNAs-miRNA-mRNA network of the upper thoracic spinal cord regions of animals with myocardial ischemia-reperfusion injury after cardiac sympathetic denervation.

LncRNAs are involved in the progression of coronary artery disease (CAD) [56]. Xu et al. reported that lncRNA AC096664.3/PPAR-gamma/ABCG1-dependent signal transduction pathway contributes to the regulation of cholesterol homeostasis [56]. As one of the differentially expressed lncRNAs between CAD patients and healthy controls, lncRNA ENST00000602558.1 plays a key role in the pathogenesis of atherosclerosis. Cai et al. showed that lncRNA ENST00000602558.1 regulated ABCG1 expression and cholesterol efflux from vascular smooth muscle cells through a p65-dependent pathway [57]. The study by Li et al. provided the characterization of lncRNA expression profile and identification of novel lncRNA biomarkers to diagnose CAD [58]. According to our study, spinal lncRNA as a sponge of miRNA mainly participates in the process of MIRI through cysteine and methionine metabolism, mTOR signaling pathway, insulin signaling pathway, and adipocytokine signaling pathway.

Circular RNAs (circRNAs) play a critical role in the physiology and pathology of cardiovascular diseases [59–62]. To further investigate the roles of these differentially expressed circRNAs in the development of MIRI, we performed GO and KEGG pathway analyses. Based on the GO and KEGG enrichment analyses of these circRNAs, our results suggested that the significantly enriched biologic processes and molecular functions of the upregulated genes after MIRI were associated with gene sets termed as follows:

(a)
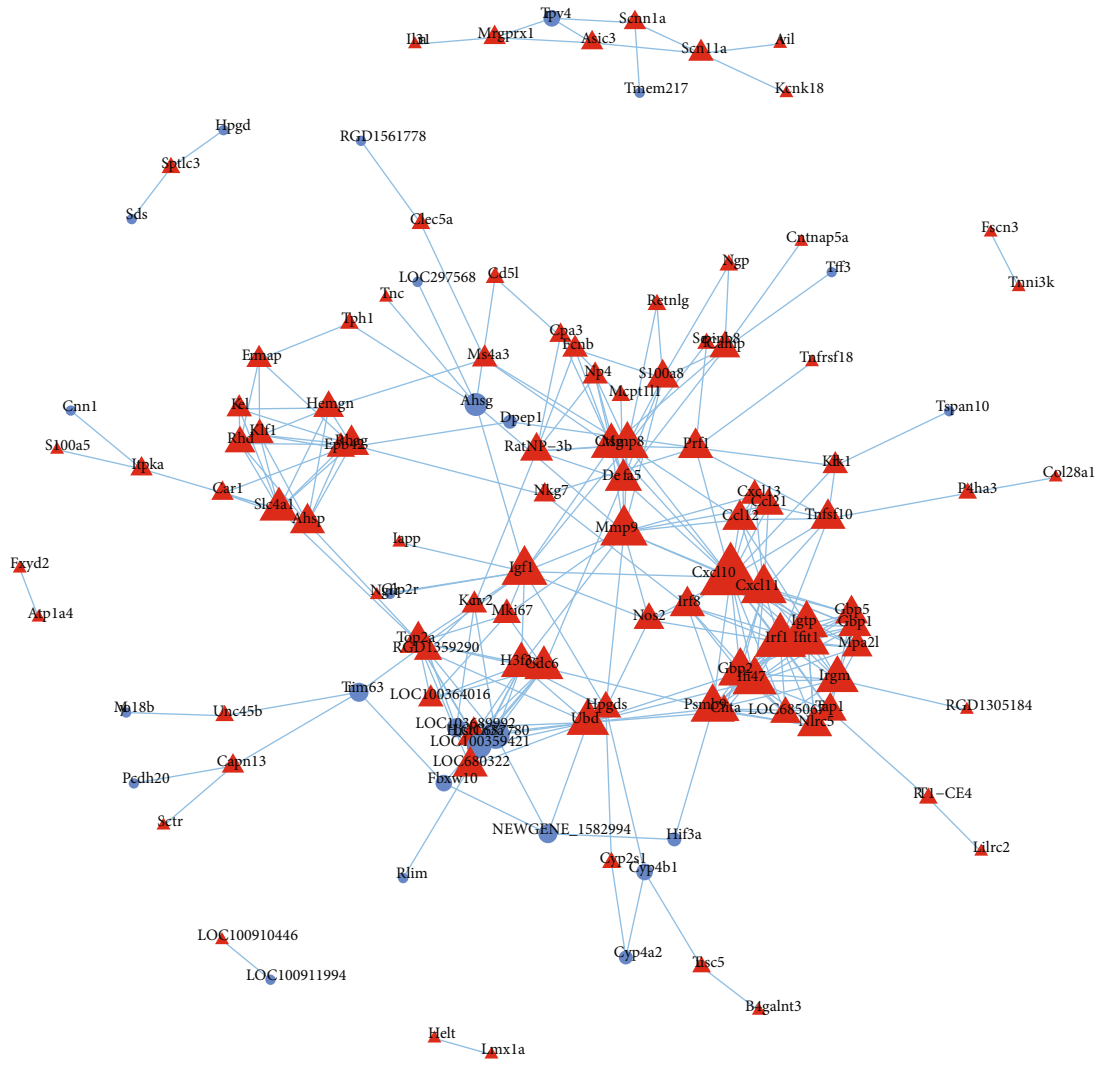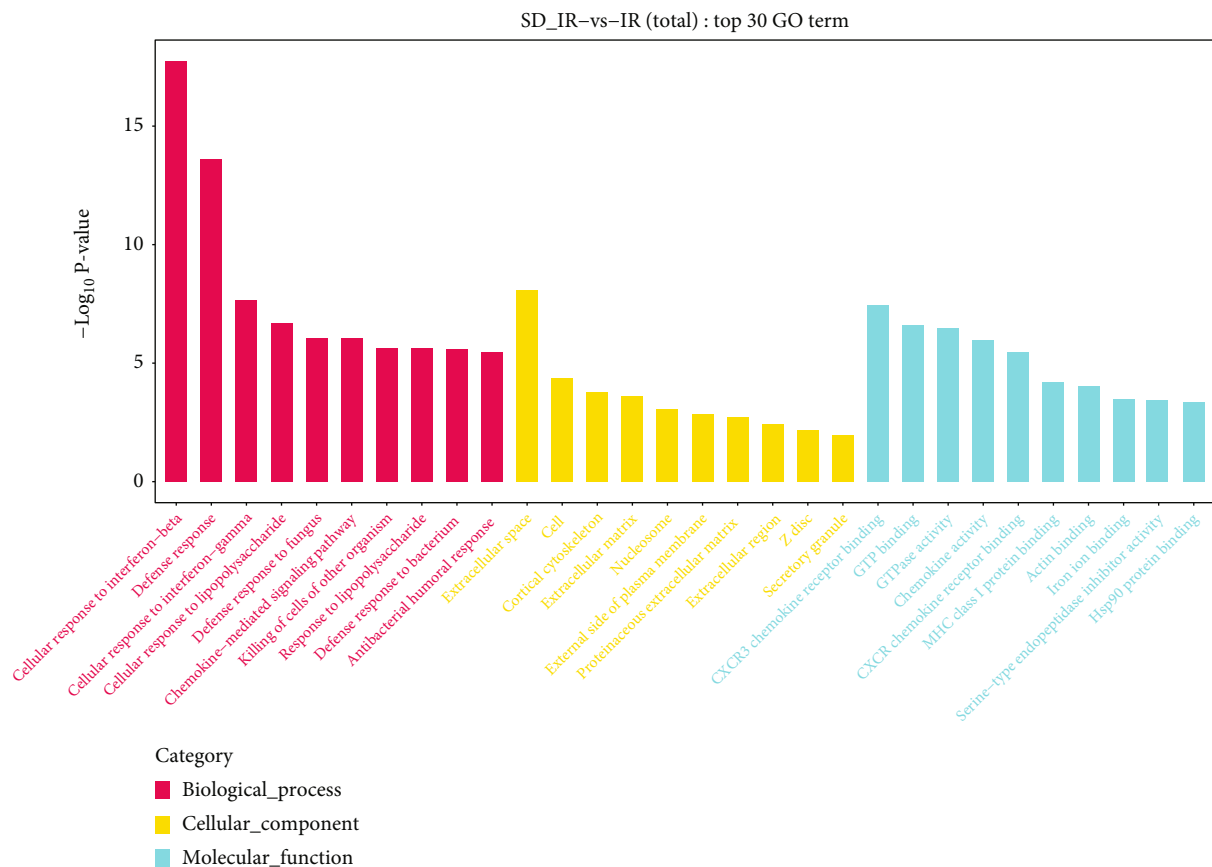
Figure 8: Continued.

(b)

Figure 8: Continued.

(c)
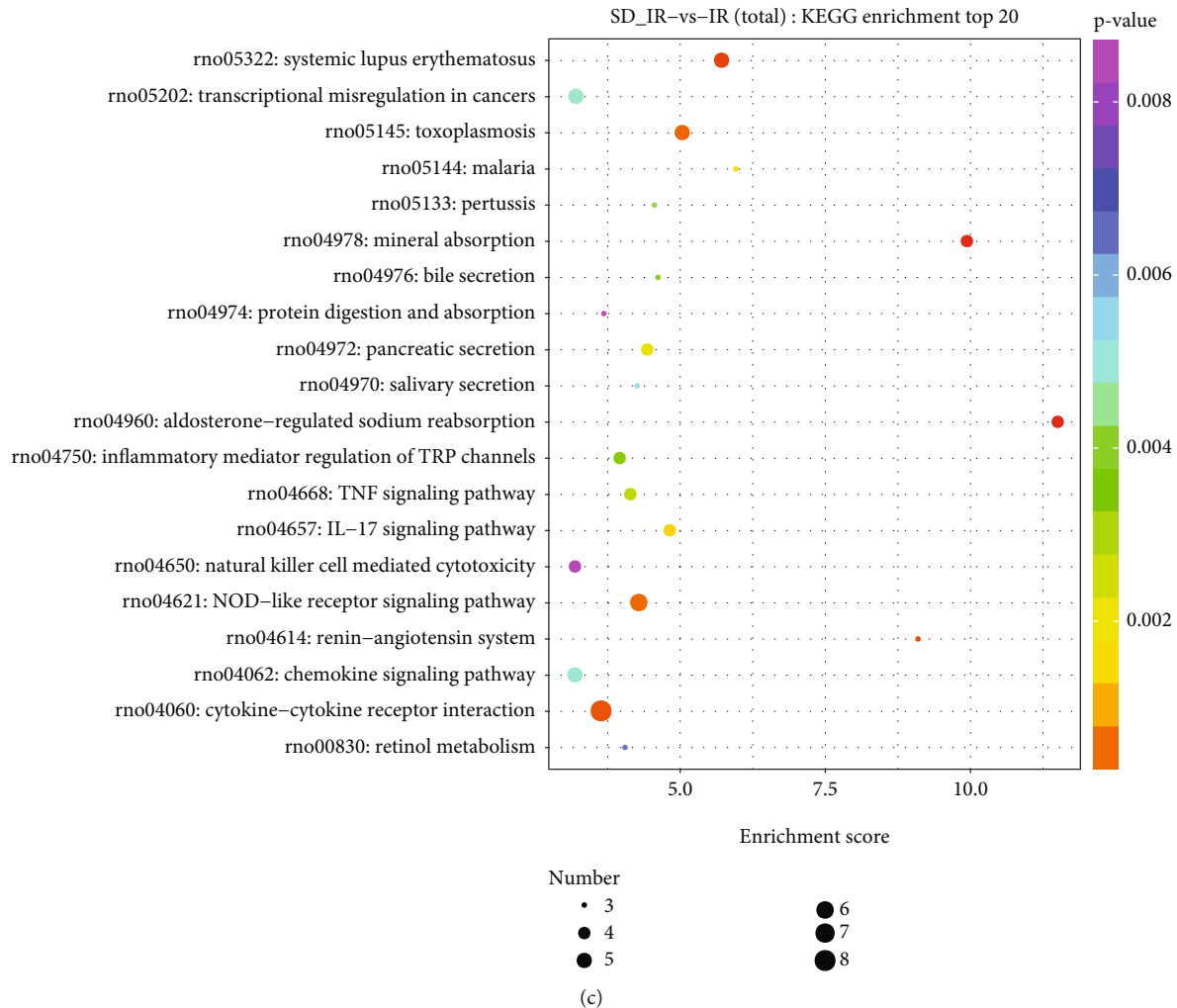
Figure 8: PPI network and functional analysis of the differentially expressed mRNAs. (a) The PPI network was constructed by differentially expressed mRNAs. (b) The top 30 Gene Ontology terms of differentially expressed mRNAs. (c) The top 20 KEGG pathway enrichment analysis of differentially expressed mRNAs.

"MAPK signaling pathway" and "cGMP-PKG signaling pathway". It is well known that MAPK pathway is involved in ischemia-reperfusion injury [63]. Previous studies have shown that cGMP-PKG pathways are implicated in cardiovascular complications of diverse etiologies [64, 65]. These data suggest that spinal circRNAs may be potential targets for MIRI.

miRNAs have been shown to modulate the translational activity of the genome and regulate protein expression and function [66–68]. According to Wang et al. [69], miRNA-493-5p promotes apoptosis and suppresses proliferation and invasion in liver cancer cells by targeting VAMP2. Previous studies have pointed out a potential cardioprotective role of phosphatidylserine in heart ischemia [70–73], suggesting that the phosphatidylserine signaling pathway is associated with MIRI. Schumacher et al. [74] indicated that phosphatidylserine significantly reduced the infarct size by 30% and improved heart function by 25% in a chronic model of acute myocardial infarction (AMI), suggesting that phosphatidylserine supplementation may be a promising

novel strategy to reduce infarct size following AMI and to prevent myocardial injury during myocardial infarction or cardiac surgery. A large number of studies have confirmed that chemokines [75–77], including C-X-C motif chemokine receptor 3 (CXCR3) [78], are closely related to the ischemia–reperfusion injury. In this study, we found that miRNAs in the spinal cord participated in the molecular progression of MIRI through the regulation of actin cytoskeleton, phospholipase D, calcium, and MAPK signaling pathways.

It has been found that the lncRNA/circRNA-miRNA-mRNA ceRNA network plays a role in multiple physiological and pathological processes [66, 79–86]. Cheng et al. [82] reported the comprehensive analysis of the circRNA-lncRNA-miRNA-mRNA ceRNA network in the prognosis of acute myeloid leukemia (AML), elucidated the post-transcriptional regulatory mechanism of AML, and identified novel AML prognostic biomarkers, which has important guiding significance for the clinical diagnosis, treatment, and further scientific research of AML. Wang et al. [87] established bronchopulmonary dysplasia (BPD)-related ceRNA

regulatory network of circRNA/lncRNA-miRNA-mRNA in the lung tissue of a mouse model, proving that it is significantly associated with the pathophysiological characteristics of BPD. In this study, we analyzed the changes in spinal lncRNA-miRNA-mRNA and circRNA-miRNA-mRNA ceRNA networks in MIRI after cardiac sympathetic denervation. Our findings offer a new direction for understanding the pathogenesis of MIRI, and suggest some effective targets in the spinal cord after cardiac sympathetic denervation.

In conclusion, the expression characteristics of coding genes, miRNAs, lncRNAs, and circRNAs in the upper thoracic spinal cord of MIRI rats were determined after cardiac sympathetic denervation induced by 6-OHDA. The preventive effect of cardiac sympathetic denervation on MIRI paves the road for further studies on the sympathetic mechanisms associated with MIRI, which is important to further explore the pathogenesis of MIRI and potentially facilitate the discovery of novel lncRNA/circRNA-miRNA-mRNA networks for therapeutic targeting in the management of MIRI.

Data Availability

The raw sequencing data presented in this paper have been deposited in the Sequence Read Archive (SRA) under accession number PRJNA776390. The records are accessible with the following link: https://www.ncbi.nlm.nih.gov/sra/PRJNA776390.

Ethical Approval

The animal study was reviewed and approved by the Institutional Animal Care and Use Committee of Tongji Hospital, Tongji Medical College, Huazhong University of Science and Technology, Wuhan, China (IRB ID: TJ-A0804).

Conflicts of Interest

The authors declare that this study received assistance from OEbiotech Co. Ltd. The OEbiotech Co. Ltd. was not involved in the study design, collection, analysis, interpretation of data, the writing of this article, or the decision to submit it for publication.

Authors' Contributions

All authors listed have made a substantial, direct, and intellectual contribution to the work and approved it for publication.

Funding

References

[1] J. Bai, C. Ren, W. Hao, R. Wang, and J. M. Cao, "Chemical sympathetic denervation, suppression of myocardial transient outward potassium current, and ventricular fibrillation in the rat," *Canadian Journal of Physiology and Pharmacology*, vol. 86, no. 10, pp. 700–709, 2008.

[2] Q. Wang, Z. G. He, S. Y. Li, M. H. Feng, and H. B. Xiang, "Application of animal and human PET in cardiac research," *American journal of cardiovascular disease*, vol. 8, no. 3, pp. 24–30, 2018.

[3] X. C. Pan, Z. X. Li, D. Z. Wu, S. Y. Li, H. B. Xiang, and Y. T. Song, "Mapping changes of whole brain blood flow in rats with myocardial ischemia/reperfusion injury assessed by positron emission tomography," *Current Medical Science*, vol. 39, no. 4, pp. 653–657, 2019.

[4] M. Chen, Z. G. He, B. W. Liu, Z. X. Li, S. G. Liu, and H. B. Xiang, "Parafascicular nucleus-heart neural crosstalk: implications for seizure- induced myocardial stunning," *Epilepsy & Behavior*, vol. 63, pp. 135–137, 2016.

[5] C. Y. Li and Y. G. Li, "Cardiac sympathetic nerve sprouting and susceptibility to ventricular arrhythmias after myocardial infarction," *Cardiology Research and Practice*, vol. 2015, 8 pages, 2015.

[6] B. A. Habecker, M. E. Anderson, S. J. Birren et al., "Molecular and cellular neurocardiology: development, and cellular and molecular adaptations to heart disease," *The Journal of Physiology*, vol. 594, no. 14, pp. 3853–3875, 2016.

[7] J. H. Coote and R. A. Chauhan, "The sympathetic innervation of the heart: important new insights," *Autonomic Neuroscience*, vol. 199, pp. 17–23, 2016.

[8] R. F. Gilmour, "Life out of balance: the sympathetic nervous system and cardiac arrhythmias," *Cardiovascular Research*, vol. 51, no. 4, pp. 625-626, 2001.

[9] J. Lu, X. Gao, J. Gu et al., "Nerve sprouting contributes to increased severity of ventricular tachyarrhythmias by upregulating iGluRs in rats with healed myocardial necrotic injury," *Journal of Molecular Neuroscience*, vol. 48, no. 2, pp. 448–455, 2012.

[10] N. Herring, J. Cranley, M. N. Lokale et al., "The cardiac sympathetic co-transmitter galanin reduces acetylcholine release and vagal bradycardia: implications for neural control of cardiac excitability," *Journal of Molecular and Cellular Cardiology*, vol. 52, no. 3, pp. 667–676, 2012.

[11] M. Palkeeva, I. Studneva, A. Molokoedov et al., "Galanin/-GalR1-3 system: a promising therapeutic target for myocardial ischemia/reperfusion injury," *Biomedicine & Pharmacotherapy*, vol. 109, pp. 1556–1562, 2019.

[12] M. T. Foster and T. J. Bartness, "Sympathetic but not sensory denervation stimulates white adipocyte proliferation," *American Journal of Physiology-Regulatory, Integrative and Comparative Physiology*, vol. 291, no. 6, pp. R1630–R1637, 2006.

[13] M. A. Samuels, "The brain-heart connection," *Circulation*, vol. 116, no. 1, pp. 77–84, 2007.

[14] A. T. Mazzeo, A. Micalizzi, L. Mascia, A. Scicolone, and L. Siracusano, "Brain-heart crosstalk: the many faces of stress-related cardiomyopathy syndromes in anaesthesia and intensive care," *British Journal of Anaesthesia*, vol. 112, no. 5, pp. 803–815, 2014.

[15] Q. Wang, Z. X. Li, Y. J. Li et al., "Alterations in amino acid levels and metabolite ratio of spinal cord in rat with myocardial ischemia-reperfusion injury by proton magnetic resonance spectroscopy," *American Journal of Translational Research*, vol. 11, p. 3101, 2019.

[16] Q. Wang, Z. X. Li, Y. J. Li et al., "Identification of lncRNA and mRNA expression profiles in rat spinal cords at various time-points following cardiac ischemia/reperfusion," *International Journal of Molecular Medicine*, vol. 43, no. 6, pp. 2361–2375, 2019.

[17] S. Y. Li, Z. X. Li, Z. G. He et al., "Quantitative proteomics reveal the alterations in the spinal cord after myocardial ischemia-reperfusion injury in rats," *International Journal of Molecular Medicine*, vol. 44, no. 5, pp. 1877–1887, 2019.

[18] S. Hombach and M. Kretz, "Non-coding RNAs: classification, biology and functioning," *Advances in Experimental Medicine and Biology*, vol. 937, pp. 3–17, 2016.

[19] J. S. Mattick and I. V. Makunin, "Non-coding RNA," *Human Molecular Genetics*, vol. 15, no. 1, pp. R17–R29, 2006.

[20] C.-H. Jung, M. A. Hansen, I. V. Makunin, D. J. Korbie, and J. S. Mattick, "Identification of novel non-coding RNAs using profiles of short sequence reads from next generation sequencing data," *Genomics*, vol. 11, no. 1, 2010.

[21] B. Wang, J. Wu, Q. L. Huang et al., "Comprehensive analysis of differentially expressed lncRNA, circRNA and mRNA and their ceRNA networks in mice with severe acute pancreatitis," *Frontiers in Genetics*, vol. 12, p. 14, 2021.

[22] F. Kopp and J. T. Mendell, "Functional classification and experimental dissection of long noncoding RNAs," *Cell*, vol. 172, no. 3, pp. 393–407, 2018.

[23] M. Esteller, "Non-coding RNAs in human disease," *Nature Reviews Genetics*, vol. 12, no. 12, pp. 861–874, 2011.

[24] M. J. Picklo, "Methods of sympathetic degeneration and alteration," *Journal of the Autonomic Nervous System*, vol. 62, no. 3, pp. 111–125, 1997.

[25] P. Jiang, D. Ma, Y. Jiang et al., "Preventive effect of different compatibilities of Ramulus Cinnamomi and radix Paeomlae alba in Guizhi decoction on cardiac sympathetic denervation induced by 6-OHDA," *Chinese Journal of Integrated Traditional and Western Medicine*, vol. 36, no. 5, pp. 608–613, 2016.

[26] Q. Wang, Z. G. He, Z. X. Li et al., "Bioinformatics analysis of gene expression profile data to screen key genes involved in cardiac ischemia-reperfusion injury," *International Journal of Clinical and Experimental Medicine*, vol. 11, pp. 4955–4966, 2018.

[27] M. H. Feng, Z. X. Li, Q. Wang et al., "Neurochemical alterations of different cerebral regions in rats with myocardial ischemia-reperfusion injury based on proton nuclear magnetic spectroscopy analysis," *Aging*, vol. 13, no. 2, pp. 2294–2309, 2021.

[28] B. A. Boughton, D. L. Callahan, C. Silva et al., "Comprehensive profiling and quantitation of amine group containing metabolites," *Analytical Chemistry*, vol. 83, no. 19, pp. 7523–7530, 2011.

[29] J. Wang, L. Zhou, H. Lei et al., "Simultaneous quantification of amino metabolites in multiple metabolic pathways using ultra-high performance liquid chromatography with tandem-mass spectrometry," *Scientific Reports*, vol. 7, no. 1, 2017.

[30] L. Gu, A. D. Jones, and R. L. Last, "LC-MS/MS assay for protein amino acids and metabolically related compounds for large-scale screening of metabolic phenotypes," *Analytical Chemistry*, vol. 79, no. 21, pp. 8067–8075, 2007.

[31] K. Dettmer, P. A. Aronov, and B. D. Hammock, "Mass spectrometry-based metabolomics," *Mass Spectrometry Reviews*, vol. 26, no. 1, pp. 51–78, 2007.

[32] Y. F. Cheng, Y. T. Chang, W. H. Chen et al., "Cardioprotection induced in a mouse model of neuropathic pain via anterior nucleus of paraventricular thalamus," *Nature Communications*, vol. 8, no. 1, p. 826, 2017.

[33] S. Bohl, D. J. Medway, J. Schulz-Menger, J. E. Schneider, S. Neubauer, and C. A. Lygate, "Refined approach for quantification of in vivo ischemia-reperfusion injury in the mouse heart," *American Journal of Physiology-Heart and Circulatory Physiology*, vol. 297, no. 6, pp. H2054–H2058, 2009.

[34] X. F. Liang, Y. C. Lai, W. Z. Wu et al., "LncRNA-miRNA-mRNA expression variation profile in the urine of calcium oxalate stone patients," *BMC Medical Genomics*, vol. 12, no. 1, p. 57, 2019.

[35] J. A. Moffitt, "Role for neural growth factor in autonomically driven arrhythmogenesis? Focus on: "structural neuroplasticity following T5 spinal cord transection: increased cardiac sympathetic innervation density and SPN arborization"," *American Journal of Physiology-Regulatory, Integrative and Comparative Physiology*, vol. 299, no. 4, pp. R983–R984, 2010.

[36] H. L. Lujan, G. Palani, and S. E. DiCarlo, "Structural neuroplasticity following T5 spinal cord transection: increased cardiac sympathetic innervation density and SPN arborization," *American Journal of Physiology-Regulatory, Integrative and Comparative Physiology*, vol. 299, no. 4, pp. R985–R995, 2010.

[37] L. Fan, B. Xiang, J. Xiong, Z. He, and H. B. Xiang, "Use of viruses for interrogating viscera-specific projections in central nervous system," *Journal of Neuroscience Methods*, vol. 341, p. 108757, 2020.

[38] M. Chen, L. Yu, X. Sheng, Q. Liu, H. Jiang, and S. Zhou, "Cardiac autonomic tone modulators: promising feasible options for heart failure with hyper-sympathetic activity," *International Journal of Cardiology*, vol. 198, pp. 185-186, 2015.

[39] Y. Lai, L. Yu, and H. Jiang, "Autonomic neuromodulation for preventing and treating ventricular arrhythmias," *Frontiers in Physiology*, vol. 10, 2019.

[40] G. Meng, X. Zhou, M. Wang et al., "Gut microbe-derived metabolite trimethylamine N-oxide activates the cardiac autonomic nervous system and facilitates ischemia-induced ventricular arrhythmia via two different pathways," *eBioMedicine*, vol. 44, pp. 656–664, 2019.

[41] L. Yu, L. Zhou, G. Cao et al., "Optogenetic modulation of cardiac sympathetic nerve activity to prevent ventricular arrhythmias," *Journal of the American College of Cardiology*, vol. 70, no. 22, pp. 2778–2790, 2017.

[42] Z. X. Li, Y. J. Li, Q. Wang, Z. G. He, M. H. Feng, and H. B. Xiang, "Characterization of novel lncRNAs in upper thoracic spinal cords of rats with myocardial ischemia-reperfusion injury," *Experimental and Therapeutic Medicine*, vol. 21, p. 15, 2021.

[43] Q. Q. Liu, H. Liu, Z. G. He et al., "Differential gene and lncRNA expression in the lower thoracic spinal cord following ischemia/reperfusion-induced acute kidney injury in rats," *Oncotarget*, vol. 8, no. 32, pp. 53465–53481, 2017.

[44] B. W. Liu, Z. X. Li, Z. G. He, C. Liu, J. Xiong, and H. B. Xiang, "Altered expression of target genes of spinal cord in different itch models compared with capsaicin assessed by RT-qPCR validation," *Oncotarget*, vol. 8, no. 43, pp. 74423–74433, 2017.

[45] M. I. O. Milanez, E. E. Nishi, A. A. Rocha, C. T. Bergamaschi, and R. R. Campos, "Interaction between angiotensin II and GABA in the spinal cord regulates sympathetic vasomotor activity in Goldblatt hypertension," *Neuroscience Letters*, vol. 728, p. 134976, 2020.

[46] B. R. Bowman, P. Bokiniec, S. McMullan, A. K. Goodchild, and P. G. R. Burke, "Somatostatin 2 receptors in the spinal cord tonically restrain thermogenic, cardiac and other sympathetic outflows," *Frontiers in Neuroscience*, vol. 13, 2019.

[47] S. A. Deuchars, "How sympathetic are your spinal cord circuits?," *Experimental Physiology.*, vol. 100, no. 4, pp. 365–371, 2015.

[48] P. Pilowsky, I. J. Llewellyn-Smith, L. Arnolda, J. Minson, and J. Chalmers, "Intracellular recording from sympathetic preganglionic neurons in cat lumbar spinal cord," *Brain Research.*, vol. 656, no. 2, pp. 319–328, 1994.

[49] Y.-Y. Poon, C.-Y. Tsai, C.-D. Cheng, A. Y. W. Chang, and S. H. H. Chan, "Endogenous nitric oxide derived from NOS I or II in thoracic spinal cord exerts opposing tonic modulation on sympathetic vasomotor tone via disparate mechanisms in anesthetized rats," *American Journal of Physiology-Heart and Circulatory Physiology.*, vol. 311, no. 3, pp. H555–H562, 2016.

[50] K. C. Cowley, "A new conceptual framework for the integrated neural control of locomotor and sympathetic function: implications for exercise after spinal cord injury," *Applied Physiology Nutrition and Metabolism.*, vol. 43, no. 11, pp. 1140–1150, 2018.

[51] S. Wang, X. Zhou, B. Huang et al., "Spinal cord stimulation suppresses atrial fibrillation by inhibiting autonomic remodeling," *Heart Rhythm*, vol. 13, no. 1, pp. 274–281, 2016.

[52] X. Ding, J. L. Ardell, F. Hua et al., "Modulation of cardiac ischemia-sensitive afferent neuron signaling by preemptive C2 spinal cord stimulation: effect on substance P release from rat spinal cord," *American Journal of Physiology-Regulatory, Integrative and Comparative Physiology*, vol. I, no. 294, pp. R93–R101, 2008.

[53] S. Wang, X. Zhou, B. Huang et al., "Spinal cord stimulation protects against ventricular arrhythmias by suppressing left stellate ganglion neural activity in an acute myocardial infarction canine model," *Heart Rhythm*, vol. 12, no. 7, pp. 1628–1635, 2015.

[54] C. Zhu, P. Hanna, P. S. Rajendran, and K. Shivkumar, "Neuromodulation for ventricular tachycardia and atrial fibrillation: a clinical scenario-based review," *JACC: Clinical Electrophysiology*, vol. 5, no. 8, pp. 881–896, 2019.

[55] N. H. Waldron, M. Fudim, J. P. Mathew, and J. P. Piccini, "Neuromodulation for the treatment of heart rhythm disorders," *JACC: Basic to Translational Science*, vol. 4, no. 4, pp. 546–562, 2019.

[56] B. M. Xu, L. Xiao, C. M. Kang et al., "LncRNA AC096664.3/P-PAR-γ/ABCG1-dependent signal transduction pathway contributes to the regulation of cholesterol homeostasis," *Journal of Cellular Biochemistry*, vol. 120, no. 8, pp. 13775–13782, 2019.

[57] C. Cai, H. J. Zhu, X. T. Ning et al., "LncRNA ENST0000 0602558.1 regulates ABCG1 expression and cholesterol efflux from vascular smooth muscle cells through a p65-dependent pathway," *Atherosclerosis*, vol. 285, pp. 31–39, 2019.

[58] L. Li, L. Y. Wang, H. F. Li et al., "Characterization of LncRNA expression profile and identification of novel LncRNA biomarkers to diagnose coronary artery disease," *Atherosclerosis*, vol. 275, pp. 359–367, 2018.

[59] A. F. Gabriel and M. C. Costa, Eds.F. J. Enguita, "Interactions among regulatory non-coding RNAs involved in cardiovascular diseases," *Advances in Experimental Medicine and Biology*, A. F. Gabriel and M. C. Costa, Eds., vol. 1229, pp. 79–104, 2020.

[60] B. W. Li, Y. Z. Li, L. G. Hu et al., "Role of circular RNAs in the pathogenesis of cardiovascular disease," *Journal of Cardiovascular Translational Research*, vol. 13, no. 4, pp. 572–583, 2020.

[61] M. Y. Li, W. Ding, T. Sun et al., "Biogenesis of circular RNAs and their roles in cardiovascular development and pathology," *The FEBS Journal*, vol. 285, no. 2, pp. 220–232, 2018.

[62] Q. L. Zhou, Z. Zhang, Y. Bei, G. Li, and T. Wang, "Circular RNAs as novel biomarkers for cardiovascular diseases," in *Circular RNAs. Advances in Experimental Medicine and Biology, Vol 1087*, J. Xiao, Ed., pp. 159–170, Springer, Singapore, 2018.

[63] F. F. Li, X. Zhou, S. F. Chu, and N. H. Chen, "Inhibition of CKLF1 ameliorates hepatic ischemia-reperfusion injury via MAPK pathway," *Cytokine*, vol. 141, p. 7, 2021.

[64] X. X. Wan, K. Belanger, S. G. Widen, M. N. Kuyurncu-Martinez, and N. J. Garg, "Genes of the cGMP-PKG-Ca2+ signaling pathway are alternatively spliced in cardiomyopathy: role of RBFOX2," *Biochimica et Biophysica Acta-Molecular Basis of Disease*, vol. 1866, no. 3, p. 165620, 2020.

[65] Y. Q. Liu, S. J. Oh, K. H. Chang, Y. G. Kim, and M. Y. Lee, "Antiplatelet effect of AMP-activated protein kinase activator and its potentiation by the phosphodiesterase inhibitor dipyridamole," *Biochemical Pharmacology*, vol. 86, no. 7, pp. 914–925, 2013.

[66] S. Charles and J. Natarajan, "Two way network construction and analysis of mRNA, miRNA and lncRNA reveals critical regulators and regulatory modules in cardiovascular diseases," *Genes & Genomics*, vol. 42, no. 8, pp. 855–867, 2020.

[67] R. Kreutz, J. Ipe, K. Kassab et al., "P741 next generation miRNA sequencing and changes in coagulation measured by thrombelastography (TEG) in patients with cardiovascular disease," *European Heart Journal*, vol. 40, no. 1, pp. 346–346, 2019.

[68] W. Zhu, H. L. Wang, G. C. Sartor et al., "RNA sequencing analyses reveal eight miRNA/mRNA pairs that may mediate the effects of cocaine in cardiovascular diseases," *Circulation*, vol. 134, 2016.

[69] G. Wang, X. Fang, M. Han, X. Wang, and Q. Huang, "MicroRNA-493-5p promotes apoptosis and suppresses proliferation and invasion in liver cancer cells by targeting VAMP2," *International Journal of Molecular Medicine*, vol. 41, no. 3, pp. 1740–1748, 2018.

[70] T. Harel-Adar, T. Ben Mordechai, Y. Amsalem, M. S. Feinberg, J. Leor, and S. Cohen, "Modulation of cardiac macrophages by phosphatidylserine-presenting liposomes improves infarct repair," *Proceedings of the National Academy of Sciences of the United States of America*, vol. 108, no. 5, pp. 1827–1832, 2011.

[71] J. H. Rosenberg, J. H. Werner, M. J. Moulton, and D. K. Agrawal, "Current modalities and mechanisms underlying

cardioprotection by ischemic conditioning," *Journal of Cardiovascular Translational Research*, vol. 11, no. 4, pp. 292–307, 2018.

[72] B. Z. Simkhovich, K. Przyklenk, and R. A. Kloner, "Role of protein kinase C in ischemic "conditioning": from first evidence to current perspectives," *Journal of Cardiovascular Pharmacology and Therapeutics*, vol. 18, no. 6, pp. 525–532, 2013.

[73] R. Gupta, L. Liu, X. Zhang et al., "IL-10 provides cardioprotection in diabetic myocardial infarction via upregulation of Heme clearance pathways," *Insight*, vol. 5, no. 17, 2020.

[74] D. Schumacher, A. Curaj, M. Staudt et al., "Phosphatidylserine supplementation as a novel strategy for reducing myocardial infarct size and preventing adverse left ventricular remodeling," *International Journal of Molecular Sciences*, vol. 22, no. 9, p. 4401, 2021.

[75] M. Bujak, M. Dobaczewski, C. Gonzalez-Quesada et al., "Induction of the CXC chemokine interferon-gamma-inducible protein 10 regulates the reparative response following myocardial infarction," *Circulation Research*, vol. 105, no. 10, pp. 973–983, 2009.

[76] M. Cavalera and N. G. Frangogiannis, "Targeting the chemokines in cardiac repair," *Current Pharmaceutical Design*, vol. 20, no. 12, pp. 1971–1979, 2014.

[77] B. Chen and N. G. Frangogiannis, "Chemokines in myocardial infarction," *Journal of Cardiovascular Translational Research*, vol. 14, no. 1, pp. 35–52, 2021.

[78] W. Xian, J. Wu, Q. Li et al., "CXCR3 alleviates renal ischemia-reperfusion injury via increase of Tregs," *Molecular Medicine Reports*, vol. 24, no. 1, 2021.

[79] X. Jiang, X. Wu, F. Chen et al., "The profiles and networks of miRNA, lncRNA, mRNA, and circRNA in benzo(a)pyrene-transformed bronchial epithelial cells," *Journal of Toxicological Sciences*, vol. 43, no. 4, pp. 281–289, 2018.

[80] Q. Xu, X. Jia, Q. Wu et al., "Esomeprazole affects the proliferation, metastasis, apoptosis and chemosensitivity of gastric cancer cells by regulating lncRNA/circRNA-miRNA-mRNA ceRNA networks," *Oncology Letters*, vol. 20, 2020.

[81] K. Hu, C. He, X. Sun et al., "Integrated study of circRNA, lncRNA, miRNA, and mRNA networks in mediating the effects of testicular heat exposure," *Cell and Tissue Research*, p. 2021, 2021.

[82] Y. Cheng, Y. Su, S. Wang et al., "Identification of circRNA-lncRNA-miRNA-mRNA competitive endogenous RNA network as novel prognostic markers for acute myeloid leukemia," *Genes*, vol. 11, no. 8, p. 868, 2020.

[83] C. Li, Z. Wang, J. Zhang et al., "Crosstalk of mRNA, miRNA, lncRNA, and circRNA and their regulatory pattern in pulmonary fibrosis," *Molecular Therapy-Nucleic Acids*, vol. 18, pp. 204–218, 2019.

[84] Y. Huang, "The novel regulatory role of lncRNA-miRNA-mRNA axis in cardiovascular diseases," *Journal of Cellular and Molecular Medicine*, vol. 22, no. 12, pp. 5768–5775, 2018.

[85] M. Li, L. W. Duan, Y. X. Li, and B. Liu, "Long noncoding RNA/circular noncoding RNA-miRNA-mRNA axes in cardiovascular diseases," *Life Sciences*, vol. 233, p. 116440, 2019.

[86] W. Xiong, M. R. Yao, Y. Q. Yang, Y. Qu, and J. Q. Qian, "Implication of regulatory networks of long noncoding RNA/circular RNA-miRNA-mRNA in diabetic cardiovascular diseases," *Epigenomics*, vol. 12, no. 21, pp. 1929–1947, 2020.

[87] J. Wang, J. Yin, X. Wang et al., "Changing expression profiles of mRNA, lncRNA, circRNA, and miRNA in lung tissue reveal the pathophysiological of bronchopulmonary dysplasia (BPD) in mouse model," *Journal of Cellular Biochemistry*, vol. 120, no. 6, pp. 9369–9380, 2019.

Research Article

SRC-3 Knockout Attenuates Myocardial Injury Induced by Chronic Intermittent Hypoxia in Mice

Wanyu Wang ,[1] Hongbo Gu ,[2] Weihua Li ,[3] Yihua Lin ,[1] Xiangyang Yao ,[4] Wen Luo ,[1] Fang Lu ,[1] Shenhui Huang ,[1] Yonghong Shi ,[1] and Zhengrong Huang [3]

[1]*Department of Pulmonary and Critical Care Medicine of the First Affiliated Hospital of XiaMen University, The Third Clinical Medical College of Fujian Medical University, Teaching Hospital of Fujian Medical University, Xiamen, China*
[2]*Department of Cardiology, Affiliated Hospital of Weifang Medical University, Weifang, China*
[3]*Department of Cardiology, Xiamen Key Laboratory of Cardiac Electrophysiology, Xiamen Institute of Cardiovascular Diseases, the First Affiliated Hospital of Xiamen University, School of Medicine, Xiamen University, Xiamen, China*
[4]*Department of Pulmonary Diseases of Xinglin branch of the First Affiliated Hospital of Xiamen University, Xiamen City, China*

Correspondence should be addressed to Yonghong Shi; shiyonghxm@163.com
and Zhengrong Huang; huangzhengrong@xmu.edu.cn

This study investigated the effects of chronic intermittent hypoxia (CIH), a model of sleep apnea syndrome (SAS), on cardiac function. SRC-3 was extremely lowly expressed in the adult mouse heart tissue, while SRC-3 was highly expressed in the adult mouse heart tissue after CIH, suggesting that SRC-3 is involved in CIH model. We further studied the role of SRC-3 in CIH-induced myocardial injury in mice. Twenty-four healthy Balb/c male mice ($n = 16$, wild type; $n = 8$, SRC-3 knockout (SRC3-KO)) were randomly divided into three groups: air control (Ctrl), CIH, and CIH+SRC3-KO. Mice were exposed to CIH for 12 weeks. qRT-PCR was used to evaluate cardiac expression of the following genes: 11HSD1, 11HSD2, GR, MR, COX-2, OPN, NOX2, HIF-1-α, IL-1β, IL-6, iNOS, TNF-α, PC-1, and TGF-β. Enzymatic levels of SOD, CAT, MDA, NOS, and NO in the mouse hearts were determined using commercially available kits. Immunohistochemistry (IHC) was used to evaluate NF-κB expression in cardiac tissues. A transmission electron microscope (TEM) was used to evaluate myocardial ultrastructure. TUNEL staining was used to assess myocardial cell apoptosis. CIH induced cardiac damage, which was ameliorated in the SRC-3 KO mice. CIH significantly increased the heart-to-body weight ratio, expression of all aforementioned genes except 11HSD1, GR, and MR, and increased the levels of MDA, NOS, NO, and NF-κB, which were attenuated in the SRC-3 KO mice. The CIH group had the lowest SOD and CAT levels, which were partially recovered in the CIH+SRC3-KO group. 11HSD2 gene expression was elevated in both the CIH and CIH+SRC3-KO groups compared to the Ctrl group. The CIH group had severe myocardial cell apoptosis and mitochondrial dysfunction, which were alleviated in the CIH+SRC3-KO group. CIH causes cardiac damage through inducing oxidative stress and inflammation. Knockout of SRC-3 ameliorates CIH-induced cardiac damage through antagonizing CIH-triggered molecular changes in cardiac tissue.

1. Introduction

Sleep apnea syndrome (SAS) is prevalent in the general population and associated with cardiovascular diseases (CVDs) [1]. Chronic intermittent hypoxia (CIH) is a distinct pathophysiological feature of SAS and contributes to the development of SAS-associated CVDs [2]. CIH induces myocardial damage mainly through increasing oxidative stress and inflammation [3, 4], ultimately leading to CVD [5]. It should be noted that there is a positive feedback loop between oxidative stress and inflammation. Reactive oxygen species (ROS) induced by CIH activate hypoxia inducible fator-1α (HIF-1α), which in turn promotes sustained oxidative stress, further exacerbating myocardial inflammation [6] and

consequently resulting in myocardial damage, atherosclerosis, and hypertension. CIH was also shown to increase vascular endothelial growth factor (VEGF) and endothelin-1 (ET-1) expression through HIF-1α, a pathophysiological process that may play an important role in the pathogenesis of SAS and cardiovascular damage [7]. Given that ROS, HIF-1α, and nuclear factor-κB (NF-κB) play a pivotal role in CIH-induced myocardial injury [6–8], it is critical to attenuate oxidative stress and inflammation to protect against CIH-induced myocardial injury.

Steroid receptor coactivator-3 (SRC-3) is a member of the p160 steroid receptor coactivator family and a coactivator of nuclear receptors (NR) and some transcription factors. The mineralocorticoid receptor (MR), as a member of the NR superfamily, binds to aldosterone and triggers oxidative stress and inflammation, eventually resulting in myocardial remodeling, fibrosis, and heart failure [9]. In recent years, SRC-3 has also been found to be involved in a variety of signal transduction pathways. For instance, SRC-3 overexpression promotes glycolysis in bladder cancer cells through activating HIF-1α [10]. SRC-3 has also been shown to promote inflammation by activating NF-κB signaling pathways and promoting CXCL2 (CXC chemokine ligands 2) expression, thereby recruiting neutrophils [11]. SRC-3 deletion reduces NF-κB nuclear translocation by inhibiting downregulation of IκB-α (inhibitor of NF-κB) levels in the early stages of inflammation, resulting in decreased expression of inflammatory factors including tumor necrosis factor-α (TNF-α), interleukin- (IL-) 2, IL-6, IL-8, and inducible nitric oxide synthase (iNOS) [12]. SRC-3 can also be recruited to the promoters of HIF-1α target genes. Given that HIF-1α is an important transcription factor involved in oxidative stress and that many of its downstream targets are closely related to CVDs, we postulate that SRC-3 contributes to the pathogenesis of CVDs through activating HIF-1α and NF-κB, as well as promoting oxidative stress and inflammation.

In the present study, we investigated the mechanisms underlying CIH-induced myocardial injury and the involvement of SRC-3 in this pathology. We also explored the molecular basis related to SRC-3 function. We hypothesized that knockout of SRC-3 may protect the heart from CIH-induced damage by suppressing oxidative stress and inflammation.

2. Materials and Methods

2.1. Reagents. The following reagents were purchased from Roche: FastStart Universal SYBR Green Master ROX (2×) kit (Roche Cat# 4913914001), Tripure isolation reagent (Cat# 11667165001), FastStart Universal SYBR Master (Cat# 04913850001), and In Situ Cell Death Detection Kit (Cat# 11684817910). The ReverTra Ace quantitative real-time polymerase chain reaction (qPCR RT) kit was obtained from TOYOBO (Cat# FSQ-101). The Animal Total RNA Rapid Extraction Kit was from JieRui (Cat# GK3016). The RevertAid First Strand cDNA Synthesis Kit (K1622) was from Thermo Scientific (Cat# 1622). The following measurement kits were purchased from Nanjing Jiancheng Bioengi-

neering Institute: superoxide dismutase (SOD) (Cat# A001-1), catalase (CAT) (Cat# A007-1), malondialdehyde (MDA) (Cat# A003-1), nitric oxide synthase (NOS) (Cat# A014-2), and NO (Cat# A012). Rabbit-anti-mouse NF-κB antibody was from Abcam (Cat# Ab32536). The immuno-histochemistry (IHC) and enhanced DAB chromogenic kits were obtained from Mai Xin.

2.2. SRC-3 Knockout (KO) Mice and Generation of the CIH Mouse Model. The animal protocol was approved by the Laboratory Animal Ethics Committee of the First Affiliated Hospital of Xiamen University. All methods were performed in accordance with ethical guidelines and regulations. This study was carried out in compliance with the ARRIVE guidelines. SPF grade SRC-3 KO mice on a Balb/c genetic background were generated at Baylor College of Medicine in the United States and donated by professor Chundong Yu, Life Sciences College, Xiamen University. SRC-3 KO mice were genotyped using PCR with the following oligos as previously described [13]: P76 5′GATGAGTGGACTAG GCGAAAGCT3′, P77 5′GCTGAGATTTGCAGAGATG AGTCC3′, and P78 5′GGCGATTAAGTTGGGTAACGC CAG3′.

A total of 24 SPF grade male mice, including 16 Balb/c wild type (WT) and 8 SRC3-KO (age, 8 to 10 weeks; body weight, 18~25 g) were divided into three groups: control (Ctrl), CIH, and CIH+SRC3-KO.

The CIH model was generated using an intermittent hypoxia system as described in our previous work [5, 7]. Mice in the CIH and CIH+SRC3-KO groups were placed in the CIH system. The Ctrl group underwent the same procedure as the other groups, except that these mice received only air.

In the CIH and CIH+SRC3-KO groups, CIH lasted for 8 h/day from 9:00-17:00 h for a duration of 12 weeks. All mice were anesthetized by intraperitoneal administration of 3% phenobarbital (30 mg/kg), perfused through the left ventricle with cold 100 mM phosphate buffer (pH 7.4). A small part of the apex of the heart was cut into small pieces within 1 mm cubes for transmission electron microscope (TEM) observation. A part of the heart was stored at −80°C for subsequent Western blot and qRT-PCR analyses. The remaining part of the heart was fixed in 10% neutral buffered formalin, stored in 70% ethanol, embedded in paraffin, and sectioned for subsequent histochemical assays.

2.3. Western Blot Analysis. Western blot analysis was performed on protein lysates purified from mouse hearts. Briefly, hearts were homogenized and lysates were purified in radioimmunoprecipitation assay (RIPA) buffer containing 1 mM phenylmethane sulfonylfluoride and a proteinase inhibitor cocktail (Roche). Protein concentrations were determined using a BCA protein quantification kit (Thermo). Equal amounts of total protein from each heart were separated using SDS-PAGE and transferred onto PVDF membranes (Millipore). The membranes were then immersed in 5% nonfat milk for 1 h and probed overnight with diluted primary antibodies against SRC-3 (1 : 1,000; Cell signaling) at 4°C. The membranes were then incubated with

the appropriate HRP-conjugated antibody at room temperature for 2 h. Protein bands were visualized using an ECL reagent (Bio-Rad). GAPDH (Santa Cruz) was used as an internal control. The intensity of the specific band was quantified using ImageJ software and normalized to GAPDH.

2.4. qRT-PCR. qRT-PCR was performed to detect cardiac expression of the following genes: 11 beta-hydroxysteroid dehydrogenase type 1 and type 2 (11HSD1 and 11HSD2), glucocorticoid receptor (GR), MR, cyclooxygenase-2 (COX-2), osteopontin (OPN), NAPDH oxidase 2 (NOX2), HIF-1α, IL-1β, IL-6, iNOS, TNF-α, proprotein convertase 1 (PC-1), and transforming growth factor-β (TGF-β). Briefly, total RNAs were purified from mouse hearts of each group ($n = 8$ per group) using the Animal Total RNA Rapid Extraction Kit, and cDNA Synthesis was performed using the RevertAid First Strand cDNA Synthesis Kit. PCR was performed in a 20 μL mixture consisting of 10 μL of FastStart Universal SYBR Master, 2 μL of Primer mix, and 8 μL of template. GAPDH was used for normalization. Premier 5.0 software was used to design primers which were synthesized by Takara Bio Inc. (Takara, Japan). The primer sequences are listed in Table 1.

2.5. Measurement of Myocardial Enzymes. Total protein concentration in mouse myocardial homogenates was determined using the BCA protein quantification kit. SOD activity was measured using the xanthine oxidase method (hydroxylamine method). Malondialdehyde (MDA) was analyzed using the thiobarbituric acid method. NOS was measured using a colorimetry method. NO was detected using the nitrate reductase method. Catalase (CAT) was detected using the visible light method. The above methods were carried out according to the manufacturers' instructions.

2.6. IHC. IHC (The PV9001/DAB two-stage method) was used to determine NF-κB cardiac expression. NF-κB-positive cells were detected by pale yellow or brown staining. The average optical density values were calculated using IPP6.0 software.

2.7. TEM. Heart samples were fixed with 2% glutaraldehyde in 0.1 M phosphate-buffered saline (PBS) at 4°C overnight, followed by another fix with 0.5% potassium ferricyanide and 2% osmium tetroxide in 25 mM cacodylate buffer at 22°C. Samples were then dehydrated, infiltrated, and embedded in Spurr's resin. Sections were prepared at a thickness of 70 nm, poststained with lead citrate and uranyl acetate, and viewed under a JEM-2100HC TEM with a charge-coupled device camera (Japan Electronics Co., Ltd.). Images were captured at magnifications of 10,000~40,000.

2.8. TUNEL Assay. The In Situ Cell Death Detection Kit (Roche, POD, Cat# 11684817910) was used for TUNEL staining according to the instructions. Ten fields (×400) were randomly selected and scored, and the percentage of TUNEL-positive cells was determined by dividing the number of positively stained nuclei by the number of total nuclei in the field.

TABLE 1: qRT-PCR primer sequences.

Primer name	Primer sequence (5′-3′)
MusTNF-F	CACAGAAAGCATGATCCGCG
MusTNF-R	ACTGATGAGAGGGAGGCCAT
MusIL-1β-F	GCAGTGGTTCGAGGCCTAAT
MusIL-1β-R	GCTGCGAGATTTGAAGCTGG
MusIL-6-F	AGCCAGAGTCCTTCAGAGAGA
MusIL-6-R	GGATGGTCTTGGTCCTTAGCC
MusiNOS-F	AGAATCCCTGGACAAGCTGC
MusiNOS-R	TTGTCTCTGGGTCCTCTGGT
MusCOX-2-F	TCCCCATTAGCAGCCAGTTG
MusCOX-2-R	TGCTCATACATTCCCCACGG
MusNOX2-F	GGGAACTGGGCTGTGAATGA
MusNOX2-R	CTGGCAGCAGGATCAGCATA
MusHIF-1α-F	TCATCAGTTGCCACTTCCCC
MusHIF-1α-R	TGTAAACCATGTCGCCGTCA
MusPC-1-F	CCAGCCGCAAAGAGTCTACA
MusPC-1-R	GGGTTTCCACGTCTCACCAT
MusTGF-β-F	CACCTTTGCCGAGGGTTCC
MusTGF-β-R	GTTTCACCAGCTCCATGTCG
Mus11HSD1-F	GTGTCTCGCTGCCTTGAAC
Mus11HSD1-R	ACCTCCATGACTCTTCGCAC
Mus11HSD2-F	TGACCAAGGCAGAGGACATC
Mus11HSD2-R	ACTGGAGACAGTTCCACGTC
MusOPN-F	TCTCAGAAGCAGAATCTCCTTGC
MusOPN-R	ATGTGGTCATGGCTTTCATTGG
MusGR-F	GGGGCTATGAACTTCGCAGG
MusGR-R	CTTCATCGGAGCACACCAGG
MusMR-F	TGAGTTCCTTTCCGCCTGTC
MusMR-R	CTCATCTCCACACACCAAGCAG
MusGAPDH-F	AGGCCGGTGCTGAGTATGTC
MusGAPDH-R	TGCCTGCTTCACCACCTTCT

2.9. Statistical Analysis. Data are presented as the means ± standard deviation (SD). Data from multiple groups were compared with ANOVA followed by the Bonferroni post hoc test. A p value less than 0.05 was considered significant. Statistical analyses were performed using SPSS 20.0 and GraphPad Prism software.

3. Results

3.1. SRC-3 KO Ameliorated CIH-Induced Cardiac Hypertrophy. To examine the role of SRC-3 in CIH-induced cardiac hypertrophy, we first determined if CIH altered the expression of SRC-3 in mouse hearts. As shown in Figure 1(a), Western blot analysis revealed that CIH mice exhibited significantly higher cardiac SRC-3 expression compared to Ctrl mice. As expected, CIH induced cardiac hypertrophy as evaluated by the heart weight/body weight ratio (Figure 1(b), ****$p < 0.0001$ vs. Ctrl), which was significantly attenuated in the SRC-3 KO mice (Figure 1(b), *$p < 0.05$ *vs.* CIH). These findings indicate that CIH

(a)

(b)
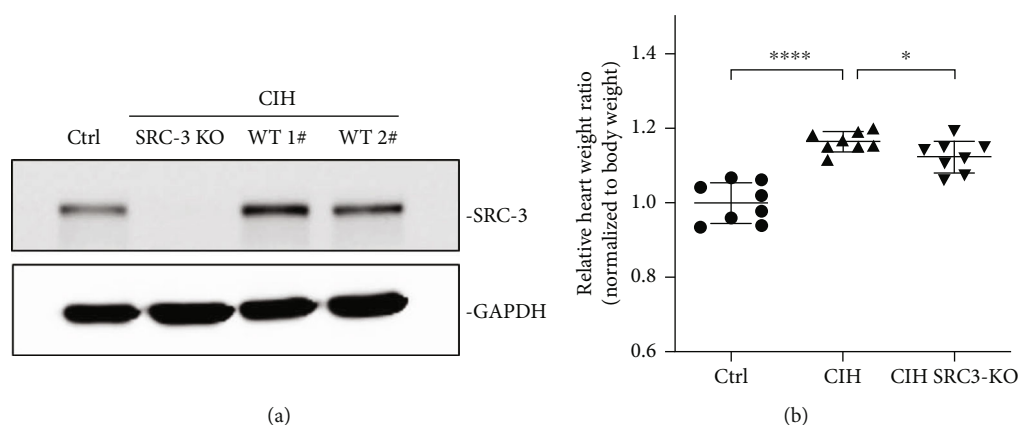
FIGURE 1: SRC-3 KO ameliorated CIH-induced cardiac hypertrophy. (a). Western blot analysis was used to evaluate the expression of SRC-3 in the mouse hearts from the three groups. GAPDH served as an internal control. (b) Heart weight/body weight ratios of mice were calculated. $N = 8$ per group. $^{****}p < 0.0001$, $^{*}p < 0.05$. Data are expressed as the means ± SD.

(a)

(b)
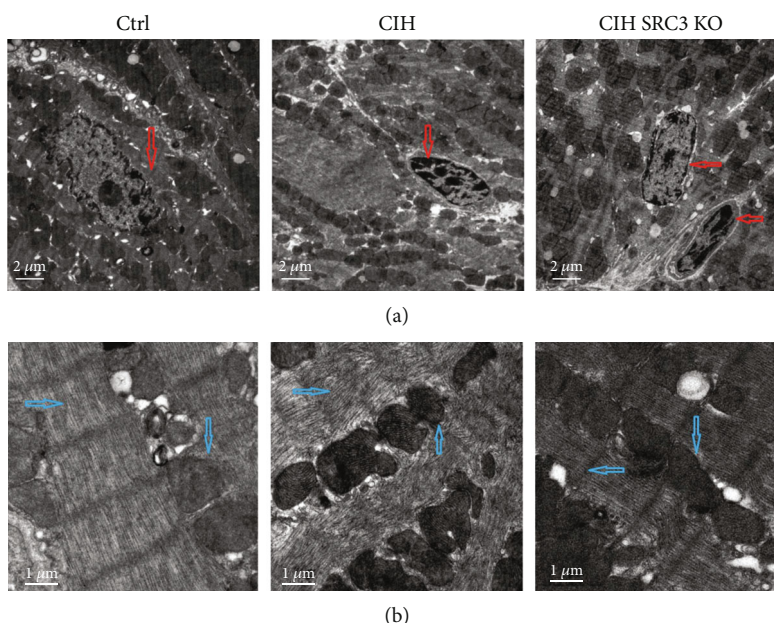
FIGURE 2: SRC-3 KO ameliorated CIH-induced myocardial pathological changes. (a) Pathological changes in myocardial cell nuclei in mice from the three groups were assessed using TEM. Red arrows point to the myocardial cell apoptosis in the CIH and CIH+SRC3-KO groups, while normal in the Ctrl group. Magnification: 10,000x, scale bar, $2\,\mu$m. (b) Pathological changes in myocardial cell mitochondria and myonemes in mice from the three groups were assessed using TEM. Blue arrows point to the mitochondria structure, mitochondrial matrix, and coarse and fine filaments in three groups. Magnification: 40,000x; scale bar, $1\,\mu$m.

increases myocardial SRC-3 expression and that SRC-3 ablation protects the heart against CIH-induced cardiac hypertrophy.

3.2. SRC-3 KO Ameliorated CIH-Induced Pathological Changes in Cardiac Tissues. We evaluated the pathological changes in the apical myocardium of mice using TEM. As expected, Ctrl mice had uniform chromatin in the myocardial nuclei and intact nuclear membranes (Figure 2(a)). However, the CIH group had pyknotic nuclei, disrupted nucleoli, and heterochromatin clustered in the perinuclear region. Analysis showed myocardial cell apoptosis in all CIH mouse hearts examined ($n = 8$). In the CIH+SRC3-

KO group, the chromatin of the myocardial nuclei was mostly uniform and the nuclear membranes were intact, but some cardiomyocyte apoptosis was indicated by nuclear consolidation and nucleolus dissolution and disappearance. In addition, heterochromatin clusters around the nucleus were detected in 2 of the 8 CIH+SRC3-KO hearts (Figure 2(a)). These data suggest that SRC-3-KO alleviates the cardiac pathological changes induced by CIH.

Myocardial mitochondria and filaments were also evaluated using TEM. In the Ctrl mouse hearts, the mitochondria had a normal structure with intact membranes. The mitochondrial cristae were arranged in parallel and abundant in number. The electron density of the mitochondrial matrix

(a)

(b)

(c)

(d)

(e)
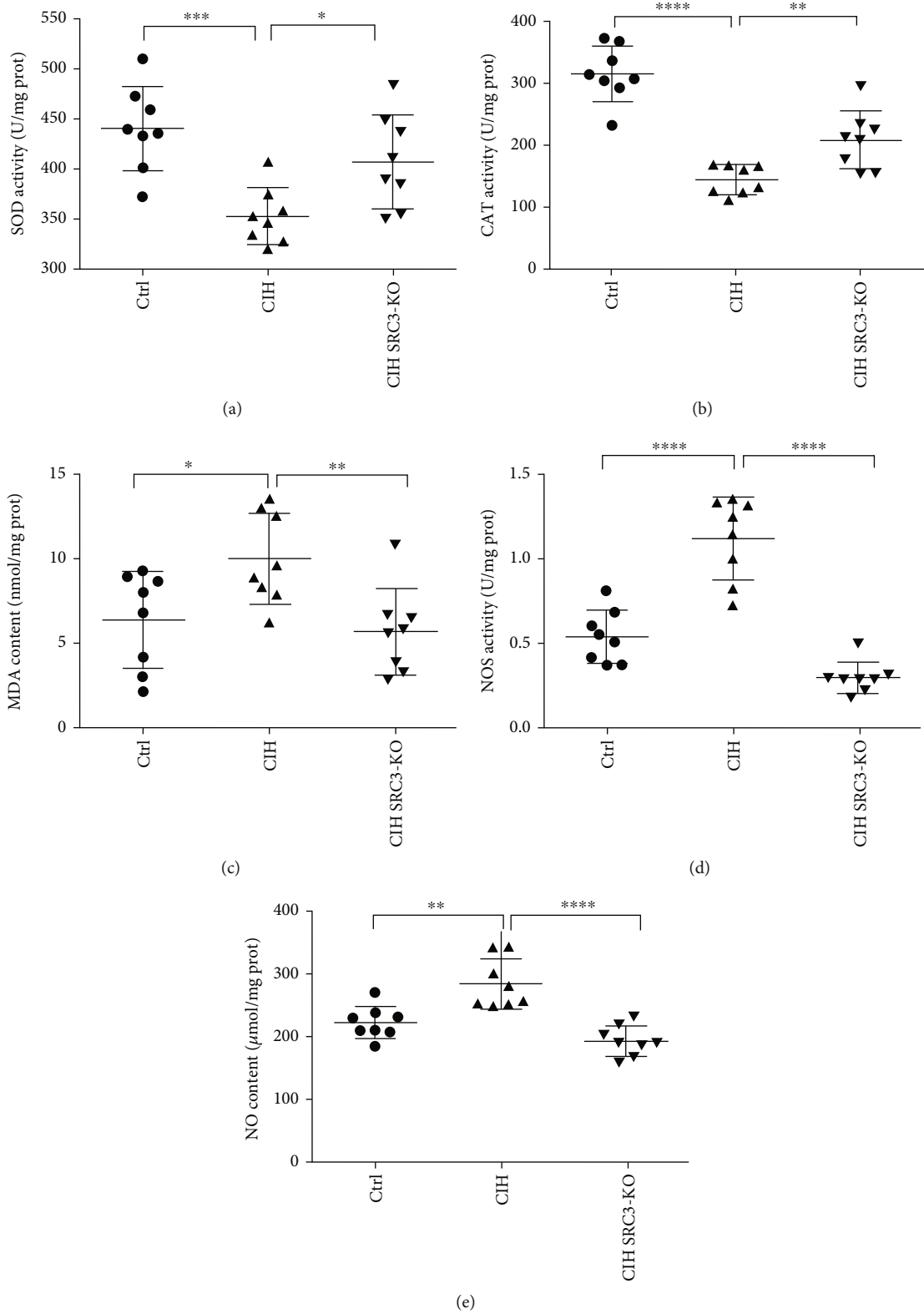
FIGURE 3: SRC-3 KO attenuated CIH-induced changes in level of oxidative stress-related enzymes in cardiac tissues. Assays were performed to measure the levels of the following enzymes in the mouse hearts from the three groups: SOD (***$p < 0.001$, *$p < 0.05$), CAT (****$p < 0.0001$, **$p < 0.01$), MDA (*$p < 0.05$, **$p < 0.01$), and NOS (****$p < 0.0001$). Myocardial NO levels were also measured (**$p < 0.01$, ****$p < 0.0001$). Data are expressed as the means ± SD. $N = 8$ per group.

(a)

(b)

(c)

(d)

(e)

(f)

(g)

(h)

FIGURE 4: Continued.

(i)

(j)

(k)

(l)

(m)

(n)
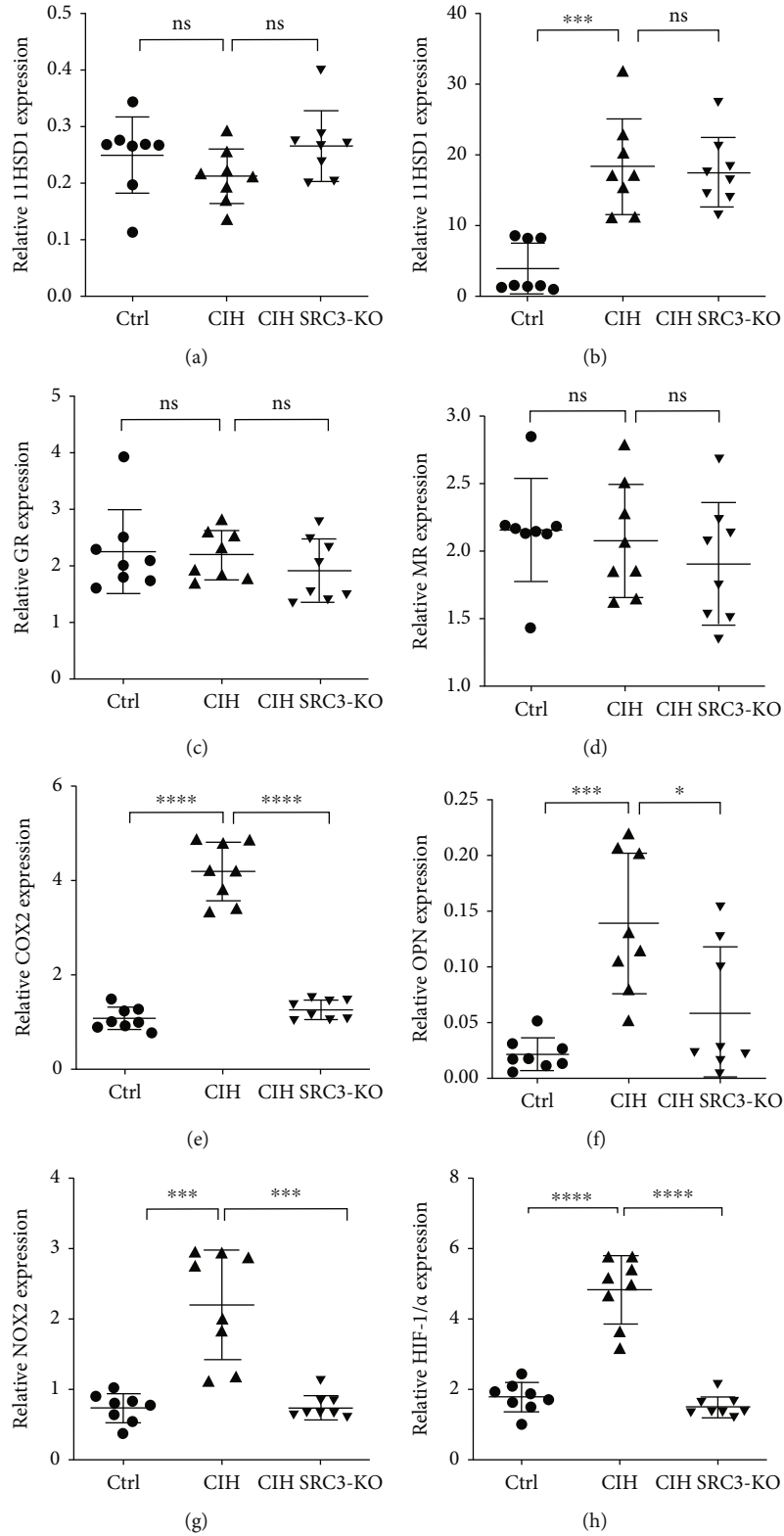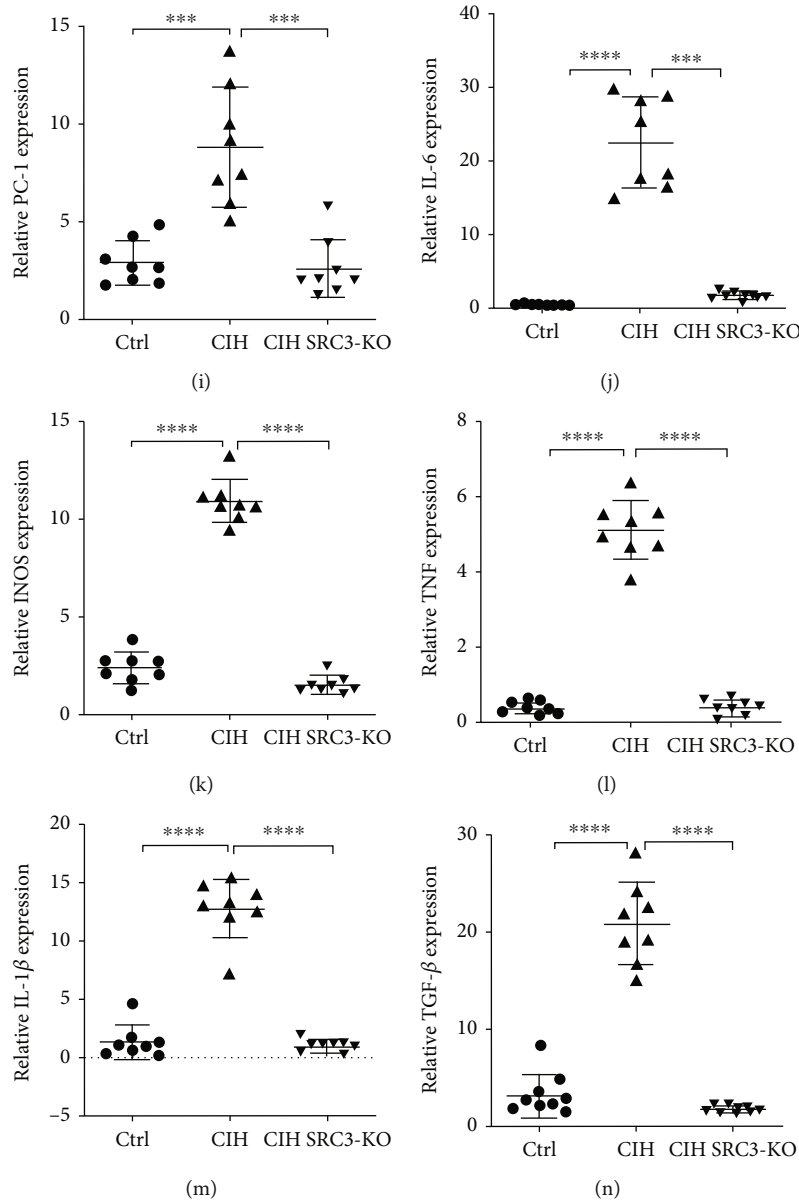
Figure 4: SRC-3 KO attenuated CIH-induced changes in transcription of inflammatory and fibrotic genes in cardiac tissues. qRT-PCR was performed to evaluate the transcription of the following inflammatory and fibrotic genes in the mouse hearts from the three groups: 11HSD1, 11HSD2, GR, MR, COX-2, OPN, NOX2, HIF-1α, IL-1β, IL-6, iNOS, TNF, PC-1, and TGF-β. GAPDH served as an internal control. ns: no significant difference. $^*p < 0.05$, $^{***}p < 0.001$, $^{****}p < 00001$. Data are expressed as the means $\pm$ SD. $N = 8$ per group.

was normal, and the coarse and fine filaments were well arranged, with clearly visible bands and Z lines (Figure 2(b)). However, in the CIH mouse hearts, the following mitochondrial effects were observed: the number of mitochondria decreased; sizes were abnormal and variable; shapes were malformed; some mitochondrial membranes were incomplete; cristae were reduced in number and were broken, dissolved, destroyed, flocculent, with widening gaps, and disordered; and the electron density of the mitochondrial matrix was increased. The coarse and fine filaments were loosely arranged and disordered, focally dissolved, the light and dark bands blurred, and the Z line disappeared, all of which were observed in the CIH hearts ($n = 8$)

(Figure 2(b)). The ultrastructural changes in the mitochondria and myoneme in the CIH+SRC3-KO mouse hearts were similar to the Ctrl mouse hearts, in which the Z lines were still visible and there were few necrotic foci observed in the mitochondria.

3.3. SRC-3 KO Attenuated CIH-Induced Changes in Levels of Oxidative Stress-Related Enzymes. We next examined whether CIH altered the levels of oxidative stress-related enzymes and the role of SRC-3 KO in mediating these changes. As shown in Figure 3, CIH significantly reduced the activity of SOD and CAT but increased the levels of MDA and iNOS. CIH also increased the levels of NO

(a)

(b)
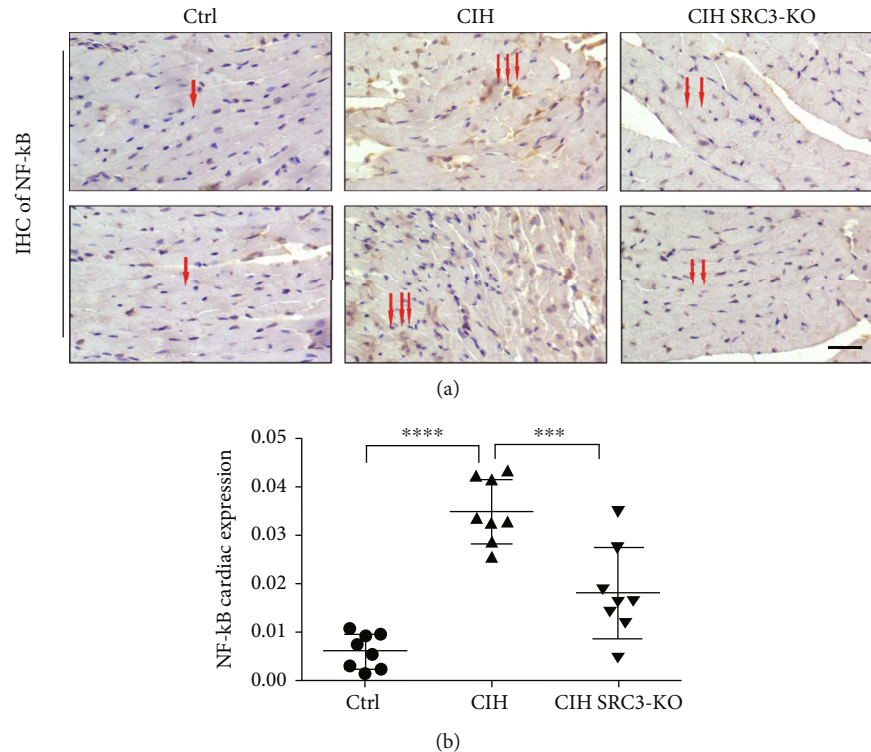
FIGURE 5: SRC-3 KO attenuated CIH-induced increases in NF-κB cardiac expression. (a) IHC was performed to evaluate myocardial expression of NF-κB in mice from the three groups. Yellow or brown staining indicates positive NF-κB expression. Red arrows point to the NF-κB staining in myocardial cells of mice. (b) The statistical analysis of (a). $^{***}p < 0.001$, $^{****}p < 00001$. Magnification: 400x; scale bar, 50 μm.

compared with the Ctrl mice. All of these changes were attenuated in the SRC-3 KO mice.

3.4. SRC-3 KO Attenuated CIH-Induced Transcription of Inflammatory and Fibrotic Genes.
We next examined whether SRC-3 KO affected transcription of steroid hormones, inflammatory markers, and fibrotic genes induced by CIH using qRT-PCR. We measured expression of the following genes: 11HSD1, GR, MR, 11HSD2, COX-2, OPN, NOX2, HIF-1α, IL-1β, iNOS, TNF, PC-1, and TGF-β. As shown in Figure 4, CIH did not induce any significant changes in the expression of 11HSD1, GR, and MR, but it substantially increased the expression of all of the other genes. With the exception of 11HSD2, CIH-induced increases in gene transcription were significantly attenuated in the SRC-3 KO mice. These findings suggest that CIH-induced changes in the transcription of cardiac inflammatory and fibrotic genes are mediated in part through SRC-3.

3.5. SRC-3 KO Attenuated CIH-Increased NF-κB Expression.
We next evaluated the effect of CIH on the expression of NF-κB, a critical transcriptional regulator of proinflammatory genes [14], in the mouse hearts using IHC. The CIH mice had significantly higher NF-κB expression than the Ctrl mice, which was attenuated in the SRC-3 KO mice (Figures 5(a) and 5(b)).

3.6. SRC-3 KO Reduced CIH-Induced Myocardial Apoptosis.
We assessed myocardial cell apoptosis using the TUNEL

assay. As shown in Figures 6(a) and 6(b), the CIH group had the highest apoptotic rate among the three groups ($^{****}p < 0.0001$), while the SRC-3 KO group had significantly reduced cardiomyocyte apoptosis ($^{****}p < 0.0001$).

4. Discussion

SAS is closely linked to the development of CVDs, and CIH plays an important role in this process. We used an SRC-3 loss of function model to investigate the role of SRC-3 in CIH-induced cardiac injury in mice. In our previous study, we have created a CIH system that mimics severe SAS [7, 15] demonstrating that no carbon dioxide accumulated.

The major findings from this study include the following: (1) SRC-3 expression was increased in mouse hearts subjected to CIH, (2) SRC-3 KO ameliorated CIH-induced pathological changes, including cardiac hypertrophy, and (3) mechanistically, SRC-3 KO attenuated CIH-induced apoptosis and changes in the activity of a number of oxidative stress-related enzymes and inflammatory genes in the mouse hearts.

It is well known that steroid hormones, including GR and MR, not only regulate electrolyte homeostasis but also play an important role in cardiovascular pathologies, such as myocardial remodeling [16, 17]. Interestingly, we found that CIH did not significantly affect the expression of GR and MR in the mouse hearts, nor did we observe any significant changes in 11HSD1 expression. However, CIH did affect 11HSD2 expression. 11HSD1 converts 11-

(a)

(b)
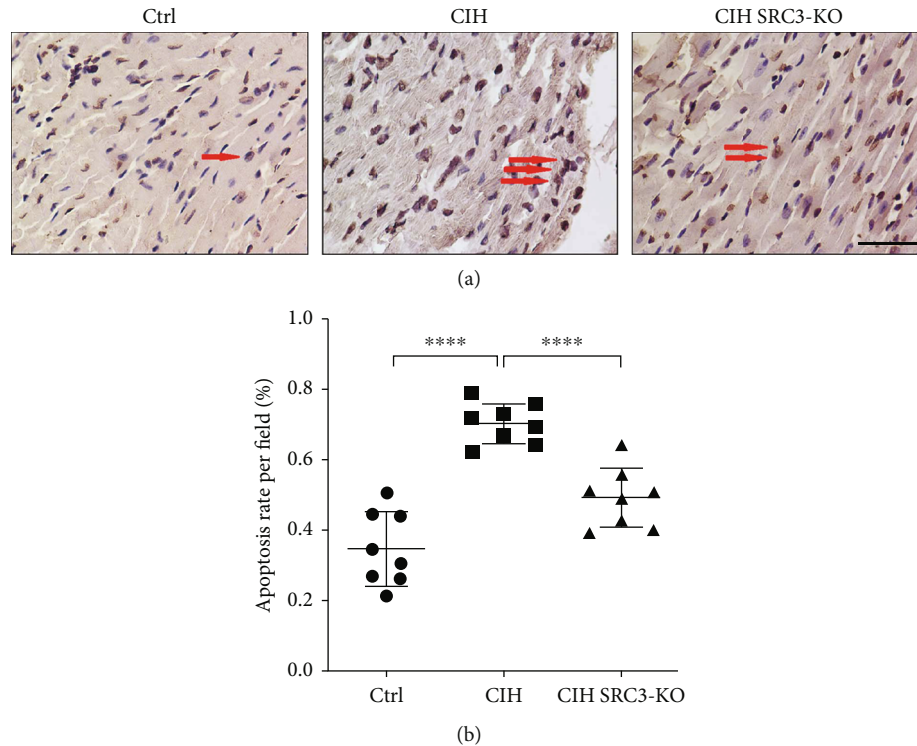
Figure 6: SRC-3 KO reduced CIH-induced myocardial apoptosis. (a) TUNEL staining was performed to assess myocardial cell apoptosis in mice from the three groups. Red arrows point to the myocardial cell apoptosis in mice. Data are expressed as the means ± SD. The CIH group exhibited the highest apoptosis rate compared to the other two experimental groups. (b) Quantification of (a). $^{****}p < 0.0001$. Magnification: 400x; scale bar, 100 μm. $N = 8$ per group.

oxo derivatives back to active glucocorticoids [18], which increases the local concentration of glucocorticoids, while 11HSD2 converts corticosterone and cortisol to their biologically inactive 11-oxo derivatives that have low affinity for MR [19]. MR mainly binds to aldosterone to induce its activation. Upregulation of 11HSD2 expression may contribute to mineralocorticoid-induced myocardial hypertrophy and remodeling [20], consistent with our finding.

Here, we found that transcription of the proinflammatory markers COX-2 and OPN was increased in the CIH-treated mouse hearts, which correlated with increased expression of the inflammatory and apoptosis marker NF-κB in the hearts of mice subjected to CIH. It has been well documented that apoptosis contributes to the pathogenesis of a variety of CVDs, including cardiac hypertrophy [21]. Therefore, we speculate that increased apoptosis played a role in CIH-induced cardiac hypertrophy in our study.

Although CIH significantly increased 11HSD2 expression, SRC-3 KO did not affect 11HSD2 expression in the CIH mouse hearts. Therefore, whether 11HSD2 plays a role in SRC-3 KO-attenuated CIH-induced cardiac hypertrophy remains to be elucidated. SRC-3 KO alleviated the severity of cardiac hypertrophy and the proinflammatory markers COX-2 and OPN partially through attenuating myocardial cell apoptosis. This result is probably due to the reduced interaction of MR and SRC-3. As mentioned above, activation of MR by aldosterone results in upregulation of COX-2 and OPN [22, 23]. Thus, blocking the adverse effects of MR binding to aldosterone in the myocardium due to

elevated levels of 11HSD2 could alleviate myocardial inflammation, hypertrophy, and remodeling caused by CIH.

CIH has been reported to cause oxidative stress and increase ROS levels [24, 25]. CIH can stimulate myocardial superoxide production via NADPH oxidase [26], a major source of ROS, to deteriorate left ventricular remodeling. Indeed, we observed that expression of NOX2, an NADPH oxidase and a biochemical marker of oxidative stress, significantly increased in the CIH mouse hearts. In contrast, CIH reduced the activity of SOD and CAT but increased the level of MDA in the mouse hearts. Therefore, we speculate that CIH-induced oxidative stress may be another mechanism leading to increased myocardial apoptosis and pathological changes. Interestingly, SRC-3 KO attenuated the CIH-induced changes in enzyme activity, which may represent another mechanism underlying SRC-3-mediated protection against CIH-induced cardiac hypertrophy. MR activation has been shown to mediate ROS production in many pathological conditions [27]. Spironolactone was demonstrated to inhibit aldosterone-mediated NADPH oxidase activation, suggesting that MR might be upstream of NADPH oxidase. SRC-3 is a coactivator of MR; thus, SRC-3 KO may alleviate myocardial oxidative stress damage [28].

Our results showed that CIH increased the expression of several inflammatory markers, including HIF-1α, IL-1β, IL-6, TNF, TGF-β, iNOS, PC-1, NO, and NF-κB, all of which were attenuated by SRC-3 KO. Hypoxia has been widely reported as the most powerful inducer of the HIF-1α transcriptional activity [29], which in turn activates the
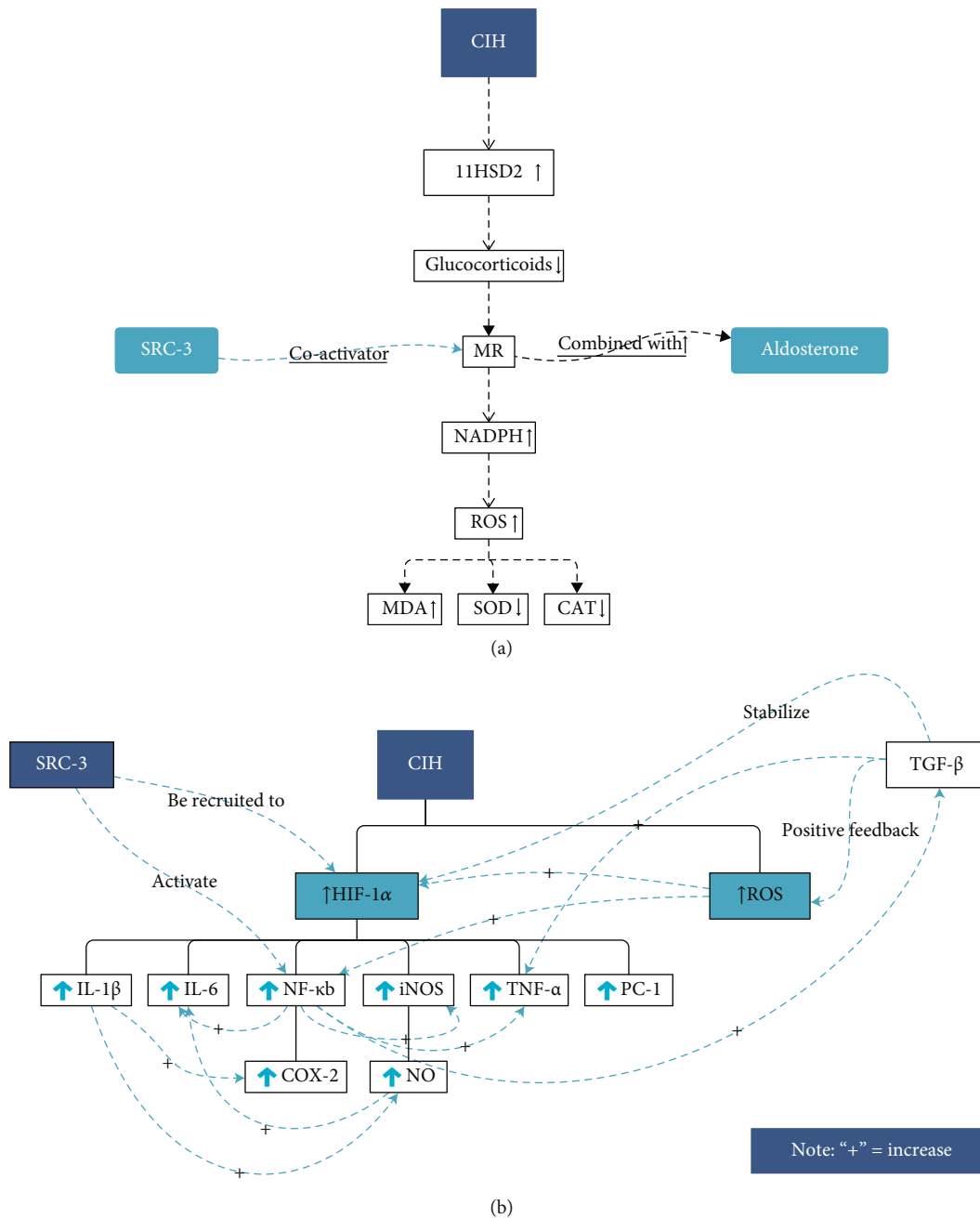
Figure 7: Hypothesis and working model for the SRC-3 function in CIH-induced myocardial injury. (a) CIH may induce myocardial oxidative stress injury via SRC-3 coactivating MR. (b) CIH may induce transcription of inflammatory and fibrotic genes and oxidative stress in the heart via activated SRC-3.

transcription of over 200 genes [30], many of which are closely related to the CIH-induced inflammatory response (IL-1β, IL-6 [31], NOS [32], TNF-α [33], PC-1 [34], and NF-κB [35]). IL-1β is a potent proinflammatory cytokine that can also induce expression of downstream proinflammatory molecules, such as COX-2 and NO [36]. iNOS produces NO, which is a messenger molecule with diverse functions in inflammation and synthesis of proinflammatory mediators (i.e., IL-6 and IL-8). TNF-α is a proinflammatory cytokine that regulates a wide spectrum of biological processes, including cell proliferation, differentiation, apoptosis,

lipid metabolism, and coagulation. PC-1 is a fibrotic marker that is secreted as abundant collagen I into the extracellular matrix after procollagen is modified by prolylhydroxilase [34]. TGF-β is another fibrotic marker that regulates cell proliferation, differentiation, and growth and can modulate expression and activation of other growth factors (i.e., TNF-α). In addition, there is a positive feedback loop between TGF-β and ROS [37, 38]; TGF-β induces and stabilizes HIF-1α expression, activates fibroblasts, and promotes collagen deposition [39]. On the other hand, there is a complex relationship between ROS, HIF-1α, and NF-κB and

other inflammatory factors. HIF-1α directly regulates the expression of NF-κB, which activates many inflammatory factors (i.e., TNF-α, TGF-β, IL-6, IL-8, COX-2, and iNOS) [40]. ROS can stimulate the production of inflammatory factors, such as NF-κB, activator protein-1, and HIF-1α. Moreover, NF-κB is closely related to apoptosis. Taken together, our data indicate that increased inflammation plays an important role in CIH-induced cardiac injury and that SRC-3 can partially reduce inflammation.

TEM revealed that CIH mouse hearts had severe myocardial cell apoptosis consistent with TUNEL assay results and abnormal ultrastructural changes in the mitochondria and cristae. These effects were ameliorated in the SRC-3 KO mice. Combined with the aforementioned findings, we propose that CIH induces cardiac injury through multiple mechanisms, including increasing oxidative stress and inflammation. These pathophysiological changes lead to elevated apoptosis and changes in myocardial ultrastructure. It should be noted that these molecular mechanisms and pathophysiological changes should not be viewed as individual independent processes; instead, they should be viewed as a part of a larger interconnected process.

SRC-3 belongs to the p160 steroid receptor coactivator family and is particularly sensitive to changes in intracellular signaling [41]. SRC-3 is ubiquitously expressed in various organs, including the heart [42, 43]. In the present study, we observed that SRC-3 KO mice exhibited reduced apoptosis, ultrastructural changes, and cardiac hypertrophy compared with CIH mice, which was accompanied by reduced expression of the inflammatory genes and oxidative enzymes. Therefore, SRC-3 mediates CIH-induced cardiac pathological changes through multiple mechanisms.

Previous studies have proved that overexpression of SRC-3 promotes glycolysis through activating HIF-1α and aggravates inflammation by activating NF-κB signaling pathways [10, 11], while SRC-3 deletion reduces NF-κB nuclear translocation, inflammatory, and iNOS [12]. Besides, SRC-3 can also be recruited to the promoters of HIF-1α target genes [44], and many of its downstream target genes (i.e., IL-1β, IL-6, iNOS, TNF, PC-1, and NF-κB) as demonstrated in this study. Furthermore, HIF-1α is an important transcription factor involved in oxidative stress and that many of its downstream targets are closely related to CVDs [6]. It is easy to come up with SRC-3 may regulate the downstream NF-κB signaling pathways [45] (Figures 7(a) and 7(b)), inflammatory, and iNOS by recruitment to the promoters of HIF-1α. We postulate that SRC-3 contributes to the pathogenesis of CVDs through activating HIF-1α and NF-κB, as well as promoting oxidative stress and inflammation.

In the present study, we used the heart weight/body weight ratio to evaluate the severity of cardiac hypertrophy. Although this index has been widely used in the field [46], it would be optimal to combine this index with cardiac functional parameters obtained by echocardiography to better evaluate cardiac hypertrophy.

Although we found that CIH increased the levels of myocardial fibrosis markers, we did not observe significant changes in myocardial fibrosis using electron microscopy. This might be because myocardial fibrosis is a late change in myocardial injury. This disparity should be clarified in a prolonged chronic intermittent hypoxia model, such as more than 12 weeks.

5. Conclusions

In summary, we found that SRC-3 KO ameliorates CIH-induced cardiac hypertrophy in mice, which is associated with attenuated myocardial oxidative stress and inflammation. Hence, SRC-3 is a potentially new target for the treatment of CVDs caused by SAS.

Abbreviations

CIH:	Chronic intermittent hypoxia
SAS:	Sleep apnea syndrome
CVDs:	Cardiovascular diseases
SRC-3:	Steroid receptor coactivator -3
WT:	Wild type
SRC3-KO:	SRC-3 knockout
Ctrl:	Air control
IHC:	Immunohistochemistry
TEM:	Transmission electron microscope
TUNEL:	TdT-mediated dUTP nick end labeling
DAB:	Diaminobenzidine
RIPA:	Radioimmunoprecipitation assay
ROS:	Reactive oxygen species
HIF-1α:	Hypoxia-inducible fator-1α
NF-κB:	Nuclear factor-κB
NR:	Nuclear receptors
GR:	Glucocorticoid receptor
MR:	Mineralocorticoid receptor
TNF-α:	Tumor necrosis factor-α
IL:	Interleukin
iNOS:	Inducible nitric oxide synthase
NOS:	Nitric oxide synthase
SOD:	Superoxide dismutase
CAT:	Catalase
MDA:	Malondialdehyde
11HSD1 and 11HSD2:	11 Beta-hydroxysteroid dehydrogenase type1 and type 2
COX-2:	Cyclooxygenase-2
OPN:	Osteopontin
NOX2:	NAPDH oxidase 2
PC-1:	Proprotein convertase 1
TGF-β:	Transforming growth factor-β
CXCL2:	CXC chemokine ligands 2
IκB-α:	Inhibitor of NF-κB
ANOVA:	Analysis of variance.

Data Availability

The datasets used and/or analyzed during the current study are available from the corresponding author on reasonable request.

Disclosure

Conflicts of Interest

The authors declare that there is no conflict of interest regarding the publication of this paper.

Authors' Contributions

WYW, HBG, and WHL performed the work. YHL, XYY, WL, FL, and SHH analyzed the data. WYW wrote the manuscript. YHS and ZRH designed the study and revised the manuscript. All authors approved the submitted version of the manuscript.

Acknowledgments

References

[1] C. Suen, J. Wong, C. M. Ryan et al., "Prevalence of undiagnosed obstructive sleep apnea among patients hospitalized for cardiovascular disease and associated in-hospital outcomes: a scoping review," *Journal of Clinical Medicine*, vol. 9, no. 4, p. 989, 2020.

[2] G. Labarca, J. Gower, L. Lamperti, J. Dreyse, and J. Jorquera, "Chronic intermittent hypoxia in obstructive sleep apnea: a narrative review from pathophysiological pathways to a precision clinical approach," *Sleep & Breathing = Schlaf & Atmung*, vol. 24, no. 2, pp. 751–760, 2020.

[3] Y. Deng, K. Liu, Y. Pan et al., "TLR2 antagonism attenuates the hippocampal neuronal damage in a murine model of sleep apnea via inhibiting neuroinflammation and oxidative stress," *Sleep & Breathing = Schlaf & Atmung*, vol. 24, no. 4, pp. 1613–1621, 2020.

[4] Y. M. Zeng, W. Y. Wan, X. Y. Chen, and Y. X. Zhang, "Effect of Telmisartan on local cardiovascular oxidative stress in mouse under chronic intermittent hypoxia condition," *Sleep & Breathing = Schlaf & Atmung*, vol. 17, no. 1, pp. 181–187, 2013.

[5] W. Wang, A. Song, Y. Zeng et al., "Telmisartan protects chronic intermittent hypoxic mice via modulating cardiac renin-angiotensin system activity," *BMC Cardiovascular Disorders*, vol. 18, no. 1, p. 133, 2018.

[6] Q. Wei, Y. Bian, F. Yu et al., "Chronic intermittent hypoxia induces cardiac inflammation and dysfunction in a rat obstructive sleep apnea model," *Journal of Biomedical Research*, vol. 30, no. 6, pp. 490–495, 2016.

[7] X. Y. Chen, Y. M. Zeng, Z. Y. Hunag et al., "Effect of chronic intermittent hypoxia on hypoxia inducible factor-1alpha in mice," *Zhonghua jie he he hu xi za zhi = Zhonghua jiehe he huxi zazhi = Chinese Journal of Tuberculosis and Respiratory Diseases*, vol. 28, no. 2, pp. 93–96, 2005.

[8] D. Song, G. Fang, S. Z. Mao et al., "Selective inhibition of endothelial NF-κB signaling attenuates chronic intermittent hypoxia-induced atherosclerosis in mice," *Atherosclerosis*, vol. 270, pp. 68–75, 2018.

[9] N. J. Brown, "Contribution of aldosterone to cardiovascular and renal inflammation and fibrosis," *Nature Reviews Nephrology*, vol. 9, no. 8, pp. 459–469, 2013.

[10] W. Zhao, C. Chang, Y. Cui et al., "Steroid Receptor Coactivator-3 Regulates Glucose Metabolism in Bladder Cancer Cells through Coactivation of Hypoxia Inducible Factor 1α *," *The Journal of Biological Chemistry*, vol. 289, no. 16, pp. 11219–11229, 2014.

[11] W. Chen, X. Lu, Y. Chen et al., "Steroid receptor coactivator 3 contributes to host defense against enteric bacteria by recruiting neutrophils via upregulation of CXCL2 expression," *Journal of Immunology*, vol. 198, no. 4, pp. 1606–1615, 2017.

[12] J. C. Tien and J. Xu, "Steroid receptor coactivator-3 as a potential molecular target for cancer therapy," *Expert Opinion on Therapeutic Targets*, vol. 16, no. 11, pp. 1085–1096, 2012.

[13] J. Xu, L. Liao, G. Ning, H. Yoshida-Komiya, C. Deng, and B. W. O'Malley, "The steroid receptor coactivator SRC-3 (p/CIP/RAC3/AIB1/ACTR/TRAM-1) is required for normal growth, puberty, female reproductive function, and mammary gland development," *Proceedings of the National Academy of Sciences of the United States of America*, vol. 97, no. 12, pp. 6379–6384, 2000.

[14] T. Liu, L. Zhang, D. Joo, and S. C. Sun, "NF-κB signaling in inflammation," *Signal Transduction and Targeted Therapy*, vol. 2, no. 1, p. 17023, 2017.

[15] A. Song, Y. Zeng, and X. Chen, "The study of an experimental mouse model of chronic hypoxia/reoxygenation," *Internationaljournal of Respiratory*, vol. 26, pp. 408–411, 2006.

[16] R. H. Oakley and J. A. Cidlowski, "Glucocorticoid signaling in the heart: a cardiomyocyte perspective," *The Journal of Steroid Biochemistry and Molecular Biology*, vol. 153, pp. 27–34, 2015.

[17] D. Fraccarollo, P. Galuppo, and J. Bauersachs, "Mineralocorticoid receptor antagonism and cardiac remodeling in ischemic heart failure," *Current Medicinal Chemistry Cardiovascular and Hematological Agents*, vol. 2, no. 4, pp. 287–294, 2004.

[18] K. Mazancová, M. Kopecký, I. Miksík, and J. Pácha, "11β-Hydroxysteroid dehydrogenase in the heart of normotensive and hypertensive rats," *The Journal of Steroid Biochemistry and Molecular Biology*, vol. 94, no. 1-3, pp. 273–277, 2005.

[19] K. E. Sheppard, "Corticosteroid Receptors, 11β-Hydroxysteroid Dehydrogenase, and the Heart," *Vitamins and Hormones*, vol. 66, pp. 77–112, 2003.

[20] P. Klusoňová, L. Řeháková, G. Borchert et al., "Chronic intermittent hypoxia induces 11β-Hydroxysteroid dehydrogenase in rat heart," *Endocrinology*, vol. 150, no. 9, pp. 4270–4277, 2009.

[21] E. Y. Kim, Y. Zhang, B. Ye et al., "Involvement of activated SUMO-2 conjugation in cardiomyopathy," *Biochimica et Biophysica Acta*, vol. 1852, no. 7, pp. 1388–1399, 2015.

[22] M. C. Rebsamen, E. Perrier, C. Gerber-Wicht, J. P. Benitah, and U. Lang, "Direct and indirect effects of aldosterone on cyclooxygenase-2 and interleukin-6 expression in rat cardiac cells in culture and after myocardial infarction," *Endocrinology*, vol. 145, no. 7, pp. 3135–3142, 2004.

[23] J. Irita, T. Okura, M. Kurata, K. I. Miyoshi, T. Fukuoka, and J. Higaki, "Osteopontin in rat renal Fibroblasts," *Hypertension*, vol. 51, no. 2, pp. 507–513, 2008.

[24] T. Kalogeris, C. P. Baines, M. Krenz, and R. J. Korthuis, "Ischemia/reperfusion," *Comprehensive Physiology*, vol. 7, no. 1, pp. 113–170, 2016.

[25] T. Inagaki, T. Akiyama, C. K. du, D. Y. Zhan, M. Yoshimoto, and M. Shirai, "Monoamine oxidase-induced hydroxyl radical production and cardiomyocyte injury during myocardial ischemia-reperfusion in rats," *Free Radical Research*, vol. 50, no. 6, pp. 645–653, 2016.

[26] T. Hayashi, C. Yamashita, C. Matsumoto et al., "Role of gp91phox-containing NADPH oxidase in left ventricular remodeling induced by intermittent hypoxic stress," *American Journal of Physiology Heart and Circulatory Physiology*, vol. 294, no. 5, pp. H2197–H2203, 2008.

[27] Q. N. Dinh, M. J. Young, M. A. Evans, G. R. Drummond, C. G. Sobey, and S. Chrissobolis, "Aldosterone-induced oxidative stress and inflammation in the brain are mediated by the endothelial cell mineralocorticoid receptor," *Brain Research*, vol. 1637, pp. 146–153, 2016.

[28] A. Taye and H. Morawietz, "Spironolactone inhibits NADPH oxidase-induced oxidative stress and enhances eNOS in human endothelial cells," *Iranian Journal of Pharmaceutical Research: IJPR*, vol. 10, no. 2, pp. 329–337, 2011.

[29] G. L. Semenza, "Oxygen sensing, hypoxia-inducible factors, and disease pathophysiology," *Annual Review of Pathology*, vol. 9, no. 1, pp. 47–71, 2014.

[30] D. J. Manalo, A. Rowan, T. Lavoie et al., "Transcriptional regulation of vascular endothelial cell responses to hypoxia by HIF-1," *Blood*, vol. 105, no. 2, pp. 659–669, 2005.

[31] F. Armando, M. Gambini, A. Corradi et al., "Oxidative stress in canine histiocytic sarcoma cells induced by an infection with canine distemper virus led to a dysregulation of HIF-1α downstream pathway resulting in a reduced expression of VEGF-B in vitro," *Viruses*, vol. 12, no. 2, p. 200, 2020.

[32] M. O. Kseibati, G. S. G. Shehatou, M. H. Sharawy, A. E. Eladl, and H. A. Salem, "Nicorandil ameliorates bleomycin-induced pulmonary fibrosis in rats through modulating eNOS, iNOS, TXNIP and HIF-1α levels," *Life Sciences*, vol. 246, article ???, 2020.

[33] X. Gao, Y. Li, H. Wang, C. Li, and J. Ding, "Inhibition of HIF-1αdecreases expression of pro-inflammatory IL-6 and TNF-αin diabetic retinopathy," *Acta Ophthalmologica*, vol. 95, no. 8, pp. e746–e750, 2017.

[34] S. McMahon, F. Grondin, P. P. McDonald, D. E. Richard, and C. M. Dubois, "Hypoxia-enhanced Expression of the Proprotein Convertase Furin Is Mediated by Hypoxia-inducible Factor-1;," *The Journal of Biological Chemistry*, vol. 280, no. 8, pp. 6561–6569, 2005.

[35] W. Feng, T. Xue, S. Huang et al., "HIF-1α promotes the migration and invasion of hepatocellular carcinoma cells via the IL-8-NF-κB axis," *Cellular & Molecular Biology Letters*, vol. 23, no. 1, p. 26, 2018.

[36] C. A. Dinarello, "The history of fever, leukocytic pyrogen and interleukin-1," *Temperature*, vol. 2, no. 1, pp. 8–16, 2015.

[37] D. Zhang, W. Jin, R. Wu et al., "High Glucose Intake Exacerbates Autoimmunity through Reactive-Oxygen-Species-Mediated TGF-β Cytokine Activation," *Immunity*, vol. 51, no. 4, pp. 671–681.e5, 2019.

[38] S. A. Park, M. J. Kim, S. Y. Park et al., "EW-7197 inhibits hepatic, renal, and pulmonary fibrosis by blocking TGF-β/Smad and ROS signaling," *Cellular and Molecular Life Sciences: CMLS*, vol. 72, no. 10, pp. 2023–2039, 2015.

[39] X. L. Zong, D. Y. Jiang, J. C. Wang, J. L. Liu, Z. Z. Liu, and J. L. Cai, "Transforming growth factor-β1 phage model peptides isolated from a phage display 7-mer peptide library can inhibit the activity of keloid fibroblasts," *Chinese Medical Journal*, vol. 124, no. 3, pp. 429–435, 2011.

[40] A. Vallée and Y. Lecarpentier, "Crosstalk between peroxisome proliferator-activated receptor gamma and the canonical WNT/β-catenin pathway in chronic inflammation and oxidative stress during carcinogenesis," *Frontiers in Immunology*, vol. 9, p. 745, 2018.

[41] R. C. Wu, C. L. Smith, and B. W. O'Malley, "Transcriptional regulation by steroid receptor coactivator phosphorylation," *Endocrine Reviews*, vol. 26, no. 3, pp. 393–399, 2005.

[42] C. S. Suen, T. J. Berrodin, R. Mastroeni, B. J. Cheskis, C. R. Lyttle, and D. E. Frail, "A Transcriptional Coactivator, Steroid Receptor Coactivator-3, Selectively Augments Steroid Receptor Transcriptional Activity," *The Journal of Biological Chemistry*, vol. 273, no. 42, pp. 27645–27653, 1998.

[43] J. Torchia, D. W. Rose, J. Inostroza et al., "The transcriptional co-activator p/CIP binds CBP and mediates nuclear- receptor function," *Nature*, vol. 387, no. 6634, pp. 677–684, 1997.

[44] F. Wang, R. Zhang, X. Wu, and O. Hankinson, "Roles of coactivators in hypoxic induction of the erythropoietin gene," *PloS One*, vol. 5, no. 4, article e10002, 2010.

[45] A. Shrestha, H. Bruckmueller, H. Kildalsen et al., "Phosphorylation of steroid receptor coactivator-3 (SRC-3) at serine 857 is regulated by the p38^{MAPK}-MK2 axis and affects NF-κB- mediated transcription," *Scientific Reports*, vol. 10, no. 1, article 11388, 2020.

[46] N. Yamaguchi, N. Takahashi, L. Xu, O. Smithies, and G. Meissner, "Early cardiac hypertrophy in mice with impaired calmodulin regulation of cardiac muscle Ca2+ release channel," *The Journal of Clinical Investigation*, vol. 117, no. 5, pp. 1344–1353, 2007.

Review Article

Targeting Ferroptosis: Pathological Mechanism and Treatment of Ischemia-Reperfusion Injury

Xinye Li [iD],[1,2] **Ning Ma,**[3] **Juping Xu,**[4] **Yanchi Zhang,**[5] **Pan Yang,**[4] **Xin Su** [iD],[1]
Yanfeng Xing [iD],[6] **Na An** [iD],[1,7] **Fan Yang** [iD],[1] **Guoxia Zhang,**[1] **Lijing Zhang** [iD],[7]
and Yanwei Xing [iD][1]

[1]*Guang'anmen Hospital, China Academy of Chinese Medical Sciences, Beijing 100053, China*
[2]*Beijing University of Chinese Medicine, Beijing 100029, China*
[3]*Dezhou Second People's Hospital, Dezhou 253000, China*
[4]*The Second People's Hospital of Jiaozuo, Jiaozuo 454001, China*
[5]*The First Affiliated Hospital, Hebei North University, Zhangjiakou 075000, China*
[6]*Shanxi University of Chinese Medicine, Taiyuan 030619, China*
[7]*Dongzhimen Hospital, Beijing University of Chinese Medicine, Beijing 100700, China*

Correspondence should be addressed to Lijing Zhang; dzmyyccu@163.com and Yanwei Xing; xingyanwei12345@163.com

Ischemia-reperfusion (I/R) is a pathological process that occurs in many organs and diseases. Reperfusion, recovery of blood flow, and reoxygenation often lead to reperfusion injury. Drug therapy and early reperfusion therapy can reduce tissue injury and cell necrosis caused by ischemia, leading to irreversible I/R injury. Ferroptosis was clearly defined in 2012 as a newly discovered iron-dependent, peroxide-driven, nonapoptotic form of regulated cell death. Ferroptosis is considered the cause of reperfusion injury. This discovery provides new avenues for the recognition and treatment of diseases. Ferroptosis is a key factor that leads to I/R injury and organ failure. Given the important role of ferroptosis in I/R injury, there is considerable interest in the potential role of ferroptosis as a targeted treatment for a wide range of I/R injury-related diseases. Recently, substantial progress has been made in applying ferroptosis to I/R injury in various organs and diseases. The development of ferroptosis regulators is expected to provide new opportunities for the treatment of I/R injury. Herein, we analytically review the pathological mechanism and targeted treatment of ferroptosis in I/R and related diseases from the perspectives of myocardial I/R injury, cerebral I/R injury, and ischemic renal injury.

1. Introduction

Ischemia-reperfusion (I/R) is a pathological process that occurs in numerous organs and diseases and can lead to cellular damage and death. Ischemia occurs when the blood supply to organs is restricted as a result of an embolus that blocks arterial blood supply. Ischemic events are related to a serious imbalance in cell metabolism, resulting in tissue hypoxia. In the affected ischemic area, reperfusion and restoration of blood flow and reoxygenation are frequently related to "reperfusion injury," including excessive tissue injury and destructive inflammatory responses [1]. I/R injury is a major pathological factor in many diseases, especially after cardiac trauma. Additionally, I/R injury delays the recovery of transplanted organs and patients undergoing treatment. Pharmacological therapy and early reperfusion therapy can reduce tissue damage and cell necrosis induced by ischemia. However, these treatments can also cause irreversible I/R injuries. Cell death is the major common I/R injury characteristic in all tissues, and consequently, it is a stable pathological index of I/R injury. Ferroptosis is a newly recognized form of programmed cell death that relies on iron and reactive oxygen species (ROS) [2] and is believed to be the cause of reperfusion injury [3]. Thus, the new manner of cell death, ferroptosis, provides new avenues for understanding and treating many diseases. Research on I/R
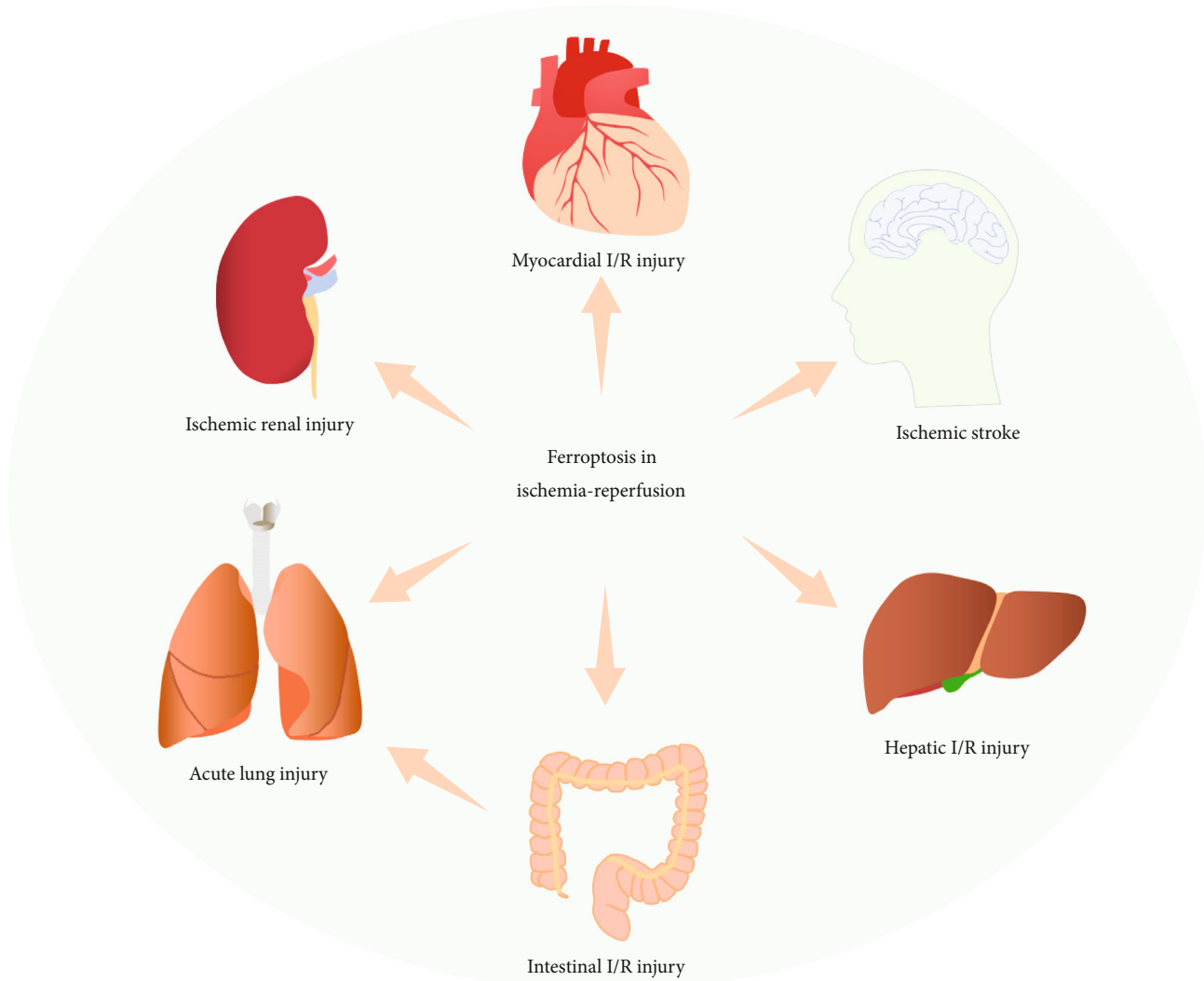
FIGURE 1: Ferroptosis plays important roles in ischemia-reperfusion (I/R) injury, including myocardial I/R injury, cerebral I/R injury, ischemic renal injury, hepatic I/R injury, intestinal I/R injury, and acute lung injury induced by intestinal I/R.

injury has been conducted in numerous organs, including the heart [4], brain [5], kidney [6], and liver [7]. Recent studies have revealed the links between ferroptosis and I/R injury (Figure 1), and ferroptosis inhibitors have successfully prevented or reduced I/R injury in various organs. Ferroptosis is a key driver of I/R injury and organ failure. Inhibiting ferroptosis may become an effective treatment strategy for related organ diseases and will help to reduce cell death during reperfusion injury. Therefore, it is worth emphasizing the importance of exploring the pathological mechanism of ferroptosis in I/R and targeted therapies. In this article, we summarize the available evidence regarding the pathological mechanism of ferroptosis, I/R injury in organs and diseases, and research progress on related therapeutic targets.

2. Regulation Mechanism of Ferroptosis

Ferroptosis is an iron-dependent, peroxidation-driven, nonapoptotic form of regulated cell death [3, 8, 9]. It is biochem-

ically, morphologically, and genetically different from apoptosis, necrosis, and other forms of cell death [2, 3, 10, 11]. Ferroptosis was clearly defined in 2012 when it was demonstrated that erastin could inhibit the antioxidant glutathione (GSH) synthesis and trigger iron-dependent cell death, which was also nonapoptotic [2]. Multiple biological regulatory pathways work simultaneously during ferroptosis. GSH deficiency or glutathione peroxidase 4 (GPX4) inactivation causes ferroptosis [2, 12–14]. Furthermore, ferroptosis is characterized by iron-mediated excessive peroxidation of polyunsaturated fatty acids (PUFAs) [15]. The immoderate accumulation of iron-dependent lipid hydroperoxides leads to ferroptosis. The mechanisms and major regulatory factors involved in ferroptosis are shown in Figure 2.

2.1. Antioxidant Mechanism of Ferroptosis. System x_c^- is a cystine-glutamate exchanger, which consists of heterodimers of the solute carrier family 3 member 2 (SLC3A2) and the catalytic subunit solute carrier family 7 member 11 (SLC7A11)
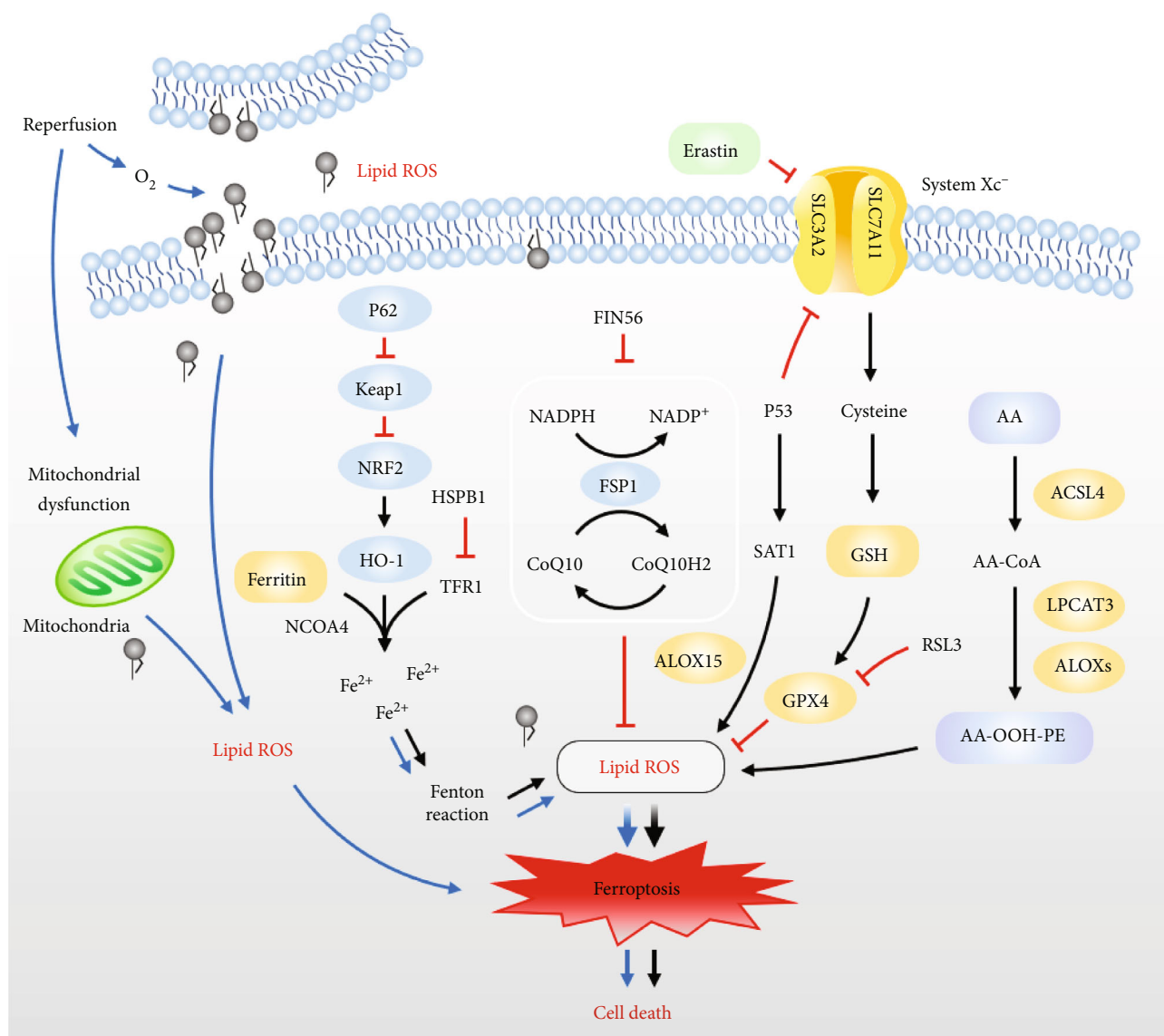
FIGURE 2: Schematic representation of the proposed mechanism of ferroptosis mediating cell death during ischemia-reperfusion and the mechanism of regulatory pathways of ferroptosis. SLC3A2: solute carrier family 3 member 2; SLC7A11: solute carrier family 7 member 11; Keap1: Kelch-like ECH-associated protein 1; NRF2: nuclear factor erythroid 2-related factor; HO-1: heme oxygenase-1; NCOA4: nuclear receptor coactivator 4; HSPB1: heat shock factor-binding protein 1; TFR1: transferrin receptor 1; FIN56: ferroptosis inducing 56; FSP1: ferroptosis suppressor protein 1; CoQ10: coenzyme Q10; RSL3: (1S, 3R)-RSL; GSH: glutathione; GPX4: glutathione peroxidase 4; ROS: reactive oxygen species; SAT1: spermidine/spermine N^1-acetyltransferase 1; ALOX-15: arachidonate lipoxygenase 15; AA: arachidonic acid; ACSL4: acyl-CoA synthetase long-chain family 4; LPCAT3: lysophosphatidylcholine acyltransferase 3; ALOXs: arachidonate lipoxygenases; PE: phosphatidylethanolamine.

[16, 17]. System x_c^- promotes the exchange process across the plasma membrane of cystine and glutamate. Cystine is necessary for cell survival and is the predominant form of cysteine in extracellular space [18]. System x_c^- imports extracellular cystine for GSH synthesis and transfers glutamate out of cells [19]. GPX4, an antioxidant enzyme that maintains cellular redox homeostasis, primarily acts as a crucial endogenous antioxidant against phospholipid peroxide, mainly using GSH as a cofactor [20]. The inhibition of system x_c^- induces GSH depletion and causes the inactivation of GPX4, resulting in the accumulation of toxic lipid ROS and triggering ferroptosis [2, 14]. To maintain the function and activity of GPX4, GSH and selenium (Se) are indispensable [3, 21]. GSH also acts as a major endogenous antioxidant [22] and participates in the regeneration of GPX4 [23]. GSH is synthesized in two steps from glutamate, cysteine, and glycine under the catalysis

of enzymes [17]. Erastin and (1S,3R)-RSL (RSL3) were identified as compounds that induce RAS-mutated tumor cell death [9, 24], and some proteins associated with GSH metabolism are related to ferroptosis [8]. GPX4 can act directly or indirectly by ferroptosis agonists, thereby reducing its activity [25]. RSL3 is a ferroptosis inducer that directly inhibits GPX4 by covalently targeting selenocysteine. It inhibits GPX4 activity, thereby causing intracellular accumulation of lipid peroxides and subsequent cell death [14, 26]. Erastin, another representative ferroptosis inducer, depletes cellular cysteine and reduces the biosynthesis of GSH by directly inhibiting system x_c^- [13]. This leads to the loss of GPX4 activity, leading to the accumulation of lipid peroxides and eventually ferroptosis. The main target of erastin is the exchange of cystine/cystathionine with glutamate [2]. Recent evidence has shown that the ferroptosis suppressor protein 1- (FSP1-) coenzyme Q10- (CoQ10-) (nicotinamide adenine dinucleotide phosphate) NAD(P)H pathway synergistically inhibits the proliferation of lipid peroxides and ferroptosis with GPX4 and GSH, as an independent system [27, 28]. FSP1 functions as an oxidoreductase that reduces CoQ10 using NAD(P)H and produces a lipophilic radical-capture antioxidant (RTA) to prevent the production of lipid peroxides [27, 28]. Ferroptosis inducing 56 (FIN56) has been shown to cause ferroptosis by blocking this pathway [29]. The tumor suppressor protein P53 plays a role in apoptosis, necrosis, and autophagy. P53 can repress SLC7A11 gene expression, affecting the activity of GPX4 and leading to the accumulation of lipid peroxidation and an increase in ferroptosis [30, 31]. P53-SAT1- (spermidine/spermine N^1-acetyltransferase 1-) arachidonate lipoxygenase 15 (ALOX-15) pathway also participates in the regulation of ferroptosis [32]. SAT1 acts as a transcriptional target of P53, and its activation can induce ROS-induced lipid peroxidation and ferroptosis.

2.2. Oxidation Mechanisms of Ferroptosis. PUFAs are oxidized to form lipid peroxides [33]. The important factors that cause ferroptosis include the accumulation of lipid peroxides [2, 3]. Oxidized arachidonic acid-containing phosphatidylethanolamine (AA-PE) acts as a signal of ferroptosis. A recent study showed that AA-OOH-PE, instead of other types of phospholipid-OOH, is the key phospholipid that induces ferroptosis [34]. Three enzymes are required for the generation of AA-OOH-PE: arachidonate lipoxygenases (ALOXs), acyl-CoA synthetase long-chain family 4 (ACSL4), and lysophosphatidylcholine acyltransferase 3 (LPCAT3) [35]. ACSL4 catalyzes PUFA (especially AA) to yield CoA-forms [36], and LPCAT3 regulates the esterification of AA-CoA into AA-PE [15]. Under the catalysis of lipoxygenase (LOXs), AA-PE can be oxidized to AA-OOH-PE and play further oxidative roles [26, 34, 37]. When the AA-OOH-PE level exceeds the limit of the reduction system, ferroptosis is induced [17, 36, 38]. In addition to lipid peroxidation, iron, a redox-active metal, is necessary for ferroptosis [39]. As the iron source of the Fenton reaction, in the labile iron pool (LIP), small amounts of iron are free and chelated. Iron released from the LIP can subsequently promote ROS accumulation through the Fenton reaction [40–42]. During ferroptosis, ROS mainly originate from the Fenton reaction. In addition, iron is a prooxidant in ferroptosis and is vital for the function of enzymes, such as lipoxygenases (LOXs) [43, 44]. Ferroptosis is also regulated by proteins involved in iron homeostasis. ShRNA-mediated iron response element binding protein 2 (IREB2) silencing has been demonstrated to reduce sensitivity to ferroptosis by modifying iron uptake, metabolism, and storage [2]. Cysteine desulfurase (NFS1) has also been shown to reduce ferroptosis in lung cancer [45]. Heat shock factor-binding protein 1 (HSPB1), a negative regulator of ferroptosis, reduces iron concentrations by inhibiting the expression of TRF1, thereby inhibiting ferroptosis [46]. Ferritin autophagy can increase the content of Fe^{2+} [47], thus promoting ferroptosis. At the same time, the ferritin receptor nuclear receptor coactivator 4 (NCOA4) mediates the autophagic degradation of ferritin, increasing free iron [48, 49]. Heme oxygenase-1 (HO-1) decomposes heme to release iron, thereby accelerating ferroptosis [50]. P62 is an autophagy receptor that can inhibit Kelch-like ECH-associated protein 1 (Keap1) directly and promotes nuclear factor erythroid 2-related factor (NRF2) activation simultaneously. An early study showed that oxidative stress induces the expression of HO-1 by activating the p62-Keap1-NRF2 pathway, thus antagonizing ferroptosis [51]. Nrf2 activates the expression of various target genes necessary to regulate ferroptosis by regulating the metabolism of GSH, lipid, iron, and mitochondrial function [51].

3. Pathological Mechanisms and Potential Targeted Therapy of Ferroptosis in Ischemia-Reperfusion Injury

3.1. Role of Ferroptosis in Ischemia-Reperfusion-Related Cell Death. Previous studies have shown that ferroptosis occurs during the reperfusion period and not during the ischemic period in I/R injury models [52]. After I/R, the endogenous mechanisms of scavenging ROS are seriously negated, and ROS cannot be effectively scavenged. Reperfusion of ischemic tissue causes excessive ROS, which mediate I/R injury [53, 54]. There is evidence that I/R injury is accompanied by several cellular events, such as reperfusion-related excessive ROS accompanied by lipid peroxidation [55] and an increase in intracellular iron concentration [56, 57]. Lipid peroxidation and ROS lead to cell injury and death. These cellular events are consistent with the manifestation of iron-dependent ferroptosis, which could be prevented by iron chelators [58]. Figure 2 shows the proposed mechanism of ferroptosis, which mediates cell death during ischemia-reperfusion. Current studies have shown that phospholipid oxidation products exist in myocardial I/R injury [59–62]. In addition to lipid peroxidation, free iron is a necessary condition for ferroptosis. Nonenzymatic production of ROS occurs when metal ions are present. There is a LIP in the cytosol, mitochondria, and lysosomes of cells [41]. The free iron in the LIP could accelerate the lipid peroxidation of saturated fatty acids in humans via the Fenton reaction [63], and iron is involved in producing ROS in mitochondria. Mitochondria of a cell are the main sites for generating

ROS [64, 65], and after the injury, they undergo alterations of structure and function. During ischemia, mitochondrial dysfunction leads to excessive ROS production. Therefore, current evidence supports the involvement of ferroptosis in the progression of organ cell injury after I/R. Ferroptosis is an important mechanism that mediates cellular damage to organs and cell death during I/R.

3.2. Myocardial I/R Injury

3.2.1. Ferroptosis in Myocardial I/R Injury. Coronary artery disease has been suggested to be the most common cardiovascular disease [66], and atherosclerosis is the main cause. Plaque rupture results in acute ischemia and myocardial infarction. A large amount of ROS is produced after reperfusion [67, 68], leading to further damage [69]. During ischemia and early reperfusion, ferritin degrades to release iron and promotes iron-mediated Fenton reaction, leading to oxidative damage and loss of cardiac function associated with I/R injury. In experimental models, inhibition of glutaminolysis, an important part of ferroptosis, was shown to reduce I/R-induced heart injury [70]. Studies have confirmed that ROS accumulation and iron content increase during I/R injury [71, 72], and iron overload is an important cause of myocardial cell injury [73]. A study by Li et al. showed that iron deposition and ROS overproduction occurred during diabetic myocardial injury, and ferroptosis was involved in the I/R injury of diabetic myocardium through the endoplasmic reticulum stress pathway [31]. These studies indicate that ferroptosis plays a key role in myocardial I/R injury. Transferrin receptor 1 (TfR1) is involved in cellular iron uptake. A novel pathway of ubiquitin-specific protease 7 (USP7)/p53/TfR1 is found in rat hearts after I/R treatment, and the upregulation of USP7 accelerates ferroptosis by activating the p53/TfR1 pathway [74]. The study has shown that ferroptosis occurs during reperfusion in rat hearts subjected to I/R [52]. With the prolongation of reperfusion time, the levels of ACSL4 protein in the cardiac tissue gradually increased, accompanied by a decrease in GPX4 levels. The exact role of ferroptosis in myocardial I/R injury remains unclear. Other studies have shown that inhibition of ferroptosis has a protective effect on myocardial I/R-induced rats [75].

3.2.2. Target and Targeted Therapy of Ferroptosis in Myocardial I/R Injury. Targeting ferroptosis is considered a feasible treatment for I/R injury. The exposure of rat cardiomyocytes to simulated I/R injury can cause nonapoptotic cell death, and the addition of ferrostatin-1 during reperfusion can attenuate this effect [76]. Fang et al. [77] found that the in vivo application of ferristatin-1 and an iron chelator plays a role in reducing heart failure caused by I/R. It has been suggested that ferroptosis is related to myocardial I/R injury, and ferristatin-1 may be a feasible treatment to alleviate reperfusion injury. In addition, many studies have demonstrated that iron chelators can block ferroptosis in vitro and in vivo. Deferoxamine (DFO) is the most widely used nontoxic iron chelator that inhibits ferroptosis mediated by lipid peroxidation under various conditions [2]. Chan et al.

showed that DFO administered before reperfusion by primary percutaneous coronary intervention could rapidly ameliorate oxidative stress but failed to limit infarct size [78]. In a study by Paraskevaidis et al., intravenous DFO infusion protected the myocardium from reperfusion injury and reduced lipid peroxidation during coronary artery bypass grafting surgery [79]. DFO, which binds iron, has been shown to have a protective effect on myocardial I/R [70]. Shan et al. demonstrated that Cyanidin-3-glucoside (C3G) treatment reduced oxidative stress and Fe^{2+} content, confirming that C3G effectively alleviated myocardial I/R injury by inhibiting ferroptosis both in vivo and in vitro [72]. C3G treatment could reduce myocardial infarction area, inhibit pathological damage, and inhibit ST-segment elevation. Baicalein (also termed 5,6,7-trihydroxyflavone) is a flavonoid that limits iron accumulation induced by erastin and lipid peroxidation by inhibiting GPX4 degradation and GSH consumption [80]. In addition, baicalein significantly reduced iron-induced lipid peroxidation and inhibited the expression of ALOX-15 in HT22 cells [81]. A recent study has shown that baicalin protects against myocardial I/R injury via inhibiting ACSL4-controlled ferroptosis in a rat model [82]. Ma et al. found that ubiquitin-specific peptidase 22 (USP22) inhibits cardiomyocyte death induced by ferroptosis in myocardial I/R injury via the SIRT1/p53/SLC7A11 axis, providing a novel therapeutic target for the treatment [83]. Chen et al. found that embryonic lethal-abnormal vision like protein 1 (ELAVL1) increased substantially during myocardial I/R injury. ELAVL1 knockout decreased ferroptosis, thus ameliorating I/R injury [84]. FOXC1-activated transcription mediates the increase in ELAVL1 induced by myocardial I/R, and FOXC1 plays a key role in myocardial I/R injury [84]. Inhibition of ELAVL1-mediated ferroptosis might be a new approach for the treatment of myocardial I/R injury. Oxidized phosphatidylcholine (OxPC) production increases during myocardial I/R injury and causes extensive cell death through ferroptosis [85]. Interventions targeting OxPCs may help reduce ferroptosis during I/R injury. Determining appropriate therapeutic targets is vital. Further studies are needed to establish more effective anti-ferroptosis-targeted therapies for patients with myocardial ischemia.

3.3. Cerebral I/R Injury

3.3.1. Ferroptosis in Cerebral I/R Injury. Ischemic stroke is the main cause of destructive cerebrovascular disease and has high mortality and morbidity rates [86]. Restoring blood supply to the ischemic area as soon as possible is crucial for ischemic cerebrovascular disease treatment [87]. Early reperfusion is the most effective therapy for acute cerebral ischemia; however, the increase in ROS and inflammation, and other phenomena in tissues after reperfusion aggravates brain tissue damage [88]. Several studies have indicated that iron chelators attenuate brain injury induced by ischemic stroke in animal models [89, 90] and play an antioxidant, neuroprotective role in stroke patients [91]. Recent studies have suggested that ferroptosis plays a significant role in ischemic stroke [92–94]. Ferroptosis inhibitors, ferrostatin-

1 or liprostatin-1, have a protective effect on neuronal injury in middle cerebral artery occlusion (MCAO) mouse models [95]. In brain I/R mice models, the expression levels of proteins related to ferroptosis are abnormal [96]. A significant increase was demonstrated in free iron content and ROS accumulation in brain tissue, whereas the levels of GPX4 and GSH significantly decreased [97]. These studies show that ferroptosis plays a key role in brain I/R injury, and inhibition of ferroptosis could protect brain tissue damage induced by I/R.

3.3.2. Target and Targeted Therapy of Ferroptosis in Cerebral I/R Injury.
A deeper understanding of the target and targeted treatment of ferroptosis will be beneficial for treating related diseases. Pharmacological Se drives GPX4 expression to reduce ferroptosis, provide neuroprotection, and have a therapeutic effect on stroke [92]. A previous study found that the tau-mediated iron export pathway prevents injury induced by ferroptosis after ischemic stroke and the therapeutic potential of ferroptotic inhibition in this injury [95]. Guan et al. observed that ROS and iron levels were increased in the brains of ischemic stroke model gerbils [98]. Carvacrol exerts neuroprotective effects in cerebral ischemia by increasing the expression of GPX4 and inhibiting ferroptosis [98]. Carthamin yellow is a flavonoid isolated from safflower. In a recent study, using MCAO model rats, carthamin yellow improved cerebral I/R injury by reducing ferroptosis [96]. Galangin is a flavonoid that is mainly extracted from Chinese medicinal herbs [99]. Galangin upregulates SLC7A11 and indirectly increases the expression of GPX4, thereby inhibiting ferroptosis and attenuating cerebral I/R injury in gerbils. Galangin treatment has been shown to increase the survival rate of neurons in the brain of gerbils and alleviate learning and memory impairment after I/R [100]. It has been hypothesized that PIEZO1 participates in cerebral I/R injury by regulating ferroptosis, which might be a potential therapeutic treatment to protect against neuronal damage [101]. Furthermore, Cui et al. identified that ACSL4 is a novel neuronal death regulator, as knockout of ACSL4 could protect mice from cerebral ischemia, while forced overexpression of ACSL4 aggravated ischemic brain injury. The intervention of ACSL4 expression could be a potential therapeutic target for ischemic stroke [102]. The therapeutic targets of ferroptosis in ischemic stroke still need to be further studied to determine appropriate and more effective anti-ferroptosis-targeted therapies.

3.4. Ischemic Renal Injury

3.4.1. Ferroptosis in Ischemic Renal Injury.
Pathophysiological renal I/R injuries include renal tubular injury, inflammation, and vascular dysfunction. The precipitating factors and major early events of acute kidney injury (AKI) are renal tubular epithelial cell injury and subsequent cell death [103]. In recent years, the role of ferroptosis in renal I/R injury has been investigated. It has been suggested that ferroptosis has pathophysiological relevance in AKI [2, 103–105]. In mice with renal I/R injury, administration of ferrostatin 1 or 16–86 15 min before ischemia, renal tissue

injury, and serum creatinine and urea were decreased 48 h after ischemia, indicating that ferroptosis plays an important role in the pathogenesis [106]. In mouse models of AKI induced by I/R injury, ferroptosis is directly related to the synchronous necrosis of renal tubules [106]. Ding et al. demonstrated that I/R induced upregulation of miR-182-5p and miR-378a-3p and induced ferroptosis in renal injury by downregulating GPX4 and SLC7A11 [107]. Recent studies have suggested that ferroptosis plays an important role in renal I/R injury; however, the exact mechanism of ferroptosis needs to be further studied.

3.4.2. Target and Targeted Therapy of Ferroptosis in Ischemic Renal Injury.
Pannexin1 (PANX1) is an ATP-releasing pathway family protein that can promote apoptosis during kidney injury. A previous study has shown that the deletion of PANX1 prevents renal I/R injury by attenuating ferroptosis activated by mitogen-activated protein kinase/extracellular signal-regulated kinase signaling [108]. Macrophage migration inhibitory factor (MIF) is a stress-regulatory cytokine. It has been reported that MIF can effectively limit necrotic ptosis, restore intracellular GSH, and reduce lipid peroxidation to alleviate oxidative stress [109]. MIF protects renal tubular epithelial cells and plays a role in renal protection during experimental I/R injury. Pachymic acid is a lanostane-type triterpenoid found in *Poria cocos*. According to research, under the treatment of pachymic acid, the renal function of mice with renal I/R injury can be improved, and renal injury can be alleviated. The protective effect of pachymic acid may be related to the inhibition of renal ferroptosis through directly or indirectly activating Nrf2 and upregulating downstream GPX4, system x_c^-, and HO-1 [110]. Additionally, XJB-5-131 is a mitochondrial-targeted nitroxide with a high affinity for tubular epithelial cells [111]. XJB-5-131 inhibits lipid peroxidation after I/R injury and inhibits I/R-induced ferroptosis in tubular epithelial cells, thus improving ischemic renal injury [111]. Irisin is a type of exercise-induced hormone that can ameliorate mitochondrial function and reduce ROS production. In renal I/R mice models, irisin treatment can reduce I/R-induced AKI by upregulating GPX4, a pivotal regulator of ferroptosis [112]. Inhibition of ferroptosis protects renal tubular epithelial cells and reduces renal I/R injury. These results indicate that the crucial endogenous antioxidant GPX4 and its cofactor GSH are important targets for protection against renal I/R injury.

3.5. Mechanism and Targeted Therapy of Ferroptosis in I/R Injury in Other Organs.
Hepatic I/R, as a surgical complication after liver transplantation, can cause inflammation and immune reactions, lead to rejection, and affect prognosis [113, 114]. Galeano et al. demonstrated that subchronic, low-level iron administration has significant hepatoprotection against I/R injury [115]. A previous study has shown that ferroptosis is a mechanism of liver I/R injury in a mouse model of hepatic injury. Li et al. demonstrated that iron overload is a new risk factor for hepatic I/R injury. Ferroptosis mediates the relationship between iron overload and liver injury, showing that ferroptosis is a prospective target for
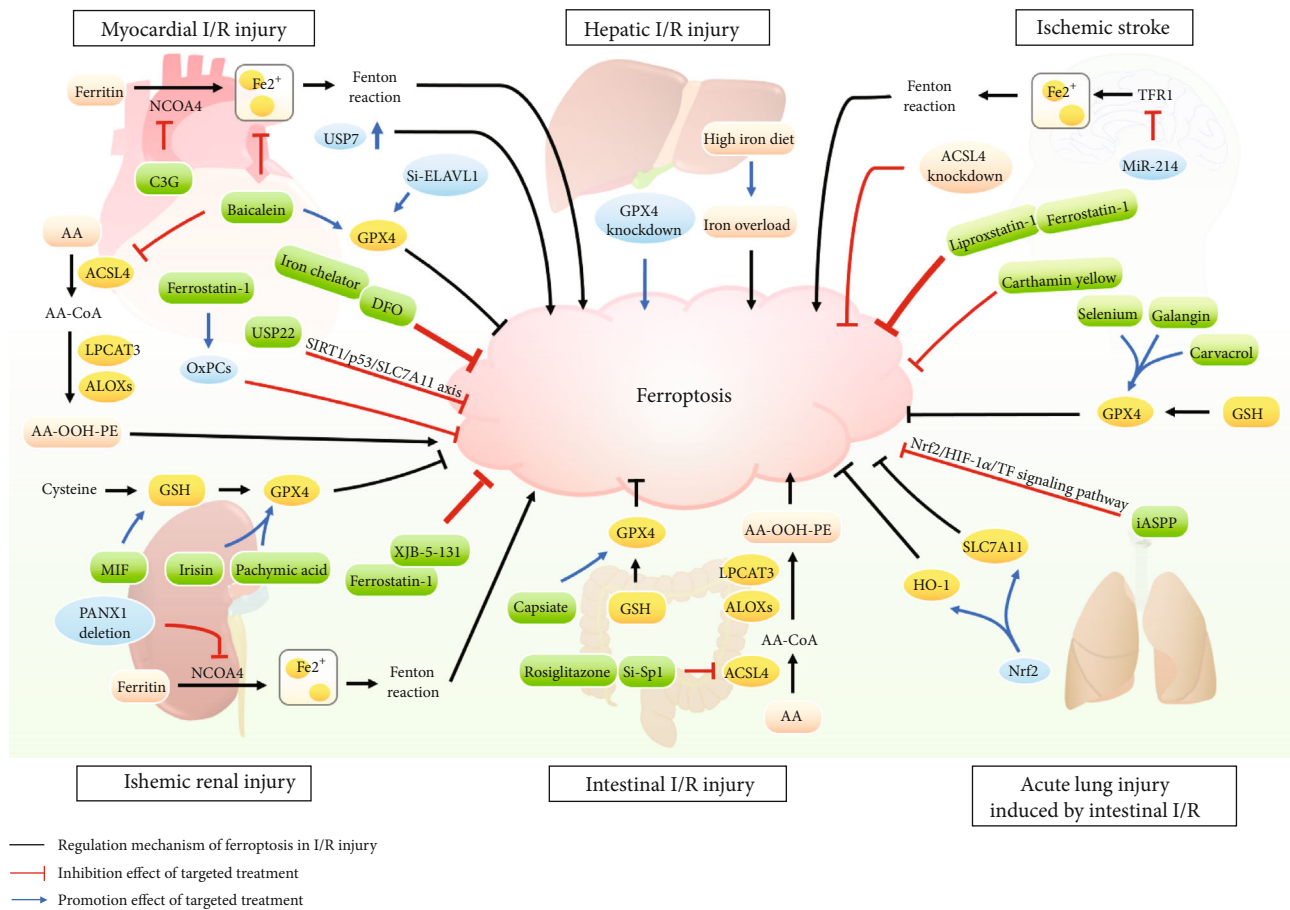
Figure 3: Pathological mechanism and targeted therapies of ferroptosis in ischemia-reperfusion (I/R) injury-related diseases. NCOA4: nuclear receptor coactivator 4; C3G: cyanidin-3-glucoside; USP7: ubiquitin-specific protease 7; USP7 ↑: the upregulation of USP7; ELAVL1: embryonic lethal-abnormal vision like protein 1; GPX4: glutathione peroxidase 4; AA: arachidonic acid; ACSL4: acyl-CoA synthetase long-chain family 4; LPCAT3: lysophosphatidylcholine acyltransferase 3; ALOXs: arachidonate lipoxygenases; PE: phosphatidylethanolamine; OxPCs: oxidized phosphatidylcholines; USP22: ubiquitin-specific peptidase 22; DFO: deferoxamine; TFR1: transferrin receptor 1; GSH: glutathione; MIF: macrophage migration inhibitory factor; Sp1: special protein 1; SLC7A11: solute carrier family 7 member 11; NRF2: nuclear factor erythroid 2-related factor; HO-1: heme oxygenase-1; iASPP: inhibitor of apoptosis-stimulating protein of P53.

preventing and treating hepatic I/R injury [116]. A recent study has also implicated that ferroptosis is associated with intestinal I/R injury [117]. Increasing evidence shows that ROS play a key role in the pathogenesis of intestinal I/R. The primary contributors of ferroptosis, including ROS generation and increase in lipid peroxidation, are related to intestinal I/R injury [118]. Deng et al. found that capsiate, a gut microbiota metabolite, can promote the expression of GPX4 by activating TRPV1 and inhibiting ferroptosis induced by intestinal I/R [119]. In addition, intestinal I/R has been shown to induce acute lung injury [120, 121]. An earlier study demonstrated ferroptosis in acute lung injury induced by intestinal I/R [122]. It has been shown that Nrf2 inhibits ferroptosis by promoting the expression of SLC7A11 and HO-1 and plays a protective role in acute lung injury following intestinal I/R [122]. The inhibitor of apoptosis-stimulating protein of p53 (iASPP) is the only inhibitor of apoptosis-stimulating protein in the p53 family. A recent study has suggested that in Nrf2-/- mice with acute

lung injury induced by intestinal I/R, iASPP can effectively alleviate acute lung injury and inhibit ferroptosis through the Nrf2/HIF-1α/TF signaling pathway [123].

4. Conclusions

In recent years, great progress has been made in applying ferroptosis in I/R injury in various organs and diseases (see Figure 3). Table 1 summarizes the main findings of studies that investigated the relevant mechanisms and targets of ferroptosis in I/R injury. However, there are several unclear mechanisms of ferroptosis in I/R injury. First, existing research on the pathological effects of ferroptosis has mostly concentrated on the animal and cell levels, and evaluation of its clinical efficacy is rare. Second, there is relatively little research on the target of ferroptosis in I/R injury in various organs and the application of targeted therapy, which requires more in-depth and extensive investigations. With the in-depth exploration of research, suppressing ferroptosis

TABLE 1: Studies reporting the mechanisms and targets of ferroptosis in ischemia-reperfusion injury.

Ferroptosis in I/R injury	Experiment	Number (n)	Model/study population	Intervention	Target	Reference
	In vitro	Not applicable	Mouse embryonic fibroblasts	Not available	Glutaminolysis	[70]
	In vitro	Not applicable	H9c2 cells	C3G	Ferroptosis-related protein, NCOA4, RSL3	[72]
	In vitro	Not applicable	Adult rat cardiomyocytes	Ferrostatin-1	OxPCs	[76]
	In vitro	Not applicable	H9c2 cells	Baicalin	ACSL4	[82]
	In vitro	Not applicable	Human cardiomyocytes	ELAVL1 knockout	Not available	[84]
	In vivo	Not applicable	I/R-treated Sprague–Dawley rats	Not available	Upregulation of USP7	[74]
Myocardial I/R injury	In vivo	Not applicable	Murine models of doxorubicin- and I/R-induced cardiomyopathy	Ferrostatin-1 and iron chelator	Not available	[77]
	In vivo	Not applicable	Sprague–Dawley rats	C3G	Ferroptosis-related protein, NCOA4, RSL3	[72]
	In vivo	Not applicable	Myocardial I/R rat model	Baicalin	ACSL4	[82]
	In vivo	Not applicable	Sprague–Dawley rats	USP22	Not available	[83]
	Clinical finding	60	Patients with ST-elevation-myocardial infarct	DFO	Not available	[78]
	Clinical finding	45	Patients undergoing coronary artery bypass grafting	DFO	Not available	[79]
	In vitro	Not applicable	Primary cortical neurons and hippocampal HT22 cells	Selenium	GPX4	[92]
	In vivo	Not applicable	C57BL/6 mice	Selenium	GPX4	[92]
	In vivo	Not applicable	Sprague–Dawley rats	Liproxstatin-1, Ferrostatin-1	Not available	[95]
Cerebral I/R injury	In vivo	Not applicable	Brain I/R mice model	Carthamin yellow	Not available	[96]
	In vivo	Not applicable	Mice models of cerebral I/R	MiR-214	PVT1, TFR1, TP53	[97]
	In vivo	Not applicable	Ischemic stroke model gerbils	Carvacrol	GPX4	[98]
	In vivo	Not applicable	Ischemic stroke model gerbils	Galangin	SLC7A11, GPX4	[100]
	In vivo	Not applicable	Mice models	Knockdown of ACSL4	Not available	[102]
	In vivo	Not applicable	C57BL/6 mice	Ferrostatin 1 or 16-86	Not available	[106]
	In vivo	Not applicable	I/R-induced renal injury rat models	Not available	GPX4, SLC7A11	[107]
	In vivo	Not applicable	Mice models	PANX1 deletion	Not available	[108]
Ischemic renal injury	In vivo	Not applicable	Mif-/- mice	MIF	GSH	[109]
	In vivo	Not applicable	Renal I/R injury mice model	Pachymic acid	GPX4, SLC7A11, and HO-1	[110]
	In vivo	Not applicable	Renal I/R mice model	XJB-5-131	Not available	[111]
	In vivo	Not applicable	Renal I/R mice model	Irisin	GPX4	[112]
Hepatic I/R injury	In vivo	Not applicable	Gpx4-/- mice	Knockout of GPX4	Not available	[6]
	In vivo	Not applicable	Murine hepatic I/R injury model	Iron overload	Not available	[116]

TABLE 1: Continued.

Ferroptosis in I/R injury	Experiment	Number (n)	Model/study population	Intervention	Target	Reference
	In vitro	Not applicable	Caco-2 cells	Rosiglitazone, si-special protein 1	ACSL4	[117]
	In vitro	Not applicable	Ileum organoid H/R model	Capsiate	GPX4, TRPV1	[119]
Intestinal I/R injury	In vivo	Not applicable	Murine model of intestinal I/R	Rosiglitazone, si-special protein 1	ACSL4	[117]
	In vivo	Not applicable	Mouse intestinal I/R model	Capsiate	GPX4, TRPV1	[119]
	In vivo	Not applicable	C57BL/6J mice and Nrf2-/- mice	Nrf2	SLC7A11, HO-1	[122]
Acute lung injury induced by intestinal I/R	In vivo	Not applicable	Nrf2-/- mice with acute lung injury induced by intestinal I/R	Inhibitor of apoptosis-stimulating protein of P53	Nrf2	[123]

could be an effective strategy for treating I/R-related organ diseases. The development of ferroptosis modulators is expected to provide new opportunities for the treatment of I/R injury and related diseases. Therefore, it is necessary to conduct such studies to screen new targeted ferroptosis therapies with potentially protective effects against I/R injury in the future.

Conflicts of Interest

The authors declare that no conflict of interest exists.

Authors' Contributions

Xinye Li, Ning Ma, Juping Xu, Yanchi Zhang, and Pan Yang contributed equally to this work.

Acknowledgments

References

[1] H. K. Eltzschig and T. Eckle, "Ischemia and reperfusion–from mechanism to translation," *Nature Medicine*, vol. 17, no. 11, pp. 1391–1401, 2011.

[2] S. Dixon, K. Lemberg, M. Lamprecht et al., "Ferroptosis: an iron-dependent form of nonapoptotic cell death," *Cell*, vol. 149, no. 5, pp. 1060–1072, 2012.

[3] B. Stockwell, J. Friedmann Angeli, H. Bayir et al., "Ferroptosis: a regulated cell death nexus linking metabolism, redox biology, and disease," *Cell*, vol. 171, no. 2, pp. 273–285, 2017.

[4] M. ten Hove, C. A. Lygate, A. Fischer et al., "Reduced inotropic reserve and increased susceptibility to cardiac ischemia/reperfusion injury in phosphocreatine-deficient guanidinoacetate-N-methyltransferase-knockout mice," *Circulation*, vol. 111, no. 19, pp. 2477–2485, 2005.

[5] L. R. Hanson, A. Roeytenberg, P. M. Martinez et al., "Intranasal deferoxamine provides increased brain exposure and significant protection in rat ischemic stroke," *The Journal of Pharmacology and Experimental Therapeutics*, vol. 330, no. 3, pp. 679–686, 2009.

[6] J. Friedmann Angeli, M. Schneider, B. Proneth et al., "Inactivation of the ferroptosis regulator Gpx4 triggers acute renal failure in mice," *Nature Cell Biology*, vol. 16, no. 12, pp. 1180–1191, 2014.

[7] E. E. Montalvo-Jave, T. Escalante-Tattersfield, J. A. Ortega-Salgado, E. Piña, and D. A. Geller, "Factors in the pathophysiology of the liver ischemia-reperfusion injury," *The Journal of Surgical Research*, vol. 147, no. 1, pp. 153–159, 2008.

[8] N. Yagoda, M. von Rechenberg, E. Zaganjor et al., "RAS-RAF-MEK-dependent oxidative cell death involving voltage-dependent anion channels," *Nature*, vol. 447, no. 7146, pp. 864–868, 2007.

[9] W. Yang and B. R. Stockwell, "Synthetic lethal screening identifies compounds activating iron-dependent, nonapoptotic cell death in oncogenic-RAS-harboring cancer cells," *Chemistry & Biology*, vol. 15, no. 3, pp. 234–245, 2008.

[10] A. Fatokun, V. L. Dawson, and T. M. Dawson, "Parthanatos: mitochondrial-linked mechanisms and therapeutic opportunities," *British Journal of Pharmacology*, vol. 171, no. 8, pp. 2000–2016, 2014.

[11] J. Wu, Q. Z. Tuo, and P. Lei, "Ferroptosis, a recent defined form of critical cell death in neurological disorders," *Journal of Molecular Neuroscience: MN*, vol. 66, no. 2, pp. 197–206, 2018.

[12] V. Bochkov, O. Oskolkova, K. Birukov, A. L. Levonen, C. J. Binder, and J. Stöckl, "Generation and biological activities of oxidized phospholipids," *Antioxidants & Redox Signaling*, vol. 12, no. 8, pp. 1009–1059, 2010.

[13] S. Dixon, D. Patel, M. Welsch et al., "Pharmacological inhibition of cystine-glutamate exchange induces endoplasmic reticulum stress and ferroptosis," *eLife*, vol. 3, article e02523, 2014.

[14] W. Yang, R. SriRamaratnam, M. Welsch et al., "Regulation of ferroptotic cancer cell death by GPX4," *Cell*, vol. 156, no. 1-2, pp. 317–331, 2014.

[15] S. Dixon, G. Winter, L. Musavi et al., "Human haploid cell genetics reveals roles for lipid metabolism genes in nonapoptotic cell death," *ACS Chemical Biology*, vol. 10, no. 7, pp. 1604–1609, 2015.

[16] S. Bröer and C. A. Wagner, "Structure-function relationships of heterodimeric amino acid transporters," *Cell Biochemistry and Biophysics*, vol. 36, no. 2-3, pp. 155–168, 2002.

[17] C. Liang, X. Zhang, M. Yang, and X. Dong, "Recent progress in ferroptosis inducers for cancer therapy," *Advanced Materials (Deerfield Beach, Fla.)*, vol. 31, no. 51, article e1904197, 2019.

[18] M. Conrad and H. Sato, "The oxidative stress-inducible cystine/glutamate antiporter, system x_c^-: cystine supplier and beyond," *Amino Acids*, vol. 42, no. 1, pp. 231–246, 2012.

[19] R. Bridges, N. R. Natale, and S. A. Patel, "System x_c^- cystine/glutamate antiporter: an update on molecular pharmacology and roles within the CNS," *British Journal of Pharmacology*, vol. 165, no. 1, pp. 20–34, 2012.

[20] B. R. Cardoso, D. J. Hare, A. I. Bush, and B. R. Roberts, "Glutathione peroxidase 4: a new player in neurodegeneration?," *Molecular Psychiatry*, vol. 22, no. 3, pp. 328–335, 2017.

[21] I. Ingold, C. Berndt, S. Schmitt et al., "Selenium utilization by GPX4 is required to prevent hydroperoxide-induced ferroptosis," *Cell*, vol. 172, no. 3, pp. 409–422.e21, 2018.

[22] A. Meister and M. E. Anderson, "Glutathione," *Annual Review of Biochemistry*, vol. 52, no. 1, pp. 711–760, 1983.

[23] M. Maiorino, M. Conrad, and F. Ursini, "GPx4, lipid peroxidation, and cell death: discoveries, rediscoveries, and open issues," *Antioxidants & Redox Signaling*, vol. 29, no. 1, pp. 61–74, 2018.

[24] S. Dolma, S. Lessnick, W. Hahn, and B. R. Stockwell, "Identification of genotype-selective antitumor agents using synthetic lethal chemical screening in engineered human tumor cells," *Cancer Cell*, vol. 3, no. 3, pp. 285–296, 2003.

[25] B. Ke, M. Tian, J. Li, B. Liu, and G. He, "Targeting programmed cell death using small-molecule compounds to improve potential cancer therapy," *Medicinal Research Reviews*, vol. 36, no. 6, pp. 983–1035, 2016.

[26] W. Yang, K. Kim, M. Gaschler, M. Patel, M. S. Shchepinov, and B. R. Stockwell, "Peroxidation of polyunsaturated fatty acids by lipoxygenases drives ferroptosis," *Proceedings of the National Academy of Sciences of the United States of America*, vol. 113, no. 34, pp. E4966–E4975, 2016.

[27] K. Bersuker, J. Hendricks, Z. Li et al., "The CoQ oxidoreductase FSP1 acts parallel to GPX4 to inhibit ferroptosis," *Nature*, vol. 575, no. 7784, pp. 688–692, 2019.

[28] S. Doll, F. Freitas, R. Shah et al., "FSP1 is a glutathione-independent ferroptosis suppressor," *Nature*, vol. 575, no. 7784, pp. 693–698, 2019.

[29] K. Shimada, R. Skouta, A. Kaplan et al., "Global survey of cell death mechanisms reveals metabolic regulation of ferroptosis," *Nature Chemical Biology*, vol. 12, no. 7, pp. 497–503, 2016.

[30] L. Jiang, N. Kon, T. Li et al., "Ferroptosis as a p53-mediated activity during tumour suppression," *Nature*, vol. 520, no. 7545, pp. 57–62, 2015.

[31] W. Li, W. Li, Y. Leng, Y. Xiong, and Z. Xia, "Ferroptosis is involved in diabetes myocardial ischemia/reperfusion injury through endoplasmic reticulum stress," *DNA and Cell Biology*, vol. 39, no. 2, pp. 210–225, 2020.

[32] Y. Ou, S. Wang, D. Li, B. Chu, and W. Gu, "Activation of SAT1 engages polyamine metabolism with p53-mediated ferroptotic responses," *Proceedings of the National Academy of Sciences of the United States of America*, vol. 113, no. 44, pp. E6806–E6812, 2016.

[33] I. Harris and G. M. DeNicola, "The Complex Interplay between Antioxidants and ROS in Cancer," *Trends in Cell Biology*, vol. 30, no. 6, pp. 440–451, 2020.

[34] V. Kagan, G. Mao, F. Qu et al., "Oxidized arachidonic and adrenic PEs navigate cells to ferroptosis," *Nature Chemical Biology*, vol. 13, no. 1, pp. 81–90, 2017.

[35] P. Lei, T. Bai, and Y. Sun, "Mechanisms of ferroptosis and relations with regulated cell death: a review," *Frontiers in Physiology*, vol. 10, p. 139, 2019.

[36] S. Doll, B. Proneth, Y. Tyurina et al., "ACSL4 dictates ferroptosis sensitivity by shaping cellular lipid composition," *Nature Chemical Biology*, vol. 13, no. 1, pp. 91–98, 2017.

[37] G. Forcina and S. J. Dixon, "GPX4 at the crossroads of lipid homeostasis and ferroptosis," *Proteomics*, vol. 19, no. 18, article e1800311, 2019.

[38] M. Lagarde, C. Calzada, C. Jouvène et al., "Functional fluxolipidomics of polyunsaturated fatty acids and oxygenated metabolites in the blood vessel compartment," *Progress in Lipid Research*, vol. 60, pp. 41–49, 2015.

[39] B. Hassannia, P. Vandenabeele, and T. vanden Berghe, "Targeting ferroptosis to iron out cancer," *Cancer Cell*, vol. 35, no. 6, pp. 830–849, 2019.

[40] D. Galaris, A. Barbouti, and K. Pantopoulos, "Iron homeostasis and oxidative stress: an intimate relationship," *Biochimica et Biophysica Acta Molecular Cell Research*, vol. 1866, no. 12, p. 118535, 2019.

[41] O. Kakhlon and Z. I. Cabantchik, "The labile iron pool: characterization, measurement, and participation in cellular processes," *Free Radical Biology & Medicine*, vol. 33, no. 8, pp. 1037–1046, 2002.

[42] M. Kruszewski, "Labile iron pool: the main determinant of cellular response to oxidative stress," *Mutation Research*, vol. 531, no. 1-2, pp. 81–92, 2003.

[43] V. Grivennikova and A. D. Vinogradov, "Generation of superoxide by the mitochondrial complex I," *Biochimica et Biophysica Acta*, vol. 1757, no. 5-6, pp. 553–561, 2006.

[44] B. Halliwell and C. E. Cross, "Oxygen-derived species: their relation to human disease and environmental stress," *Environmental Health Perspectives*, vol. 102, Supplement 10, pp. 5–12, 1994.

[45] S. Alvarez, V. Sviderskiy, E. Terzi et al., "NFS1 undergoes positive selection in lung tumours and protects cells from ferroptosis," *Nature*, vol. 551, no. 7682, pp. 639–643, 2017.

[46] X. Sun, Z. Ou, M. Xie et al., "HSPB1 as a novel regulator of ferroptotic cancer cell death," *Oncogene*, vol. 34, no. 45, pp. 5617–5625, 2015.

[47] A. Terman and T. Kurz, "Lysosomal iron, iron chelation, and cell death," *Antioxidants & Redox Signaling*, vol. 18, no. 8, pp. 888–898, 2013.

[48] M. Gao, P. Monian, Q. Pan, W. Zhang, J. Xiang, and X. Jiang, "Ferroptosis is an autophagic cell death process," *Cell Research*, vol. 26, no. 9, pp. 1021–1032, 2016.

[49] W. Hou, Y. Xie, X. Song et al., "Autophagy promotes ferroptosis by degradation of ferritin," *Autophagy*, vol. 12, no. 8, pp. 1425–1428, 2016.

[50] R. Daher, H. Manceau, and Z. Karim, "Iron metabolism and the role of the iron-regulating hormone hepcidin in health and disease," *Presse Medicale (Paris, France: 1983)*, vol. 46, no. 12, pp. e272–e278, 2017.

[51] X. Sun, Z. Ou, R. Chen et al., "Activation of the p62-Keap 1-NRF2 pathway protects against ferroptosis in hepatocellular carcinoma cells," *Hepatology (Baltimore, Md.)*, vol. 63, no. 1, pp. 173–184, 2016.

[52] L. Tang, X. Luo, H. Tu et al., "Ferroptosis occurs in phase of reperfusion but not ischemia in rat heart following ischemia or ischemia/reperfusion," *Naunyn-Schmiedeberg's Archives of Pharmacology*, vol. 394, no. 2, pp. 401–410, 2021.

[53] M. Hess and N. Manson, "Molecular oxygen: Friend and foe: The role of the oxygen free radical system in the calcium paradox, the oxygen paradox and ischemia/reperfusion injury," *Journal of Molecular and Cellular Cardiology*, vol. 16, no. 11, pp. 969–985, 1984.

[54] L. C. Becker and G. Ambrosio, "Myocardial consequences of reperfusion," *Progress in Cardiovascular Diseases*, vol. 30, no. 1, pp. 23–44, 1987.

[55] E. E. Farmer and M. J. Mueller, "ROS-mediated lipid peroxidation and RES-activated signaling," *Annual Review of Plant Biology*, vol. 64, no. 1, pp. 429–450, 2013.

[56] Y. Zhao, Z. Xin, N. Li et al., "Nano-liposomes of lycopene reduces ischemic brain damage in rodents by regulating iron metabolism," *Free Radic Biol Med*, vol. 124, pp. 1–11, 2018.

[57] Y. Scindia, J. Leeds, and S. Swaminathan, "Iron homeostasis in healthy kidney and its role in acute kidney injury," *Seminars in Nephrology*, vol. 39, no. 1, pp. 76–84, 2019.

[58] D. Galaris, A. Barbouti, and P. Korantzopoulos, "Oxidative stress in hepatic ischemia-reperfusion injury: the role of antioxidants and iron chelating compounds," *Current Pharmaceutical Design*, vol. 12, no. 23, pp. 2875–2890, 2006.

[59] C. W. White, A. Ali, D. Hasanally et al., "A cardioprotective preservation strategy employing *ex vivo* heart perfusion facilitates successful transplant of donor hearts after cardiocirculatory death," *The Journal of Heart and Lung Transplantation*, vol. 32, no. 7, pp. 734–743, 2013.

[60] C. W. White, D. Hasanally, P. Mundt et al., "A whole blood-based perfusate provides superior preservation of myocardial function during ex vivo heart perfusion," *The Journal of Heart and Lung Transplantation*, vol. 34, no. 1, pp. 113–121, 2015.

[61] R. Ganguly, D. Hasanally, A. Stamenkovic et al., "Alpha linolenic acid decreases apoptosis and oxidized phospholipids in cardiomyocytes during ischemia/reperfusion," *Molecular and Cellular Biochemistry*, vol. 437, no. 1-2, pp. 163–175, 2018.

[62] C. Yeang, D. Hasanally, X. Que et al., "Reduction of myocardial ischaemia-reperfusion injury by inactivating oxidized phospholipids," *Cardiovascular Research*, vol. 115, no. 1, pp. 179–189, 2019.

[63] M. Valko, K. Jomova, C. J. Rhodes, K. Kuča, and K. Musílek, "Redox- and non-redox-metal-induced formation of free radicals and their role in human disease," *Archives of Toxicology*, vol. 90, no. 1, pp. 1–37, 2016.

[64] M. D. Brand, "Mitochondrial generation of superoxide and hydrogen peroxide as the source of mitochondrial redox signaling," *Free Radical Biology and Medicine*, vol. 100, pp. 14–31, 2016.

[65] P. Ježek and L. Hlavatá, "Mitochondria in homeostasis of reactive oxygen species in cell, tissues, and organism," *The International Journal of Biochemistry & Cell Biology*, vol. 37, no. 12, pp. 2478–2503, 2005.

[66] J. L. Anderson and D. A. Morrow, "Acute myocardial infarction," *The New England Journal of Medicine*, vol. 376, no. 21, pp. 2053–2064, 2017.

[67] D. Granger and P. R. Kvietys, "Reperfusion injury and reactive oxygen species: the evolution of a concept," *Redox Biology*, vol. 6, pp. 524–551, 2015.

[68] N. An, Y. Gao, Z. Si et al., "Regulatory mechanisms of the NLRP3 inflammasome, a novel immune-inflammatory marker in cardiovascular diseases," *Frontiers in Immunology*, vol. 10, p. 1592, 2019.

[69] X. Yang, N. An, C. Zhong et al., "Enhanced cardiomyocyte reactive oxygen species signaling promotes ibrutinib-induced atrial fibrillation," *Redox Biology*, vol. 30, p. 101432, 2020.

[70] M. Gao, P. Monian, N. Quadri, R. Ramasamy, and X. Jiang, "Glutaminolysis and transferrin regulate ferroptosis," *Molecular Cell*, vol. 59, no. 2, pp. 298–308, 2015.

[71] Y. Baba, J. Higa, B. Shimada et al., "Protective effects of the mechanistic target of rapamycin against excess iron and ferroptosis in cardiomyocytes," *American Journal of Physiology-Heart and Circulatory Physiology*, vol. 314, no. 3, pp. H659–H668, 2018.

[72] X. Shan, Z. Lv, M. Yin, J. Chen, J. Wang, and Q. N. Wu, "The Protective Effect of Cyanidin-3-Glucoside on Myocardial Ischemia- Reperfusion Injury through Ferroptosis," *Oxidative Medicine and Cellular Longevity*, vol. 2021, Article ID 8880141, 15 pages, 2021.

[73] E. Park and S. W. Chung, "ROS-mediated autophagy increases intracellular iron levels and ferroptosis by ferritin and transferrin receptor regulation," *Cell Death & Disease*, vol. 10, no. 11, p. 822, 2019.

[74] L. Tang, Y. Zhou, X. Xiong et al., "Ubiquitin-specific protease 7 promotes ferroptosis via activation of the p53/TfR1 pathway in the rat hearts after ischemia/reperfusion," *Free Radical Biology & Medicine*, vol. 162, pp. 339–352, 2021.

[75] J. Li, F. Cao, H. Yin et al., "Ferroptosis: past, present and future," *Cell Death & Disease*, vol. 11, no. 2, p. 88, 2020.

[76] a. Stamenkovic, G. N. Pierce, and A. Ravandi, "phospholipid oxidation products in ferroptotic myocardial cell death," *American Journal of Physiology-Heart and Circulatory Physiology*, vol. 317, no. 1, pp. h156–h163, 2019.

[77] X. Fang, H. Wang, D. Han et al., "Ferroptosis as a target for protection against cardiomyopathy," *Proceedings of the National Academy of Sciences of the United States of America*, vol. 116, no. 7, pp. 2672–2680, 2019.

[78] W. Chan, A. Taylor, A. Ellims et al., "Effect of iron chelation on myocardial infarct size and oxidative stress in ST-elevation-myocardial infarction," *Circulation: Cardiovascular Interventions*, vol. 5, no. 2, pp. 270–278, 2012.

[79] I. Paraskevaidis, E. Iliodromitis, D. Vlahakos et al., "Deferoxamine infusion during coronary artery bypass grafting ameliorates lipid peroxidation and protects the myocardium against reperfusion injury: immediate and long-term significance," *European Heart Journal*, vol. 26, no. 3, pp. 263–270, 2005.

[80] Y. Xie, X. Song, X. Sun et al., "Identification of baicalein as a ferroptosis inhibitor by natural product library screening," *Biochemical and Biophysical Research Communications*, vol. 473, no. 4, pp. 775–780, 2016.

[81] Q. Li, Q. Li, J. Jia et al., "Baicalein exerts neuroprotective effects in FeCl$_3$-induced posttraumatic epileptic seizures via suppressing ferroptosis," *Frontiers in Pharmacology*, vol. 10, p. 638, 2019.

[82] Z. Fan, L. Cai, S. Wang, J. Wang, and B. Chen, "Baicalin prevents myocardial ischemia/reperfusion injury through inhibiting ACSL4 mediated ferroptosis," *Frontiers in Pharmacology*, vol. 12, p. 628988, 2021.

[83] S. Ma, L. Sun, W. Wu, J. Wu, Z. Sun, and J. Ren, "USP22 protects against myocardial ischemia-reperfusion injury via the SIRT1-p 53/SLC7A11-dependent inhibition of ferroptosis-induced cardiomyocyte death," *Frontiers in Physiology*, vol. 11, p. 551318, 2020.

[84] H. Chen, Z. Xiao, X. Ling, R. N. Xu, P. Zhu, and S. Y. Zheng, "ELAVL1 is transcriptionally activated by FOXC1 and promotes ferroptosis in myocardial ischemia/reperfusion injury by regulating autophagy," *Molecular Medicine (Cambridge, Mass.)*, vol. 27, no. 1, p. 14, 2021.

[85] A. Stamenkovic, K. A. O'Hara, D. C. Nelson et al., "Oxidized phosphatidylcholines trigger ferroptosis in cardiomyocytes during ischemia-reperfusion injury," *American Journal of Physiology-Heart and Circulatory Physiology*, vol. 320, no. 3, pp. H1170–h1184, 2021.

[86] G. Cao, N. Jiang, Y. Hu et al., "Ruscogenin attenuates cerebral ischemia-induced blood-brain barrier dysfunction by suppressing TXNIP/NLRP3 inflammasome activation and the MAPK pathway," *International Journal of Molecular Sciences*, vol. 17, no. 9, p. 1418, 2016.

[87] M. Pamenter, D. Hogg, X. Gu, L. T. Buck, and G. G. Haddad, "Painted turtle cortex is resistant to an in vitro mimic of the ischemic mammalian penumbra," *Journal of Cerebral Blood Flow and Metabolism*, vol. 32, no. 11, pp. 2033–2043, 2012.

[88] W. Li, C. Tan, Y. Liu et al., "Resveratrol ameliorates oxidative stress and inhibits aquaporin 4 expression following rat cerebral ischemia-reperfusion injury," *Molecular Medicine Reports*, vol. 12, no. 5, pp. 7756–7762, 2015.

[89] F. Groenendaal, M. Shadid, J. McGowan, O. P. Mishra, and F. van Bel, "Effects of Deferoxamine, a Chelator of Free Iron, on Na$^+$,K$^+$-ATPase Activity of Cortical Brain Cell Membrane during Early Reperfusion after Hypoxia-Ischemia in Newborn Lambs," *Pediatric Research*, vol. 48, no. 4, pp. 560–564, 2000.

[90] M. Shadid, G. Buonocore, F. Groenendaal et al., "Effect of deferoxamine and allopurinol on non-protein-bound iron concentrations in plasma and cortical brain tissue of newborn lambs following hypoxia-ischemia," *Neuroscience Letters*, vol. 248, no. 1, pp. 5–8, 1998.

[91] M. Selim, "Treatment with the iron chelator, deferoxamine mesylate, alters serum markers of oxidative stress in stroke patients," *Translational Stroke Research*, vol. 1, no. 1, pp. 35–39, 2010.

[92] I. Alim, J. Caulfield, Y. Chen et al., "Selenium drives a transcriptional adaptive program to block ferroptosis and treat stroke," *Cell*, vol. 177, no. 5, pp. 1262–1279.e25, 2019.

[93] J. Anrather and C. Iadecola, "Inflammation and stroke: an overview," *Neurotherapeutics*, vol. 13, no. 4, pp. 661–670, 2016.

[94] Q. Tuo, S. T. Zhang, and P. Lei, "Mechanisms of neuronal cell death in ischemic stroke and their therapeutic implications," *Medicinal Research Reviews*, 2021.

[95] Q. Tuo, P. Lei, K. Jackman et al., "Tau-mediated iron export prevents ferroptotic damage after ischemic stroke," *Molecular Psychiatry*, vol. 22, no. 11, pp. 1520–1530, 2017.

[96] H. Guo, L. Zhu, P. Tang et al., "Carthamin yellow improves cerebral ischemia-reperfusion injury by attenuating inflammation and ferroptosis in rats," *International Journal of Molecular Medicine*, vol. 47, no. 4, 2021.

[97] J. Lu, F. Xu, and H. Lu, "lncRNA PVT1 regulates ferroptosis through miR-214-mediated TFR1 and p53," *Life Sciences*, vol. 260, p. 118305, 2020.

[98] X. Guan, X. Li, X. Yang et al., "The neuroprotective effects of carvacrol on ischemia/reperfusion-induced hippocampal neuronal impairment by ferroptosis mitigation," *Life Sciences*, vol. 235, p. 116795, 2019.

[99] W. Zhang, Y. Lan, Q. Huang, and Z. Hua, "Galangin induces B16F10 melanoma cell apoptosis via mitochondrial pathway and sustained activation of p38 MAPK," *Cytotechnology*, vol. 65, no. 3, pp. 447–455, 2013.

[100] X. Guan, Z. Li, S. Zhu et al., "Galangin attenuated cerebral ischemia-reperfusion injury by inhibition of ferroptosis through activating the SLC7A11/GPX4 axis in gerbils," *Life Sciences*, vol. 264, p. 118660, 2021.

[101] X. Guo, Y. Lu, H. Zhang, J. Q. Huang, and Y. W. Li, "PIEZO1 might be involved in cerebral ischemia-reperfusion injury through ferroptosis regulation: a hypothesis," *Medical Hypotheses*, vol. 146, p. 110327, 2021.

[102] Y. Cui, Y. Zhang, X. Zhao et al., "ACSL4 exacerbates ischemic stroke by promoting ferroptosis-induced brain injury and neuroinflammation," *Brain, Behavior, and Immunity*, vol. 93, pp. 312–321, 2021.

[103] A. Linkermann, B. Stockwell, S. Krautwald, and H. J. Anders, "Regulated cell death and inflammation: an auto-amplification loop causes organ failure," *Nature Reviews Immunology*, vol. 14, no. 11, pp. 759–767, 2014.

[104] Y. Xie, W. Hou, X. Song et al., "Ferroptosis: process and function," *Cell Death and Differentiation*, vol. 23, no. 3, pp. 369–379, 2016.

[105] W. Yang and B. R. Stockwell, "Ferroptosis: death by lipid peroxidation," *Trends in Cell Biology*, vol. 26, no. 3, pp. 165–176, 2016.

[106] A. Linkermann, R. Skouta, N. Himmerkus et al., "Synchronized renal tubular cell death involves ferroptosis," *Proceedings of the National Academy of Sciences of the United States of America*, vol. 111, no. 47, pp. 16836–16841, 2014.

[107] C. Ding, X. Ding, J. Zheng et al., "miR-182-5p and miR-378a-3p regulate ferroptosis in I/R-induced renal injury," *Cell Death & Disease*, vol. 11, no. 10, p. 929, 2020.

[108] L. Su, X. Jiang, C. Yang et al., "Pannexin 1 mediates ferroptosis that contributes to renal ischemia/reperfusion injury," *The Journal of Biological Chemistry*, vol. 294, no. 50, pp. 19395–19404, 2019.

[109] C. Stoppe, L. Averdunk, A. Goetzenich et al., "The protective role of macrophage migration inhibitory factor in acute kidney injury after cardiac surgery," *Science Translational Medicine*, vol. 10, no. 441, article eaan4886, 2018.

[110] G. Jiang, Y. Liao, L. Huang, X. J. Zeng, and X. H. Liao, "Effects and molecular mechanism of pachymic acid on ferroptosis in renal ischemia reperfusion injury," *Molecular Medicine Reports*, vol. 23, no. 1, 2021.

[111] Z. Zhao, J. Wu, H. Xu et al., "XJB-5-131 inhibited ferroptosis in tubular epithelial cells after ischemia–reperfusion injury," *Cell Death & Disease*, vol. 11, no. 8, p. 629, 2020.

[112] J. Zhang, J. Bi, Y. Ren et al., "Involvement of GPX4 in irisin's protection against ischemia reperfusion-induced acute kidney injury," *Journal of Cellular Physiology*, vol. 236, no. 2, pp. 931–945, 2021.

[113] J. Ali, S. Davies, R. Brais et al., "Analysis of ischemia/reperfusion injury in time-zero biopsies predicts liver allograft outcomes," *Liver Transplantation*, vol. 21, no. 4, pp. 487–499, 2015.

[114] W. Kim, J. Lake, J. Smith et al., "OPTN/SRTR 2016 annual data report: liver," *American Journal of Transplantation*, vol. 18, pp. 172–253, 2018.

[115] M. Galleano, G. Tapia, S. Puntarulo, P. Varela, L. A. Videla, and V. Fernández, "Liver preconditioning induced by iron in a rat model of ischemia/reperfusion," *Life Sciences*, vol. 89, no. 7-8, pp. 221–228, 2011.

[116] N. Yamada, T. Karasawa, T. Wakiya et al., "Iron overload as a risk factor for hepatic ischemia-reperfusion injury in liver transplantation: potential role of ferroptosis," *American Journal of Transplantation*, vol. 20, no. 6, pp. 1606–1618, 2020.

[117] Y. Li, D. Feng, Z. Wang et al., "Ischemia-induced ACSL4 activation contributes to ferroptosis-mediated tissue injury in intestinal ischemia/reperfusion," *Cell Death and Differentiation*, vol. 26, no. 11, pp. 2284–2299, 2019.

[118] Y. Hu, Z. Mao, L. Xu et al., "Protective effect of dioscin against intestinal ischemia/reperfusion injury via adjusting miR-351-5p-mediated oxidative stress," *Pharmacological Research*, vol. 137, pp. 56–63, 2018.

[119] F. Deng, B. Zhao, X. Yang et al., "The gut microbiota metabolite capsiate promotes Gpx4 expression by activatingTRPV1to inhibit intestinal ischemia reperfusion-induced ferroptosis," *Gut Microbes*, vol. 13, no. 1, pp. 1902719–1902721, 2021.

[120] M. Mura, C. Andrade, B. Han et al., "Intestinal ischemia-reperfusion-induced acute lung injury and oncotic cell death

in multiple organs," *Shock (Augusta, Ga.)*, vol. 28, no. 2, pp. 227–238, 2007.

[121] A. Stallion, T. Kou, S. Latifi et al., "Ischemia/reperfusion: a clinically relevant model of intestinal injury yielding systemic inflammation," *Journal of Pediatric Surgery*, vol. 40, no. 3, pp. 470–477, 2005.

[122] H. Dong, Z. Qiang, D. Chai et al., "Nrf2 inhibits ferroptosis and protects against acute lung injury due to intestinal ischemia reperfusion via regulating SLC7A11 and HO-1," *Aging*, vol. 12, no. 13, pp. 12943–12959, 2020.

[123] Y. Li, Y. Cao, J. Xiao et al., "Inhibitor of apoptosis-stimulating protein of p53 inhibits ferroptosis and alleviates intestinal ischemia/reperfusion-induced acute lung injury," *Cell Death & Differentiation*, vol. 27, no. 9, pp. 2635–2650, 2020.

Research Article

Dioscin Attenuates Myocardial Ischemic/Reperfusion-Induced Cardiac Dysfunction through Suppression of Reactive Oxygen Species

Dayin Lyu,[1] Qing Tian,[2] Huitao Qian,[3] Chang He,[1] Tianyu Shen,[4] Jinxing Xi,[5] Pingxi Xiao [ID],[6] and Qiulun Lu [ID][1]

[1]*Key Laboratory of Cardiovascular and Cerebrovascular Medicine, Collaborative Innovation Center for Cardiovascular Disease Translational Medicine, Nanjing Medical University, Nanjing 211166, China*
[2]*Intensive Care Unit of Wuhan Asia Heart Hospital, Wuhan 430000, China*
[3]*The First Clinical Medical College of Nanjing Medical University, Nanjing 211166, China*
[4]*Department of Orthopedics Surgery, Taihe Hospital, Hubei University of Medicine, Shiyan 442000, China*
[5]*Nanjing Vocational College of Information Technology, Nanjing 211166, China*
[6]*Cardiac Department, Sir Runrun Hospital Affiliated to Nanjing Medical University, Nanjing 211166, China*

Correspondence should be addressed to Pingxi Xiao; sysu-xiao@163.com and Qiulun Lu; qiulunlu@njmu.edu.cn

Dayin Lyu and Qing Tian contributed equally to this work.

Received 15 July 2021; Accepted 2 September 2021; Published 5 October 2021

Academic Editor: Ding-Sheng Jiang

Myocardial ischemic/reperfusion (MI/R) is a leading cause of cardiovascular disease with high morbidity and mortality. However, the mechanisms underlying pathological reperfusion remain obscure. In this study, we found that dioscin, a natural product, could be a potential candidate for treating MI/R through modulating cardiac dysfunction. Mechanistically, our work revealed that dioscin could suppress the production of reactive oxygen species (ROS) *via* repressing the nicotinamide adenine dinucleotide phosphate (NADPH) oxidase 2 (*Nox2*) and enhancing the expression of antioxidant enzymes, including superoxide dismutase (SOD), catalase (CAT), glutathione (GSH), and glutathione peroxidase (GPx). These findings indicate that dioscin may be a potential candidate for therapeutic interventions in MI/R injury.

1. Introduction

Myocardial ischemic/reperfusion (MI/R), a leading cause of cardiovascular disease with high morbidity and mortality, is caused by the blood recovery after a vital period of coronary artery occlusion, which easily leads to myocardial infarction or heart failure [1–3]. Previously, literature reported that lethal reperfusion injury accounts for up to 50% of the final myocardial infarct size [4]. It is well known that the pathogenesis of MI/R injury includes oxidative stress, inflammatory response, calcium overload, and mitochondrial dysfunction [5–8]. Since

the oxidant stress is accompanied with the pathological process of cardiac dysfunction, inhibition of oxidant stress is a potential therapeutic strategy for MI/R injury [9].

Oxidative stress is originated from the overwhelmed reactive oxygen species (ROS) and the insufficient antioxidant defense systems [10]. Under the physiological condition, ROS is crucial and maintains normal cellular metabolism processes, balancing at the dynamic stage between antioxidants and oxidant response [11]. However, abundant of ROS is generated in two stages of MI/R, including ischemia and reperfusion [12]. Due to sudden overburden of the high oxygen

tensions, reperfusion contributes to elevated levels of oxygen free radical (OFR) production, which leads to oxidative damage, such as protein carbonylation and DNA oxidation [13, 14]. Nevertheless, various traditional antioxidants do not present with therapeutic efficacy [15, 16]. Some active natural products, including pentamethylquercetin, isorhychophylline, myricetin, and fisetin from medicinal plants, have shown excellent activities against MI/R injury [17–20]. Thus, it is reasonable to exploit effective natural products from herbs for the treatment of MI/R injury.

Dioscin, a natural steroid saponin isolated from the root bark of wild dioscorea nipponica, is currently widely used for cardiovascular disease treatment [21]. Our previous investigations have demonstrated that dioscin elevates lncRNA MANTIS in therapeutic angiogenesis for myocardial infarction [22]. What is more, dioscin plays a beneficial role in hepatic ischemia-reperfusion injury, intestinal ischemia-reperfusion injury, and gastric ischemia-reperfusion injury [23–25]. However, whether dioscin protects cardiac injury against MI/R remains unclear.

Hence, dioscin was systematically investigated in a MI/R-injured mouse model *in vivo* and in H9C2 cardiomyocytes *in vitro* subjected to hypoxia/reoxygenation (H/R) injury, presenting the cardioprotective role of dioscin and additionally demonstrating the beneficial function of dioscin against reactive oxygen species, in order to provide new options for the clinical treatment of MI/R.

2. Materials and Methods

2.1. Animals. Male C57BL/6 mice (22-24 g) were purchased from the Animal Core of Nanjing Medical University (Nanjing, China). The mice were kept with a standard vivarium with free access to food and water. All animal experiments were approved by the National Institutes of Health Guide for the Care and Use of Laboratory Animals, and the protocols used were also consistent with the Animal Ethics Committee of Nanjing Medical University, Nanjing, China (IACUC-2003006).

The myocardial ischemia/reperfusion injury model was produced as previously reported [26]. Briefly, the left anterior descending (LAD) coronary was tied by a slipknot with a 6-0 silk suture. After 30 min of ischemia, the slipknot was released smoothly and gently until a feeling of release was sensed, at which time, the myocardium began reperfusion and was kept for 3 days. Sham-operated control mice underwent the same surgical procedure, except the suture placed under the left coronary artery was not tied.

Dioscin (80 mg/kg/day, Di'ao Group, Chengdu, China) was administrated to mice for 3 days beginning on the day of operation. Briefly, the dioscin was first dissolved in dimethyl sulphoxide (DMSO), and then, 5% sodium carboxymethyl cellulose (CMC-Na) was added to make the volume ratio for 1 : 19. Consequently, the mice were given the dissolution by intragastric administration. The preparation and application of the drug's dissolution should be completed in one day. If precipitation occurred in the preparation process, it could be assisted by heating or ultrasound.

2.2. Measurement of Cardiac Function by Echocardiography. Echocardiographic measurements were performed on mice using a VisualSonics Vevo® 2100 Imaging System (VisualSonics, Toronto, Canada) with a 40 MHz MicroScan transducer (model MS-550D) [27]. The M-mode echocardiogram was acquired from the parasternal short axis view of the left ventricle at the midpapillary muscle level. Echocardiographic parameters were calculated using the primary measurements and accompanying software. The echocardiographer was blinded to the genetic identity of the mice for all studies.

2.3. Histological Assays. Mouse hearts were dissected out, then fixed in 4% paraformaldehyde (PFA, Electron Microscopy Sciences) overnight. After dehydration through a series of ethanol baths, samples were embedded in paraffin wax. Further, 5 μm thick samples of the heart were obtained to perform hematoxylin and eosin (HE) and Masson trichrome staining. Slides were imaged under a light microscope.

2.4. Determination of Enzyme Activities. The detection kits of superoxide dismutase (SOD), catalase (CAT), glutathione (GSH), and glutathione peroxidase (GPx) were purchased from a company (Solarbio, China). The activities of these enzymes in the heart were evaluated following the manufacturer's instructions.

2.5. Determination of Reactive Oxygen Species (ROS). The production of ROS was measured as previously described [28]. The samples of the heart section were incubated with the DHE (Beyotime, China) at 37°C for 30 min, then washed three times with PBS for 5 min, and further costained with DAPI (Beyotime, China). The fluorescence intensity was examined using a confocal scanning microscope, and all images were analyzed using ImageJ software.

2.6. Quantitative RT-PCR. Total RNA was isolated using the TRIzol Reagent (Invitrogen) from cell or tissue samples. The mRNA expression levels were determined by quantitative reverse transcription polymerase chain reaction (PCR) using SuperScript II Reverse Transcriptase (Thermo Fisher Scientific Inc.) for reverse transcription and a Power SYBR Green PCR Master Mix (Thermo Fisher Scientific Inc.) for quantitative reverse transcription PCR reaction with PCR primers. The measurable of corresponding genes were detected by real-time PCR Detection System (Bio-Rad) and were analysed by CFX Manager 3.1 software (Bio-Rad). The sequences of primers were as follows: Anp-F: 5′-ACC TCC CGA AGC TAC CTA AGT-3′, Anp-R: 3′-CAA CCT TTT CAA CGG CTC CAA-5′; Bnp-F: 5′-GAG GTC ACT CCT ATC CTC TGG-3′, Bnp-R: 3′-GCC ATT TCC TCC GAC TTT TCT C-5′; β-Mhc-F: 5′-GAG GGT GGC TCT CAC ACA TTC-3′, β-Mhc-R: 3′-TTG GCC TTC GTA AGC AAA CTG-5′; Sod1-F: 5′-AAC CAG TTG TGT TGT CAG GAC-3′, Sod1-R: 3′-CCA CCA TGT TTC TTA GAG TGA GG-5′; Sod2-F: 5′-CAG ACC TGC CTT ACG ACT ATG G-3′, Sod2-R: 3′-CTC GGT GGC GTT GAG ATT GTT-5′; Cat-F: 5′-AGC GAC CAG ATG AAG CAG TG-3′, Cat-R: 3′-TCC GCT CTC TGT CAA AGT GTG-5′; Nrf2-F: 5′-CCA TTT ACG
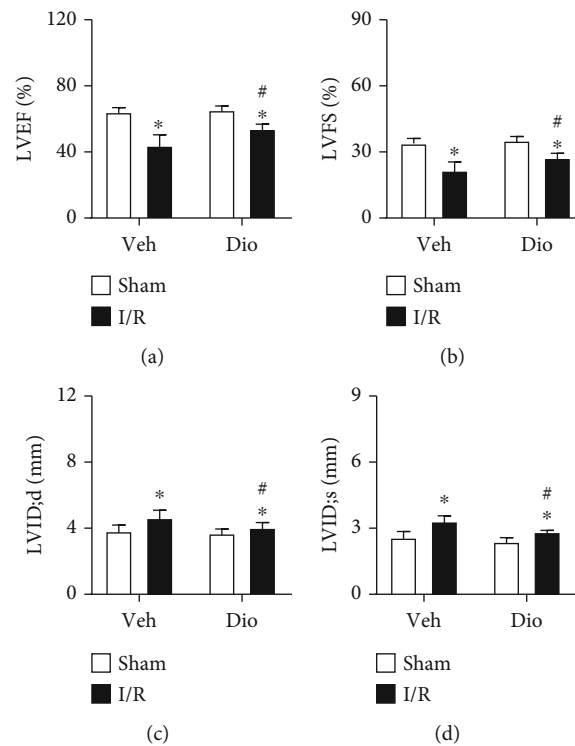
FIGURE 1: Dioscin improves cardiac function in ischemic/reperfusion mice. The C57BL/6 mice were subjected to myocardial ischemic/reperfusion (MI/R) surgery. Echocardiographic parameters for (a) left ventricular ejection fraction (LVEF, %), (b) left ventricular fractional shortening (LVFS, %), (c) left ventricular end diastolic internal dimension (LVID; d, mm), and (d) left ventricular end systolic internal dimension (LVID; s, mm). $n = 8$ each group. Data are mean ± SD. $^*P < 0.05$ vs. sham group, $^\#P < 0.05$ vs. I/R group.

GAG ACC CAC CGC CTG-3′, Nrf2-R: 3′-CTC GTG TGA GAT GAG CCT CTA AGC GG-5′; Nox2-F: 5′-ACT CCT TGG GTC AGC ACT GG-3′, Nox2-R: 3′-GTT CCT GTC CAG TTG TCT TCG-5′; and 18s-F: 5′-GCC TCC TCC TCC TCT CTC-3′, 18s-R: 3′-GCT ACT GGC AGG ATC AAC C-5′.

2.7. Statistical Analysis. Continuous variables that approximated the normal distribution were expressed as mean ± SD. Comparison between groups was subjected to ANOVA followed by the Bonferroni correction for post hoc t-test. Data expressed as proportions were assessed with a chi-square test. Two-sided tests have been used throughout, and P values < 0.05 were considered statistically significant. GraphPad Prism 8 was used to evaluate data.

3. Results

3.1. Dioscin Improves Cardiac Dysfunction in MI/R-Injured Mice. In order to explore the protective role of dioscin in response to MI/R injury in vivo, mice were subjected to myocardial ischemic/reperfusion surgery. Echocardiography exhibited that the significant increases of cardiac function markers of the left ventricular ejection fraction (LVEF) and the left ventricular fractional shortening (LVFS) were observed in the MI/R with the dioscin treatment group compared to the MI/R group (Figures 1(a) and 1(b)). Further-more, we found that mice subjected to MI/R treated with dioscin presented improved cardiac function, as evidenced by the preserved left ventricular end diastolic internal dimension (LVID; d) and left ventricular end systolic internal dimension (LVID; s), when compared with vehicle-treated mice (Figures 1(c) and 1(d)).

To examine whether the cardiac fibrosis was prevented by dioscin or not, a series of staining were performed on heart sections. Hematoxylin and eosin (HE) staining revealed widespread myocardial structural disorder, while treatment with dioscin markedly ameliorated histological features in myocardial tissue (Figure 2(a)). Moreover, collagen accumulation in the interstitial space, which was detected by Masson's trichrome staining, increased obviously in the heart sections of the MI/R group, and this increase was improved significantly in the MI/R with treatment dioscin group (Figures 2(b) and 2(c)). We further examined the expression of biomarkers for cardiac function, finding that the expression of natriuretic peptide A (Anp), natriuretic peptide B (Bnp), and beta-myosin heavy polypeptide cardiac muscle (β-Mhc) was reduced after being treated with dioscin in MI/R injury hearts compared to the MI/R group (Figures 2(d)–2(f)). These results indicated that dioscin improves cardiac function and alleviates cardiac fibrosis against MI/R injury.

3.2. Dioscin Modulates Antioxidant Status in MI/R Mice. Because of the involvement of ROS in MI/R injury, we detected the ROS levels in perfused hearts. Dihydroethidium

(a)

(b)

(c)

(d)

(e)

(f)
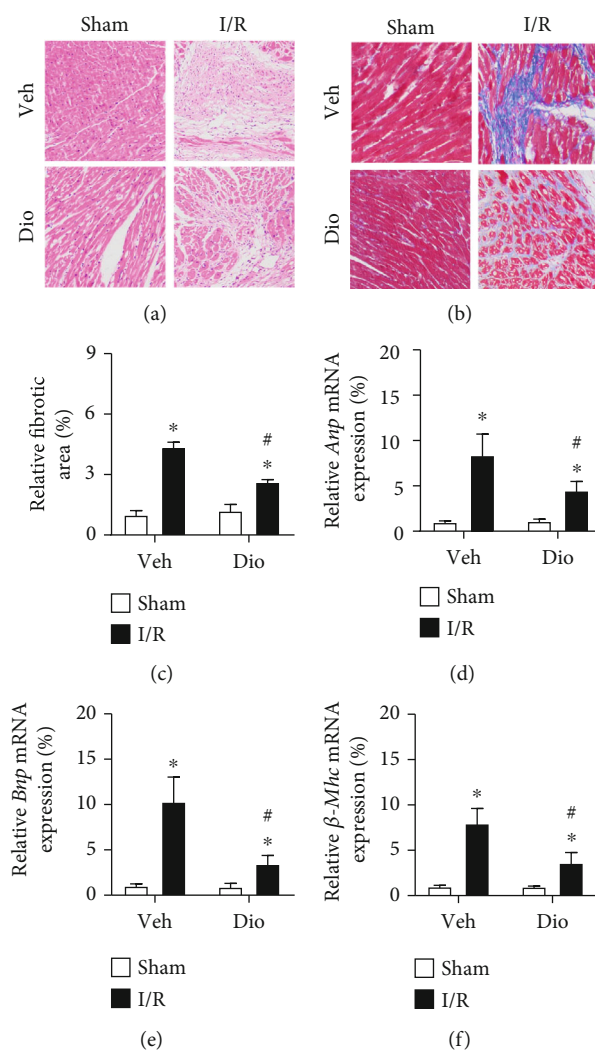
FIGURE 2: Dioscin alleviates cardiac fibrosis in MI/R injury mice. (a) Representative images of HE staining (bar = 100 μm), $n = 3$ each group. (b) Representative images of Masson trichrome-stained (bar = 100 μm), $n = 3$ each group. (c) The measurement of relative fibrosis area (%). The mRNA expression of (d) Anp, (e) Bnp, and (f) β-Mhc. $n = 6$ each group. Data are mean ± SD. *$P < 0.05$ vs. sham group, #$P < 0.05$ vs. I/R group.

(DHE) staining was performed using heart sections, indicating that the levels of ROS in MI/R-induced heart tissues were significantly increased compared with those in the sham group, and dioscin treatment markedly attenuated the elevated production of ROS (Figures 3(a) and 3(b)).

To identify the mechanism underlying how dioscin regulates antioxidant stress in response to MI/R injury, we subsequently detected the mRNA level of corresponding oxidative genes. We found that the expressions of superoxide dismutase 1 (Sod1), superoxide dismutase 2 (Sod2), catalase (Cat), and nuclear factor erythroid 2-related factor 2 (Nrf2) were upregulated in hearts from the MI/R group compared to sham mice, which was prevented by dioscin treatment (Figures 3(c)–3(f)). These results might reveal that the upregulated expression of ROS in the period of perfusion causes the increase expression of antioxidant genes, while the production of ROS is eliminated by treatment with dioscin to further suppress the expression of antioxidant genes.

To further explore the mechanism underlying the protective role of dioscin against MI/R injury, we further measured the activities of antioxidant status-related enzymes. Superoxide dismutase (SOD) is the typical antioxidant enzyme as ROS scavenger. In the MI/R group, the activities of SOD were significant decreased compared to those of sham mice, but the downregulation was prevented by dioscin (Figure 4(a)). What is more, neither catalase (CAT), glutathione (GSH), nor glutathione peroxidase (GPx) plays a protective role in cells from oxidative damage. Dioscin suppressed the declination of MI/R-induced activities of CAT, GSH, and GPx (Figures 4(b)–4(d)). We suspect that the dynamic balance between the antioxidants and oxidant response was damaged by an overburdened high ROS, which further injures these antioxidant enzymes. However, treatment with dioscin recues the decline. Taken together, dioscin could regulate the antioxidant status to repress the production of the ROS level in the MI/R heart.

(a)

(b)

(c)

(d)

(e)

(f)
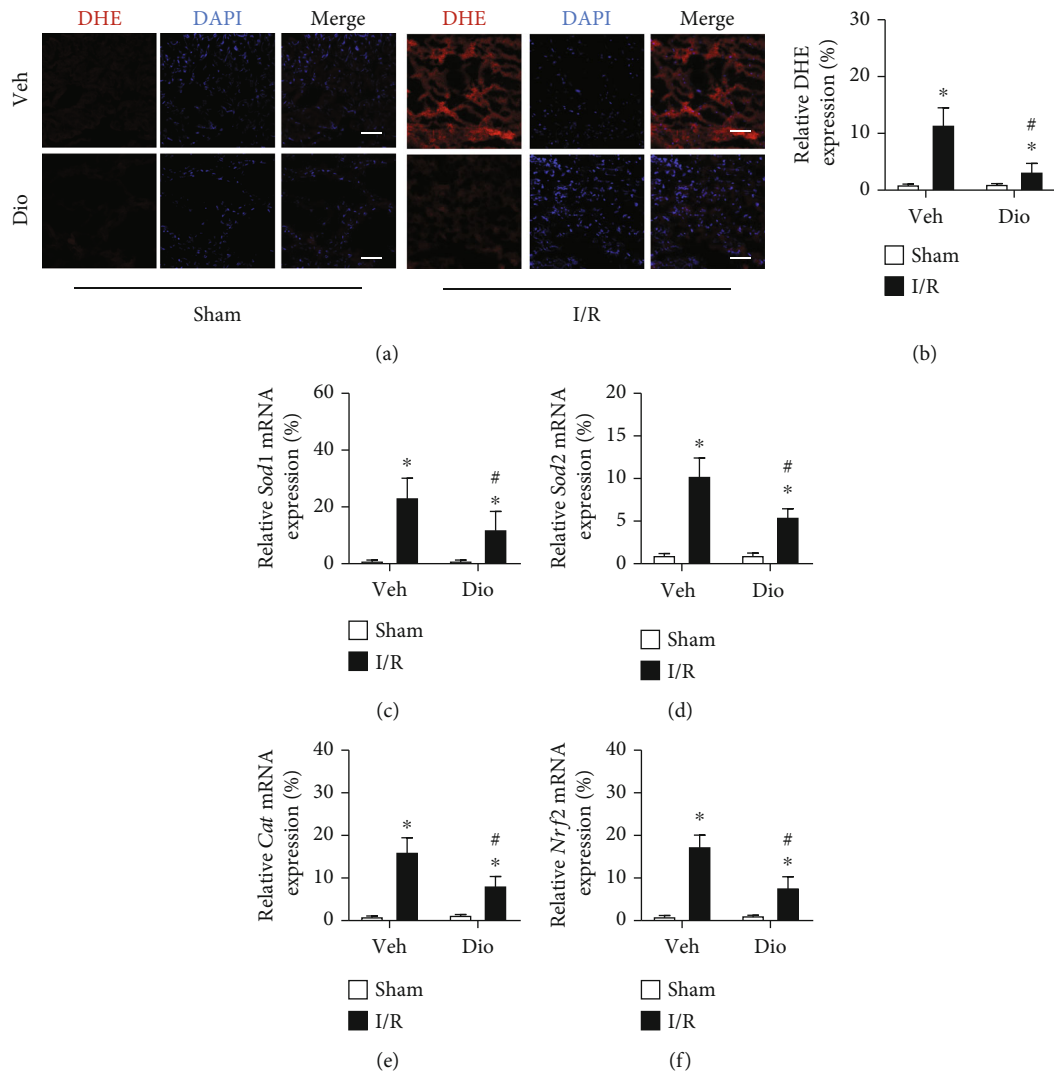
FIGURE 3: Dioscin changes the oxidant response after I/R. (a) Representative images of double staining of heart sections with dihydroethidium (DHE) (red) and DAPI (blue) (bar = 20 μm), $n = 3$ each group. (b) The quantification of relative expression of reactive oxygen species. The mRNA expression of antioxidant genes, including (c) Sod1, (d) Sod2, (e) Cat, and (f) Nrf2. $n = 6$ each group. Data are mean ± SD. $^*P < 0.05$ vs. sham group, $^#P < 0.05$ vs. I/R group.

3.3. Dioscin Scavenges ROS in Perfused H9C2 Cells. Considering the results from the in vivo experiments, we further verified whether dioscin abolishes ROS accumulation in myocytes in an oxidant condition. We further performed dihydroethidium (DHE) staining to detect the level of ROS in H_2O_2-incubated H9C2 cells, showing that dioscin treatment markedly attenuated the elevated levels of ROS production (Figures 5(a) and 5(b)). Because the nicotin-amide adenine dinucleotide phosphate (NADPH) oxidase 2 (Nox2) plays a central role in catalyzing the production of superoxide from oxygen, we identified that the expression of Nox2 was obviously increased in H_2O_2-cultured H9C2, and the increase was prevented after dioscin treatment (Figure 5(c)). These results verified that dioscin alleviates perfused injury via downregulation of the oxidant response.

4. Discussion

In this study, we demonstrated that dioscin, as a natural product, showed a cardioprotective role in response to myocardial ischemic/reperfusion (MI/R) injury. Dioscin has a therapeutic effect via downregulation of oxidant stress, reflecting from the elevated levels of the antioxidant enzyme activities, accompanying with the ROS scavenger. These results exhibited that dioscin has potent effects for the treatment of MI/R injury.

Multiple events take part in the pathogenesis of MI/R, including accumulation of ROS, inflammation, perturbation of calcium handing, and metabolic derangements. Considering ROS as the primary cause among these stimuli, the pharmacological antagonists of accumulated succinate sufficiently ameliorated in vivo myocardial ischemia/reperfusion injury

(a)

(b)

(c)

(d)
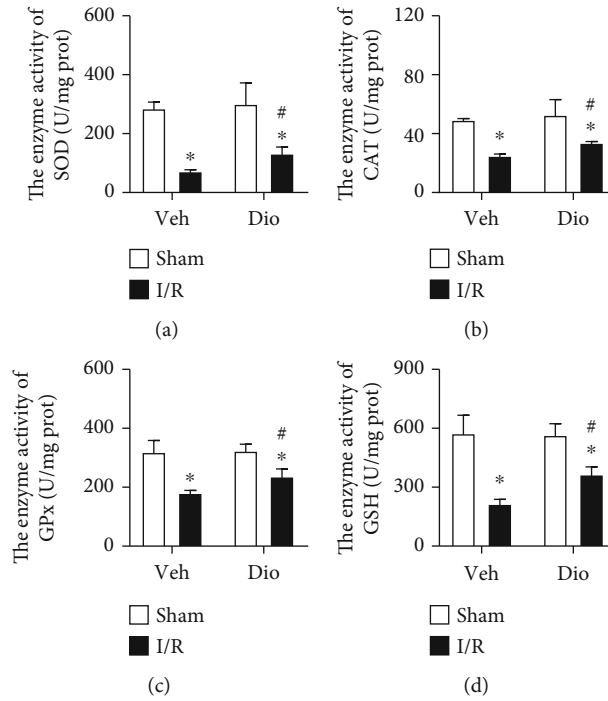
FIGURE 4: Dioscin modulates antioxidant status in IR hearts. The enzyme activities for (a) SOD, (b) CAT, (c) GPx, and (d) GSH. $n = 6$ each group, repeated twice. Data are mean ± SD. $^*P < 0.05$ vs. sham group, $^\#P < 0.05$ vs. I/R group.

(a)

(b)

(c)
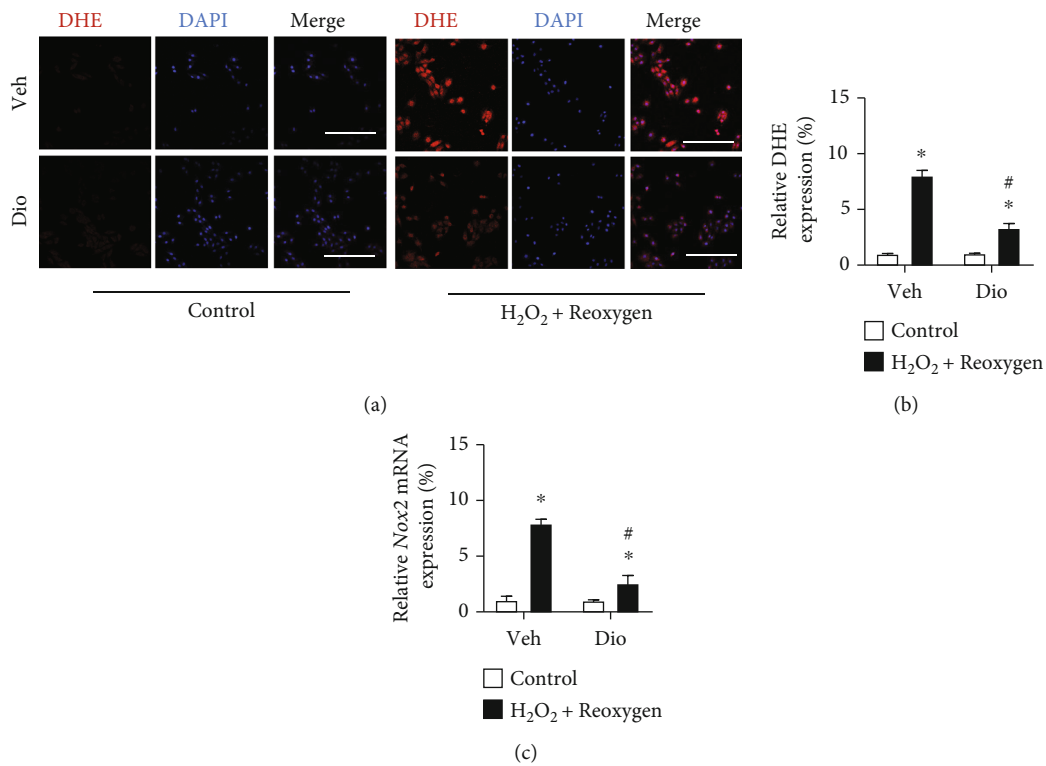
FIGURE 5: Dioscin abolishes the accumulation of ROS production in H9C2 cells. Representative images of double staining of H9C2 cells with dihydroethidium (DHE) (red) and DAPI (blue) (bar = 50 μm), $n = 3$ each group. (b) The quantification of relative expression of reactive oxygen species. (c) The mRNA expression of $Nox2$. $n = 6$ each group. Data are mean ± SD. $^*P < 0.05$ vs. control group, $^\#P < 0.05$ vs. H$_2$O$_2$+reoxygen group.

via repressing extensive ROS generation [29]. Further, uric acid aggravates MI/R-induced activation of the NOD-like receptor pyrin domain-containing protein 3 (NLRP3) inflammatory cascade and pyroptosis by promoting ROS generation, while inflammasome inhibitors and ROS scavengers partly reverse the injury [30]. What is more, ROS scavenger N-acetyl cysteine (NAC) was able to reduce the amount of ROS and prevent cell death [31]. Herein, we identified that dioscin was considered as the ROS scavenger in the process of MI/R injury.

Dioscin plays a beneficial role in cardiac protection via reducing the production of ROS. MI/R injury is mediated by the elevated production of ROS, which occurs particularly at reperfusion [32]. The nicotinamide adenine dinucleotide phosphate (NADPH) oxidase family is considered as one major source of ROS in cardiomyocytes [33]. Meanwhile, many antioxidant enzymes participate in the elimination of ROS in response to MI/R injury [34]. Additionally, it was reported that dioscin alleviated doxorubicin-induced cardiotoxicity through modulating miR-140-5p-mediated myocardial oxidative stress [35]. Furthermore, dioscin has renoprotective effects against fructose-induced renal damage via adjusting sirtuin 3-mediated oxidative stress [36]. And dioscin significantly protected against renal damage by decreasing blood urea nitrogen and creatinine levels and reversing oxidative stress [37].

Summarily, dioscin ameliorates myocardial ischemia/reperfusion injury through suppressing reactive oxygen species via downregulation of Nox2 and upregulation of the antioxidative enzyme, including SOD, CAT, GPx, and GSH, leading to alleviate cardiac dysfunction. Our results indicated that dioscin, providing a potential therapeutic strategy, would be beneficial for myocardial ischemic/reperfusion injury.

Data Availability

The data used to support the findings of this study are available from the corresponding authors upon request.

Conflicts of Interest

The authors declare that they have no conflicts of interest.

Authors' Contributions

Qiulun Lu and Pingxi Xiao designed the study and revised the manuscript. Dayin Lyu, Qing Tian, and Huitao Qian carried out the experiments, and Dayin Lyu wrote the draft manuscript. Chang He, Tianyu Shen, and Jinxing Xi consulted the corresponding literature for preparation. All authors read and approved the final manuscript. Dayin Lyu and Qing Tian contributed equally to this work.

Acknowledgments

References

[1] H. Y. Chen, Z. Z. Xiao, X. Ling, R. N. Xu, P. Zhu, and S. Y. Zheng, "ELAVL1 is transcriptionally activated by FOXC1 and promotes ferroptosis in myocardial ischemia/reperfusion injury by regulating autophagy," *Mol Med*, vol. 27, no. 1, p. 14, 2021.

[2] N. Schanze, C. Bode, and D. Duerschmied, "Platelet contributions to myocardial ischemia/reperfusion injury," *Front Immunol*, vol. 10, p. 1260, 2019.

[3] S. S. Virani, A. Alonso, E. J. Benjamin et al., "Heart disease and stroke statistics-2020 update: a report from the American Heart Association," *Circulation*, vol. 141, no. 9, pp. e139–e596, 2020.

[4] M. ten Hove, C. A. Lygate, A. Fischer et al., "Reduced inotropic reserve and increased susceptibility to cardiac ischemia/reperfusion injury in phosphocreatine-deficient guanidinoacetate-N-methyltransferase-knockout mice," *Circulation*, vol. 111, no. 19, pp. 2477–2485, 2005.

[5] M. I. Ashraf, M. Ebner, C. Wallner et al., "A p38MAPK/MK2 signaling pathway leading to redox stress, cell death and ischemia/reperfusion injury," *Cell Commun Signal*, vol. 12, no. 1, p. 6, 2014.

[6] S. Hernandez-Resendiz, K. Chinda, S. B. Ong, H. Cabrera-Fuentes, C. Zazueta, and D. . Hausenloy, "The role of redox dysregulation in the inflammatory response to acute myocardial ischaemia-reperfusion injury-adding fuel to the fire," *Curr Med Chem*, vol. 25, no. 11, pp. 1275–1293, 2018.

[7] H. Zhou, J. Wang, P. Zhu, S. Hu, and J. Ren, "Ripk3 regulates cardiac microvascular reperfusion injury: The role of IP3R-dependent calcium overload, XO-mediated oxidative stress and F-action/filopodia-based cellular migration," *Cell Signal*, vol. 45, pp. 12–22, 2018.

[8] M. Yang, B. S. Linn, Y. Zhang, and J. Ren, "Mitophagy and mitochondrial integrity in cardiac ischemia-reperfusion injury," *Biochim Biophys Acta Mol Basis Dis*, vol. 1865, no. 9, pp. 2293–2302, 2019.

[9] K. Raedschelders, D. M. Ansley, and D. D. Chen, "The cellular and molecular origin of reactive oxygen species generation during myocardial ischemia and reperfusion," *Pharmacol Ther*, vol. 133, no. 2, pp. 230–255, 2012.

[10] A. van der Pol, W. H. van Gilst, A. A. Voors, and P. van der Meer, "Treating oxidative stress in heart failure: past, present and future," *Eur J Heart Fail*, vol. 21, no. 4, pp. 425–435, 2019.

[11] J. Farías, V. M. Molina, R. A. Carrasco et al., "Antioxidant therapeutic strategies for cardiovascular conditions associated with oxidative stress," *Nutrients*, vol. 9, no. 9, p. 966, 2017.

[12] S. J. Forrester, D. S. Kikuchi, M. S. Hernandes, Q. Xu, and K. K. Griendling, "Reactive oxygen species in metabolic and inflammatory signaling," *Circ Res*, vol. 122, no. 6, pp. 877–902, 2018.

[13] J. I. Goldhaber and J. N. Weiss, "Oxygen free radicals and cardiac reperfusion abnormalities," *Hypertension*, vol. 20, no. 1, pp. 118–127, 1992.

[14] R. Rodrigo, "Prevention of postoperative atrial fibrillation: novel and safe strategy based on the modulation of the antioxidant system," *Front Physiol*, vol. 3, p. 93, 2012.

[15] S. Bae, M. Park, C. Kang et al., "Hydrogen peroxide-responsive nanoparticle reduces myocardial ischemia/reperfusion injury," *J Am Heart Assoc*, vol. 5, no. 11, 2016.

[16] F. Tullio, C. Angotti, M. G. Perrelli, C. Penna, and P. Pagliaro, "Redox balance and cardioprotection," *Basic Res Cardiol*, vol. 108, no. 6, p. 392, 2013.

[17] B. Dong, C. Liu, R. Xue et al., "Fisetin inhibits cardiac hypertrophy by suppressing oxidative stress," *J Nutr The Biochemist*, vol. 62, pp. 221–229, 2018.

[18] J. du, W. He, C. Zhang et al., "Pentamethylquercetin Attenuates Cardiac Remodeling via Activation of the Sestrins/Keap1/Nrf2 Pathway in MSG-Induced Obese Mice," *Biomed Res Int*, vol. 2020, article 3243906, pp. 1–10, 2020.

[19] H. H. Liao, N. Zhang, Y. Y. Meng et al., "Myricetin alleviates pathological cardiac hypertrophy via TRAF6/TAK1/MAPK and Nrf 2 signaling pathway," *Oxid Med Cell Longev*, vol. 2019, p. 6304058, 2019.

[20] Y. Zhang, Y. Cui, S. Dai et al., "Isorhynchophylline enhances Nrf 2 and inhibits MAPK pathway in cardiac hypertrophy," *Naunyn Schmiedebergs Arch Pharmacol*, vol. 393, no. 2, pp. 203–212, 2020.

[21] L. Zhao, X. Tao, Y. Qi, L. Xu, L. Yin, and J. Peng, "Protective effect of dioscin against doxorubicin-induced cardiotoxicity via adjusting microRNA-140-5p-mediated myocardial oxidative stress," *Redox Biol*, vol. 16, pp. 189–198, 2018.

[22] C. Kong, D. Lyu, C. He, R. Li, and Q. Lu, "DioscinelevateslncRNA MANTIS in therapeutic angiogenesis for heart diseases," *Aging Cell*, vol. 20, no. 7, p. e13392, 2021.

[23] X. Tao, X. Wan, Y. Xu et al., "Dioscin attenuates hepatic ischemia-reperfusion injury in rats through inhibition of oxidative-nitrative stress, inflammation and apoptosis," *Transplantation*, vol. 98, no. 6, pp. 604–611, 2014.

[24] L. Zheng, X. Han, Y. Hu et al., "Dioscin ameliorates intestinal ischemia/reperfusion injury via adjusting miR-351-5p/MAPK13-mediated inflammation and apoptosis," *Pharmacol Res*, vol. 139, pp. 431–439, 2019.

[25] Y. Hu, X. Tao, X. Han et al., "Dioscin attenuates gastric ischemia/reperfusion injury through the down- regulation of PKC/ERK1/2 signaling via PKC_{α} and $PKC_{\beta 2}$ inhibition," *Chem Biol Interact*, vol. 258, pp. 234–244, 2016.

[26] E. Gao, Y. H. Lei, X. Shang et al., "A novel and efficient model of coronary artery ligation and myocardial infarction in the mouse," *Circ Res*, vol. 107, no. 12, pp. 1445–1453, 2010.

[27] J. Chen, Z. P. Huang, H. Y. Seok et al., "mir-17-92 cluster is required for and sufficient to induce cardiomyocyte proliferation in postnatal and adult hearts," *Circ Res*, vol. 112, no. 12, pp. 1557–1566, 2013.

[28] M. Zhang, J. Lin, S. Wang et al., "Melatonin protects against diabetic cardiomyopathy through Mst1/Sirt3 signaling," *J Pineal Res*, vol. 63, no. 2, 2017.

[29] E. T. Chouchani, V. R. Pell, E. Gaude et al., "Ischaemic accumulation of succinate controls reperfusion injury through mitochondrial ROS," *Nature*, vol. 515, no. 7527, pp. 431–435, 2014.

[30] S. Shen, F. He, C. Cheng, B. L. Xu, and J. L. Sheng, "Uric acid aggravates myocardial ischemia-reperfusion injury _via_ ROS/NLRP3 pyroptosis pathway," *Biomed Pharmacother*, vol. 133, p. 110990, 2021.

[31] C. Beltran, R. Pardo, D. Bou-Teen et al., "Enhancing glycolysis protects against ischemia-reperfusion injury by reducing ROS production," *Metabolites*, vol. 10, no. 4, p. 132, 2020.

[32] S. Cadenas, "ROS and redox signaling in myocardial ischemia-reperfusion injury and cardioprotection," *Free Radic Biol Med*, vol. 117, pp. 76–89, 2018.

[33] K. Bedard and K. H. Krause, "The NOX family of ROS-generating NADPH oxidases: physiology and pathophysiology," *Physiol Rev*, vol. 87, no. 1, pp. 245–313, 2007.

[34] J. M. Yoo, B. D. Lee, D. E. Sok, J. Y. Ma, and M. R. Kim, "Neuroprotective action of N-acetyl serotonin in oxidative stress-induced apoptosis through the activation of both TrkB/CREB/BDNF pathway and Akt/Nrf2/Antioxidant enzyme in neuronal cells," *Redox Biol*, vol. 11, pp. 592–599, 2017.

[35] L. Zhao, X. Tao, Y. Qi, L. Xu, L. Yin, and J. Peng, "Corrigendum to 'Protective effect of dioscin against doxorubicin-induced cardiotoxicity via adjusting microRNA-140-5p-mediated myocardial oxidative stress' [Redox Biol.], 2018, 16: 189-198," *Redox Biol*, vol. 26, p. 101303, 2019.

[36] Y. Qiao, L. Xu, X. Tao et al., "Protective effects of dioscin against fructose-induced renal damage via adjusting Sirt3-mediated oxidative stress, fibrosis, lipid metabolism and inflammation," *Toxicol Lett*, vol. 284, pp. 37–45, 2018.

[37] M. Qi, L. Yin, L. Xu et al., "Dioscin alleviates lipopolysaccharide-induced inflammatory kidney injury _via_ the microRNA let-7i/TLR4/MyD88 signaling pathway," *Pharmacol Res*, vol. 111, pp. 509–522, 2016.

Research Article

Effects of Insomnia on Peptic Ulcer Disease Using Mendelian Randomization

Ling-Feng Zha [1], **Jiang-Tao Dong,** [2] **Jing-Lin Wang,** [1] **Qian-Wen Chen,** [3] **Jian-Fei Wu,** [4] **Ying-Chao Zhou,** [5] **Shao-Fang Nie** [1] **and Xin Tu** [4]

[1]*Department of Cardiology, Union Hospital, Tongji Medical College, Huazhong University of Science and Technology, Wuhan 430022, China*

[2]*Department of Cardiovascular Surgery, Union Hospital, Tongji Medical College, Huazhong University of Science and Technology, Wuhan 430022, China*

[3]*Hubei Maternal and Child Health Hospital, Wuhan 430070, China*

[4]*College of Life Science and Technology, Center for Human Genome Research, Cardio-X Institute, Huazhong University of Science and Technology, Wuhan 430074, China*

[5]*Heart Center, Qingdao Women and Children's Hospital, Qingdao University, Qingdao 266000, China*

Correspondence should be addressed to Shao-Fang Nie; 317933339@qq.com and Xin Tu; xtu@hust.edu.cn

Objectives. Observational studies indicate that insomnia may increase risk of peptic ulcer disease (PUD). Our purpose is to clarify the possible causal relationship between insomnia and PUD by Mendelian randomization analyses. *Methods*. We carried out analyses using summary statistics data for genetic variants reported from a GWAS of insomnia ($N =$ up to 1,331,010 individuals) and from a GWAS of PUD ($N =$ up to 456,327 individuals). Three Mendelian randomization approaches were used to explore whether insomnia might play a causal role in PUD, and pathway and functional enrichment analyses were conducted to anticipate the underlying mechanisms. *Results*. Conventional Mendelian randomization analysis showed clear causality between insomnia and PUD; 1 SD increased insomnia incident was related to a 19% higher risk of PUD ($P = 6.69 \times 10^{-16}$; OR, 1.19 (95% CI, 1.14-1.24)). The associations between insomnia and PUD were consistent in the other two analyses performed using the weighted median method ($P = 7.75 \times 10^{-7}$; OR, 1.16 (95% CI, 1.09-1.23)) and MR-Egger regression ($P = 5.00 \times 10^{-3}$; OR, 1.27 (95% CI, 1.07-1.50)). Moreover, no evidence indicated a reverse causality between PUD events and insomnia symptoms. Pathway and functional enrichment analyses indicated that the mechanisms of insomnia effect on PUD may be through various ways, such as the immune system and oxidative stress. *Conclusions*. This Mendelian randomization study suggests insomnia as a causal risk factor for PUD. The potential mechanisms included may be immune and oxidative stress. These findings indicate that improving sleep quality could have substantial health benefits.

1. Introduction

Insomnia is a common mental disorder; it is by far the most common sleep disorder in medical practice. About 30% of the common population report symptoms of insomnia [1]. Insomnia is considered as a key factor referring to the occurrence and progress of chronic inflammatory diseases; it is closely associated with gastrointestinal symptoms, high blood pressure, asthma, systemic lupus erythematosus, auto-nomic nervous system dysfunction, impaired blood sugar control, and increased inflammation [2].

Peptic ulcer disease (PUD) is a common gastrointestinal disease involving rupture (ulceration) of the alimentary canal mucosa, mainly occurring in the gastric area and duodenum. Epidemiology shows that the annual incidence of PUD is 0.1-0.3%, and the lifetime prevalence in the general population is about 5-10% [3]. More than 4 million people suffer from the disease each year, resulting in high medical

costs [4]. People with PUD have a lower quality of life. The cardinal symptoms of PUD are upper abdominal pain but also can have increasing saliva secretion, heartburn, belching, vomiting, and other gastrointestinal symptoms [5]. It is called peptic ulcer because it was thought that gastric and duodenal are included caused by the digestion of the mucous membrane itself by gastric acid and pepsin. Although the etiology of PUD is not yet clear, H. pylori infection, gastric acid overproduction, and weakened gastric mucosal protection mechanism are recognized as the main pathogenesis in recent years [3].

It is well known that sleep quality is closely related to gastrointestinal health. It is reported that the sleep quality of patients with peptic ulcer is worse than that of normal people. Evidence suggests that in older populations, PUD patients have poorer sleep quality compared to the healthy [6]. Recently, a study found that among women, those who slept less than seven hours a night had twice the risk of developing PUD compared to those who slept more than nine hours a night [7]. Another study investigated whether poor sleep quality predicted recurrence of PUD in 1,538 elderly patients who had been inoculated with H. pylori; the result shows that the recurrence rate of PUD was higher in poor sleepers than in good sleepers [8]. With the deepening of the research on peptic ulcer, scholars believe that there is a certain correlation between sleep quality and peptic ulcer, which is both the cause of the disease and the rehabilitation disorder. Studies have shown that sleep disorders (especially insomnia) can increase the incidence of PUD. Peptic ulcer patients will be due to upper abdominal pain or discomfort from sleep to wake up, occurring a variety of forms of sleep disorders, such as difficulty in falling asleep, increased wakefulness, and prolonged wakefulness. Although a growing number of clinical studies suggest a close relationship between insomnia and PUD, the causal relationship between them remains uncertain. Clarifying the causal relationship between insomnia and PUD is of great significance for understanding the pathogenesis of PUD, as well as for providing potentially new prevention strategies.

Mendelian randomization is a flourishing branch of genetic epidemiological methodology. Its core is to use genetic data as a bridge to clarify thoroughly the causality between the exposure and the outcome. MR is based on the most basic Mendelian law of heredity that parental alleles are randomly assigned to offspring and that genotype determines phenotype [9]. Since genotype is innate, it must be ahead of the time of outcome, and it is not disturbed by other confounding factors such as acquired environment, so it can be used as a powerful tool to study the causality between exposure and outcome. Compared with traditional epidemiological methods, this approach can indicate the direction of exposure and outcome, and therefore, the causal relationship between the two, not just the association [10]. The design strategy of two-sample MR is to establish two independent samples from the same population that are associated with the study population. MR of the two samples is based on long-term data from genome-wide association studies (GWASs). Given its enlarged sample size, the statis-

tical ability is greatly improved [11]. Currently, the two-sample MR is widely used due to the large amount of public data from GWAS cooperative groups around the world.

In this study, we explored a possible causal relationship between insomnia and PUD by bidirectional Mendelian randomization analyses, using available public data from two recent large-scale GWAS for insomnia [12] and PUD [13].

2. Methods

2.1. Genetic Variants Associated with Insomnia. In the first phase analysis, 12 independent single nucleotide polymorphisms (SNPs) ($P < 5 \times 10^{-8}$ for GWAS significant level; $r^2 < 0.1$ for linkage disequilibrium) that were susceptible to insomnia in the dataset (SSGAC) (113,006 participants) were included in the analysis [14]. Eight of 12 SNPs associated with insomnia were included in the PUD GWAS dataset and were selected for our instrumental variable analyses (Table 1). For our secondary phase analysis, in order to make our sensitivity analysis to achieve sufficient statistical power, another larger set of SNPs was used in our main analysis, which was retrieved from a recent GWAS for insomnia involving 1,331,010 European people [12]. In this analysis, 248 independent SNPs were significantly associated with insomnia ($P < 5 \times 10^{-8}$; $r^2 < 0.1$). 242 of them were included in the PUD GWAS dataset and were chosen for the MR analysis (see supplementary Table 1). This is enough to produce a powerful genetic tool that can be used to obtain an unbiased causal assessment.

2.2. Genetic Variants Associated with PUD. GWAS and GWGAS involving 456,327 participants from UK Biobank indicated that 8 independent SNPs were strongly associated with PUD ($P < 5 \times 10^{-8}$; $r^2 < 0.1$) [13]. Seven of 8 SNPs associated with PUD were included in the insomnia GWAS dataset and selected for the reverse causality analysis (Table 2).

2.3. Mendelian Randomization Analyses. Three Mendelian randomization analyses were carried out to explore the causal relationship between insomnia and PUD.

Firstly, conventional Mendelian randomization analyses, also called the inverse-variance weighted method, were implemented to regress the exposure (genetic variants in susceptibility to insomnia) against the outcome (genetic variants in susceptibility to PUD), with each variant as a data point.

Secondly, two sensitivity analyses were performed to evaluate the effect of pleiotropism on Mendelian random causality, relaxing the Mendelian randomization hypothesis partly. For instance, MR-Egger analysis is based on the InSIDE hypothesis, which requests that the size of any pleiotropic effect (from genetic variants to PUD, bypassing insomnia) should not be related to the size of the main effect (from genetic variants to insomnia). Another approach based on median assumes that when analyzing a large number of variants (some of which may be pleiotropic), these pleiotropies may well be material difference and therefore unlikely to be concentrated on a common median estimate.

TABLE 1: Characteristics of the studied insomnia-associated SNPs in both insomnia and PUD GWAS.

SNP	Gene	EA	NA	Insomnia results			PUD results		
				BETA	SE	P	BETA	SE	P
rs375216017	MEIS1	GT	G	0.089574	0.015720	$1.21E-08$	—	—	—
rs62144051	MEIS1	G	A	0.096151	0.016318	$3.81E-09$	0.018165	0.019416	0.35
rs62144053	MEIS1	A	G	0.098931	0.016272	$1.20E-09$	0.026932	0.019223	0.16
rs62144054	MEIS1	A	G	0.097846	0.016237	$1.68E-09$	0.026976	0.019221	0.16
rs113851554	MEIS1	T	G	0.178239	0.020371	$2.14E-18$	0.019566	0.025498	0.44
rs182588061	MEIS1	T	G	0.228449	0.036320	$3.18E-10$	0.029322	0.051821	0.57
rs139775539	MEIS1	A	AC	0.186994	0.022403	$7.00E-17$	—	—	—
rs11679120	MEIS1	A	G	0.187813	0.022461	$6.18E-17$	0.021005	0.027931	0.45
rs115087496	MEIS1	C	G	0.177042	0.022576	$4.43E-15$	0.009710	0.029911	0.73
rs549771308	MEIS1	C	CT	0.090546	0.015777	$9.51E-09$	—	—	—
rs11693221	MEIS1	T	C	0.170821	0.022572	$3.79E-14$	0.009066	0.028027	0.75
rs574753165	SCFD2	G	A	0.394740	0.067503	$4.98E-09$	—	—	—

PUD: peptic ulcer disease; EA/NA: effect allele/no effect allele; BETA: effect size; SE: standard error of the effect size; P: P values indicate genome-wide significance in GWAS.

TABLE 2: Characteristics of the studied PUD-associated SNPs in both insomnia and PUD GWAS.

SNP	Gene	EA	NA	PUD results			Insomnia results		
				BETA	SE	P	BETA	SE	P
rs681343	FUT2	C	T	-0.088770	0.011169	$1.9E-15$	-0.006920	0.005108	0.18
rs2976388	PSCA	G	A	0.086730	0.011318	$1.8E-14$	0.004309	0.005152	0.40
rs10500661	CCKBR	T	C	-0.101570	0.013439	$4.1E-14$	0.004008	0.006322	0.53
rs147048677	MUC1	C	T	-0.152180	0.022310	$9.0E-12$	—	—	—
rs78459074	MUC6	A	G	0.115348	0.018241	$2.6E-10$	0.002804	0.008030	0.73
rs34074411	GAST	C	T	-0.072050	0.011397	$2.6E-10$	-0.010940	0.005242	0.04
rs687621	ABO	A	G	0.073539	0.012116	$1.3E-09$	-0.007970	0.005474	0.13
rs9581957	CDX2	C	T	-0.069730	0.011819	$3.6E-09$	0.001601	0.005474	0.77

PUD: peptic ulcer disease; EA/NA: effect allele/no effect allele; BETA: effect size; SE: standard error of the effect size; P: P values indicate genome-wide significance in GWAS.

Conversely, effective variants without pleiotropy are more possibly to display more accordant and homogeneous effects (on insomnia and subsequent PUD), more possibly to cluster at the estimated median point. Causal reasoning is strengthened by the consistency of results among different approaches which propose s different hypothesis about pleiotropy; nevertheless, different results may suggest that some of the results were influenced by genetic pleiotropy.

Thirdly, in the case of a large number of pleiotropies, the genetic risk of PUD may also forecast the outcome of insomnia; we conducted reverse Mendelian randomization analysis using 8 SNPs associated with PUD (only 7 of 8 SNPs associated with PUD were included in the insomnia GWAS dataset and selected for the reverse causality analysis).

2.4. Functional Annotation. FUMA was used to functionally annotate; three gene mapping strategies were applied in FUMA to identify genes that are associated with the 242 SNPs, which were included in the MR analysis. In the positional mapping, we mapped 242 SNPs and SNPs in LD

$(r^2 \geq 0.6)$ with them to genes. The other two gene-mapping strategies were gene mapping based on eQTL and gene mapping based on chromatin interaction.

2.5. Pathway and Functional Enrichment Analyses. Enrichment analyses including GO (http://geneontology.org/) analysis and KEGG (https://www.kegg.jp/) analysis were carried out on David (https://david-d.ncifcrf.gov/).

2.6. Statistical Analyses. All SNPs were matched to the same effect allele among the different datasets. All statistical tests were 2-sided, and statistical significance was assessed by Bonferroni correction. All analyses were conducted in Stata (version 15), FUMA (version 1.2.4), and R (version 3.2.5).

3. Results

3.1. Causal Effect from Insomnia to PUD. There is a first stage analysis using 8 SNPs that significant correlation to insomnia in the GWAS dataset (SSGAC) included 113,006
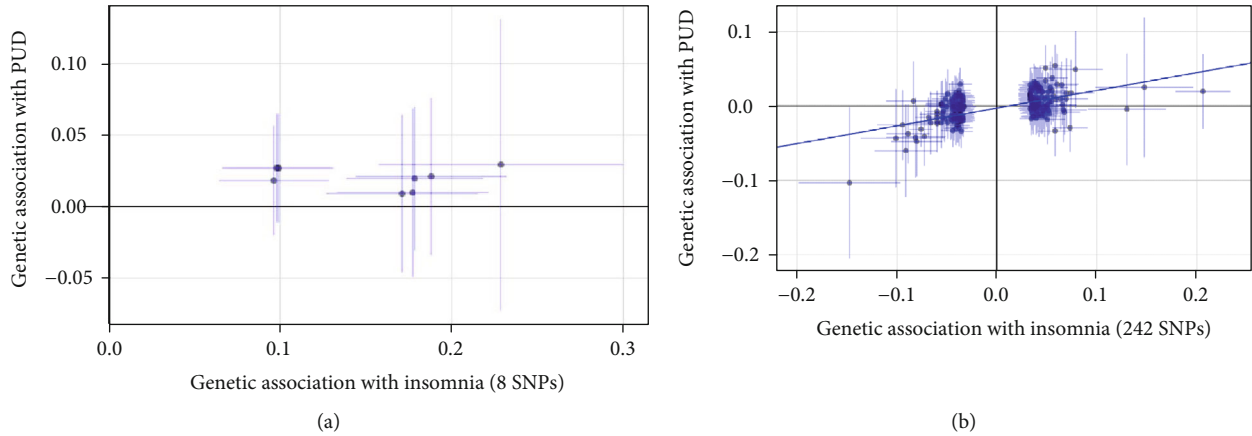
(a)

(b)

FIGURE 1: Comparison plot of the association between insomnia-related SNPs associated with insomnia and PUD: (a) 8 insomnia-related SNP analysis; (b) 242 insomnia-related SNP analysis. Each point displays the influence of the SNP on the insomnia and PUD. The slope of the line represents the causal association.

participants ($P < 5.00 \times 10^{-8}$, $r^2 < 0.1$). All these 8 SNPs did not reach the Bonferroni-corrected significance level in the PUD GWAS ($P > 0.006$) (Table 1). The results in the conventional Mendelian randomization analysis showed that in a comparison of the effects of 8 SNPs on insomnia and PUD, the effects on insomnia and PUD were clearly consistent, indicating a significant causal relationship between insomnia and PUD ($P = 0.03$; OR, 1.15 (95% CI, 1.02-1.29)) (Figures 1 and 2). However, results were inconsistent between the other two methods, using the weighted median method ($P = 0.15$; OR, 1.12 (95% CI, 0.96-1.30)) and MR-Egger regression ($P = 0.72$; OR, 0.93 (95% CI, 0.63-1.38)), both with a wider CI (Figure 2). Those divergent results among those methods may indicate a bias of genetic pleiotropy towards these results.

Considering the limited number of SNPs and the limited sample size in this stage analysis which were insufficient to derive unbiased causal estimates, in order to make our sensitivity analysis to achieve sufficient statistical power, we retrieved 248 independent SNPs associated with insomnia from the most recent GWAS data involving 1,331,010 European people ($P < 5.00 \times 10^{-8}$; $r^2 < 0.1$), which explained 2.6% of the variance in insomnia. 242 of 248 SNPs associated with insomnia were included in the PUD GWAS dataset, and all these 242 SNPs did not reach the Bonferroni-corrected significance level in the PUD GWAS ($P < 0.0002$) (see supplementary Table 1). The secondary set of analyses using 242 SNPs yielded consistent results. The conventional Mendelian randomization analysis indicated a causal relationship between insomnia and prevalent PUD; 1 SD increased insomnia incident was associated with a 19% higher risk of PUD ($P = 6.69 \times 10^{-16}$; OR, 1.19 (95% CI, 1.14-1.24)) (Figures 1 and 2).

Complementary analyses showed the consistent associations between insomnia and PUD through the weighted median method ($P = 7.75 \times 10^{-7}$; OR, 1.16 (95% CI, 1.09-1.23)) and MR-Egger regression method ($P = 5.00 \times 10^{-3}$; OR, 1.27 (95% CI, 1.07-1.50)) (Figure 2). There are no pleiotropy (MR-Egger intercept; $\beta = -0.003$, -0.001 to 0.004; P

$= 0.416$) or heterogeneity between the Mendelian randomization estimates obtained for different SNPs ($I^2 = 9.8\%$, $P = 0.0028$ for heterogeneity). All the sensitivity analyses make it unlikely that pleiotropy would seriously affect our primary cause analysis. Causal reasoning is strengthened by the consistency of findings among diverse approaches that propose a different hypothesis about pleiotropy, which is consistent with the assumptions that pleiotropy was not responsible for this finding.

3.2. Causal Effect from PUD to Insomnia. Consider that PUD is also likely to be the causal factor of insomnia symptoms, reverse MR analysis was carried out using 7 SNPs associated with PUD, which were not associated with insomnia after Bonferroni corrected ($P > 0.007$) (Table 2). However, no evidence was found for the assumption that PUD event is related to insomnia outcomes in the conventional Mendelian randomization analysis ($P = 0.43$; OR, 1.02 (95% CI, 0.97-1.09)) (Figure 3). Results were unchanged after using the weighted median analysis ($P = 0.34$; OR, 1.03 (95% CI, 0.97-1.11)) and MR-Egger analysis ($P = 0.93$; OR, 1.00 (95% CI, 0.97-1.04)) (Figure 3). Those evidences indicated no reverse causality between PUD events and insomnia symptoms.

3.3. Functional Annotation. Three gene mapping methods were applied in FUMA to identify genes of interest on account of 242 SNPs included in the MR analysis. For mapping based on position, 412 genes were identified by mapping SNPs in the risk loci and in LD with the independent GAWS SNPs ($r^2 \geq 0.6$). Mapping based on eQTL implicated 594 genes and mapping based on chromatin interaction implicated 159 genes (Figure 4). A total of 748 genes were identified by the three methods; 91 of them were identified by all three methods, which were distributed on multiple chromosomes (see supplementary Table 2-4).

3.4. Gene Set Enrichment Analyses. To investigate the possible mechanism of insomnia leading to PUD, all 748 genes identified by the methods above were used to conduct GO

Analysis	No. of sample	OR (95 %CI)	OR (95 %CI)	p value
8 SNPs				
Conventional MR (IVW)	113006		1.15 (1.02–1.29)	0.03
MR–Egger	113006		0.93 (0.63–1.38)	0.72
Weighted median MR	113006		1.12 (0.96–1.30)	0.15
242 SNPs				
Conventional MR (IVW)	1331010		1.19 (1.14–1.24)	6.69×10^{-16}
MR–Egger	1331010		1.27 (1.07–1.50)	5.00×10^{-3}
Weighted median MR	1331010		1.16 (1.09–1.23)	7.75×10^{-7}

0.0   0.5   1.0   1.5   2.0
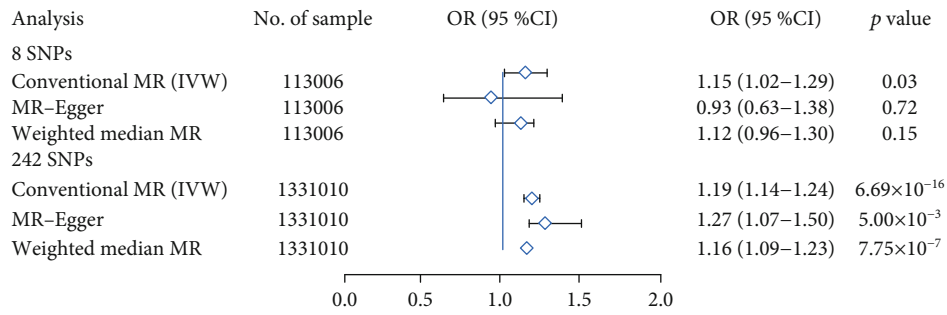
FIGURE 2: Forest plot estimates the effect of genetically increased insomnia risk on PUD. EA/NA: effect allele/no effect allele; OR: odds ratio; CI: confidence interval.

(a)

Analysis	No. of sample	OR (95 %CI)	OR (95 %CI)	p value
7 SNPs				
Conventional MR (IVW)	456327		1.02 (0.97–1.09)	0.43
MR–Egger	456327		1.00 (0.97–1.04)	0.93
Weighted median MR	456327		1.03 (0.97–1.11)	0.34

0.00 0.50 1.00 1.50 2.00
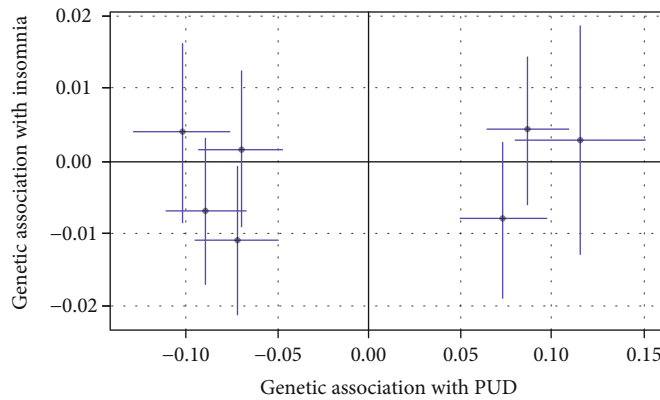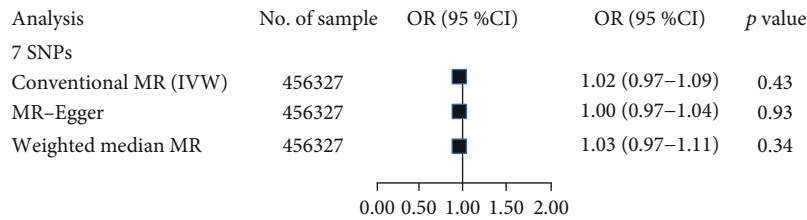
(b)

FIGURE 3: Causal effect from PUD to insomnia: (a) comparison plot of the association between PUD-related SNPs associated with insomnia and PUD; (b) forest plot estimates the effect of genetically increased PUD risk on insomnia. Each point displays the influence of the SNP on the insomnia and PUD.

enrichment analysis at the online Functional Annotation Tool (DAVID). These genes were classified from three levels of molecular function, cellular component, and biological process to further understand their related functions. At the same time, the KEGG database was used for gene signaling pathway analysis to understand the signaling pathways involved in these genes. The results showed that in terms of cell components, the genes mainly focused on nucleus, cytoplasm, plasma membrane, etc. In terms of molecular function, the genes were mainly related to GTPase activity, MHC class I and MHC class II receptor activity, and transcription regulator activity. In terms of biological processes, genes are mainly related to the immune system, innate immune system, NOTCH, and mitochondrial tRNA aminoacylation (Figures 5 and 6). KEGG enrichment pathway analysis suggested that those genes were significant enrich-

ment in the adaptive immune system, synaptic membrane adhesion, regulation of cellular response to stress, viral process and cytokine production, etc. (Figures 5 and 6).

4. Discussion

PUD is a chronic inflammatory disease; insomnia is closely related to gastroesophageal reflux and peptic ulcer [15]. Clinical studies have found that patients with poor sleep quality have a higher recurrence rate of PUD [8]. Despite observational studies indicate an association between insomnia and PUD, it is lacking of causal evidence for effects of insomnia on PUD. Both insomnia and PUD have a genetic predisposition. This causal study shows that insomnia is related to the increasing risk of PUD. The findings corroborate the results of several observational studies which

(a)

(b)
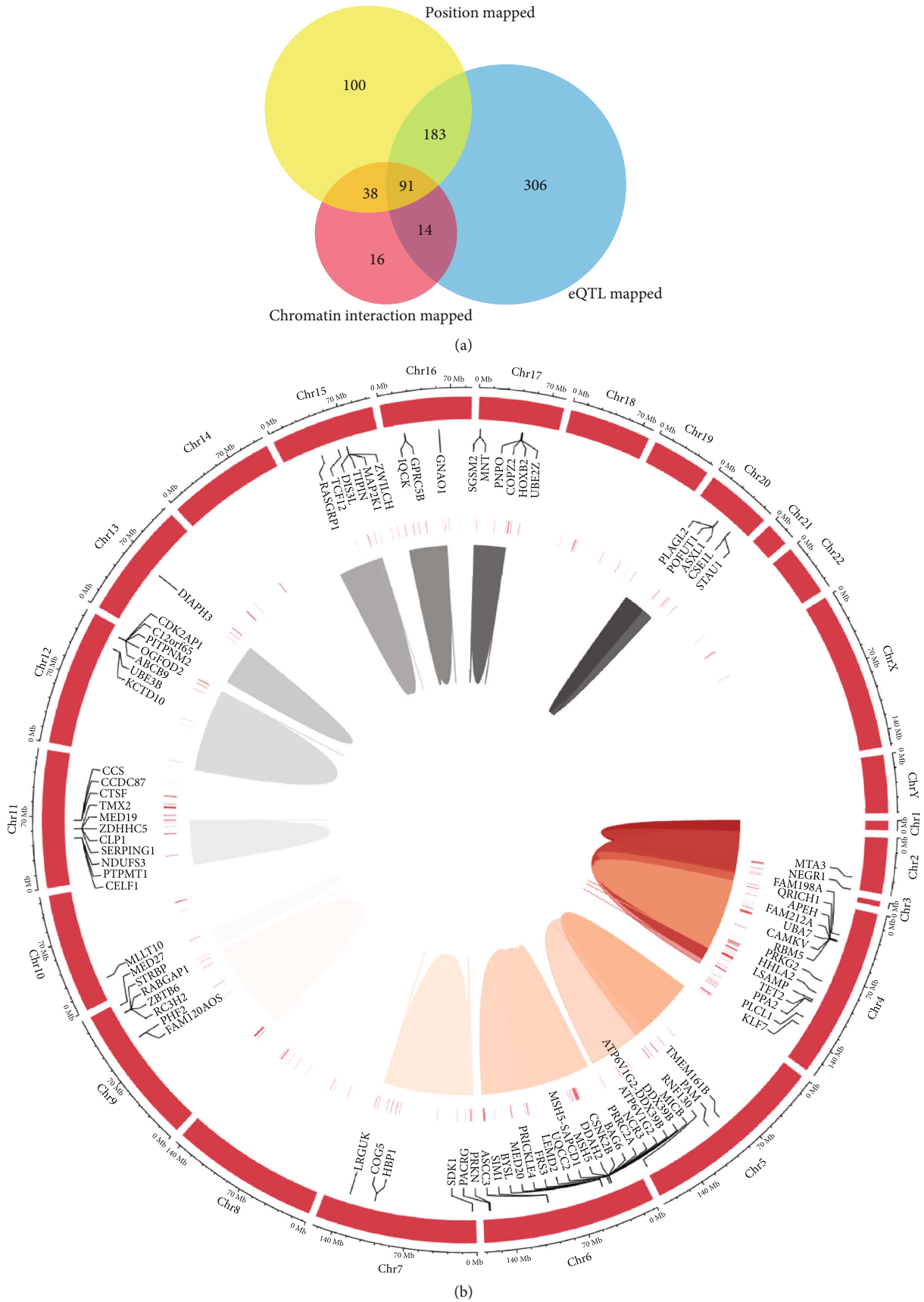
FIGURE 4: Genes mapped to insomnia-related SNPs: (a) venn diagram; (b) circos plot heatmap.
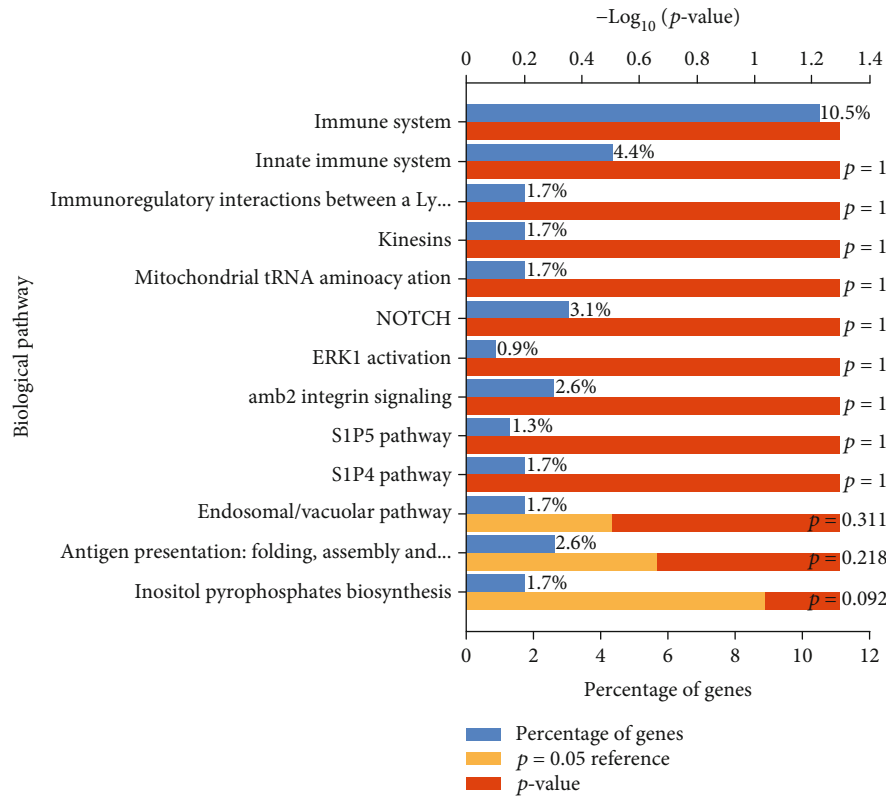
(a)
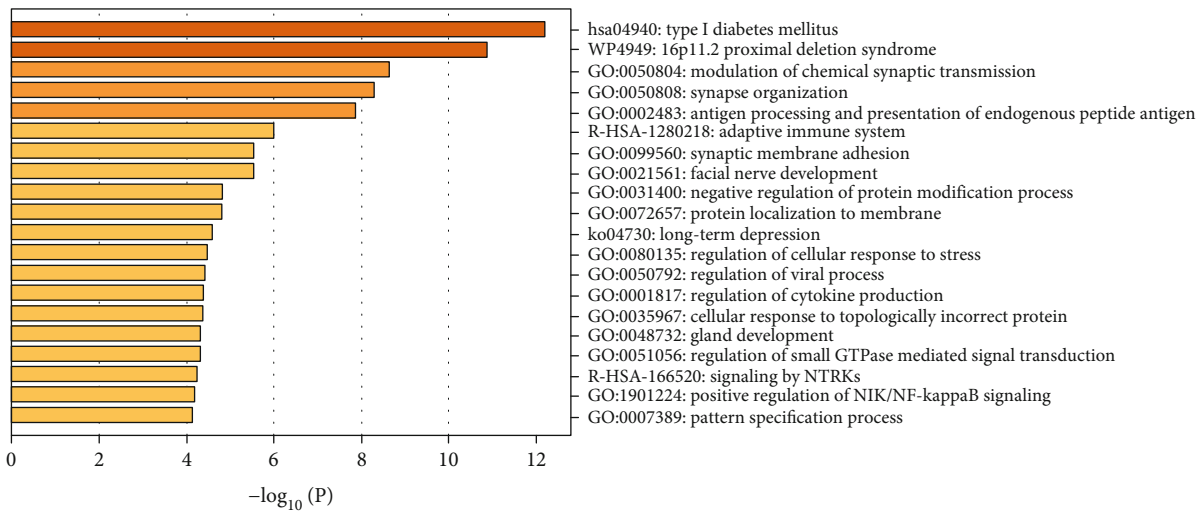
(b)

FIGURE 5: Enrichment analysis: (a) biological pathway of enrichment genes; (b) enrichment heatmap for selected GO.

suggested a positive correlation between insomnia and PUD risk.

Although the etiology of PUD is not yet clear, H. pylori infection, gastric acid overproduction, and weakened gastric mucosal protection mechanism are recognized as the main pathogenesis in recent years. Modern medicine suggests that abnormal sleep patterns may be a vital factor for the development of chronic inflammatory diseases. Abnormal sleep affects gastrointestinal function and is associated with worsening of functional gastrointestinal diseases. Sleep distur-

bances can increase the incidence of peptic ulcer. Sleep deprivation can lead to gastric mucosal erosion, which may involve the reduction of gastric mucosal blood flow, the suppression of cell proliferation, the influence of gastric mucosal repair, and the decrease of gastric mucosal ion barrier. The study found that after entering deep sleep, gastric mucous outflow, gastric mucosal blood flow, and melatonin secretion increased, whereas gastrin secretion decreased, which were helpful to prevent PUD development and recurrence. Recently, researchers found that the stomach and small

(a)

(b)

Figure 6: Gene cluster: (a) gene clusters and interactions between genes; (b) genes in the enrichment GO.

intestine produce a chemical called TFF2 protein that repairs the ruptures at night, and lack of sleep reduces the production of this protein and increases the risk of stomach ulcers [16].

Insomnia is a neurological disease that can lead to complications in a variety of other systems. Insomnia can cause central nervous system and gastrointestinal function regulation imbalance, and long-term insomnia can also lead to anxiety and depression, which in turn can cause gastrointestinal nerve, endocrine, and immune disorders, which may produce somatization symptoms of the digestive system in

different degrees. As stimulation of the vagus nerve can promote gastric acid secretion, vagotomy is commonly used to treat PUD clinically. The autonomic nervous system is closely related to the enteric nervous system. It is widely accepted that the enterobrain axis participates in the regulation of the alimentary canal and the maintaining of the intestinal immunity system through the mechanisms of intestinal permeability, intestinal endocrine signaling, and immune activation. But sleep disturbances or circadian rhythm disturbances may disrupt its normal function and may affect gastrointestinal sensitivity to ulcer preparations

[17]. Further study suggests that melatonin may prevent PUD recurrence through clearing oxidative free radicals, promoting cell proliferation and gastric mucosal microcirculation, whereas sleep disorders cause a lack of melatonin, affecting the underlying protective effect of melatonin against PUD recurrence [18].

We conducted pathway-enrichment analysis for the genes associated with insomnia using gene clustering tools to explore the potential biological mechanisms between insomnia and PUD. We found that the subnetworks of the genes are enriched in multiple processes, including the immune system, regulation of viral process, facial nerve development, long-term depression, regulation of cytokine process, regulation of cellular response to stress, and mitochondrial tRNA aminoacylation. It is well-known that lacking sleep can lead to decreased immunity, so that the body including gastrointestinal is susceptible to bacteria or viruses. The interesting thing is that many genes involved in oxidative stress and mitochondrial function were found such as GPX1, DARS2, PRDX6, HAAO, RBM14-RBM4, NDUFS3, OGFOD2, and ATP5G1, suggesting insomnia may affect PUD through oxidative stress and mitochondrial function. Evidences suggest that reactive oxygen species (ROS) refer to the pathogenesis of PUD as well as possibly gastric cancer [19]. Sleep deprivation directly affects the oxidative state of the mucosa [20]. Recently, tests on fly and mouse have shown that sleep expropriation resulted in the amassment of ROS in the gut and consequent oxidative stress [21]. Alzoubi et al. reported that sleep deprivation increases oxidative stress as well as impairs learning and memory processes [22]. Similar with Reimund's hypothesis, sleep deprivation is an oxidative challenge, and adequate sleep may have a protective effect against oxidative damage [23]. Oxidative stress is thought to be a latent condition connected with insomnia. Systemic oxidative stress was increased, and serum antioxidant enzyme levels were decreased in insomnia patients in contrast with healthy people [24]. Mitochondrial respiratory complexes were reduced, and superoxide dismutase 2 (SOD2) was significantly increased in fatal familial insomnia (FFI) patient, suggesting that mitochondrial and protein synthesis mechanisms are reduced [25]. Mitochondrial damage increases and leads to an increase in oxidative stress [26]. Sleep disorders may promote the accumulation of neurotoxic proteins and oxidative stress [27].

Redox signal is involved in gastrointestinal physiology and pathophysiology. Redox signal regulates the Notch and Wnt signaling pathway principally by NADPH oxidase (NOx), thereby regulating the physiological self-renewal, propagation, transference, and differentiation of gastrointestinal epidermal cell. Broken redox homeostasis participates in the development and progression of diverse gastrointestinal diseases, like peptic ulcer, inflammatory bowel diseases, and colorectal cancer. Harmful "oxygen free radical overload" has serious impacts on intestinal mucosa and is relevant to the clinical outcome of inflammatory bowel disease [28, 29]. Oxidative stress is now recognized as an underlying causative factor and a key factor for the progress and severity of diseases, instead of the accompanying consequence of chronic gastrointestinal inflammations [30, 31]. Oxidative

stress take part in the inflammatory reaction of H. pylori infection through a variety of redox signals. H. pylori infection results in the occurrence as well as the development of PUD, but the mechanism of it leading to various clinical manifestations is still unclear. During infection, changes in the balance of cell proliferation and apoptosis may lead to changes in the gastric mucosa. Existing studies reveal that H. pylori infection is closely relevant to an increasing synthesis of free radicals, which are thought as a major cause of cell death. Oxidative stress induced by H. pylori activates apoptosis through the intrinsic pathways. The alteration in structure and function of mitochondrial organelles caused by these processes are the fundamental causes of gastric mucosal toxicity and result in the occurrence of a variety of manifestations related to the infection. Accumulating evidences indicate that antioxidant therapy may contribute to the clinical therapies of patients with H. pylori infection. Many factors, including genetics, stress, and hygiene, take part in the pathogenic mechanisms of H. pylori infection. A link is found between H. pylori infection and increasing free radicals [32, 33]. The increasing of ROS in gastric mucosa in gastritis patients infected with H. pylori was considered to be related to bacterial load. As we all know, oxidative stress is one of the factors that lead to accelerated cell cycles and premature cell death, resulting in various degenerative and psychiatric diseases. From a physiological perspective, cell protects itself against oxidative stress through arousing antioxygen defense mechanisms referring to oxygen-scavenger enzymes like superoxide dismutase, catalase, and glutathione peroxidase [34]. Spirulina improves gastric ulcer induced by aspirin in albino mice through enhancing antioxidant and cell-protective defenses alleviating oxidative stress and inflammation [35].

In this study, we found that insomnia is an important risk factor for PUD, rather than a complication of PUD. The mechanism of insomnia effect on PUD may be through a variety of ways, such as the immune system; it is worth noting that oxidative stress might also take part in it. The advantages in this study are the design of the MR as well as the use of data from large-scale GWASs of insomnia and PUD, which provide sufficient statistical power. Another advantage is that the studies included in these MR analyses mainly included individuals of European ancestry, which reduces the bias attributable to demographic stratification. In addition, because genetic information is used as an instrumental variable, the method is less susceptible to confounder, and because common exposures (such as weight) do not negatively affect human genetic information (such as DNA sequence), this method is not affected by reverse causality.

This study may be limited because the validity of the results of MR studies may be threatened by pleiotropy. However, our results were consistent across all analyses based on different MR methods, and there was no indication of directional pleiotropy. Another drawback is that the MR study evaluated whether insomnia susceptibility is associated with PUD. However, our findings do not necessarily mean that insomnia itself is a cause of PUD. We cannot rule out that there are other causes of insomnia leading to PUD. In

addition, the definition of insomnia includes a different set of chief complaints of insomnia. Another limitation is the overlap of individual segments included in GWASs for insomnia and PUD. This may introduce some bias in the MR estimates.

5. Conclusions

In conclusion, we found a significant association between insomnia and adverse PUD outcomes, highlighting the need to address sleep concerns as part of PUD management, and improving the quality of sleep might be a valuable way for populations suffering from insomnia to prevent PUD. Considering that patients with poor sleep quality are more prone to PUD recurrence, it is necessary to check up on these patients regularly. In addition, healthy people should also get enough sleep to prevent digestive problems.

Data Availability

All data are available on reasonable request from the corresponding author.

Conflicts of Interest

The authors declare that they have no conflicts of interest.

Authors' Contributions

Ling Feng Zha provided experimental ideas; Jiang Tao Dong and Qian Wen Chen processed the data; Jing Lin Wang, Ying Chao Zhou, and Jian Fei Wu contributed materials/analysis tools; Xin Tu and Shao Fang Nie wrote the paper. All authors reviewed the manuscript. The authors thank the public data from the GWAS consortia of SSGAC and the Program in Complex Trait Genomics. Ling-Feng Zha and Jiang-Tao Dong contributed equally to this study.

Acknowledgments

Supplementary Materials

Supplementary Table 1: insomnia-associated SNPs. Supplementary Table 2: position mapping genes. Supplementary Table 3: eQTL mapping genes. Supplementary Table 4: chromatin interaction mapping genes. *(Supplementary Materials)*

References

[1] C. M. Morin and R. Benca, "Chronic insomnia," *Lancet*, vol. 379, no. 9821, pp. 1129–1141, 2012.

[2] T. Roth and T. Roehrs, "Insomnia: epidemiology, characteristics, and consequences," *Clinical Cornerstone*, vol. 5, no. 3, pp. 5–15, 2003.

[3] A. Lanas and F. K. L. Chan, "Peptic ulcer disease," *Lancet*, vol. 390, no. 10094, pp. 613–624, 2017.

[4] R. S. Sandler, J. E. Everhart, M. Donowitz et al., "The burden of selected digestive diseases in the United States," *Gastroenterology*, vol. 122, no. 5, pp. 1500–1511, 2002.

[5] P. Malfertheiner, F. K. Chan, and K. E. McColl, "Peptic ulcer disease," *Lancet*, vol. 374, no. 9699, pp. 1449–1461, 2009.

[6] I. Räihä, M. Seppälä, O. Impivaara, M. T. Hyyppä, L. R. Knuts, and L. Sourander, "Chronic illness and subjective quality of sleep in the elderly," *Aging (Milano)*, vol. 6, no. 2, pp. 91–96, 1994.

[7] S. H. Ko, M. K. Baeg, S. Y. Ko, and K. D. Han, "Women who sleep more have reduced risk of peptic ulcer disease; Korean National Health and Nutrition Examination Survey (2008-2009)," *Scientific Reports*, vol. 6, no. 1, 2016.

[8] B. Fang, S. Yang, R. Xu, and G. Chen, "Association between poor sleep quality and subsequent peptic ulcer recurrence in older patients with mild cognitive impairment: examining the role of social engagement," *Scientific Reports*, vol. 9, no. 1, p. 2188, 2019.

[9] D. A. Lawlor, R. M. Harbord, J. A. Sterne, N. Timpson, and G. Davey Smith, "Mendelian randomization: using genes as instruments for making causal inferences in epidemiology," *Statistics in Medicine*, vol. 27, no. 8, pp. 1133–1163, 2008.

[10] J. Zheng, D. Baird, M.-C. Borges et al., "Recent developments in Mendelian randomization studies," *Curr Epidemiol Rep*, vol. 4, no. 4, pp. 330–345, 2017.

[11] S. Burgess, C. N. Foley, E. Allara, J. R. Staley, and J. M. M. Howson, "A robust and efficient method for Mendelian randomization with hundreds of genetic variants," *Nature Communications*, vol. 11, no. 1, p. 376, 2020.

[12] P. R. Jansen, The 23andMe Research Team, K. Watanabe et al., "Genome-wide analysis of insomnia in 1,331,010 individuals identifies new risk loci and functional pathways," *Nature Genetics*, vol. 51, no. 3, pp. 394–403, 2019.

[13] Y. Wu, G. K. Murray, E. M. Byrne, J. Sidorenko, P. M. Visscher, and N. R. Wray, "GWAS of peptic ulcer disease implicates _Helicobacter pylori_ infection, other gastrointestinal disorders and depression," *Nature Communications*, vol. 12, no. 1, 2021.

[14] A. R. Hammerschlag, S. Stringer, C. A. de Leeuw et al., "Genome-wide association analysis of insomnia complaints identifies risk genes and genetic overlap with psychiatric and metabolic traits," *Nature Genetics*, vol. 49, no. 11, pp. 1584–1592, 2017.

[15] S. S. Vege, G. R. Locke, A. L. Weaver, S. A. Farmer, L. J. Melton, and N. J. Talley, "Functional gastrointestinal disorders among people with sleep disturbances: a population-based study," *Mayo Clinic Proceedings*, vol. 79, no. 12, pp. 1501–1506, 2004.

[16] J. I. Semple, J. L. Newton, B. R. Westley, and F. E. May, "Dramatic diurnal variation in the concentration of the human trefoil peptide TFF2 in gastric juice," *Gut*, vol. 48, no. 5, pp. 648–655, 2001.

[17] V. Khanijow, P. Prakash, H. A. Emsellem, M. L. Borum, and D. B. Doman, "Sleep dysfunction and gastrointestinal diseases," *Gastroenterol Hepatol (N Y)*, vol. 11, 2015.

[18] K. Kato, I. Murai, S. Asai et al., "Circadian rhythm of melatonin and prostaglandin in modulation of stress-induced gastric mucosal lesions in rats," *Alimentary Pharmacology & Therapeutics*, vol. 16, Supplement 2, pp. 29–34, 2002.

[19] P. S. Phull, C. J. Green, and M. R. Jacyna, "A radical view of the stomach: the role of oxygen-derived free radicals and antioxidants in gastroduodenal disease," *European Journal of Gastroenterology & Hepatology*, vol. 7, no. 3, pp. 265–274, 1995.

[20] Q. Zhang, J. B. Dawodu, G. Etolhi, A. Husain, C. G. Gemmell, and R. I. Russell, "Relationship between the mucosal production of reactive oxygen radicals and density of Helicobacter pylori in patients with duodenal ulcer," *European Journal of Gastroenterology & Hepatology*, vol. 9, no. 3, pp. 261–265, 1997.

[21] A. Vaccaro, Y. K. Dor, K. Nambara et al., "Sleep loss can cause death through accumulation of reactive oxygen species in the gut," *Cell*, vol. 181, no. 6, pp. 1307–1328.e15, 2020.

[22] K. H. Alzoubi, O. F. Khabour, H. A. Salah, and B. E. Abu Rashid, "The combined effect of sleep deprivation and Western diet on spatial learning and memory: role of BDNF and oxidative stress," *Journal of Molecular Neuroscience*, vol. 50, no. 1, pp. 124–133, 2013.

[23] E. Reimund, "The free radical flux theory of sleep," *Medical Hypotheses*, vol. 43, no. 4, pp. 231–233, 1994.

[24] B. Liang, Y. H. Li, and H. Kong, "Serum paraoxonase, arylesterase activities and oxidative status in patients with insomnia," *European Review for Medical and Pharmacological Sciences*, vol. 17, no. 18, pp. 2517–2522, 2013.

[25] M. A. Frau-Méndez, I. Fernández-Vega, B. Ansoleaga et al., "Fatal familial insomnia: mitochondrial and protein synthesis machinery decline in the mediodorsal thalamus," *Brain Pathology*, vol. 27, no. 1, pp. 95–106, 2017.

[26] M. Glatzel and D. Sepulveda-Falla, "Losing sleep over mitochondria: a new player in the pathophysiology of fatal familial insomnia," *Brain Pathology*, vol. 27, no. 1, pp. 107-108, 2017.

[27] L. Palagini, P. A. Geoffroy, M. Miniati et al., "Insomnia, sleep loss, and circadian sleep disturbances in mood disorders: a pathway toward neurodegeneration and neuroprogression? A theoretical review," *CNS Spectrums*, pp. 1–11, 2021.

[28] F. Biasi, G. Leonarduzzi, P. I. Oteiza, and G. Poli, "Inflammatory bowel disease: mechanisms, redox considerations, and therapeutic targets," *Antioxidants & Redox Signaling*, vol. 19, no. 14, pp. 1711–1747, 2013.

[29] Y. Naito, T. Takagi, and T. Yoshikawa, "Molecular fingerprints of neutrophil-dependent oxidative stress in inflammatory bowel disease," *Journal of Gastroenterology*, vol. 42, no. 10, pp. 787–798, 2007.

[30] I. Moret-Tatay, M. Iborra, E. Cerrillo, L. Tortosa, P. Nos, and B. Beltrán, "Possible Biomarkers in Blood for Crohn's Disease: Oxidative Stress and MicroRNAs-Current Evidences and Further Aspects to Unravel," *Oxidative Medicine and Cellular Longevity*, vol. 2016, Article ID 2325162, 9 pages, 2016.

[31] H. Zhu and Y. R. Li, "Oxidative stress and redox signaling mechanisms of inflammatory bowel disease: updated experimental and clinical evidence," *Experimental Biology and Medicine (Maywood, N.J.)*, vol. 237, no. 5, pp. 474–480, 2012.

[32] G. R. Davies, N. J. Simmonds, T. R. Stevens et al., "Helicobacter pylori stimulates antral mucosal reactive oxygen metabolite production in vivo," *Gut*, vol. 35, no. 2, pp. 179–185, 1994.

[33] D. Bagchi, G. Bhattacharya, and S. J. Stohs, "Production of reactive oxygen species by gastric cells in association with Helicobacter pylori," *Free Radical Research*, vol. 24, no. 6, pp. 439–450, 1996.

[34] M. Mori, H. Suzuki, M. Suzuki, A. Kai, S. Miura, and H. Ishii, "Catalase and superoxide dismutase secreted from Helicobacter pylori," *Helicobacter*, vol. 2, no. 2, pp. 100–105, 1997.

[35] Y. I. Mahmoud and E. A. Abd El-Ghffar, "Spirulina ameliorates aspirin-induced gastric ulcer in albino mice by alleviating oxidative stress and inflammation," *Biomedicine & Pharmacotherapy*, vol. 109, pp. 314–321, 2019.

Research Article

PAK1 Silencing Attenuated Proinflammatory Macrophage Activation and Foam Cell Formation by Increasing PPARγ Expression

Wen-Lin Cheng,[1,2] **Quan Zhang,**[3] **Bo Li,**[4] **Jian-Lei Cao,**[1,2] **Lin Jiao,**[1,2] **Sheng-Ping Chao,**[1,2] **Zhibing Lu** ⓘ **,**[1,2] **and Fang Zhao** ⓘ [1,2]

[1]*Department of Cardiology, Zhongnan Hospital, Wuhan University, Wuhan 430071, China*
[2]*Institute of Myocardial Injury and Repair, Wuhan University, Wuhan 430071, China*
[3]*Department of Obstetrics and Gynecology, Union Hospital, Tongji Medical College, Huazhong University of Science and Technology, Wuhan 430022, China*
[4]*Department of Oral Radiology, School and Hospital of Stomatology, Wuhan University, Wuhan 430060, China*

Correspondence should be addressed to Zhibing Lu; luzhibing222@163.com and Fang Zhao; zhao_fang_zn@126.com

Macrophage polarization in response to environmental cues has emerged as an important event in the development of atherosclerosis. Compelling evidences suggest that P21-activated kinases 1 (PAK1) is involved in a wide variety of diseases. However, the potential role and mechanism of PAK1 in regulation of macrophage polarization remains to be elucidated. Here, we observed that PAK1 showed a dramatically increased expression in M1 macrophages but decreased expression in M2 macrophages by using a well-established *in vitro* model to study heterogeneity of macrophage polarization. Adenovirus-mediated *loss-of-function* approach demonstrated that PAK1 silencing induced an M2 macrophage phenotype-associated gene profiles but repressed the phenotypic markers related to M1 macrophage polarization. Additionally, dramatically decreased foam cell formation was found in PAK1 silencing-induced M2 macrophage activation which was accompanied with alternation of marker account for cholesterol efflux or influx from macrophage foam cells. Moderate results in lipid metabolism and foam cell formation were found in M1 macrophage activation mediated by AdshPAK1. Importantly, we presented mechanistic evidence that PAK1 knockdown promoted the expression of PPARγ, and the effect of macrophage activation regulated by PAK1 silencing was largely reversed when a PPARγ antagonist was utilized. Collectively, these findings reveal that PAK1 is an independent effector of macrophage polarization at least partially attributed to regulation of PPARγ expression, which suggested PAK1-PPARγ axis as a novel therapeutic strategy in atherosclerosis management.

1. Introduction

Macrophages play crucial roles in regulation of inflammation, innate immunity, and adaptive immunity that the pathophysiology processes induced by macrophage are widely involved in a broad spectrum of acute and chronic inflammatory diseases [1–3]. It is well accepted that macrophages are characterized as remarkable diversity and plasticity which can plasticize to different phenotypes after integrating various environmental signals. Administrated with integration of interferon-γ (IFN-γ) and Toll-like receptor 4 (TLR4) ligand lipopolysaccharide (LPS), macrophages turns to a classical proinflammatory macrophage phenotype (M1) that regulate inflammatory response by degradation of basement membrane by secretion of extracellular matrix metalloproteinases (MMPs), production of cytokines, and chemokines. On the contrary, macrophages undergo alternative activation (M2) change upon IL-4 and IL-13 stimulation that are associated with resolution of inflammation and tissue repair mediated by secretion of anti-inflammatory cytokines [4–7]. In the past dozens of years, a spectrum of activation programs and underlying molecular mechanisms in M1 and M2 polarized

macrophage field have been deeply investigated [8, 9], especially in the development of atherosclerosis in which macrophages are important sources and targets of inflammatory mediators [10]. Accumulative evidences have indicated that a continuum of M1 and M2 macrophages can be expressed in both mouse and human atherosclerotic lesions [11], which, respectively, accelerate or attenuate foam cell formation and atherosclerotic lesion formation [5, 12]. The distinct function of M1 and M2 macrophage polarization implicated in atherogenesis prompts us to explore important regulators and underlying molecular mechanisms.

The P21-activated kinase (PAK) family belongs to the larger nonreceptor serine/threonine protein kinase family with six members (PAK1-6) and initially serves as important effectors for Rho GTPases [13]. Among the PAK family proteins, PAK1 plays a crucial role in a wide variety of diseases, including cancers, inflammation, viral infection, malaria, immunosuppression, ageing, and diabetes [14–18]. Increasing evidences have demonstrated that PAK1 participates in cardiovascular diseases by engaging different signaling pathways [19]. PAK1 acts as a regulator of ion channels and contractile proteins which can prevent arrhythmias by modifying Ca^{2+} homoeostasis in myocytes [20]. *In vitro* and *in vivo* studies demonstrate that PAK1 phosphorylation protects the heart from pressure overload-induced hypertrophy through the JNK/NFAT signaling pathway in response to various hypertrophic stresses [21]. A more recent study demonstrates that PAK1 is a novel therapeutic target for the treatment of ischemia-reperfusion (I/R) injury, as suggested by the evidences that PAK1 deficiency leads to phosphorylation of myofilament proteins and subsequently impedes the recovery of cardiac function after I/R [22]. However, supporting data for the potential functional involvement of PAK1 in macrophage polarization are scarce.

In the present study, we observed that PAK1 expression was positively related with M1 macrophages but negatively associated with M2 macrophages. In functional studies, we demonstrated that PAK1 silencing shaped macrophage towards to anti-inflammatory M2 macrophage, and it mediated M2 macrophage activation dramatically decreased foam cell formation by released cellular cholesterol constituents characterized as upregulated ATP-binding cassette transporter A1 (ABCA1) and ATP-binding cassette transporter G1 (ABCG1) expression but downregulated CD36 and scavenger receptor type A (SR-A) expression. In addition, PAK1 inhibition led to a moderate attenuating effect on M1 macrophage activation. Mechanistically, we demonstrated that the aforementioned effects mediated by PAK1 knockdown were reversed upon inhibited peroxisome proliferator-activated receptor γ (PPARγ) expression.

2. Materials and Methods

2.1. Cell Culture and Adenovirus Infection.
Peritoneal macrophages (PMs) were isolated from ApoE-deficient mice and harvested followed with peritoneal lavage treatment for 4 days after intraperitoneal injection of 1 ml of 4% thioglycolate. Then, the cells were collected and cultured in conditioned medium constitute with Roswell Park Memorial Institute (RPMI) containing 10% fetal bovine serum and 1% penicillin-streptomycin. Femurs and tibias from ApoE-deficient mice were flushed with Dulbecco's modified eagle medium (DMEM), and isolated bone marrow-derived macrophages (BMDMs) were centrifuged and cultured in RPMI containing 10% fetal bovine serum and MCSF (50 ng/ml). PLVX-shRNA vector was utilized for PAK1-specific short hairpin RNA- (shRNA-) expressing (shPAK1) construction which then generates AdshPAK1 recombinant adenoviral vectors, while adenoviral vector with short hairpin RNA (AdshRNA) as a control group. BMDMs were infected with adenovirus in diluted media for 24 hours at a 100 multiplicity of infection (MOI) of 100 particles per cell. The collected BMDMs were treated with LPS (50 ng/ml) or IL-4 (10 ng/ml) for 24 hours and harvested for mRNA and protein test. The animal protocols were approved by the Animal Care and Use Committee of Zhongnan Hospital of Wuhan University.

2.2. RNA Isolation and Quantitative Real-Time PCR.
For real time-PCR analysis, total mRNA was extracted from macrophages with a TRIzol reagent (Invitrogen) manage and then reverse transcribed into cDNA using a Transcriptor First-Strand cDNA Synthesis Kit. PCR amplifications were quantified using a QuantStudio 6 Flex System (Life technologies) in accordance with manufacturer's protocol. The mRNA expressions were normalized to GAPDH expression. The primers were showed in Table 1.

2.3. Western Blotting.
Cultured macrophages were lysed using a RIPA assay buffer, and protein concentrations were determined using a Pierce BCA Protein Assay kit. Five micrograms of protein were separated via sodium dodecyl-sulphate polyacrylamide gel electrophoresis (SDS-PAGE) and transferred to a polyvinylidene fluoride (PVDF) membrane, which then probed with particular primary antibodies overnight at 4°C. Following incubation with secondary antibodies for 1 hour at room temperature, the signals were visualized using a FluorChem E Imager. The protein expression levels were normalized against GAPDH. The antibodies were showed in Table 2.

2.4. Foam Cell Formation.
BMDMs infected with AdshPAK1 upon stimulation with LPS or IL-4 were cultured on chamber slides for overnight incubation. To further visualize cholesterol accumulation, the treated macrophages were fixed on cover slips and stimulated with 15ug/ml of oxidation low lipoprotein (Ox-LDL) for additional 24 hours. Macrophages were then fixed with 4% paraformaldehyde in PBS and stained with 0.3% Oil Red O in 60% isopropanol and captured by microscopy.

2.5. Immunofluorescence Staining.
Macrophages were cultured on cover slips and were fixed with 3.7% formaldehyde and permeabilized with 0.1% Triton X-100 in PBS for 45 min. Subsequently, the slides were blocked in 10% goat serum diluted with PBS for 1 h and incubated overnight with various primary antibodies overnight at 4°C. After rewarming at 37°C for 1 h, the sections then were washed in PBS and incubated with the appropriate secondary antibodies

Table 1: The primers for real-time PCR.

Primer	Sequence (5$'$ to 3$'$)
PAK1-F	GATGTAGCCACAGGGCAGGA
PAK1-R	GAGCCTCCAGCCAAGTATTCC
Arg-1-F	ACACGGCAGTGGCTTTAACC
Arg-1-R	GGCGTTTGCTTAGTTCTGTCTG
Mrc-1-F	TACAGCCGGGAAGACAATAACT
Mrc-1-R	AGGAGTCGGTTAGCAGTATGTTG
IL-10-F	AGTCCTTCAGAGGGGGTTCACC
IL-10-R	TTGTCTTGTGGAGCAGGTGTG
KLF4-F	GCCACCCACACTTGTGACTA
KLF4-R	CTGTGTGTTTGCGGTAGTGC
chi3I3-F	TGAAGGAGCCACTGAGGTCT
chi3I3-R	TGAAGGAGCCACTGAGGTCT
Retnla-F	TCCCTCCACTGTAACGAAGAC
Retnla-R	AAGATCCACAGGCAAAGCCA
TNF-α-F	TCCCCAAAGGGATGAGAAGTT
TNF-α-R	GAGGAGGTTGACTTTCTCCTGG
IL-6-F	CTTCTTGGGACTGATGCTGGT
IL-6-R	CACAACTCTTTTCTCATTTCCACG
iNOs-F	ACATCAGGTCGGCCATCACT
iNOs-R	CAGAGGCAGCACATCAAAGC
IL-1β-F	TAATGAAAGACGGCACACCCA
IL-1β-R	GTTTCCCAGGAAGACAGGCT
Cox2-F	ATTGCCCTCCCCTCTCTACG
Cox2-R	CGGCTCATGAGTGGAGAACG
MCP-1-F	ATGCAGGTCCCTGTCATG
MCP-1-R	GCTTGAGGTGGTTGTGGA
SR-A-F	TGGAGGAGAGAATCGAAAGCA
SR-A-R	CTGGACTGACGAAATCAAGGAA
CD36-F	GACTGGGACCATTGGTGATGA
CD36-R	AAGGCCATCTCTACCATGCC
ABCA1-F	AGGCACTCAAGCCACTGCTTGT
ABCA1-R	TGCCTCTGCTGTCTAACAGCGT
ABCG1-F	GGTTGCGACATTTGTGGGTC
ABCG1-R	TTCTCGGTCCAAGCCGTAGA
GAPDH-F	TGAAGGGTGGAGCCAAAAG
GAPDH-R	AGTCTTCTGGGTGGCAGTGAT

Table 2: Antibody for immunoblot.

Primary antibody	Cat no.	Manufacturer	Sources of species
PAK1	ab223849	Abcam	Rabbit
TNF-a	ab6671	Abcam	Rabbit
IL-6	66146-1-Ig	Proteintech group	Mouse
Arg-1	16001-1-AP	Proteintech group	Rabbit
IL-10	20850-1-AP	Proteintech group	Rabbit
CD36	sc-21772	Santa	Mouse
SR-A	sc-166139	Santa	Mouse
ABCA1	ab66217	Abcam	Mouse
ABCG1	ab52617	Abcam	Rabbit
PPARγ	sc-7273	Santa	Mouse
GAPDH	ab181602	Abcam	Rabbit

were further washed five times with lysis buffer, boiled with 2× SDS loading buffer, separated with SDS–PAGE, and electrophoretically transferred to PVDF membrane. The membranes were blocked with 5% BSA in Tris-buffered saline containing 0.1% Tween-20 and were immunoreacted with the indicated primary antibodies and secondary antibodies.

2.7. Statistical Analysis. All results were presented as the means ± SD. For comparisons between two groups, Student's two-tailed t-test was applied. One-way analysis of variance (ANOVA) was applied for comparison of multiple groups. All statistical analyses were performed. The software SPSS, version 22.0, was used for all statistical analyses. P values less than 0.05 were considered significant.

3. Result

3.1. Altered PAK1 Expression in M1 and M2 Macrophage. To examine whether PAK1 is involved in regulation of macrophage activation, we first investigated the expression of PAK1 in classically (M1) or alternatively (M2) activated macrophage upon LPS or IL-4 stimulation, respectively. RT-PCR analysis showed that PAK1 mRNA levels were significantly increased in M1 macrophage but decreased in M2 macrophage as assessed with PMs (Figure 1(a)) and BMDM population (Figure 1(b)). As expected, we observed a similar pattern in PAK1 protein expression examined by Western blot analyses (Figures 1(c) and 1(d)). In addition, double immunofluorescence staining for PAK1 and the macrophage-specific marker CD68 in BMDMs showed stronger immunoreactivity of PAK1 in M1 macrophage than that in M2 macrophage (Figure 1(e)). Collectively, these findings suggested a positive relationship between PAK1 and macrophages with the proinflammatory phenotype.

3.2. PAK1 Silencing Promoted Alternative M2 Activation. Since the notable change of PAK1 expression in M1 and M2 macrophages suggested a possible role for PAK1 in the regulation of macrophage polarization, we next tested the

for another 1 h. Images were captured with a fluorescence microscope (Olympus, Tokyo, Japan) using DP2-BSW software and were analyzed with Image-Pro Plus 6.0.

2.6. Co-IP. Immunoprecipitation was performed to determine protein-protein interactions. For immunoprecipitation, cells were washed with cold PBS and lysed with lysis buffer containing Protease Inhibitor Cocktail Tablets (AS1005C, ASPEN). After being precleared with immunoglobulin G and Sure Beads™Starter Kit Protein A (#1614813, BIO-RAD), lysates were incubated with the indicated primary antibodies and protein A-agarose at 4℃ overnight with gentle shaking. The immunoprecipitated proteins

Figure 1: PAK1 expression is induced in M1 but reduced in M2 macrophages. (a, b) PAK1 mRNA levels in PMs and BMDMs subjected to PBS, IL-4, or LPS stimulation for 24 hours. $n = 3$. (c, d) Western blot analysis of PAK1 protein levels in PMs and BMDMs administrated with PBS, IL-4, or LPS for 24 hours. $n = 3$. (e) Representative images of double immunofluorescence staining of BMDMs with an anti-PAK1 antibody (red) and macrophage marker (CD68, green) treated with PBS, IL-4, or LPS for 24 hours. The integral optical density of PAK1 was presented. Scale bar = 50 μm. $n = 3$. $^*P < 0.05$ versus PBS group, $^#P < 0.05$ versus IL-4 group. PMs: peritoneal macrophages; BMDMs: bone marrow-derived macrophages; PBS: phosphate-buffered saline; IL-4: interleukin-4; LPS: lipopolysaccharides.

expression of represented markers of M1 or M2 activation in BMDMs regulated by PAK1. A *loss-of-function* study with adenovirus harboring PAK1 short hairpin RNA (AdshPAK1) was performed, and we noticed that PAK1 expression was dramatically decreased in the BMDMs transfected with AdshPAK1 (Figures 2(a) and 2(b)). In response
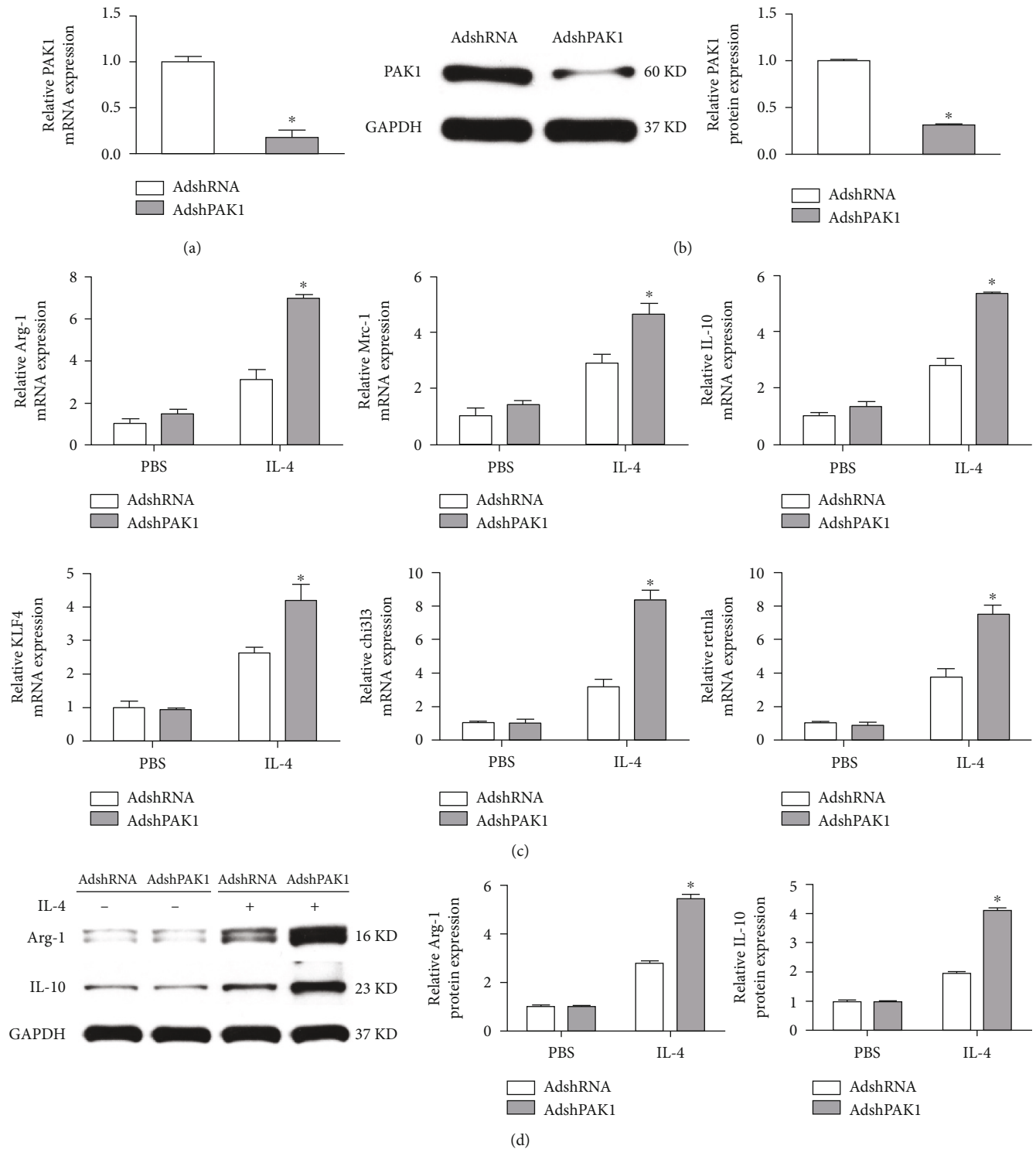
Figure 2: PAK1 promotes M2 polarized macrophages. (a, b) The PAK1 expression in BMDMs infected with AdshPAK1 or AdshRNA. $n = 3$. (c) mRNA expression levels of M2 macrophage markers in BMDMs by PAK1 knockdown with IL-4 stimulation. $n = 3$. (d) Protein expression levels of Arg-1 and IL-10 in BMDMs by PAK1 knockdown with IL-4 stimulation. $n = 3$. $^*P < 0.05$ compared with control group. Arg-1: arginase-1.

to IL-4 administration, higher mRNA levels of anti-inflammatory M2 makers were found in BMDMs mediated by PAK1 knockdown, including arginase-1 (Arg-1), Mrc-1, interleukin (IL)-10, KLF4, chi3I3, and Retnla, whereas there was no difference under basal conditions in response to PBS stimulation (Figure 2(c)). Furthermore, these changes in the mRNA levels of Arg-1 and IL-10 were recapitulated at the protein level, as determined by Western blot analyses (Figure 2(d)).

3.3. PAK1 Knockdown Inhibited Classical M1 Activation.
Next, we evaluated the effect of PAK1 silencing on M1

(a)

(b)

(c)

(d)

(e)

(f)

(g)
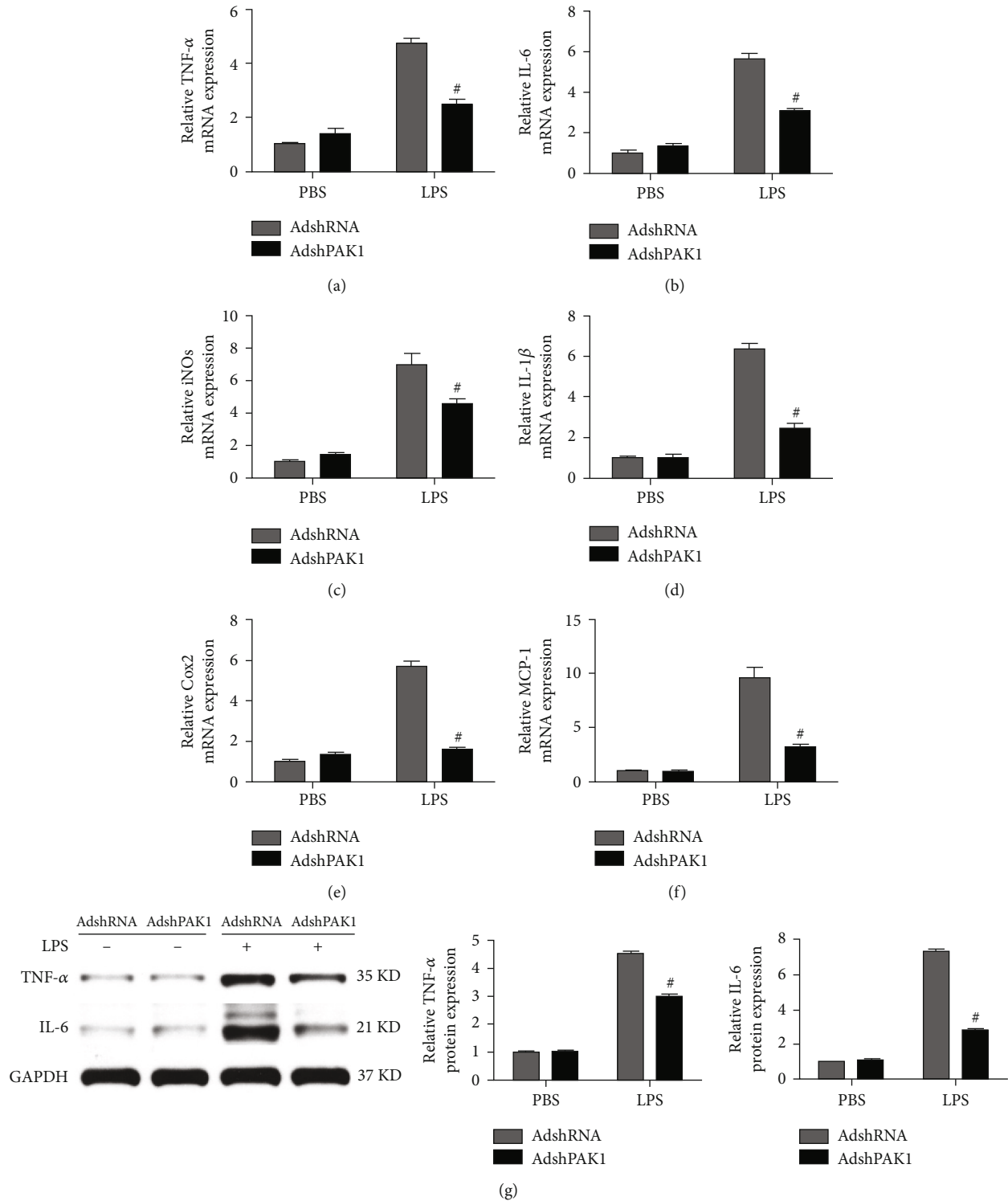
Figure 3: PAK1 attenuates the M1 polarized macrophages. (a–f) RT-PCR analysis of expression levels of M1 macrophage markers in BMDMs by PAK1 knockdown upon LPS treatment. $n = 3$. (g) Western blot analysis of TNF-α and IL-6 protein level in BMDMs by PAK1 knockdown upon LPS treatment. $n = 3$. $^{\#}P < 0.05$ compared with control group. TNF-α: tumor necrosis factor-α; iNOs: inducible no synthase.

polarization by testing the prototypical proinflammatory M1 macrophage target genes. In contrast with the observations of AdshPAK1-mediated M2 macrophages, the expression of LPS-induced M1 markers, including the characteristic tumor

necrosis factor-α (TNF-α), IL-6, inducible no synthase (iNOs), IL-1β, Cox2, and MCP-1 genes, was significantly decreased by PAK1 knockdown, whereas slight differences were observed in the PBS-treated group (Figures 3(a)–3(f)). As expected, the
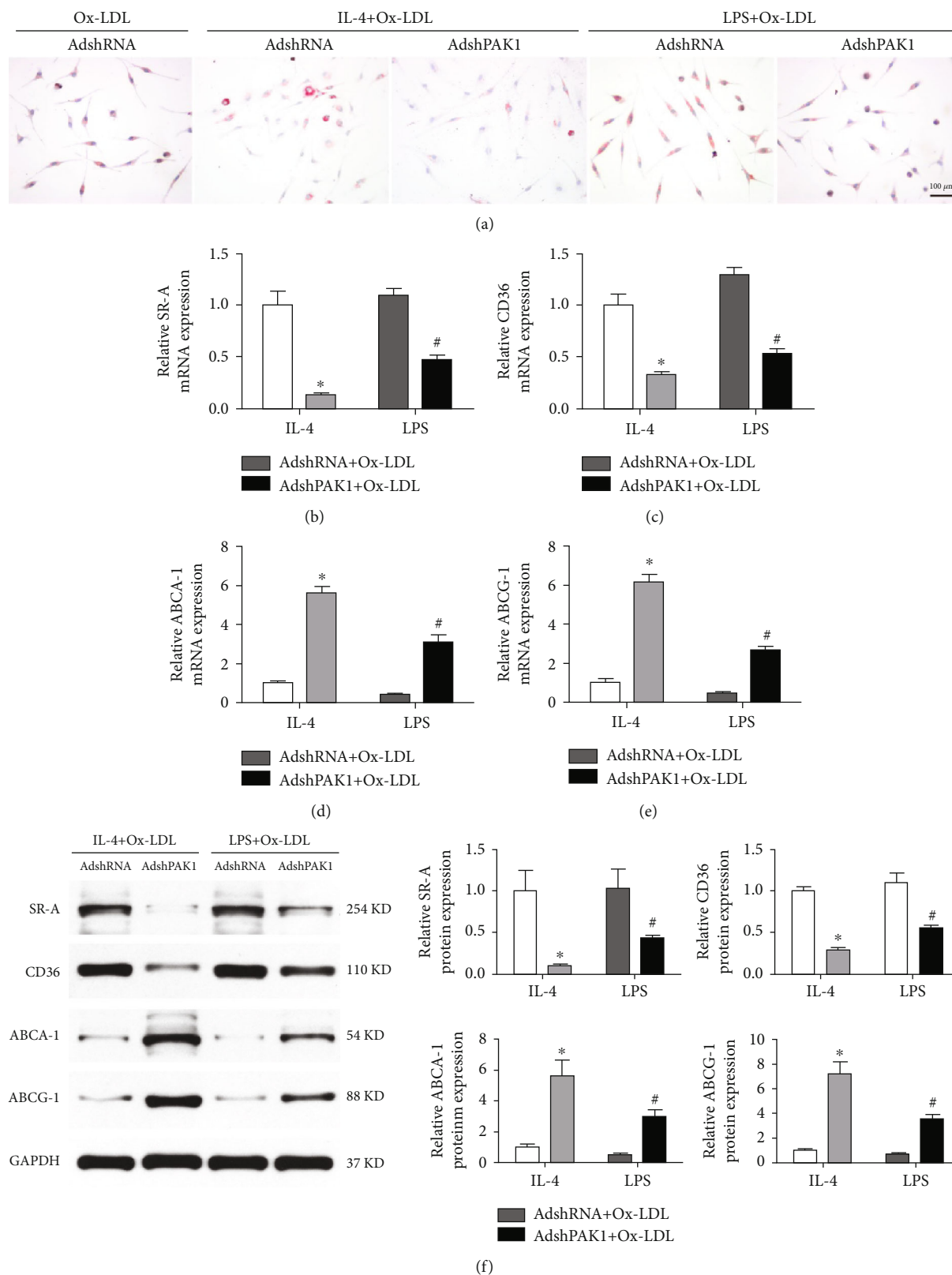
Figure 4: Decreased foam cell formation by PAK1 silencing. (a) Oil-red staining of BMDMs infected with AdshPAK1 or AdshRNA, which previously stimulated with IL-4 or LPS and administrated with Ox-LDL. Scale bar = 100 μm. n = 6-10. (b–f) Alternation of the expression of SR-A and CD36, and ABCA1 and ABCG1 in BMDMs infected with AdshPAK1, which previous stimulated with IL-4 or LPS and administrated with Ox-LDL at mRNA (b–e) and protein (f) levels, respectively. n = 3. $^*P < 0.05$ or $^#P < 0.05$ compared with control group. SR-A: scavenger receptor type A; ABCA1: ATP-binding cassette transporter A1; ABCG1: ATP-binding cassette transporter G1 (ABCG1).

(a)

(b)

(c)

(d)

FIGURE 5: Continued.

(e)

(f)

(g)

(h)
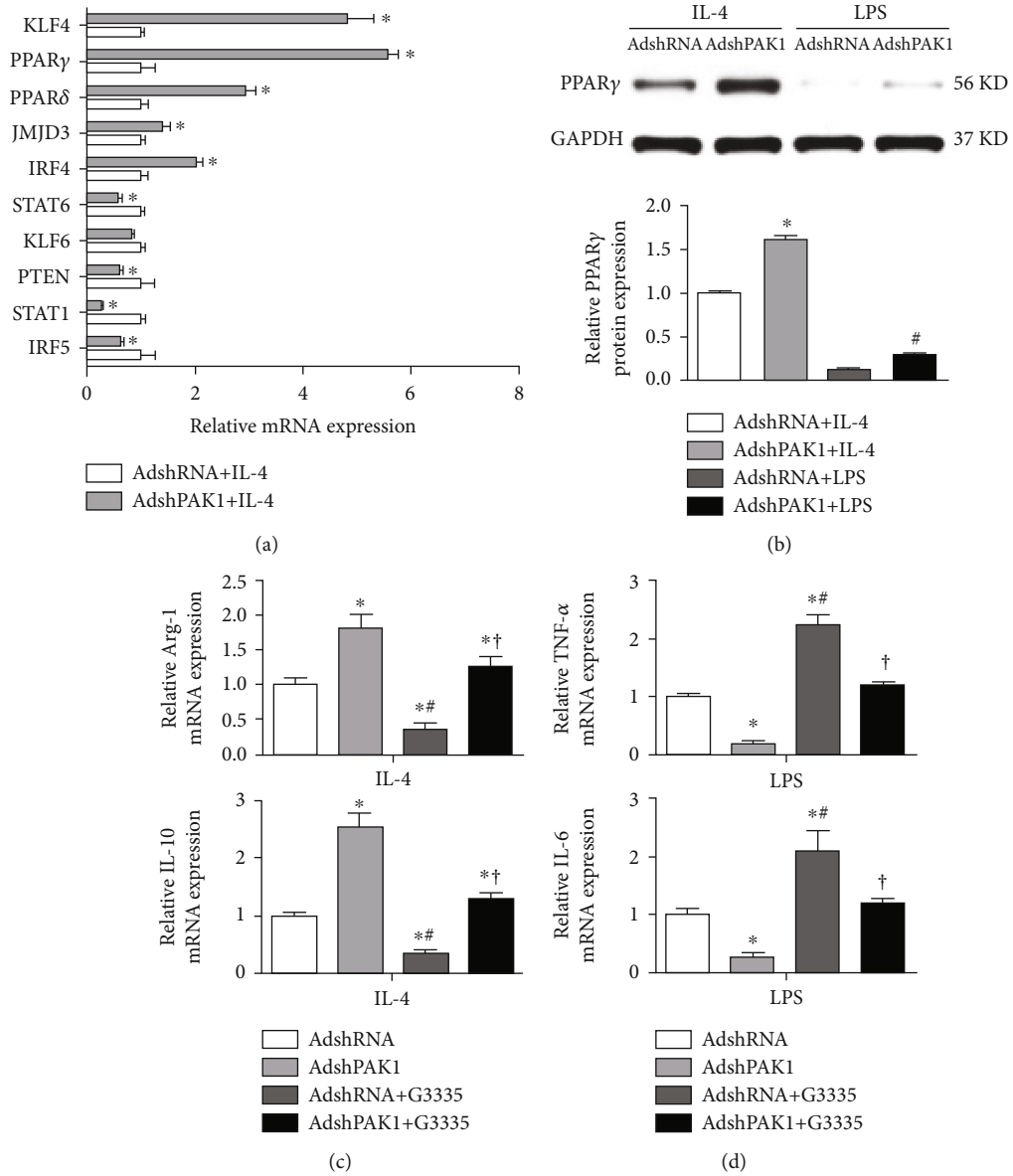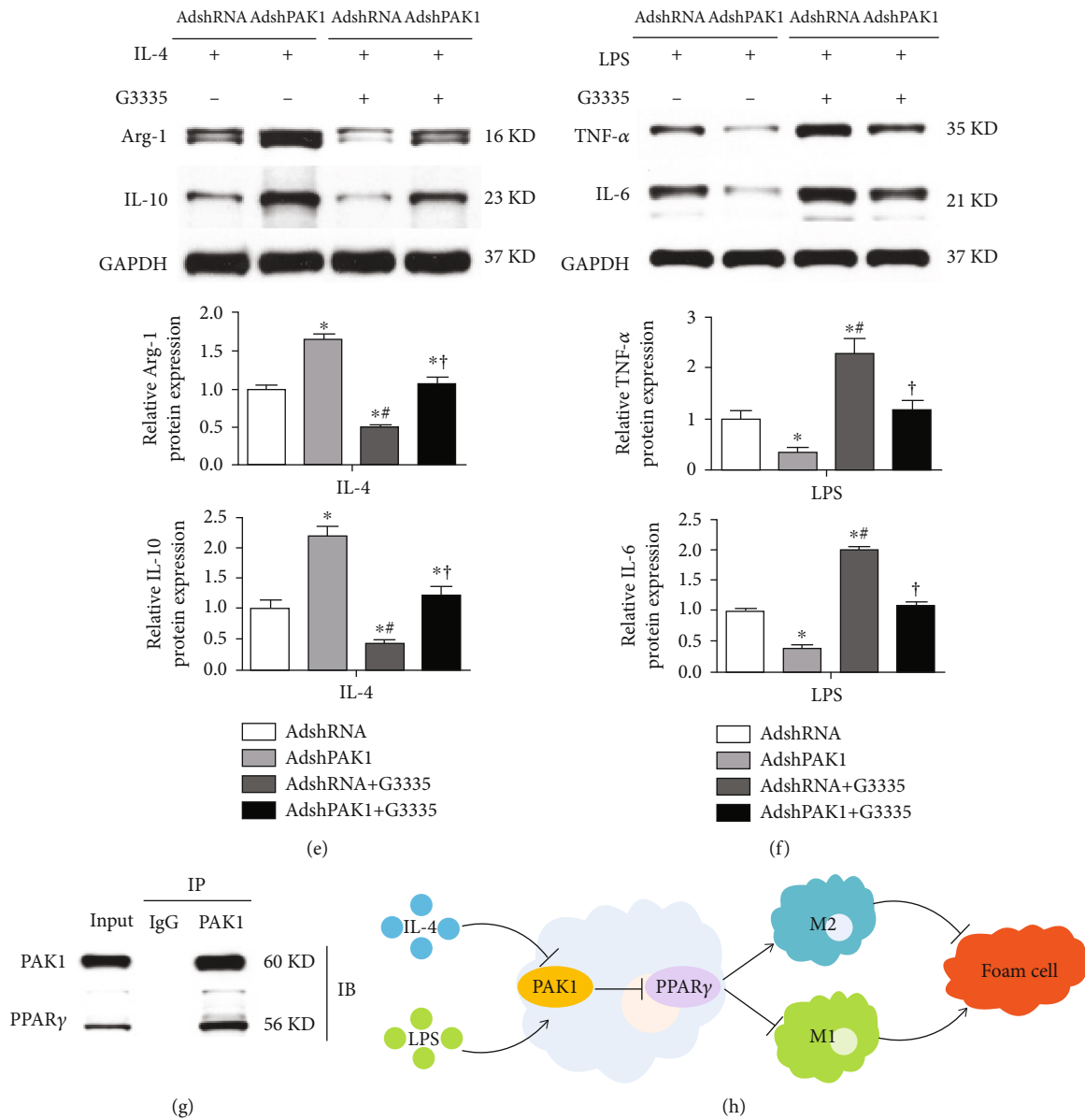
FIGURE 5: Upregulated PPARγ expression by PAK1 silencing. (a) mRNA levels of the representative regulators for macrophage polarization in BMDMs by PAK1 knockdown with IL-4 stimulation. $n = 3$. $^*P < 0.05$ compared with AdshRNA group. (b) Protein level of PPARγ in BMDMs by PAK1 knockdown with IL-4 or LPS stimulation. $n = 3$. $^*P < 0.05$ or $^\#P < 0.05$ compared with control group. (c–f). RT-PCR (c, d) and Western blot (e, f) analysis of M2 and M1 marker gene expression in macrophage transfected with AdshRNA or AdshPAK1 and treated with LPS or IL-4, which then cultured with G3335 or control. $n = 3$. $^*P < 0.05$ compared with AdshRNA group; $^\#P < 0.05$ vs. AdshPAK1 group; $^\dagger P < 0.05$ vs. AdshRNA with G3335 group. (g) Immunoblotting with PPARγ or PAK1antibody was performed on co-IP of PAK1 using PAK1 antibody. (h) Schematic diagram of the molecular mechanisms underlying PAK1-regulated macrophage polarization and foam cell. PPARγ: peroxisome proliferator-activated receptor γ.

differences in mRNA expression of TNF-α and IL-6 were confirmed by Western blot analyses to be similar for the corresponding proteins (Figure 3(g)).

3.4. Decreased Foam Cell Formation Was Mediated by PAK1 Knockdown.

Foam cells formed by the accumulation of oxidized modified LDL (Ox-LDL) in macrophages play an important role in the development of atherosclerosis, and recent studies have suggested that macrophage polarization may substantially contribute to foam cell precursors. Consis-

tently, we noticed that accumulated foam cells were found in the M1-polarized macrophage population treated with Ox-LDL, but fewer foam cells were found among the M2-polarized macrophages treated with Ox-LDL, as determined by neutral lipid staining with Oil Red O (Figure 4(a)). Importantly, dramatically decreased lipid accumulation was observed in the M2 macrophages activated by AdshPAK1 after treatment with Ox-LDL compared with those treated with AdshRNA, whereas moderately decreased lipid accumulation was found in the M1 macrophages in which

activation was mediated by AdshPAK1 (Figure 4(a)). The RT-PCR analysis revealed significantly or moderately decreased marker expression accounted for cholesterol influx (SR-A and CD36) and increased markers related to cholesterol efflux (ABCA1 and ABCG1) in IL-4-induced M2 macrophages and LPS-induced M1 macrophages regulated by PAK1 knockdown, respectively (Figures 4(b)–4(e)). The expression of protein markers related to cholesterol influx and efflux was similar to that observed for the corresponding mRNAs (Figure 4(f)).

3.5. PAK1 Silencing Upregulated PPARγ Expression. Accumulating evidence has strongly demonstrated that multiple transcription factors are required for management of macrophage polarization [9]. Thus, intensively exploring the underlying mechanism by which PAK1 knockdown alleviated classical M1 macrophages but promoted alternative M2 macrophage activation, we determined changes in the potential aforementioned target genes upon PAK1 silencing. We found that upon PAK1 silencing, PPARγ mRNA levels were increased the most in M2 macrophages (Figure 5(a)), which was confirmed by Western blot analysis (Figure 5(b)). Next, we tested the functional requirement of PPARγ in PAK1-knockdown-mediated macrophage polarization. By using a PPARγ-specific antagonist (G3335), we noticed that PPARγ inactivation blunted the PAK1-knockdown-mediated increased anti-inflammatory M2 phenotype marker expression (Arg-1 and IL-10) and decreased proinflammatory M1 phenotype marker expression (TNF-α and IL-6) at both the mRNA (Figures 5(c) and 5(e)) and protein levels (Figures 5(d) and 5(f)). The regulation of PPARγ activity by PAK1 prompted us to ask whether PAK1 could directly interact with PPARγ. Endogenous interaction between PAK1 and PPARγ was identified in BMDMs (Figure 5(g)).

4. Discussion

Understanding the switching of macrophages polarization may provide promising targets and novel strategies to protect against the development of atherosclerosis. The current study showed a remarkable enhanced M2 polarized macrophage genes but reduced M1 polarized macrophage marker expression in BMDMs infected with AdshPAK1. Additionally, dramatically decreased foam cell formation was found in PAK1 silencing-induced M2 macrophage activation concomitantly with increased ABCA1 and ABCG1 expression and decreased CD36 and SR-A expression. Mechanistically, the shift in macrophage phenotype acquisition mediated by PAK1 knockdown was largely reversed by PPARγ inactivation. Thus, this evidence establishes the PAK1-PPARγ axis as an attractive therapeutic target for the regulation of macrophage polarization implicated in atherosclerosis (Figure 5(h)).

As a member of the highly conserved family of serine-/threonine protein kinases regulated by Ras-related small G-proteins, PAK1 plays diverse roles in cell signaling through catalytic and scaffolding activities, as well as regulation of proliferation and survival pathways, including the MAPK, AKT, Wnt1/β-catenin, ERα, BAD, and nuclear factor kappa beta (NF-κB) pathways [17, 23, 24]. In addition, PAK1 plays a crucial role in multiple cardiovascular diseases, including cardiac arrhythmias, cardiac contractility dysfunction, hypertrophy, and I/R [19]. Besides, considerable evidences have suggested that PAK1 is involved in inflammation-related diseases. PAK1 promotes the expression of target genes involved in NF-κB signaling [17], while PAK1 deficiency increases Treg cell numbers which are critical for attenuating the local inflammatory response and facilitating a significant improvement in immunopathology during schistosome infection [25]. Moreover, PAK1 interacts with Signal Transducer and Activator of Transcription (STAT3) to form PAK1/STAT3 complex and subsequently regulates the transcription of the IL-6 gene by binding to the IL-6 promoter [26]. Notably, published paper demonstrates that genetic deletion of PAK1 in ApoE-deficient mice leads to reduced atherosclerotic lesion by decreasing IL-6 and MCP-1 levels, whereas the detailed molecule mechanism instead of phenotypic observation remains unexplored. By using PMs and BMDMs isolated from ApoE knockout mice which were utilized as a classical in vitro model for atherosclerosis, we aimed to investigate the potential role of PAK1 in macrophage activation that may contribute to the development of atherosclerosis. Our present data have established that PAK1 may act as an important regulator for macrophage polarization characterized as dramatically increased expression in proinflammatory M1 macrophages but decreased expression in anti-inflammatory M2 macrophages. More importantly, functional study showed that PAK1 silencing suppressed proinflammatory M1 maker expression induced by LPS and restored anti-inflammatory M2 genes subjected to IL-4. Although the present study demonstrated PAK1 as a novel target for regulation of macrophage polarization, the effect of PAK1, especially macrophage-specific PAK1 deficiency, on macrophage activation in vivo should be deeply investigated in the future study.

Substantial evidences have demonstrated that the pathogenesis and evolution of atherosclerotic lesion are significantly influenced by macrophage polarization that M1 or M2 macrophages can, respectively, exert pro- or antiatherogenic functions. Understanding the underlying regulators and mechanisms that are responsible for the dynamic plasticity and distinct functional characteristics of classical M1 macrophage and alternative M2 macrophage activation in the development of atherosclerosis could provide effective strategies to prevent the atherosclerotic lesion development and outcome. Overwhelming suggestive evidences have demonstrated that macrophage polarization is controlled by the interplay between extrinsic factor, intrinsic developmental pathways, and the tissue environment [9]. Stimulated by interferon- (IFN-) γ and its receptor with TLR, IL-1R signaling, and TNF induction, macrophages are polarized to M1 phenotype by engaging a set of transcription factors, such as NF-κB, IRF5, STAT1, PTEN, KLF6, and AKT2. By contrast, induced by IL-4, IL-13, and IL-4Ra, the alternative M2 macrophages are polarized with simultaneous activation of key downstream transcription factor that are central to M2 polarization, including STAT6, IRF4, JMJD3, PPARδ, PPARγ, KLF4, and AKT1 [9, 12]. Thus, we continued to

elucidate the underlying mechanism by which PAK1 knockdown regulated macrophage polarization. The results showed that PPARγ was the most significantly upregulated gene in macrophages infected with AdshPAK1 upon IL-4 stimulation among those screened targets. Consistently, it has been reported that suppression of PPARγ is responsible for the effect of PAK1 overexpression on NF-κB signaling activation in inflammation and colitis-associated cancer. The nuclear hormone receptor PPARγ has recently emerged as a central switch that determines the pro- or anti-inflammatory potential macrophage *in vitro* and *in vivo* [12, 27]. PPARγ overexpression attenuates the induction of inflammatory gene expression by modulating the downstream transcription factor activity through protein-protein interaction subjected to LPS and IFNγ stimulation [28]. By contrast, IL-4- and IL-13-induced differentiation of monocytes into alternative macrophages is enhanced by PPARγ, while secretion of proinflammatory mediators in M1 macrophages is attenuated cocultured with the supernatant obtained from the culture of M2 macrophages with high PPARγ expression [29]. Consistent with these results *in vitro*, selective inactivation of PPARγ in macrophages cause an impairment of alternatively activated M2 macrophages and accelerate diet-induced obesity, insulin resistance, and glucose intolerance, as well as exacerbate atherosclerotic lesion formation in ApoE-deficient mice [12]. In administration of a PPARγ-specific antagonist, it largely reversed the effect of PAK1 silencing on macrophage polarization, while PAK1 can also interact with PPARγ. Considering this evidence, we demonstrated that PAK1 knockdown regulated macrophage polarization partially through the activation of PPARγ.

In addition to its important role in the regulation of macrophage polarization, PPARγ also plays a crucial role in cholesterol transport and foam cell formation. Reduction of SR-A and apoB-48 receptor expression and inhibition of LPL secretion and activity are implicated in attenuated foam cell formation mediated by PPARγ activation [30–32]. Moreover, PPARγ decreases ACAT1 expression to decrease the rate of cholesterol esterification and is positively associated with cholesterol efflux in macrophage through upregulated expression of SR-B1, caveolin-1, ABCA1, and ABCG1 [33–36]. Although foam cell formation has been traditionally linked to the proinflammatory macrophage phenotype, the underlying mechanisms associated with cholesterol loading in reaction to the inflammatory response by macrophages have not yet been defined, and little is known about the propensity of individual polarized macrophage to become foam cells. It has been reported that M4 and Mhem macrophages inhibit the capacity of cholesterol influx but promotes cholesterol efflux depending by increased liver X receptor (LXR) expression, which indicated that M1 or M2 macrophages can act as the main foam cell precursors upon alteration of the key determinates of cholesterol transport [37, 38]. Another important finding in our present study was that increased foam cells were observed in the M1-polarized macrophage population, but fewer foam cells were found in the M2-polarized macrophage population. Importantly, less-significant lipid accumulation was found in

AdshPAK1-mediated M2 polarized macrophages induced by IL-4, and this reduction was accompanied by increased expression of markers involved in cholesterol efflux and decreased expression of genes associated with cholesterol influx. Therefore, we suspected that the upregulated PPARγ expression in M2 macrophages mediated by PAK1 knockdown was required for decreased foam cell formation. Collectively, the clearly delineated effect of the "PAK1-PPARγ" axis on macrophage polarization and subsequent foam cell formation indicated the important role of this axis in the development of atherosclerosis.

In summary, our study first demonstrated that PAK1 was a novel regulator of macrophage polarization characterized as positive association between PAK1 expression and proinflammatory macrophage phenotype, increased alternative inflammation-resolving M2 macrophage activation, and more significantly, decreased foam cell formation in PAK1 silencing-induced M2 macrophage activation. Our work provides a promising mechanism and highlights the important role of PAK1 as a promising therapeutic target for atherosclerosis management.

Data Availability

The data used to support the findings of this study are available from the corresponding author upon request.

Conflicts of Interest

The authors declare that they have no conflicts of interest.

Authors' Contributions

Wen-Lin Cheng, Quan Zhang, and Bo Li contributed equally to this work.

Acknowledgments

References

[1] A. Sica and V. Bronte, "Altered macrophage differentiation and immune dysfunction in tumor development," *The Journal of Clinical Investigation*, vol. 117, no. 5, pp. 1155–1166, 2007.

[2] S. K. Biswas and A. Mantovani, "Macrophage plasticity and interaction with lymphocyte subsets: cancer as a paradigm," *Nature Immunology*, vol. 11, no. 10, pp. 889–896, 2010.

[3] S. Gordon and F. O. Martinez, "Alternative activation of macrophages: mechanism and functions," *Immunity*, vol. 32, no. 5, pp. 593–604, 2010.

[4] A. Sica and A. Mantovani, "Macrophage plasticity and polarization: in vivo veritas," *The Journal of Clinical Investigation*, vol. 122, no. 3, pp. 787–795, 2012.

[5] N. Leitinger and I. G. Schulman, "Phenotypic polarization of macrophages in atherosclerosis," *Arteriosclerosis, Thrombosis, and Vascular Biology*, vol. 33, no. 6, pp. 1120–1126, 2013.

[6] D. Zhou, C. Huang, Z. Lin et al., "Macrophage polarization and function with emphasis on the evolving roles of coordinated regulation of cellular signaling pathways," *Cellular Signalling*, vol. 26, no. 2, pp. 192–197, 2014.

[7] I. Tabas and K. E. Bornfeldt, "Macrophage phenotype and function in different stages of atherosclerosis," *Circulation Research*, vol. 118, no. 4, pp. 653–667, 2016.

[8] L. B. Ivashkiv, "Epigenetic regulation of macrophage polarization and function," *Trends in Immunology*, vol. 34, no. 5, pp. 216–223, 2013.

[9] P. J. Murray, "Macrophage polarization," *Annual Review of Physiology*, vol. 79, no. 1, pp. 541–566, 2017.

[10] P. Libby, "Inflammation in atherosclerosis," *Nature*, vol. 420, no. 6917, pp. 868–874, 2002.

[11] J. L. Stoger, M. J. Gijbels, S. van der Velden et al., "Distribution of macrophage polarization markers in human atherosclerosis," *Atherosclerosis*, vol. 225, no. 2, pp. 461–468, 2012.

[12] I. F. Charo, "Macrophage polarization and insulin resistance: PPARγ in control," *Cell Metabolism*, vol. 6, no. 2, pp. 96–98, 2007.

[13] R. Kumar, R. Sanawar, X. Li, and F. Li, "Structure, biochemistry, and biology of PAK kinases," *Gene*, vol. 605, pp. 20–31, 2017.

[14] M. A. Sells, U. G. Knaus, S. Bagrodia, D. M. Ambrose, G. M. Bokoch, and J. Chernoff, "Human p21-activated kinase (Pak1) regulates actin organization in mammalian cells," *Current Biology*, vol. 7, no. 3, pp. 202–210, 1997.

[15] V. D. Delorme-Walker, J. R. Peterson, J. Chernoff et al., "Pak1 regulates focal adhesion strength, myosin IIA distribution, and actin dynamics to optimize cell migration," *The Journal of Cell Biology*, vol. 193, no. 7, pp. 1289–1303, 2011.

[16] M. Radu, G. Semenova, R. Kosoff, and J. Chernoff, "PAK signalling during the development and progression of cancer," *Nature Reviews. Cancer*, vol. 14, no. 1, pp. 13–25, 2014.

[17] K. Dammann, V. Khare, M. Lang et al., "PAK1 modulates a PPARgamma/NF-kappaB cascade in intestinal inflammation," *Biochimica et Biophysica Acta*, vol. 1853, pp. 2349–2360, 2015.

[18] J. Wang, Y. Zhu, J. Chen et al., "Identification of a novel PAK1 inhibitor to treat pancreatic cancer," *Acta Pharmaceutica Sinica B*, vol. 10, no. 4, pp. 603–614, 2020.

[19] Y. Wang, S. Wang, M. Lei et al., "The p21-activated kinase 1 (Pak1) signalling pathway in cardiac disease: from mechanistic study to therapeutic exploration," *British Journal of Pharmacology*, vol. 175, no. 8, pp. 1362–1374, 2018.

[20] Y. Wang, H. Tsui, Y. Ke et al., "Pak1 is required to maintain ventricular Ca(2)(+) homeostasis and electrophysiological stability through SERCA2a regulation in mice," *Circulation. Arrhythmia and Electrophysiology*, vol. 7, no. 5, pp. 938–948, 2014.

[21] W. Liu, M. Zi, R. Naumann et al., "Pak1 as a novel therapeutic target for antihypertrophic treatment in the heart," *Circulation*, vol. 124, no. 24, pp. 2702–2715, 2011.

[22] E. E. Egom, T. M. Mohamed, M. A. Mamas et al., "Activation of Pak1/Akt/eNOS signaling following sphingosine-1-phosphate release as part of a mechanism protecting cardiomyocytes against ischemic cell injury," *American Journal of Physiology. Heart and Circulatory Physiology*, vol. 301, no. 4, pp. H1487–H1495, 2011.

[23] Z. Wang, E. Oh, D. W. Clapp, J. Chernoff, and D. C. Thurmond, "Inhibition or ablation of p21-activated kinase (PAK1) disrupts glucose homeostatic mechanisms in vivo," *The Journal of Biological Chemistry*, vol. 286, no. 48, pp. 41359–41367, 2011.

[24] D. Z. Ye, S. Jin, Y. Zhuo, and J. Field, "p21-activated kinase 1 (Pak1) phosphorylates BAD directly at serine 111 in vitro and indirectly through Raf-1 at serine 112," *PLoS One*, vol. 6, no. 11, article e27637, 2011.

[25] H. Chang, K. Y. He, C. Li et al., "P21 activated kinase-1 (PAK1) in macrophages is required for promotion of Th17 cell response during helminth infection," *Journal of Cellular and Molecular Medicine*, vol. 24, no. 24, pp. 14325–14338, 2020.

[26] J. H. Kim, H. S. Choi, S. L. Kim, and D. S. Lee, "The PAK1-Stat3 signaling pathway activates IL-6 gene transcription and human breast cancer stem cell formation," *Cancers (Basel)*, vol. 11, 2019.

[27] E. Rigamonti, G. Chinetti-Gbaguidi, and B. Staels, "Regulation of macrophage functions by PPAR-α, PPAR-γ, and LXRs in mice and men," *Arteriosclerosis, Thrombosis, and Vascular Biology*, vol. 28, no. 6, pp. 1050–1059, 2008.

[28] J. S. Welch, M. Ricote, T. E. Akiyama, F. J. Gonzalez, and C. K. Glass, "PPARgamma and PPARdelta negatively regulate specific subsets of lipopolysaccharide and IFN-gamma target genes in macrophages," *Proceedings of the National Academy of Sciences of the United States of America*, vol. 100, no. 11, pp. 6712–6717, 2003.

[29] J. I. Odegaard, R. R. Ricardo-Gonzalez, M. H. Goforth et al., "Macrophage-specific PPARγ controls alternative activation and improves insulin resistance," *Nature*, vol. 447, no. 7148, pp. 1116–1120, 2007.

[30] K. J. Moore, E. D. Rosen, M. L. Fitzgerald et al., "The role of PPAR-γ in macrophage differentiation and cholesterol uptake," *Nature Medicine*, vol. 7, no. 1, pp. 41–47, 2001.

[31] F. G. Gbaguidi, G. Chinetti, D. Milosavljevic et al., "Peroxisome proliferator-activated receptor (PPAR) agonists decrease lipoprotein lipase secretion and glycated LDL uptake by human macrophages," *FEBS Letters*, vol. 512, no. 1-3, pp. 85–90, 2002.

[32] G. Haraguchi, Y. Kobayashi, M. L. Brown et al., "PPARα and PPARγ activators suppress the monocyte-macrophage apoB-48 receptor^1," *Journal of Lipid Research*, vol. 44, no. 6, pp. 1224–1231, 2003.

[33] G. Chinetti, F. G. Gbaguidi, S. Griglio et al., "CLA-1/SR-BI is expressed in atherosclerotic lesion macrophages and regulated by activators of peroxisome proliferator-activated receptors," *Circulation*, vol. 101, no. 20, pp. 2411–2417, 2000.

[34] G. Chinetti, S. Lestavel, V. Bocher et al., "PPAR-α and PPAR-γ activators induce cholesterol removal from human macrophage foam cells through stimulation of the ABCA1 pathway," *Nature Medicine*, vol. 7, no. 1, pp. 53–58, 2001.

[35] R. Galetto, M. Albajar, J. I. Polanco, M. M. Zakin, and J. C. Rodriguez-Rey, "Identification of a peroxisome-proliferator-activated-receptor response element in the apolipoprotein E gene control region," *The Biochemical Journal*, vol. 357, no. 2, pp. 521–527, 2001.

[36] G. Llaverias, M. Vazquez-Carrera, R. M. Sanchez et al., "Rosiglitazone upregulates caveolin-1 expression in THP-1 cells through a PPAR-dependent mechanism," *Journal of Lipid Research*, vol. 45, no. 11, pp. 2015–2024, 2004.

[37] C. A. Gleissner, I. Shaked, K. M. Little, and K. Ley, "CXC chemokine ligand 4 induces a unique transcriptome in monocyte-derived macrophages," *Journal of Immunology*, vol. 184, no. 9, pp. 4810–4818, 2010.

[38] A. V. Finn, M. Nakano, R. Polavarapu et al., "Hemoglobin directs macrophage differentiation and prevents foam cell formation in human atherosclerotic plaques," *Journal of the American College of Cardiology*, vol. 59, no. 2, pp. 166–177, 2012.

Research Article

Melatonin Exerts Cardioprotective Effects by Inhibiting NLRP3 Inflammasome-Induced Pyroptosis in Mice following Myocardial Infarction

Lianghe Wen ⓘ,[1] **Minnan Wang ⓘ,**[2] **Peiyao Luo ⓘ,**[3] **Xianglin Meng ⓘ,**[3] **and Mingyan Zhao ⓘ**[3]

[1]*Department of Critical Care Medicine, The Second Affiliated Hospital of Harbin Medical University, No. 246 Xuefu Road, Harbin, 150086 Heilongjiang Province, China*

[2]*Department of Endocrinology and Metabolism, The Second Affiliated Hospital of Harbin Medical University, No. 246 Xuefu Road, Harbin, 150086 Heilongjiang Province, China*

[3]*Department of Critical Care Medicine, The First Affiliated Hospital of Harbin Medical University, No. 23 Youzheng Street, Harbin, 150001 Heilongjiang Province, China*

Correspondence should be addressed to Mingyan Zhao; zhaomingyan2020@163.com

Myocardial infarction- (MI-) induced myocardial damage is mainly attributed to the loss of cardiomyocytes. Pyroptosis is a newly recognized form of programmed cell necrosis that is associated with the progression of MI. Melatonin has been shown to exert cardioprotective effects against cardiac damage in multiple cardiovascular diseases. However, the effect of melatonin on pyroptosis-induced cardiac injury in MI has not been elucidated. Herein, we found that melatonin administration ameliorated cardiac dysfunction and reduced cardiomyocyte death both in mice following coronary artery ligation and in H9C2 cells exposed to hypoxia. The results also showed that pyroptosis was induced both *in vivo* and *in vitro*, as evidenced by increased NLRP3, cleaved caspase-1, GSDMD-N, and mature IL-1β and IL-18 levels, and these changes were decreased by melatonin treatment. Furthermore, we observed that TLR4 and NF-κB levels were increased by MI or hypoxia, and these increases were reversed by melatonin. The antipyroptotic action of melatonin was abrogated by treatment with an agonist of the TLR4/NF-κB signaling pathway. Our results indicate that melatonin can exert cardioprotective effects by inhibiting NLRP3 inflammasome-induced pyroptosis through modulation of the TLR4/NF-κB signaling pathway and provide strong evidence for the utility of melatonin in the treatment of MI.

1. Introduction

Myocardial infarction (MI) is a leading cause of morbidity and mortality worldwide. It is widely acknowledged that MI can deteriorate left ventricle cardiomyocytes and aggravate cardiac remodeling, eventually resulting in heart failure [1–3]. Cardiomyocyte death occurs at the onset of MI and ultimately contributes to myocardial damage [4, 5]. Although reperfusion therapy is an effective strategy to reduce infarct size, it also potentiates myocardial damage, known as ischemia-reperfusion injury [6, 7]. Thus, the identification of effective and innovative therapies for reducing cardiomyocyte loss may play a critical role in the treatment of MI.

Pyroptosis is a type of programmed cell necrosis mediated by the gasdermin family. Inflammasomes, which are multiprotein complexes, are activated under distinct pathological stimuli and subsequently trigger the activation of caspase-1. On the one hand, active caspase-1 contributes to pyroptosis by cleaving gasdermin D (GSDMD) to produce an N-terminal fragment of GSDMD (GSDMD-N), which is widely considered a pyroptosis executor. On the other hand, active caspase-1 also leads to an inflammatory response by

inducing interleukin (IL)-1β or IL-18 maturation [8–11]. Recent studies have demonstrated that pyroptosis is involved in cardiomyocyte loss induced by MI [12, 13]. The nucleotide-binding oligomerization domain-like receptor family pyrin domain-containing 3 (NLRP3) inflammasome, one of the best-known inflammasomes, was found to be activated upon MI and to induce cardiomyocyte pyroptosis by triggering caspase-1 and cleaved GSDMD [14, 15]. However, inhibition of the NLRP3 inflammasome by MCC950 significantly reduced infarct size and improved cardiac remodeling [16]. Inhibition of pyroptosis could ameliorate the damage to cardiomyocytes caused by MI [17]. These studies indicate that targeting NLRP3 inflammasome-mediated pyroptosis may be an effective strategy for reducing MI-induced myocardial injury.

The neuroendocrine hormone melatonin has multiple effects, including regulating circadian rhythm and immunity; influencing sleep; delaying aging via effects against oxidation, apoptosis, fibrosis, and autophagy; and protecting against mitochondria and endoplasmic reticulum stress [18]. It has been widely demonstrated that melatonin has a cardioprotective effect in MI [19]. For example, melatonin can ameliorate cardiac remodeling by activating the Notch1/Mfn2 pathway in the hearts of mice following MI [20]. Melatonin exerts anti-inflammatory activity by inhibiting the release of inflammatory cytokines, including IL-1β, IL-18, TNF-α, C-reactive protein, Nrf2, and IL-1α, during the development of MI [21, 22]. However, whether melatonin can regulate cardiomyocyte pyroptosis in MI remains unclear.

The aim of this study was to evaluate the possible effect of melatonin on cardiomyocyte pyroptosis in MI and to further identify the underlying molecular mechanisms. Our results demonstrated that melatonin alleviated cardiomyocyte loss by inhibiting NLRP3 inflammasome-mediated pyroptosis by modulating the Toll-like receptor 4 (TLR4)/NF-κB signaling pathway and further clarified that melatonin may be a promising agent for MI treatment.

2. Methods and Materials

2.1. Animals.
Male C57BL/6 mice (weighing 20 ± 2 g) were obtained from The Second Affiliated Hospital of Harbin Medical University. This study was approved by the Animal Protection and Use Committee of Harbin Medical University and was performed in line with the recommendations in the Guide for the Care and Use of Laboratory Animals issued by the National Institutes of Health.

2.2. MI Model and Drug Treatment.
The mice were randomly divided into three groups: the sham group ($n = 12$), the MI group (MI, $n = 12$), and the melatonin treatment group (MI+MLT, $n = 12$). The MI model was generated with a method similar to that in previous studies [23, 24]. Briefly, the mice were anaesthetized by avertin (0.2 g/kg) injection. The left anterior descending coronary artery was exposed and ligated with a 7-0 nylon suture for 24 h. The mice in the sham group underwent the same surgical procedures without coronary artery ligation. The mice in the MI+MLT group were administered 10 mg/kg melatonin (M5250, Sigma-Aldrich) per day by intragastric gavage for 14 days

prior to MI surgery [25]. The mice in the sham and MI groups were given an equivalent volume of ddH$_2$O.

2.3. Echocardiography.
Cardiac function was detected by using an ultrasound system (VisualSonics, Toronto, ON, Canada) after MI for twenty-four hours. The mice were anaesthetized by avertin injection and fixed onto a flat plate. After exposing the chest, left ventricular systolic diameter (LVDs), left ventricular diastolic diameter (LVDd), left ventricular ejection fraction (EF), and left ventricular fractional shortening (FS) were detected and analyzed.

2.4. Western Blot Assay.
Tissues or cells were fully dissolved in RIPA buffer (P0013B, Beyotime, China) containing protease inhibitor (4693159001, Roche, Germany) and phosphatase inhibitor (4906837001, Roche, Germany). Sample were separated by SDS-PAGE gel and then transferred onto a nitrocellulose membrane. After the membranes were blocked with 5% nonfat milk, they were incubated at 4°C overnight with the following antibodies: NLRP3 (1 : 500, bs-10021R, Bioss), cleaved caspase-1 (1 : 200, ab207802, Abcam), GSDMD-N (1 : 200, ab215203, Abcam, USA), TLR4 (1 : 200, sc-293072, Santa Cruz Biotechnology), NF-κB (p-65, 1 : 200, sc-8008, Santa Cruz Biotechnology), IL-1β (1 : 200, ab254360, Abcam), IL-18 (1 : 100, ab207324, Abcam), and β-actin (1 : 2000, TA-09, ZSGB). Then, the secondary antibody was added, and the membrane was incubated at room temperature. After a washing step, the gray values were evaluated by Quantity One software and subjected to statistical analysis.

2.5. Real-Time PCR Assay.
Cells and tissues were fully lysed with TRIzol (15596026, Invitrogen, USA) according to manufacturer's instructions. The RNA concentration was determined by a NanoDrop instrument. A reverse transcription kit (FSQ-101, Toyobo) was used to synthesize cDNA. Real-time PCR was performed using an ABI 7500 Fast PCR instrument with the SYBR Green Real-time PCR Master Kit (QPK-201, Toyobo). The primer sequences were as follows: NLRP3 (forward: 5$'$-CAACCTCACGTCACAC TGCT-3$'$; reverse: 5$'$-TTTCAGACAACCCCAGGTTC-3$'$), caspase-1 (forward: 5$'$-ACACGTCTTGCCCTCATTATCT-3$'$; reverse: 5$'$-ATAACCTTGGGCTTGTCTTTCA-3$'$), and GAPDH (forward: 5$'$-AAGAAGGTGGTGAAGCAGGC-3$'$; reverse: 5$'$-TCCACCACCCAGTTGCTGTA-3$'$). GAPDH was used to normalize target expression levels. RNA expression levels were computed by the $2^{-\triangle\triangle CT}$ method.

2.6. Cell Culture, Drug Treatment, and Hypoxic Conditions.
H9C2 cells were purchased from American Type Culture Collection (Manassas, USA) and cultured in Dulbecco's modified Eagle's medium (DMEM, SH30022.01, HyClone) supplemented with 10% fetal calf serum and 1% penicillin-streptomycin in an incubator (5% CO$_2$, 95% O$_2$, 37°C). When the cell density reached 70-80%, the cells were moved into a hypoxic chamber (95% N$_2$, 5% O$_2$, 37°C) and incubated for 120 min with or without melatonin (10 μM, M5250, Sigma-Aldrich) [26].
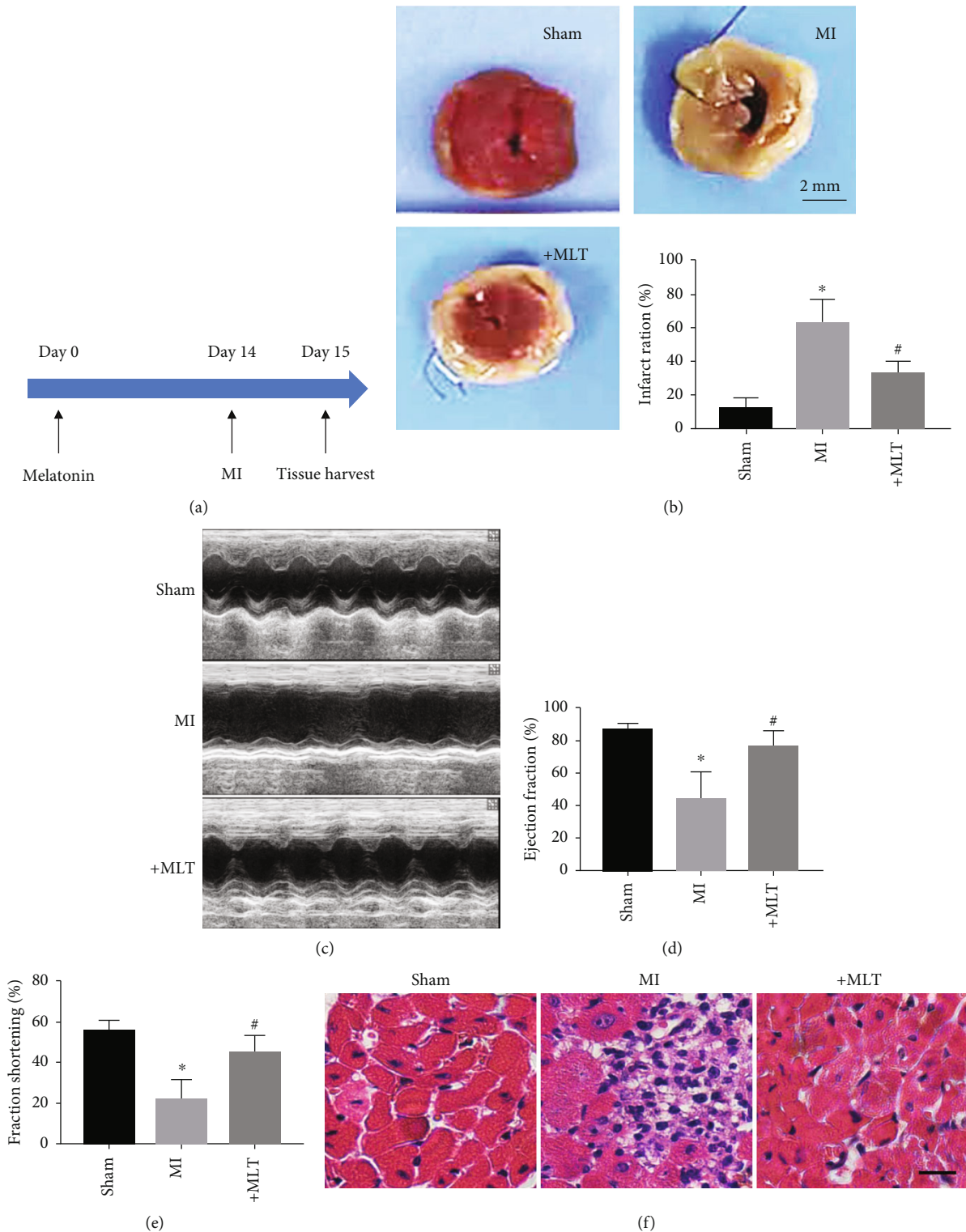
Figure 1: Cardiac injury was reversed by melatonin treatment in MI mice. (a) Diagram of the experimental protocol. (b) Representative LV sections stained with TTC and statistical analysis of infarct area data in mice. The infarct region is labeled in white. $^*P < 0.05$ vs. sham, $^#P < 0.05$ vs. MI. Number of trials = 5-6. (c) Representative echocardiography images from different groups. (d, e) Statistical analysis of echocardiographic EF% and FS% data in MI mice treated with or without melatonin. $^*P < 0.05$ vs. sham, $^#P < 0.05$ vs. MI. Number of trials = 6. (f) Representative images of H&E staining of the mouse heart. Scale bar, 20 μm. MI: myocardial infarction; MLT: melatonin.

(a)

(b)

(c)

(d)

(e)

(f)

FIGURE 2: Continued.

(g)

(h)

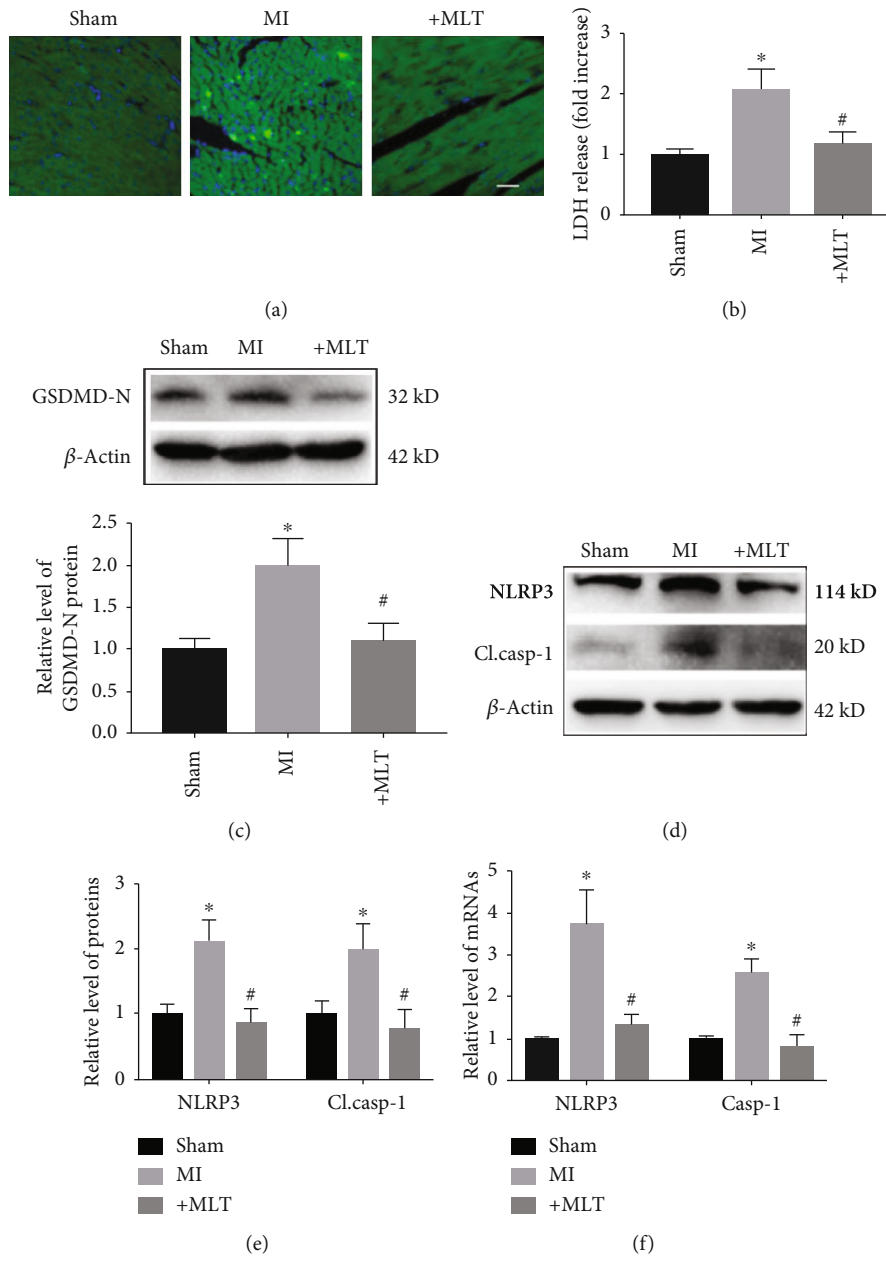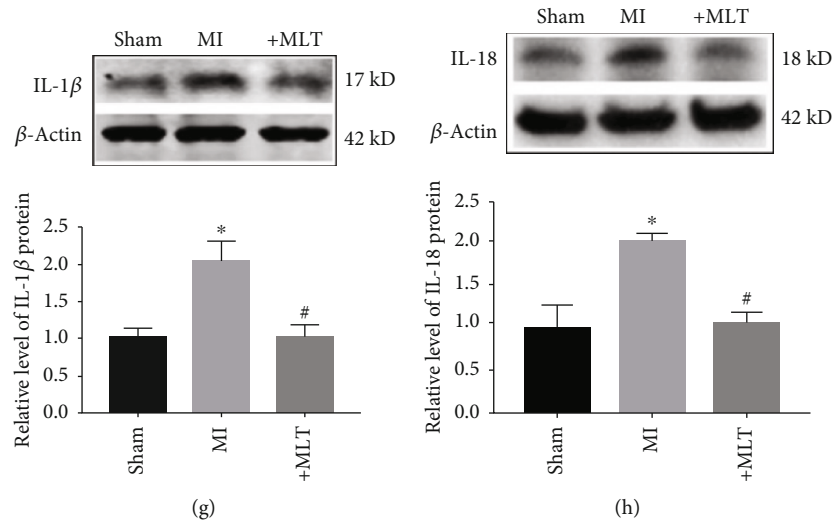Figure 2: Effect of melatonin on NLRP3 inflammasome-mediated cardiac pyroptosis in MI mice. (a) Representative images from TUNEL staining in different groups. Scale bar, 20 μm. (b) Melatonin treatment decreased the release of LDH in MI mice. $*P < 0.05$ vs. sham, $^{\#}P < 0.05$ vs. MI. Number of trials = 6. (c) The level of GSDMD-N was decreased by melatonin treatment. $*P < 0.05$ vs. sham, $^{\#}P < 0.05$ vs. MI. Number of trials = 5. (d, e) Melatonin treatment reduced the levels of NLRP3 and cl.casp-1 in the hearts of MI mice. $*P < 0.05$ vs. sham, $^{\#}P < 0.05$ vs. MI. Number of trials = 5-6. (f) The mRNA levels of NLRP3 and caspase-1 in the different groups were detected by real-time PCR. $*P < 0.05$ vs. sham, $^{\#}P < 0.05$ vs. MI. Number of trials = 6. (g, h) The levels of IL-1β and IL-18 in heart tissue from different groups. $*P < 0.05$ vs. sham, $^{\#}P < 0.05$ vs MI. Number of trials = 4-5. MI: myocardial infarction; cl.casp-1: cleaved caspase-1; MLT: melatonin.

2.7. Immunofluorescence Staining. Treated or untreated H9C2 cells were fixed with 4% paraformaldehyde. After a blocking step, anti-NLRP3 (1 : 100, bs-10021R, Bioss) or anti-TLR4 (1 : 100, sc-293072, Santa Cruz Biotechnology) was added, and the cells were incubated at 4°C overnight. Then, secondary antibody conjugated to Alexa Fluor 488 (A11034, Invitrogen) was added for 1 h at room temperature. Finally, the nucleus was stained with 4′,6-diamino-2-phenylindole (DAPI, C0065, Solarbio). All images were acquired under a fluorescence microscope (Nikon 80i, Japan).

2.8. Immunohistochemical Staining. The heart tissues were removed, fixed, and embedded in paraffin. After a blocking step, a primary anti-TLR4 antibody (1 : 100, sc-293072, Santa Cruz Biotechnology) was added, and the tissues were incubated overnight at 4°C. The next day, the secondary antibody was added for 20 min at room temperature. The images were captured by a microscope (Zeiss, Germany).

2.9. Calcein AM/EthD-III Staining. Calcein AM/EthD-III staining was performed according to manufacturer's instructions (30002, Biotium, USA). Briefly, untreated and treated H9C2 cells were washed three times with PBS, and then, 200 μL of calcein-AM/EthD-III staining solution was added. After incubation for 40 min, images of the cells were captured by using a fluorescence microscope (Nikon 80i, Japan).

2.10. Lactate Dehydrogenase (LDH) Release Assay. The supernatants from different groups were collected, and LDH was detected using an LDH assay kit (A020-2-2, Nanjingjiancheng, China) according to manufacturer's instructions. A

microplate reader was used to analyze the absorbance value of each sample at 450 nm.

2.11. Hematoxylin and Eosin (HE) Staining. Heart tissues were fixed and embedded in paraffin. After cutting the paraffin tissue blocks into 5 μm thick sections, HE staining was performed by using an HE kit (G1120, Solarbio) according to manufacturer's instructions. Images were collected under a microscope (Zeiss, Germany).

2.12. TUNEL Staining. Heart tissues from different groups were embedded in paraffin and then cut into 5 μm sections. The In Situ Cell Death Detection Kit (11684817910, Roche, Germany) was used to detect cell death following manufacturer's instructions with some modifications. After deparaffinization, the TUNEL reaction mixture was added to the paraffin sections, which were then incubated for 1 h at 37°C. The nuclei were stained with DAPI (C0065, Solarbio) for 15 min at room temperature. Fluorescence microscopy was used to capture the images (Nikon 80i, Japan).

2.13. Statistical Analysis. The data are presented as the mean ± SEM. One-way ANOVA was used to compare the differences between groups with SPSS 22.0 software. $P < 0.05$ was considered to indicate statistical significance.

3. Results

3.1. Melatonin Alleviates Cardiac Injury in MI Mice. To determine whether melatonin has cardioprotective effects after MI, we established a mouse model of MI and pretreated the mice with melatonin for 14 days prior to coronary artery ligation (Figure 1(a)). TTC staining was used to measure the
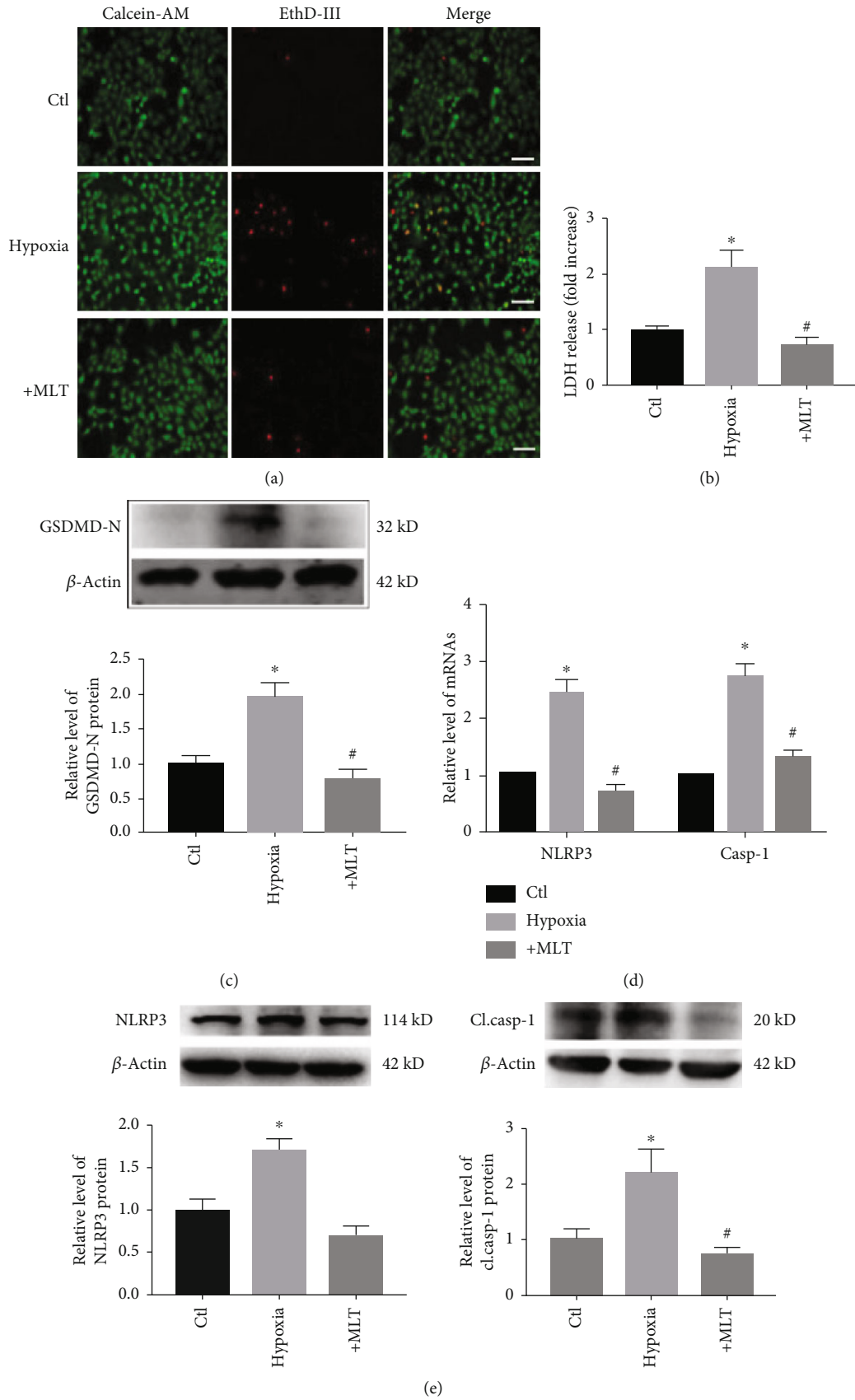
(a)

(b)

(c)

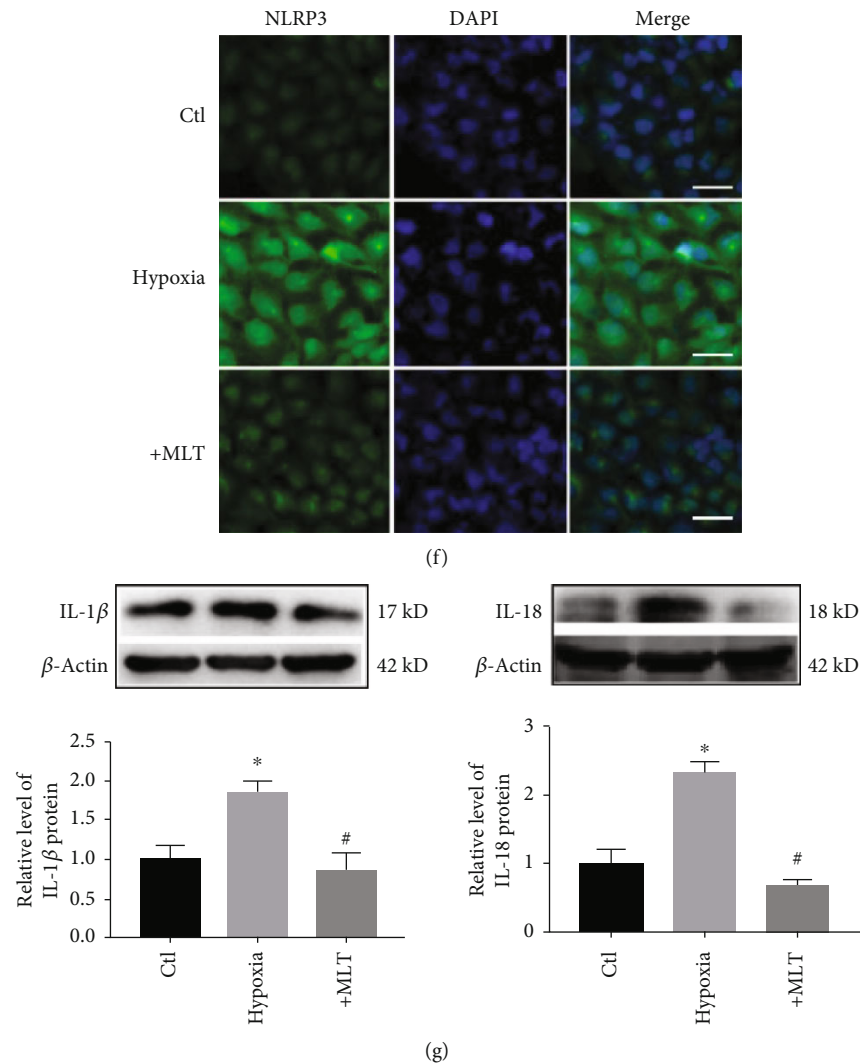
(d)

(e)

Figure 3: Continued.

(f)

(g)

FIGURE 3: Effect of melatonin on NLRP3 inflammasome-mediated cardiac pyroptosis in H9C2 cells exposed to hypoxia. (a) Melatonin reduced hypoxia-induced cardiomyocyte loss. Live cells were stained with calcein-AM (green), and dead cells were stained with EthD-III (red). Scale bar, 40 μm. (b) Melatonin treatment decreased the release of LDH in H9C2 cells. $^*P < 0.05$ vs. ctl, $^\#P < 0.05$ vs. hypoxia. Number of trials = 3. (c) GSDMD-N levels were decreased by melatonin treatment. $^*P < 0.05$ vs. ctl, $^\#P < 0.05$. Number of trials = 3. (d) The mRNA levels of NLRP3 and caspase-1 in the different groups were detected by real-time PCR. $^*P < 0.05$ vs. ctl, $^\#P < 0.05$. Number of trials = 3. (e) Melatonin treatment reduced the levels of NLRP3 and cl.casp-1 in hypoxia-treated H9C2 cells. $^*P < 0.05$ vs. ctl, $^\#P < 0.05$ vs. hypoxia. Number of trials = 3. (f) NLRP3 levels were detected by immunofluorescence. Scale bar, 50 μm. (g) The levels of IL-1β and IL-18 were decreased by melatonin in H9C2 cells. $^*P < 0.05$ vs. ctl, $^\#P < 0.05$ vs. hypoxia. Number of trials = 3. cl.casp-1: cleaved caspase-1; MLT: melatonin.

infarct area 24 h after MI. The infarct area was markedly increased in the MI group compared with the sham group, while melatonin administration significantly decreased the infarct area induced by MI (Figure 1(b)). As shown in Figures 1(c)–1(e), the echocardiographic data showed that the EF and FS values were significantly lower in MI mice than in sham mice, suggesting that cardiac damage was induced by MI in mice. Notably, the EF and FS values were both effectively restored by melatonin administration in MI mice. Additionally, the melatonin-treatment group had reduced infiltration of inflammatory cells compared with the MI group (Figure 1(f)).

3.2. Melatonin Attenuates NLRP3 Inflammasome-Mediated Cardiac Pyroptosis in MI Mice. Previous studies have demonstrated that pyroptosis contributes to cardiomyocyte loss in the development of MI [27, 28]. Therefore, we next determined whether the cardioprotective effect of melatonin in the hearts of MI mice was associated with pyroptosis. TUNEL staining showed that melatonin treatment reversed the MI-induced cardiomyocyte loss (Figure 2(a)). Moreover, LDH levels were significantly increased in the serum of MI mice, suggesting that the plasma membrane was ruptured. Importantly, melatonin administration decreased LDH levels (Figure 2(b)). As shown in Figure 2(c), the level of GSDMD-

(a)

(b)

(c)

Figure 4: Continued.

(d)

(e)
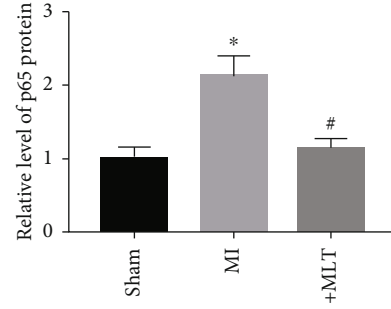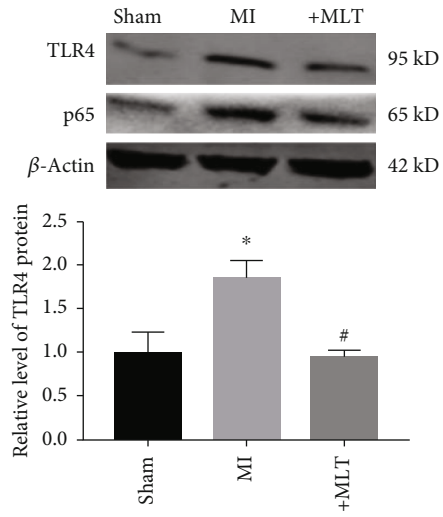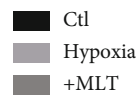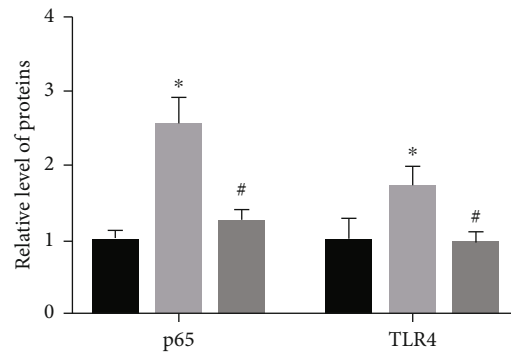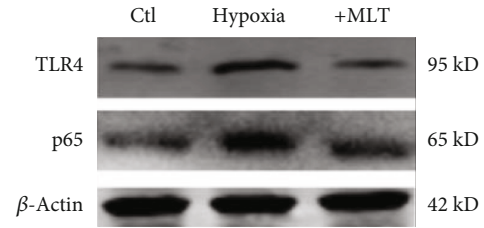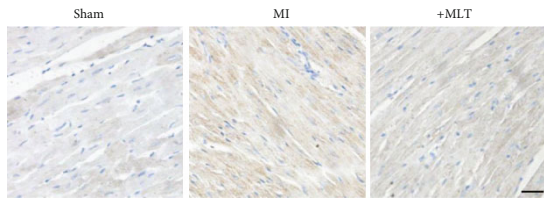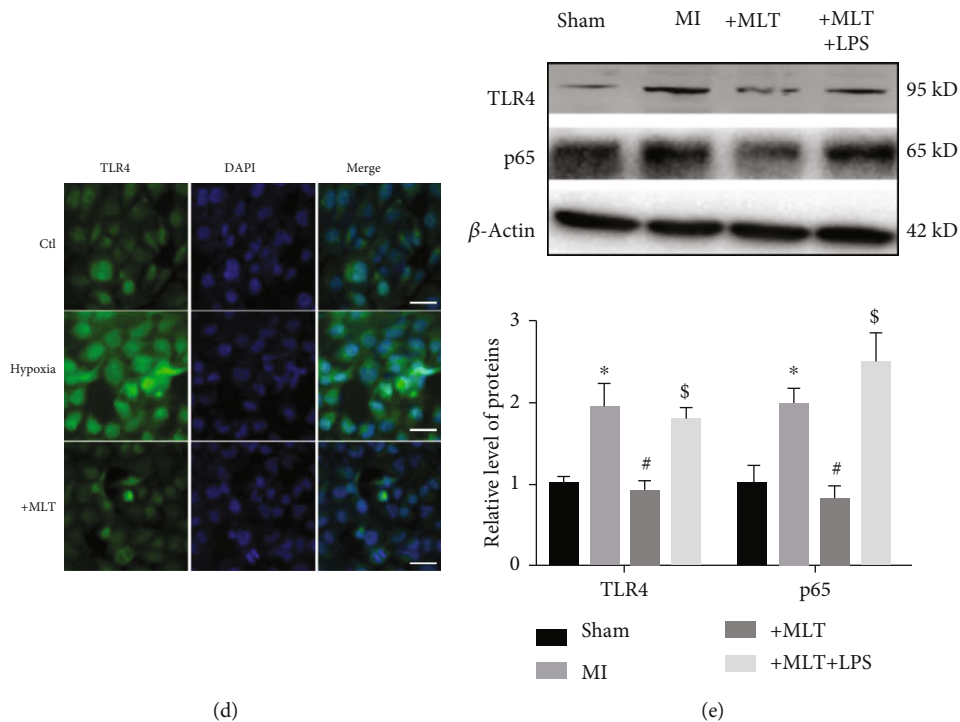
FIGURE 4: Effect of melatonin on the TLR4/NF-κB signaling pathway both *in vivo* and *in vitro*. (a) Melatonin treatment reduced the levels of TLR4 and p65 in the hearts of MI mice. $^*P < 0.05$ vs. sham, $^#P < 0.05$ vs. MI. Number of trials = 4. (b) Representative staining of TLR4 by immunohistochemistry. Scale bar, 20 μm. (c) The levels of TLR4 and p65 were decreased in H9C2 cells by melatonin treatment. $^*P < 0.05$ vs. ctl, $^#P < 0.05$ vs. hypoxia. Number of trials = 3. (d) TLR4 levels were detected by immunofluorescence. Scale bar, 50 μm. (e) The protein levels of TLR4 and p65 in the hearts of MI mice with or without LPS treatment (2 mg/kg). $^*P < 0.05$ vs. sham, $^#P < 0.05$ vs. MI, $^$P < 0.05$ vs. MLT. Number of trials = 4. MLT: melatonin.

N, a pyroptosis executor, was significantly increased in the hearts of MI mice compared with sham mice; however, this increase was reversed by melatonin treatment. These data suggest that melatonin can inhibit pyroptotic cardiomyocyte death induced by MI.

The NLRP3 inflammasome has been shown to be involved in cell death by inducing pyroptosis, and inhibition of the NLRP3 inflammasome exerts protective effects in various diseases [29–31]. To ascertain whether the antipyroptotic effect of melatonin in MI is associated with the NLRP3 inflammasome, we detected changes in this large multiprotein complex. In this study, we found that the protein and mRNA levels of NLRP3 and cleaved caspase-1 were decreased in the MI+MLT group compared with the MI group (Figures 2(d)–2(f)). Caspase-1 activation is known to lead to cardiac damage by inducing the maturation of IL-1β or IL-18. Thus, we also detected the effect of melatonin on IL-1β and IL-18 in heart tissue. As shown in Figures 2(g) and 2(h), the protein levels of IL-1β and IL-18 were increased by MI but were reduced by melatonin administration.

3.3. Melatonin Inhibits NLRP3 Inflammasome-Mediated Cardiac Pyroptosis In Vitro.

Next, we aimed to determine whether melatonin can attenuate NLRP3 inflammasome-mediated cardiac pyroptosis *in vitro*. Hypoxia plays a critical role in the onset of MI; thus, we established an *in vitro*

model of hypoxia in H9C2 cardiac cells to mimic MI conditions. We found that melatonin significantly decreased hypoxia-induced cardiac cell death, as detected by EthD-III staining (Figure 3(a)). Moreover, LDH levels were significantly increased in cardiac cells exposed to hypoxia and were decreased by melatonin administration (Figure 3(b)). As shown in Figure 3(c), the level of GSDMD-N was significantly increased after hypoxia exposure compared with the control; however, this increase was reversed by melatonin treatment. In addition, the levels of NLRP3 and cleaved caspase-1 were increased in cardiac cells after hypoxia exposure and were significantly decreased by melatonin treatment (Figures 3(d) and 3(e)). A similar change in NLRP3 was observed by immunofluorescence (Figure 3(f)). We also detected the effect of melatonin on IL-1β and IL-18 in H9C2 cells exposed to hypoxia. As shown in Figure 3(g), the protein levels of IL-1β and IL-18 were increased by hypoxia and reduced by melatonin administration.

3.4. Melatonin Attenuates NLRP3 Inflammasome-Mediated Pyroptosis by Inhibiting the TLR4/NF-κB Signaling Pathway Both In Vivo and In Vitro.

Previous studies have demonstrated that the Toll-like receptor 4 (TLR4)/nuclear factor-κB (NF-κB) signaling pathway not only plays a critical role in MI-induced myocardial inflammation but also is involved in the NLRP3 inflammasome-mediated inflammatory response [32, 33]. Therefore, we investigated whether the
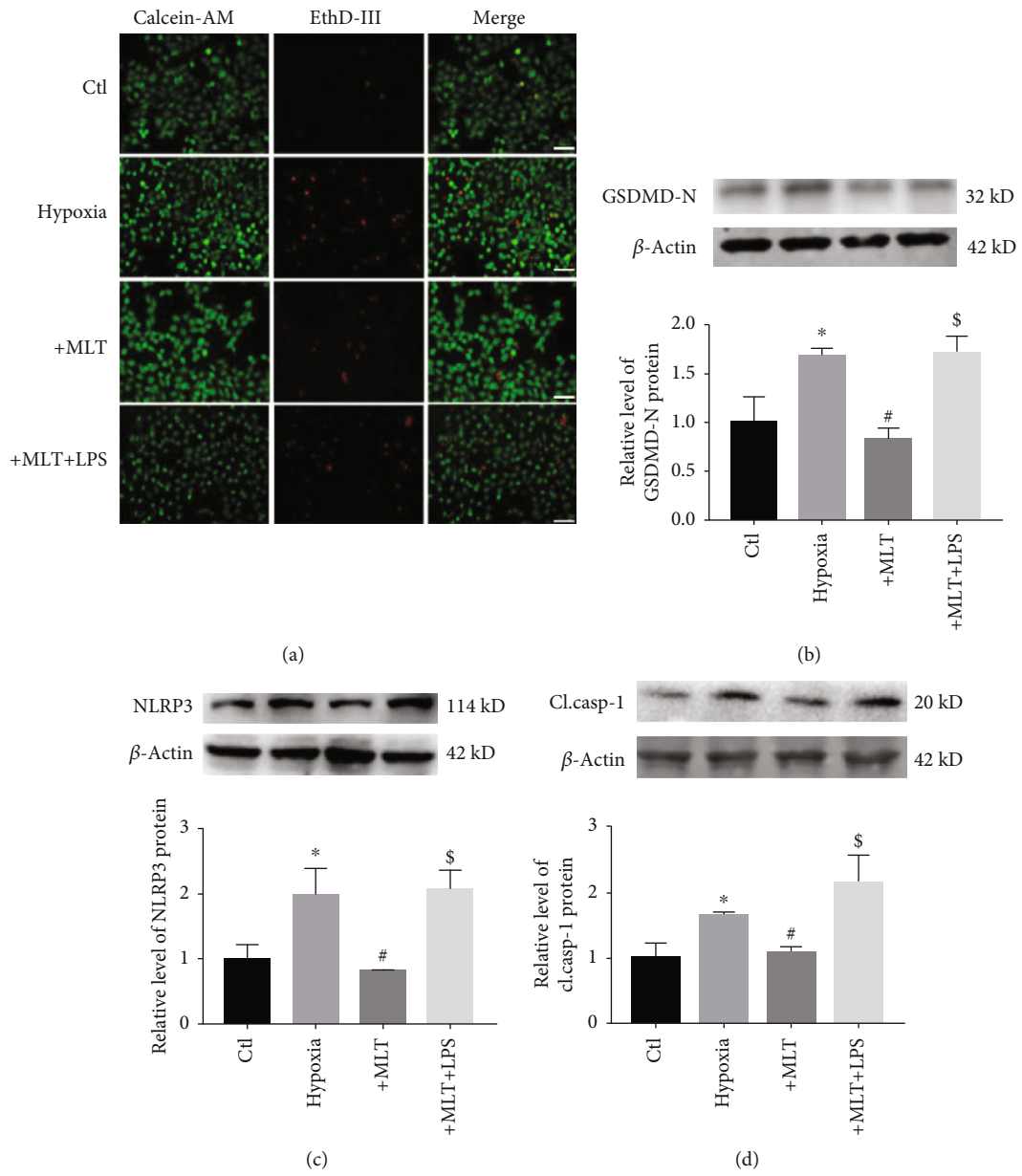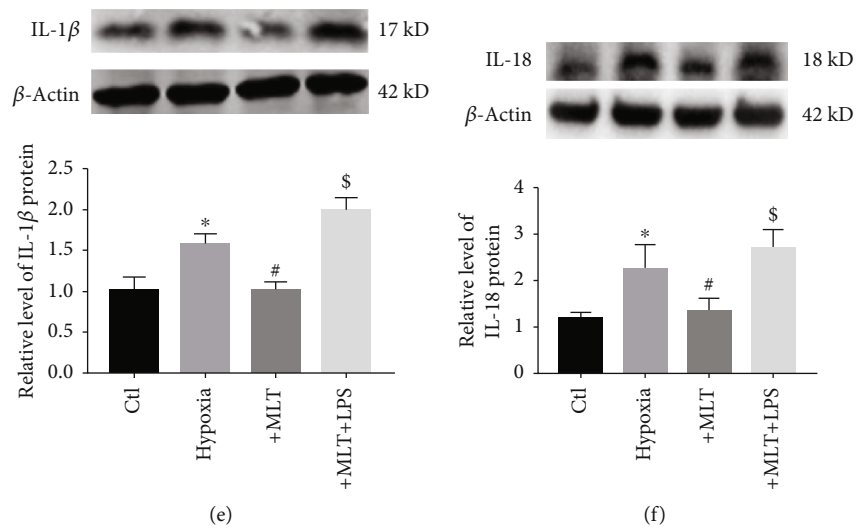
(a)

(b)

(c)

(d)

FIGURE 5: Continued.

(e)

(f)

Figure 5: Effect of melatonin on NLRP3 inflammasome-mediated pyroptosis through inhibition of the TLR4/NF-κB signaling pathway. (a) LPS (1 μg/mL) blocked the effect of melatonin on H9C2 cardiomyocyte cell death. Live cells were stained with calcein-AM (green), and dead cells were stained with EthD-III (red). Scale bar, 40 μm. (b–f) Representative images and statistical analysis of GSDMD-N (b), NLRP3 (c), and cl.casp-1 (d), mature IL-1β (e), and mature IL-18 (f) data from different groups. $^*P < 0.05$ vs. ctl, $^#P < 0.05$ vs. hypoxia, $^\$P < 0.05$ vs. MLT. Number of trials = 3. MLT: melatonin.

antipyroptotic effect of melatonin in MI is associated with the TLR4/NF-κB signaling pathway. As shown in Figures 4(a) and 4(b), the protein levels of TLR4 and NF-κB (p-65) were increased in the hearts of mice following MI, and these increases were reversed by melatonin treatment. Consistent with the *in vivo* data, hypoxia also induced increases in TLR4 and p-65 levels in H9C2 cells, and melatonin administration significantly downregulated these hypoxia-induced increases (Figure 4(c)). A similar change in TLR4 was observed by immunofluorescence assay (Figure 4(d)). Lipopolysaccharide (LPS) is a common agonist of the TLR4/NF-κB signaling pathway [34, 35]. Interestingly, we found that the effect of melatonin on the TLR4/NF-κB signaling pathway was blocked by LPS (Figure 4(e)).

We also found that LPS treatment abrogated the ability of melatonin to reduce hypoxia-induced cardiomyocyte loss (Figure 5(a)). Importantly, as shown in Figures 5(b)–5(f), the antipyroptotic effect of melatonin was blocked by LPS treatment, as evidenced by decreased GSDMD-N, NLRP3, cleaved caspase-1, and mature IL-1β and IL-18 levels in H9C2 cells exposed to hypoxia. These data suggest that melatonin, at least in part, attenuates NLRP3 inflammasome-mediated pyroptosis by inhibiting the TLR4/NF-κB signaling pathway.

4. Discussion

In the present study, we observed that melatonin ameliorated cardiac damage in an MI mouse model and hypoxia-induced cardiomyocyte injury in H9C2 cells. We also demonstrated that melatonin exerted cardioprotective effects by inhibiting cardiomyocyte death induced by NLRP3 inflammasome-mediated pyroptosis at the cellular level. The antipyroptotic effect of melatonin can likely be attributed to suppression of the TLR4/NF-κB signaling

pathway. These findings provide further support for melatonin as an effective agent for MI treatment.

MI-induced cardiac damage is a major cause of death worldwide and is mainly attributed to cardiomyocyte loss. Because cardiomyocytes have little potential for division, preventing cardiac cell death is considered an effective therapy for the treatment of MI. Numerous studies have found that myocardial inflammation is an important factor for cardiac dysfunction in MI progression [36, 37]. Inhibiting the inflammatory response is a potential strategy to reduce the loss of cardiomyocytes during MI [38–40]. Pyroptosis is inflammation-related cell death that has been shown to be involved in cardiomyocyte loss in cardiovascular disorders, such as MI and ischemia/reperfusion injury [41, 42]. Similar to previous studies, our present study found that the level of GSDMD-N, a pyroptosis executor, was significantly increased in the hearts of MI mice and in hypoxia-treated H9C2 cardiac cells. Moreover, the LDH assay data showed that MI induced marked pyroptosis-related morphological changes. However, strategies for preventing the loss of cardiomyocytes induced by pyroptosis in the progression of MI remain unclear.

Melatonin is a neuroendocrine hormone secreted by the pineal gland. Numerous studies have demonstrated that melatonin has beneficial effects in cardiovascular disorders, including MI, ischemia/reperfusion injury, atherosclerosis, heart failure, and hypertension [43, 44]. Similar to the results of previous studies, we found that melatonin administration significantly ameliorated cardiac dysfunction by normalizing the EF and FS values and reducing the number of inflammatory cells in the hearts of MI mice. Therefore, we next considered the mechanism by which melatonin prevents cardiac dysfunction. Previous studies have demonstrated that the underlying mechanisms of the cardioprotective effects of melatonin in MI are related to its abilities to inhibit

the inflammatory response, decrease oxidative stress, maintain mitochondrial function, reduce cardiomyocyte apoptosis, and regulate receptor or nonreceptor signaling pathways (such as the MAPK/ERK, AMPK, PI3K/Akt, SAFE, and Notch pathways) [45–47]. However, whether the cardioprotective role of melatonin in MI is related to cardiac pyroptosis inhibition has not yet been proven. The results herein show that melatonin can significantly inhibit cardiac pyroptosis, as shown by the decreased GSDMD-N levels in both the hearts of MI mice and H9C2 cells exposed to hypoxia. Meanwhile, the levels of NLRP3, cleaved caspase-1, and mature IL-1β and IL-18 were markedly reduced by melatonin treatment both *in vivo* and *in vitro*. These data are the first to show that melatonin could prevent cardiac injury in part by inhibiting NLRP3 inflammasome-mediated cardiac pyroptosis.

TLR4, the first characterized mammalian Toll-like receptor, is widely accepted to play an important role in facilitating inflammatory responses during cardiovascular disease [48, 49]. For instance, TLR4 and its downstream gene NF-κB were induced in the hearts of mice following MI [50]. Treatment with siRNA against TLR4 or a TLR4 inhibitor significantly reduced infarct size and restored cardiac function in MI mice [51]. The cardiomyocyte injury induced by hypoxia was inhibited by silencing TLR4 [52]. Moreover, the TLR4/NF-κB signaling pathway has been shown to function upstream of the NLRP3 inflammasome during MI [53, 54]. However, whether the beneficial effect of melatonin on NLRP3 inflammasome-mediated pyroptosis is associated with the TLR4/NF-κB signaling pathway in MI is still unclear. As predicted, we found that the activation of TLR4 and NF-κB (p-65) in MI was inhibited by melatonin both *in vivo* and *in vitro*, whereas administration of LPS, an agonist of the TLR4/NF-κB signaling pathway, abrogated the beneficial effect of melatonin on cardiac pyroptosis.

5. Conclusion

Taken together, our present study provides strong evidence that melatonin modulates MI-associated NLRP3 inflammasome-mediated cardiac pyroptosis by affecting the TLR4/NF-κB signaling pathway, suggesting its utility in the treatment of MI.

Data Availability

The data used to support the findings of this study are available from the corresponding author upon rational request.

Conflicts of Interest

The authors declare no competing interests.

Authors' Contributions

Z. MY and W. LH contributed to the study design and article preparation. W. LH, W. MN, and L. PY performed the *in vivo* experiments. W. LH, W. MN, and M. XL were responsible for the *in vitro* experiments.

References

[1] J. L. Anderson and D. A. Morrow, "Acute myocardial infarction," *The New England Journal of Medicine*, vol. 376, no. 21, pp. 2053–2064, 2017.

[2] R. W. Yeh, S. Sidney, M. Chandra, M. Sorel, J. V. Selby, and A. S. Go, "Population trends in the incidence and outcomes of acute myocardial infarction," *The New England Journal of Medicine*, vol. 362, no. 23, pp. 2155–2165, 2010.

[3] E. J. Benjamin, P. Muntner, A. Alonso et al., "Heart disease and stroke statistics-2019 update: a report from the American Heart Association," *Circulation*, vol. 139, no. 10, pp. e56–e528, 2019.

[4] C. Yoshimura, A. Nagasaka, H. Kurose, and M. Nakaya, "Efferocytosis during myocardial infarction," *Journal of Biochemistry*, vol. 168, no. 1, pp. 1–6, 2020.

[5] P. Patel and J. Karch, "Regulation of cell death in the cardiovascular system," in *International Review of Cell and Molecular Biology 353*, pp. 153–209, Elsevier, 2020.

[6] D. J. Hausenloy and D. M. Yellon, "Myocardial ischemia-reperfusion injury: a neglected therapeutic target," *The Journal of Clinical Investigation*, vol. 123, no. 1, pp. 92–100, 2013.

[7] D. Garcia-Dorado, M. Ruiz-Meana, J. Inserte, A. Rodriguez-Sinovas, and H. M. Piper, "Calcium-mediated cell death during myocardial reperfusion," *Cardiovascular Research*, vol. 94, no. 2, pp. 168–180, 2012.

[8] H. Che, H. Li, Y. Li et al., "Melatonin exerts neuroprotective effects by inhibiting neuronal pyroptosis and autophagy in STZ-induced diabetic mice," *The FASEB Journal*, vol. 34, no. 10, pp. 14042–14054, 2020.

[9] P. Broz, P. Pelegrin, and F. Shao, "The gasdermins, a protein family executing cell death and inflammation," *Nature Reviews. Immunology*, vol. 20, no. 3, pp. 143–157, 2020.

[10] X. Liu, Z. Zhang, J. Ruan et al., "Inflammasome-activated gasdermin D causes pyroptosis by forming membrane pores," *Nature*, vol. 535, no. 7610, pp. 153–158, 2016.

[11] H. Liu, Z. Chen, X. Weng et al., "Enhancer of zeste homolog 2 modulates oxidative stress-mediated pyroptosis in vitro and in a mouse kidney ischemia-reperfusion injury model," *The FASEB Journal*, vol. 34, no. 1, pp. 835–852, 2020.

[12] E. Mezzaroma, S. Toldo, D. Farkas et al., "The inflammasome promotes adverse cardiac remodeling following acute myocardial infarction in the mouse," *Proceedings of the National Academy of Sciences of the United States of America*, vol. 108, no. 49, pp. 19725–19730, 2011.

[13] M. Kawaguchi, M. Takahashi, T. Hata et al., "Inflammasome activation of cardiac fibroblasts is essential for myocardial ischemia/reperfusion injury," *Circulation*, vol. 123, no. 6, pp. 594–604, 2011.

[14] S. Toldo and A. Abbate, "The NLRP3 inflammasome in acute myocardial infarction," *Nature Reviews. Cardiology*, vol. 15, no. 4, pp. 203–214, 2018.

[15] A. G. Mauro, A. Bonaventura, E. Mezzaroma, M. Quader, and S. Toldo, "NLRP3 inflammasome in acute myocardial

infarction," *Journal of Cardiovascular Pharmacology*, vol. 74, no. 3, pp. 175–187, 2019.

[16] R. Gao, H. Shi, S. Chang et al., "The selective NLRP3-inflammasome inhibitor MCC950 reduces myocardial fibrosis and improves cardiac remodeling in a mouse model of myocardial infarction," *International Immunopharmacology*, vol. 74, p. 105575, 2019.

[17] Q. Lei, T. Yi, and C. Chen, "NF-kappaB-gasdermin D (GSDMD) axis couples oxidative stress and NACHT, LRR and PYD domains-containing protein 3 (NLRP3) inflammasome-mediated cardiomyocyte pyroptosis following myocardial infarction," *Medical Science Monitor*, vol. 24, pp. 6044–6052, 2018.

[18] L. Carrascal, P. Nunez-Abades, A. Ayala, and M. Cano, "Role of melatonin in the inflammatory process and its therapeutic potential," *Current Pharmaceutical Design*, vol. 24, no. 14, pp. 1563–1588, 2018.

[19] Z. Fu, Y. Jiao, J. Wang et al., "Cardioprotective role of melatonin in acute myocardial infarction," *Frontiers in Physiology*, vol. 11, p. 366, 2020.

[20] H. Pei, J. du, X. Song et al., "Melatonin prevents adverse myocardial infarction remodeling via Notch1/Mfn2 pathway," *Free Radical Biology & Medicine*, vol. 97, pp. 408–417, 2016.

[21] S. H. Zhang, H. M. Wu, S. Li, M. Z. Wang, L. Fang, and R. Y. Liu, "Melatonin Enhances Autophagy and Decreases Apoptosis Induced by nanosilica in RAW264.7 cells," *IUBMB Life*, vol. 71, pp. 1021–1029, 2019.

[22] G. M. Yu, H. Kubota, M. Okita, and T. Maeda, "The anti-inflammatory and antioxidant effects of melatonin on LPS-stimulated bovine mammary epithelial cells," *PLoS One*, vol. 12, no. 5, article e0178525, 2017.

[23] G. P. Fan, W. Wang, H. Zhao et al., "Pharmacological inhibition of focal adhesion kinase attenuates cardiac fibrosis in mice cardiac fibroblast and post-myocardial-infarction models," *Cellular Physiology and Biochemistry*, vol. 37, no. 2, pp. 515–526, 2015.

[24] Z. Li, H. Xu, X. Liu et al., "GDF11 inhibits cardiomyocyte pyroptosis and exerts cardioprotection in acute myocardial infarction mice by upregulation of transcription factor HOXA3," *Cell Death & Disease*, vol. 11, no. 10, p. 917, 2020.

[25] H. F. Pei, J. N. Hou, F. P. Wei et al., "Melatonin attenuates postmyocardial infarction injury via increasing Tom70 expression," *Journal of Pineal Research*, vol. 62, no. 1, article e12371, 2017.

[26] L. Yu, H. Liang, Z. Lu et al., "Membrane receptor-dependent Notch1/Hes1 activation by melatonin protects against myocardial ischemia-reperfusion injury: in vivo and in vitro studies," *Journal of Pineal Research*, vol. 59, no. 4, pp. 420–433, 2015.

[27] F. Chen, Z. Q. Chen, G. L. Zhong, and J. J. Zhu, "Nicorandil inhibits TLR4/MyD88/NF-κB/NLRP3 signaling pathway to reduce pyroptosis in rats with myocardial infarction," *Experimental Biology and Medicine*, p. 153537022110134, 2021.

[28] Q. Mao, X. L. Liang, C. L. Zhang, Y. H. Pang, and Y. X. Lu, "LncRNA KLF3-AS1 in human mesenchymal stem cell-derived exosomes ameliorates pyroptosis of cardiomyocytes and myocardial infarction through miR-138-5p/Sirt1 axis," *Stem Cell Research & Therapy*, vol. 10, p. 393, 2019.

[29] F. Zheng, S. Xing, Z. Gong, W. Mu, and Q. Xing, "Silence of NLRP3 suppresses atherosclerosis and stabilizes plaques in

apolipoprotein E-deficient mice," *Mediators of Inflammation*, vol. 2014, Article ID 507208, 8 pages, 2014.

[30] C. Yao, T. Veleva, L. Scott Jr. et al., "Enhanced cardiomyocyte NLRP3 inflammasome signaling promotes atrial fibrillation," *Circulation*, vol. 138, no. 20, pp. 2227–2242, 2018.

[31] H. Jiang, H. He, Y. Chen et al., "Identification of a selective and direct NLRP3 inhibitor to treat inflammatory disorders," *The Journal of Experimental Medicine*, vol. 214, no. 11, pp. 3219–3238, 2017.

[32] X. Zhong, M. Liu, W. Yao et al., "Epigallocatechin-3-gallate attenuates microglial inflammation and neurotoxicity by suppressing the activation of canonical and noncanonical inflammasome via TLR4/NF-κB pathway," *Molecular Nutrition & Food Research*, vol. 63, no. 21, 2019.

[33] C. Ma, Y. Jiang, X. Zhang, X. Chen, Z. Liu, and X. Tian, "Isoquercetin ameliorates myocardial infarction through anti-inflammation and anti-apoptosis factor and regulating TLR4-NF-κB signal pathway," *Molecular Medicine Reports*, vol. 17, pp. 6675–6680, 2018.

[34] M. Zusso, V. Lunardi, D. Franceschini et al., "Ciprofloxacin and levofloxacin attenuate microglia inflammatory response via TLR4/NF-kB pathway," *Journal of Neuroinflammation*, vol. 16, no. 1, 2019.

[35] T. Kawai and S. Akira, "Signaling to NF-κB by Toll-like receptors," *Trends in Molecular Medicine*, vol. 13, no. 11, pp. 460–469, 2007.

[36] J. Liu, M. Nishida, H. Inui et al., "Rivaroxaban suppresses the progression of ischemic cardiomyopathy in a murine model of diet-induced myocardial infarction," *Journal of Atherosclerosis and Thrombosis*, vol. 26, no. 10, pp. 915–930, 2019.

[37] Z. Shao, M. Nazari, L. Guo et al., "The cardiac repair benefits of inflammation do not persist: evidence from mast cell implantation," *Journal of Cellular and Molecular Medicine*, vol. 19, no. 12, pp. 2751–2762, 2015.

[38] J. T. Thackeray, H. C. Hupe, Y. Wang et al., "Myocardial inflammation predicts remodeling and neuroinflammation after myocardial infarction," *Journal of the American College of Cardiology*, vol. 71, no. 3, pp. 263–275, 2018.

[39] X. Wang, Z. Guo, Z. Ding, and J. L. Mehta, "Inflammation, autophagy, and apoptosis after myocardial infarction," *Journal of the American Heart Association*, vol. 7, no. 9, 2018.

[40] L. K. Newby, "Inflammation as a treatment target after acute myocardial infarction," *The New England Journal of Medicine*, vol. 381, no. 26, pp. 2562-2563, 2019.

[41] Y. Bian, X. Li, P. Pang et al., "Kanglexin, a novel anthraquinone compound, protects against myocardial ischemic injury in mice by suppressing NLRP3 and pyroptosis," *Acta Pharmacologica Sinica*, vol. 41, no. 3, pp. 319–326, 2020.

[42] B. Ye, X. Chen, S. Dai et al., "Emodin alleviates myocardial ischemia/reperfusion injury by inhibiting gasdermin D-mediated pyroptosis in cardiomyocytes," *Drug Design, Development and Therapy*, vol. Volume 13, pp. 975–990, 2019.

[43] R. J. Reiter, D. X. Tan, S. D. Paredes, and L. Fuentes-Broto, "Beneficial effects of melatonin in cardiovascular disease," *Annals of Medicine*, vol. 42, no. 4, pp. 276–285, 2010.

[44] S. Tengattini, R. J. Reiter, D.-X. Tan, M. P. Terron, L. F. Rodella, and R. Rezzani, "Cardiovascular diseases: protective effects of melatonin," *Journal of Pineal Research*, vol. 44, pp. 16–25, 2007.

[45] A. Galano and R. J. Reiter, "Melatonin and its metabolites vs oxidative stress: from individual actions to collective

protection," *Journal of Pineal Research*, vol. 65, no. 1, article e12514, 2018.

[46] G. P. Luo, Z. Jian, R. Y. Ma et al., "Melatonin alleviates hypoxia-induced cardiac apoptosis through PI3K/Akt pathway," *International Journal of Clinical and Experimental Pathology*, vol. 11, no. 12, pp. 5840–5849, 2018.

[47] H. Che, Y. Wang, H. Li et al., "Melatonin alleviates cardiac fibrosis via inhibiting lncRNA MALAT1/miR-141-mediated NLRP3 inflammasome and TGF-β1/Smads signaling in diabetic cardiomyopathy," *The FASEB Journal*, vol. 34, no. 4, pp. 5282–5298, 2020.

[48] D. J. Kaczorowski, A. Nakao, K. R. McCurry, and T. R. Billiar, "Toll-like receptors and myocardial ischemia/reperfusion, inflammation, and injury," *Current Cardiology Reviews*, vol. 5, no. 3, pp. 196–202, 2009.

[49] M. Fujiwara, T. Matoba, J. I. Koga et al., "Nanoparticle incorporating Toll-like receptor 4 inhibitor attenuates myocardial ischaemia-reperfusion injury by inhibiting monocyte-mediated inflammation in mice," *Cardiovascular Research*, vol. 115, no. 7, pp. 1244–1255, 2019.

[50] Y. Sun, J. Huang, and K. Song, "BET protein inhibition mitigates acute myocardial infarction damage in rats via the TLR4/TRAF6/NF-kappaB pathway," *Experimental and Therapeutic Medicine*, vol. 10, no. 6, pp. 2319–2324, 2015.

[51] X. Jin, C. Chen, D. Li et al., "PRDX2 in myocyte hypertrophy and survival is mediated by TLR4 in acute infarcted myocardium," *Scientific Reports*, vol. 7, no. 1, p. 6970, 2017.

[52] O. Avlas, S. Srara, A. Shainberg, D. Aravot, and E. Hochhauser, "Silencing cardiomyocyte TLR4 reduces injury following hypoxia," *Experimental Cell Research*, vol. 348, no. 2, pp. 115–122, 2016.

[53] B. Leng, Y. Zhang, X. Liu et al., "Astragaloside IV Suppresses High Glucose-Induced NLRP3 Inflammasome Activation by Inhibiting TLR4/NF-κB and CaSR," *Mediators of Inflammation*, vol. 2019, Article ID 1082497, 16 pages, 2019.

[54] Y. Dai, S. Wang, S. Chang et al., "M2 macrophage-derived exosomes carry microRNA-148a to alleviate myocardial ischemia/reperfusion injury _via_ inhibiting TXNIP and the TLR4/NF- κB/NLRP3 inflammasome signaling pathway," *Journal of Molecular and Cellular Cardiology*, vol. 142, pp. 65–79, 2020.

Research Article

The Suppression of Pin1-Alleviated Oxidative Stress through the p38 MAPK Pathway in Ischemia- and Reperfusion-Induced Acute Kidney Injury

Xiaojie Zhao,[1] Dan Wang,[2] Shanshan Wan,[3] Xiuheng Liu ⬤,[1] Wei Wang ⬤,[4] and Lei Wang ⬤[1]

[1]*Department of Urology, Renmin Hospital of Wuhan University, Wuhan, 430060 Hubei, China*
[2]*Department of Pharmacy Intravenous Admixture Service, Renmin Hospital of Wuhan University, Wuhan, 430060 Hubei, China*
[3]*Department of Ophthalmology, Renmin Hospital of Wuhan University, Wuhan, 430060 Hubei, China*
[4]*Department of Urology and Institute of Urology, The First Affiliated Hospital of Anhui Medical University, Anhui Province Key Laboratory of Genitourinary Diseases, Anhui Medical University, Hefei, 230022 Anhui, China*

Correspondence should be addressed to Xiuheng Liu; drliuxh@126.com, Wei Wang; wangweimiwai@126.com, and Lei Wang; drwanglei@whu.edu.cn

Background. Pin1, as the peptidyl-prolyl isomerase, plays a vital role in cellular processes. However, whether it has a regulatory effect on renal ischemia and reperfusion (I/R) injury still remains unknown. *Methods.* The hypoxia/reoxygenation (H/R) model in human kidney (HK-2) cells and the I/R model in rats were assessed to investigate the role of Pin1 on I/R-induced acute kidney injury. Male Sprague-Dawley rats were used to establish the I/R model for 15, 30, and 45 min ischemia and then 24 h reperfusion, with or without the Pin1 inhibitor, to demonstrate the role of Pin1 in acute kidney injury. HK-2 cells were cultured and experienced the H/R model to identify the molecular mechanisms involved. *Results.* In this study, we found that Pin1 and oxidative stress were obviously increased after renal I/R. Inhibition of Pin1 with juglone decreased renal structural and functional injuries, as well as oxidative stress. Besides, Pin1 inhibition with the inhibitor, juglone, or the small interfering RNA showed significant reduction on oxidative stress markers caused by the H/R process in vitro. Furthermore, the results indicated that the expression of p38 MAPK was increased during H/R in vitro and Pin1 inhibition could reduce the increased expression of p38 MAPK. *Conclusion.* Our results illustrated that Pin1 aggravated renal I/R injury via elevating oxidative stress through activation of the p38 MAPK pathway. These findings indicated that Pin1 might become the potential treatment for renal I/R injury.

1. Introduction

Acute kidney injury (AKI), which is characterized by fast deterioration of renal function, becomes a worldwide public issue with high incidence and mortality [1]. Renal ischemia/reperfusion (I/R) injury, associated with partial nephrectomy, transplantation, shock, and cardiac bypass surgery, is a major risk for AKI and subsequent chronic kidney disease [2]. The mechanism of renal I/R injury is complex and involves a series of cellular processes, including oxidative stress, inflammation, apoptosis, and endoplasmic reticulum stress, which together lead to serious renal damage [3]. Previous research indicated that oxidative stress, characterized by

rapid overproduction of reactive oxygen species (ROS), was considered one of the primary pathogeneses of I/R [4]. Therefore, it is urgent and beneficial for developing therapeutic strategy on reducing oxidative stress during renal I/R and thus attenuating AKI.

The phosphorylation of Ser/Thr residues on protein is a key mechanism to change their functional activity during the cellular process [5]. Pin1, as the peptidyl-prolyl isomerase, is an important regulator of phosphorylation-induced protein activation [6, 7]. Pin1 has important effect on the regulation of organic I/R injury. A previous report found that at early reperfusion times, Pin1 protein levels exhibited a rapid decline after cardiac ischemia, which was with a pattern

(a)

(b)

(c)

(d)

(e)

(f)

(g)

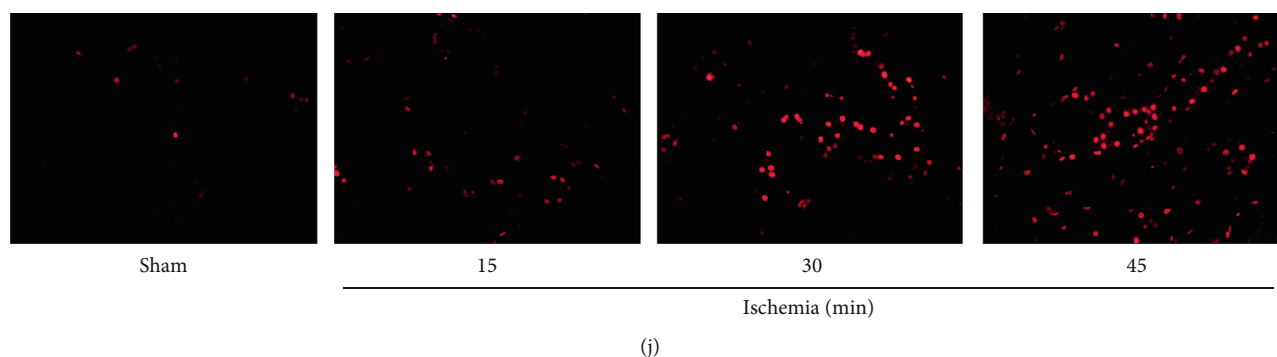(h)

(i)

Sham | 15 | 30 | 45

Ischemia (min)

(j)
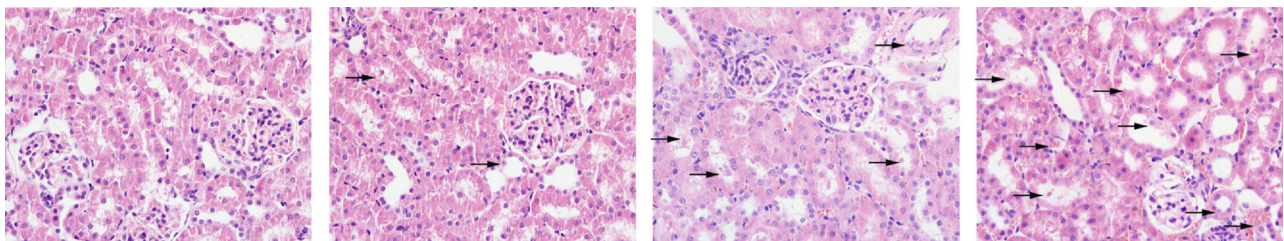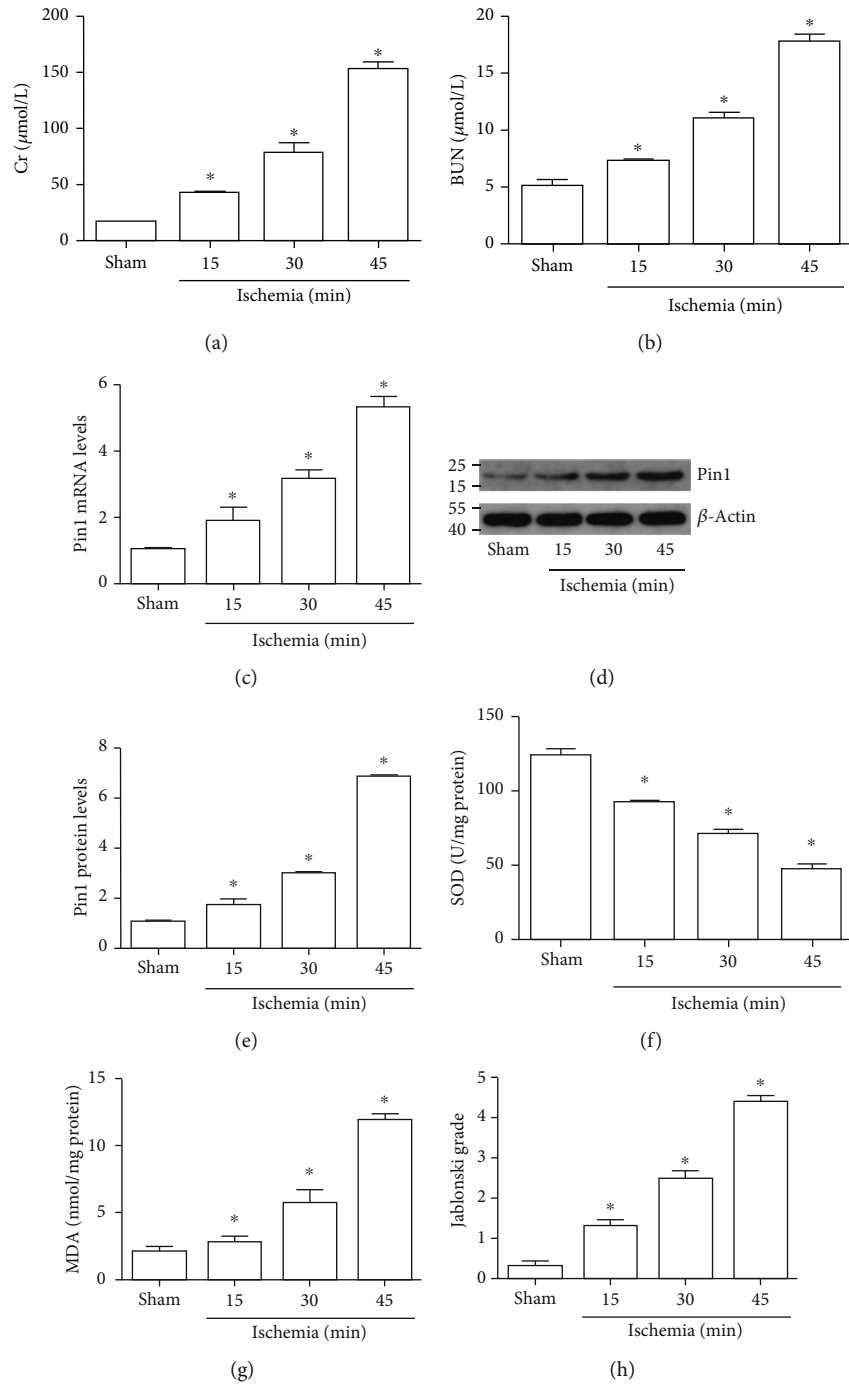
Figure 1: Pin1 expression was increased during renal I/R injury in rats. The model was established with 15, 30, and 45 min ischemia and 24 h reperfusion. (a, b) The Cr and BUN levels in serum were detected. (c) The Pin1 mRNA level was increased in RT-PCR. (d, e) The Pin1 protein level was increased in Western blot, and the quantification was performed. (f, g) The SOD activity and MDA content were detected after I/R injury in rats. (h, i) The pathological change was examined by H&E staining and its quantification (×400). (j) The renal ROS level was examined by DHE staining (×400) ($n = 5$). The values were presented as mean ± SEM. *$P < 0.05$ vs. the sham group.

resembling that of AKT protein, indicating a relationship between Pin1 loss and AKT stability decreased [8]. Another study showed that Pin1, which regulated p53 transactivation under stress, aggravated the pathogenesis via Notch signaling during ischemic stroke [9]. However, the effect of Pin1 on AKI induced by I/R injury remains unclear.

The mitogen-activated protein kinase (MAPK) pathway participates in numerous biological processes, including cell differentiation, cell proliferation, and adaptation to environmental stress [10]. p38 MAPK is a subclass of MAPKs, which is involved in the pathogenesis and progression of AKI [11]. Previous research indicated that the JNK/p38 MAPK pathway was activated following renal I/R, which was accompanied by the overproduction of ROS [12]. However, whether pin1 regulated p38 MAPK expression during AKI induced by I/R was still unclear. In the present study, we investigated whether Pin1 played an important role on renal I/R injury. Also, we tested the possible mechanisms that was involved in Pin1 regulating on oxidative stress.

2. Material and Methods

2.1. Animal. Male adult Sprague-Dawley (SD) rats (200–250 g) were provided by the center of experimental animals in the Medical College of Wuhan University. The animals were placed in a room with suitable temperature and humidity and free access to rat edibles and tap water. This experiment was authorized by the Ethics Committee of Renmin Hospital of Wuhan University, and the procedures were carried out in accordance with the principles of animal care of our university.

2.2. I/R Model Establishment. Rats were acclimated for a week and the model of renal I/R injury in rats was performed as previously reported [13]. After the rats were fully anesthetized with pentobarbital sodium (50 mg/kg, i.p.), they were subjected to the midline laparotomy. And then, all the rats experienced the right nephrectomy, followed by the left kidney vessels being clamped for 15, 30, and 45 min ischemia and then unclamped for 24 h reperfusion.

2.3. Animal Treatment. Rats were treated with various doses of the Pin1 inhibitor, juglone (2 or 10 mg/kg, once a day), three consecutive days before renal I/R injury establishment. The dimethyl sulfoxide (DMSO) group was injected with the equal DMSO solution as a control.

2.4. Serum Assays. Blood samples were collected to detect the level of blood urea nitrogen (BUN) and serum creatinine (Cr) through commercial kit instructions (Nanjing Jiancheng, China). The results were calculated and indicated through spectrophotometric methods.

2.5. Cell Treatment. The human kidney (HK-2) cells were cultured in DMEM (Invitrogen, USA) supplemented with 10% fetal bovine serum under 5% CO_2 and 21% O_2 at 37°C. To establish the cell model, the H/R process was performed as previously described [14]. Briefly, the HK-2 cells were incubated in the hypoxic condition (1% O_2, 94% N_2, and 5% CO_2) for 3, 6, and 12 hours with the nonnutrient medium and then changed with normal medium and cultured in the normoxic condition for 6 hours. The control group was incubated in normal medium under normoxic condition.

2.6. Small Interfering RNA (siRNA) Transfection. For transfection of si-Pin1, the cells were transfected with two different si-RNA against Pin1 or si-NC for 48 h through lipofectamine 3000. Western blot was used to assess the effect of si-RNA against Pin1.

2.7. Histological Examinations. After the rats were sacrificed, renal tissue samples were fixed in 4% paraformaldehyde, embedded in paraffin, and incised with an average thickness of 4 μm. Then, the samples were experiencing being deparaffinized, hydrated, and stained with hematoxylin and eosin (H&E). An established grading scale of 0–4, outlined by Jablonski et al. [15], was used for the histopathological assessment of I/R-induced damage.

2.8. RT-PCR. RNA was extracted with the RNAiso Plus (TaKaRa Biotechnology). Reverse transcriptase reactions were performed using a SuperScript First-strand Synthesis System (Invitrogen). Real-time PCR reactions were

(a)

(b)

(c)

(d)

(e)

(f)

(g)

(h)

Figure 2: Continued.

| Sham | DMSO | 2 | 10 |

I/R+Juglone (mg/kg)

(i)
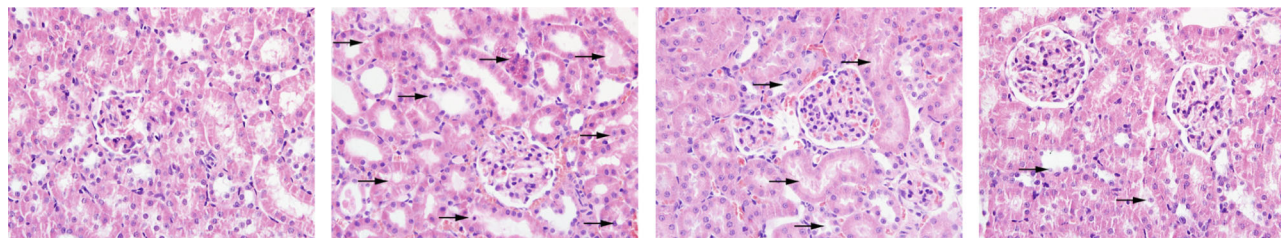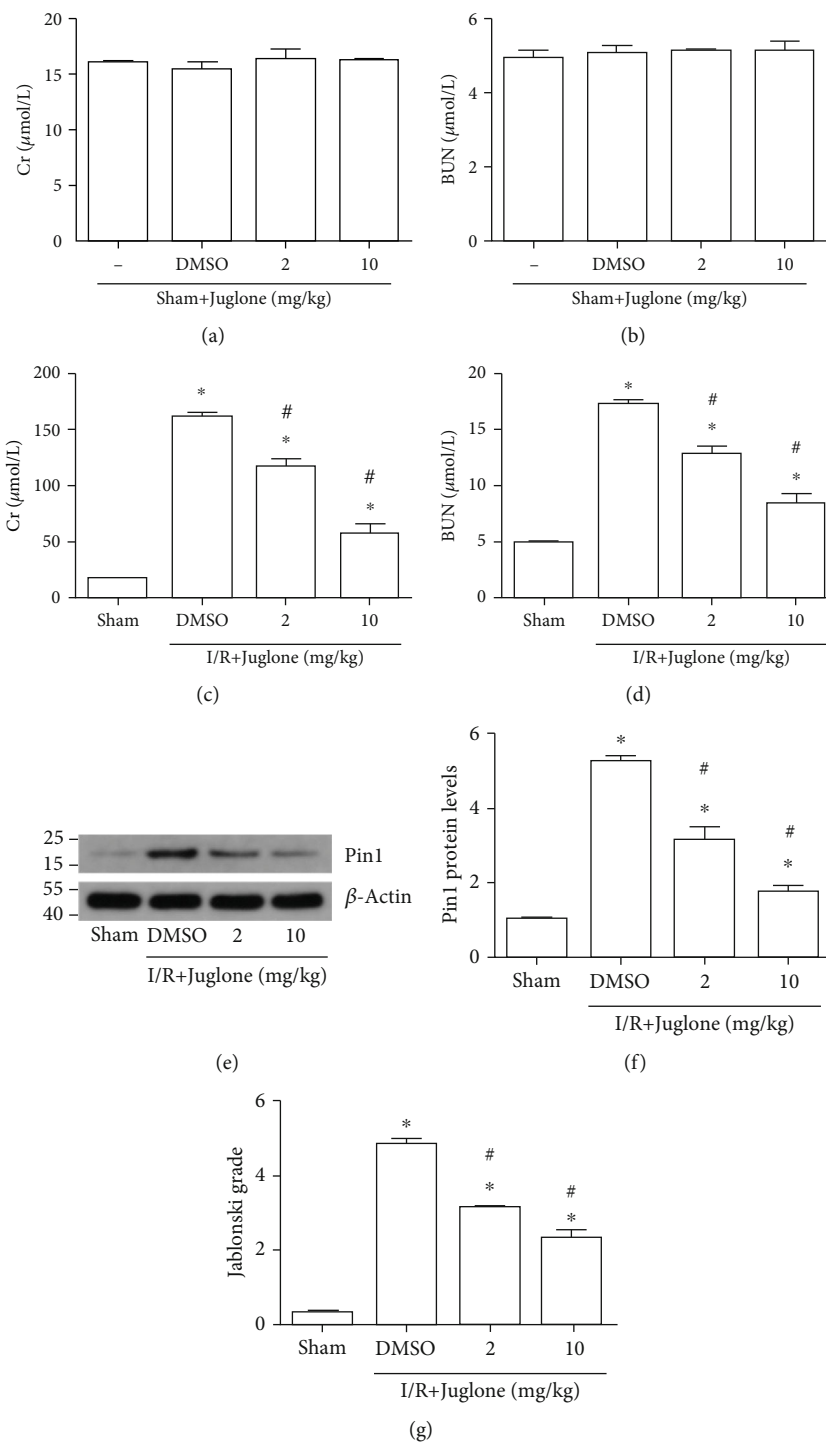
FIGURE 2: The Pin1 inhibitor, juglone, prevented renal tissue against I/R injury in rats. The model was established with 45 min ischemia and then 24 h reperfusion. (a, b) The effect of juglone at different concentrations (2 mg/kg, 10 mg/kg) on the Cr and BUN levels in the sham group. (c, d) The effect of juglone at different concentrations (2 mg/kg, 10 mg/kg) on the Cr and BUN levels in the I/R group. (e, f) The effect of juglone at different concentrations (2 mg/kg, 10 mg/kg) on Pin1 expression in rats and the quantification. (g, h) The effect of juglo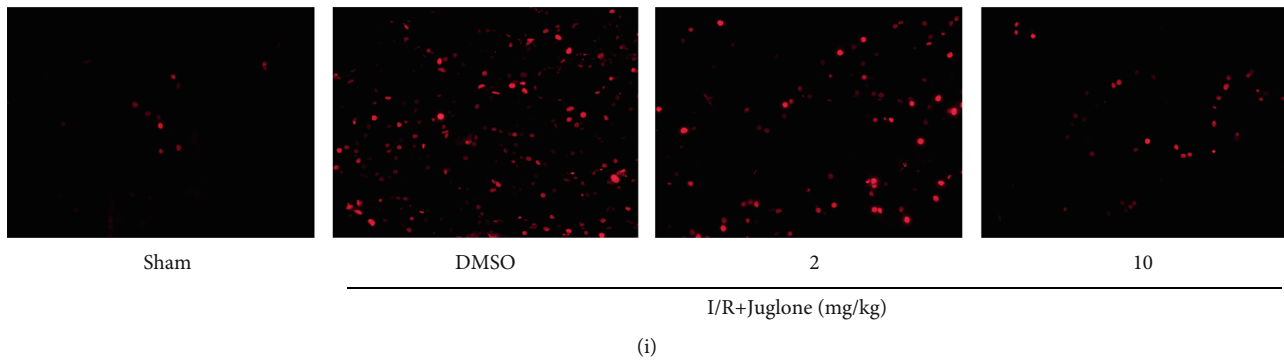ne at different concentrations (2 mg/kg, 10 mg/kg) on the structure change was examined by H&E staining and its quantification (×400). (i) The effect of juglone on oxidative stress was examined by DHE staining (×400) ($n = 5$). The values were presented as mean ± SEM. $^*P < 0.05$ vs. the sham group and $^\#P < 0.05$ vs. the I/R group.

performed with β-actin as internal control. Gene levels were shown as fold change relative to control. The primers were included as follows:

R-Pin1: 5′-GCTCAGGCCGTGTCTACTACTTC-3′ (F); 5′-TCCGAGATTGGCTGTGCTTC-3′ (R); R-β-actin: 5′-TGCTATGTTGCCCTAGACTTCG-3′ (F); 5′-GTTGGCATAGAGGTCTTTACGG-3′ (R); H-Pin1: 5′-TCAACCACATCACTAACGCCAG-3′ (F); 5′-GCAAACGAGGCGTCTTCAAAT-3′ (R); H-β-actin: 5′-CACCCAGCACAATGAAGATCAAGAT-3′ (F); and 5′-CCAGTTTTTAAATCCTGAGTCAAGC-3′ (R).

2.9. Western Blotting. Kidney tissue was collected and then protein was extracted and quantified. Briefly, the sample was separated and then transferred to the polyvinylidene difluoride membrane. Subsequently, it was blocked with 5% nonfat milk and then incubated at 4°C overnight with primary antibodies against Pin1 (#192036, Abcam), 4-hydroxynonenal (4-HNE) (#46545, Abcam), COX2 (cyclooxygenase 2) (#179800, Abcam), myeloperoxidase (MPO) (#208670, Abcam), p38 (#31828, Abcam), p-p38(#4822, Abcam), and β-actin (#BA2305, Boster Biological Technology). Then, it was washed and incubated with secondary antibody. Specific bands were detected and the densities were quantified using ImageJ software.

2.10. Measurement of Malondialdehyde (MDA) and Superoxide Dismutase (SOD). The detection of SOD activity and MDA content were performed through the instructions of the Nanjing Jiancheng Bioengineering Institute. Cell lysates from in vivo and in vitro experiments were collected and detected the level of SOD and MDA. The specific procedures were according with the manufacturer's direction.

2.11. ROS Production Detection. The ROS levels were determined based on our previous study [16] through the commercial kit instruction (Nanjing Jiancheng, China). The samples were incubated with dichloro-dihydro-fluorescein

diacetate (20 μM) at room temperature for 30 min, and the result of the ROS level was quantified through flow cytometry.

2.12. Detection for the Production of Hydrogen Peroxide (H_2O_2). The renal tissue and HK-2 cells were perfused and homogenized. And then, hydrogen peroxide was detected through the commercial kit instruction (Nanjing Jiancheng, China). The results were shown as fold change relative to the control group.

2.13. DHE Staining. Frozen kidney sections (4 μM) were stained with dihydroethidium (DHE) (2 μmol/L, Sigma) in a light-protected humidified chamber at 37°C for 15 min. The images were visualized using a fluorescence microscope (Olympus IX51).

2.14. Statistical Analysis. All data was expressed as mean ± standard error of the mean (SEM). Statistical analyses included two-way analysis of variance and the Student–Newman–Keuls test. Statistically significant differences were considered when $p < 0.05$.

3. Results

3.1. Pin1 Expression Was Elevated during Renal I/R. The levels of Bun and Cr were continuing to increase as the ischemic time extended (Figures 1(a) and 1(b)). Also, the levels of Pin1 were examined by RT-PCR and Western blot and the results showed that Pin1 mRNA and the protein level were continuing to increase as the extension of ischemic time, especially at 45 min ischemia (Figures 1(c)–1(e)). Then, we found that oxidative stress was increased during renal I/R. The results showed that SOD activity (Figure 1(f)) continued to decrease and MDA content (Figure 1(g)) continued to increase in the course of I/R progress, especially at 45 min ischemia. H&E staining (Figures 1(h) and 1(i)) and DHE staining (Figure 1(j)) indicated that renal I/R injury exhibited acute tubular damage and increased ROS level at ischemia
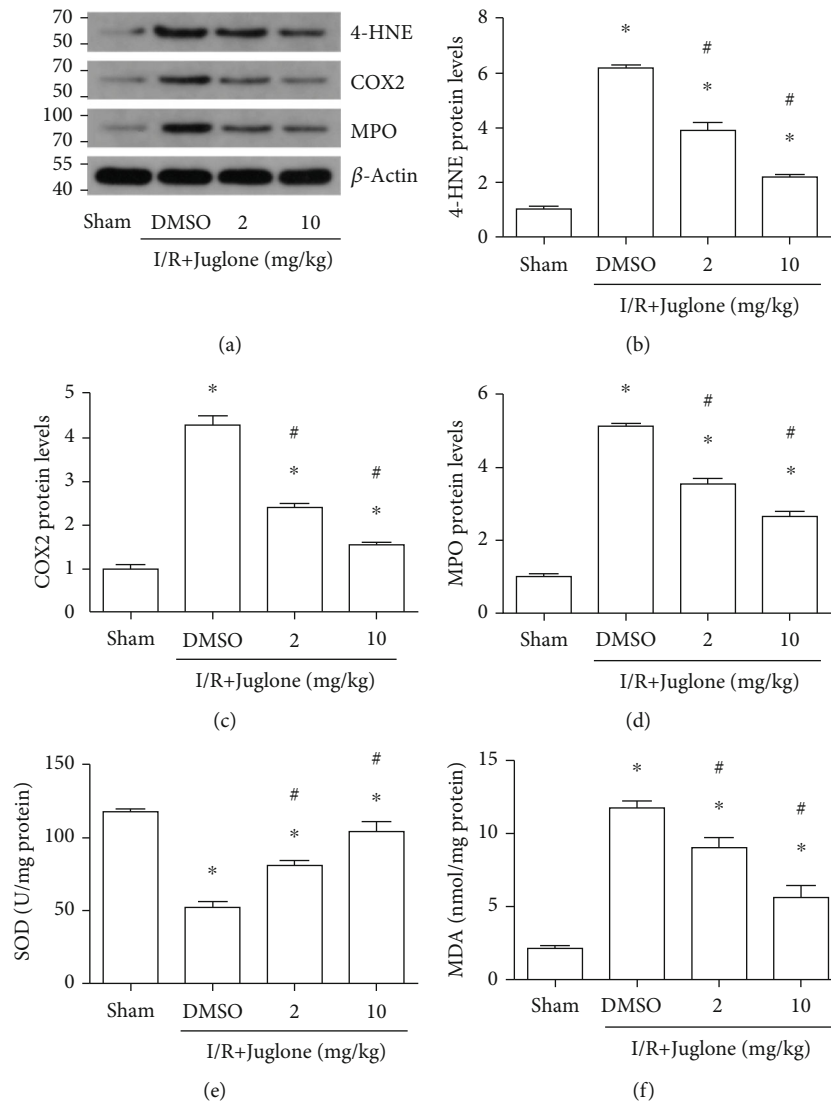
(a)

(b)

(c)

(d)

(e)

(f)

FIGURE 3: The Pin1 inhibitor, Juglone, reduced oxidative stress induced by renal I/R in rats. The model was established with 45 min ischemia and then 24 h reperfusion. (a–d) The regulatory effect of the Pin1 inhibitor on 4-HNE, COX2, and MPO expression after renal I/R, and quantification was performed. (e) The effect of the Pin1 inhibitor on the SOD activity after renal I/R. (f) The effect of the Pin1 inhibitor on MDA content after renal I/R ($n = 5$). The values were presented as mean ± SEM. $^{*}P < 0.05$ vs. the sham group and $^{\#}P < 0.05$ vs. the I/R group.

45 min. Therefore, we chose ischemia 45 min and reperfusion 24 h in the following experiments.

3.2. Pin1 Inhibition Protected against Renal Injury Induced by I/R. Firstly, different concentrations of the Pin1 inhibitor, juglone, were applied in the sham group. The results indicated that juglone did not affect renal function, as BUN and Cr levels did not have difference between groups (Figures 2(a) and 2(b)). Then, we found that the increased BUN and Cr levels induced by I/R obviously decreased after juglone treatment (Figures 2(c) and 2(d)). The results of Western blot showed that the treatment of juglone could inhibit the elevated expression of Pin1 caused by renal I/R (Figures 2(e) and 2(f)). Besides, H&E staining showed that renal I/R injury exhibited acute tubular damage, including the loss of the brush border and tubular dilatation in the proximal tubules (Figures 2(g) and 2(h)). However, the different

concentration of juglone protected renal tissue from acute tubular damage, with better effects at 10 mg/kg. The DHE staining also showed that juglone could reduce the elevated ROS levels induced by I/R (Figure 2(i)).

3.3. Pin1 Inhibition Attenuated Oxidative Stress Caused by Renal I/R. Next, we investigated the relationship of Pin1 and oxidative stress induced by renal I/R injury. Western blot results showed that the 4-HNE, COX2, and MPO expression was elevated after renal I/R injury and Pin1 inhibition could alleviate their expression (Figures 3(a)–3(d)). Also, the results indicated that the reduced SOD level (Figure 3(e)) and the elevated MDA content (Figure 3(f)) induced by renal I/R were reversed by the Pin1 inhibitor. Therefore, it indicated that Pin1 inhibition might alleviate oxidative stress induced by renal I/R.

(a)

(b)

(c)

(d)

(e)

(f)

(g)
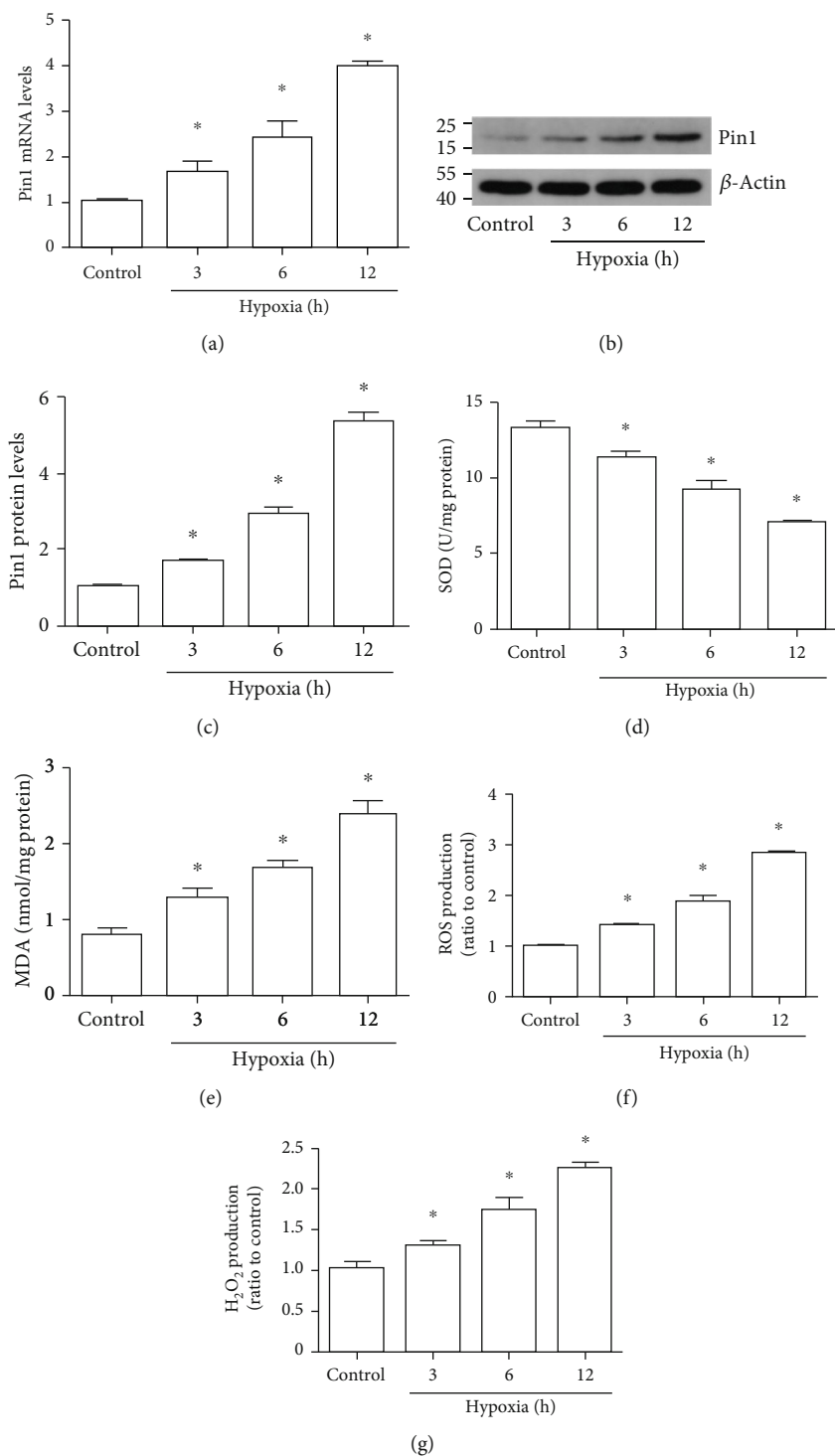
FIGURE 4: Pin1 expression and oxidative stress were elevated during the H/R process in vitro. The model was established with 3, 6, and 12 h hypoxia and 6 h reoxygenation. (a) The mRNA was detected by RT-PCR after the H/R process. (b, c) Western blot was used to detect Pin1 expression and the quantification was analyzed. (d–g) The SOD, MDA, ROS, and H_2O_2 levels were detected after H/R injury in vitro ($n = 5$). The values were presented as mean ± SEM. $^*P < 0.05$ vs. the control group.

3.4. Pin1 Level and Oxidative Stress Were Elevated during H/R In Vitro.

RT-PCR and Western blot results indicated that the Pin1 mRNA and protein levels were increased after different hypoxia time and reoxygenation 6 h in HK-2 cells,

especially at hypoxia 12 h (Figures 4(a)–4(c)). We also found that the SOD activity (Figure 4(d)) continued to decrease during the H/R course in HK-2 cells. However, the MDA content (Figure 4(e)), ROS (Figure 4(f)), and H_2O_2

(a)

(b)

(c)

(d)

(e)

(f)

(g)

(h)

(i)

(j)
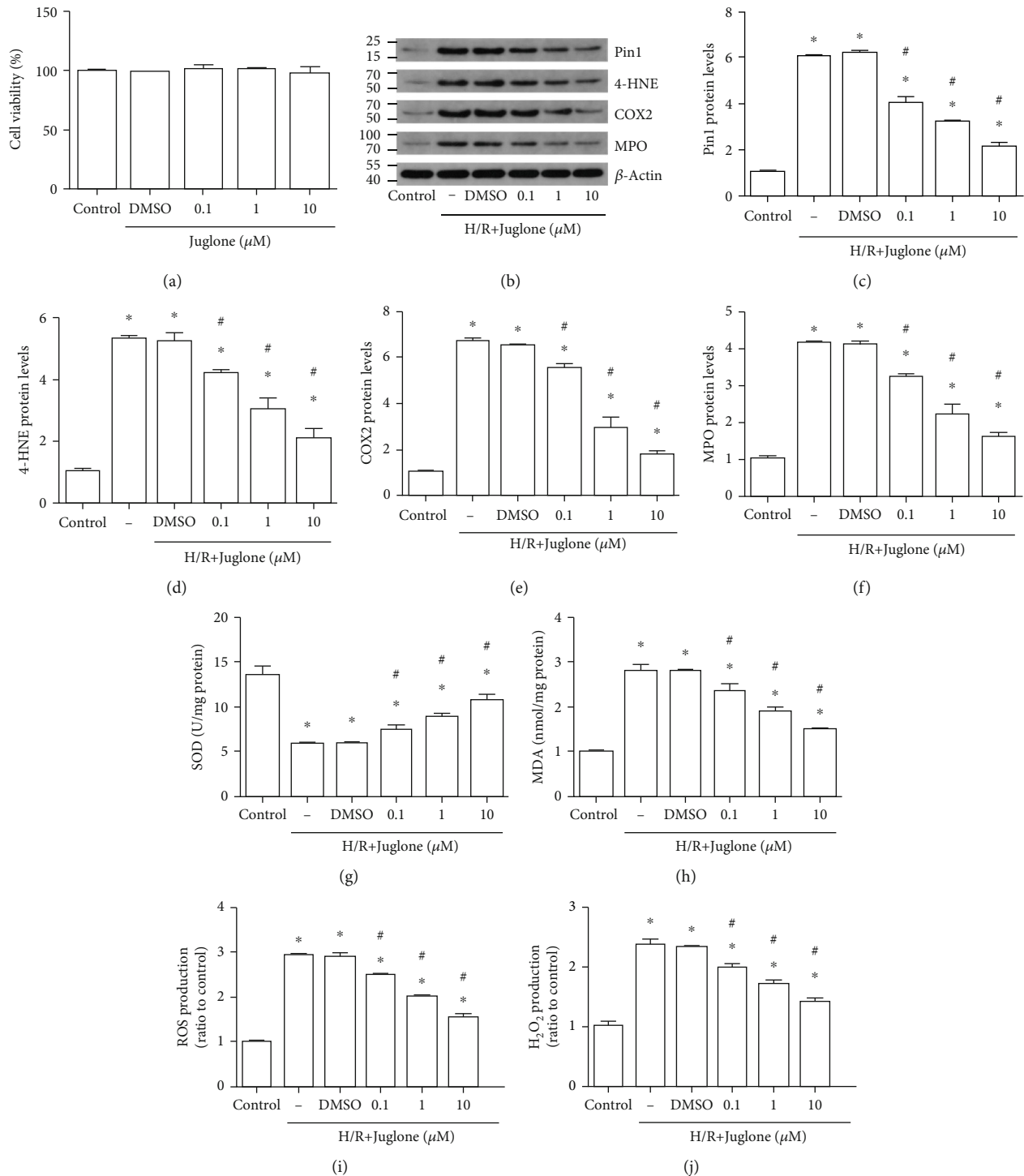
Figure 5: The Pin1 inhibitor, Juglone, regulated oxidative stress caused by H/R injury in vitro. The model was established with 12 h hypoxia and 6 h reoxygenation. HK-2 cells were treated with the Pin1 inhibitor (0.1,1, and 10 μM) for 1 h and then experienced the H/R process. (a) The effect of different concentrations of juglone on the control group. (b–f) Western blot was used to detect the expression of Pin1, 4-HNE, COX2, and MPO and quantification was performed. (g–j) The SOD, MDA, ROS, and H$_2$O$_2$ levels were detected after the H/R process in vitro ($n = 5$). The values were presented as mean ± SEM. $^{*}P < 0.05$ vs. the control group and $^{\#}P < 0.05$ vs. the H/R group.

production (Figure 4(g)) were increased in response to H/R. So, we chose 12 h hypoxia and 6 h reoxygenation in the following experiments.

3.5. Juglone Decreased Oxidative Stress Caused by H/R In Vitro. Firstly, the different concentration of juglone was used in the control group and the CCK-8 results showed that cell

(a)
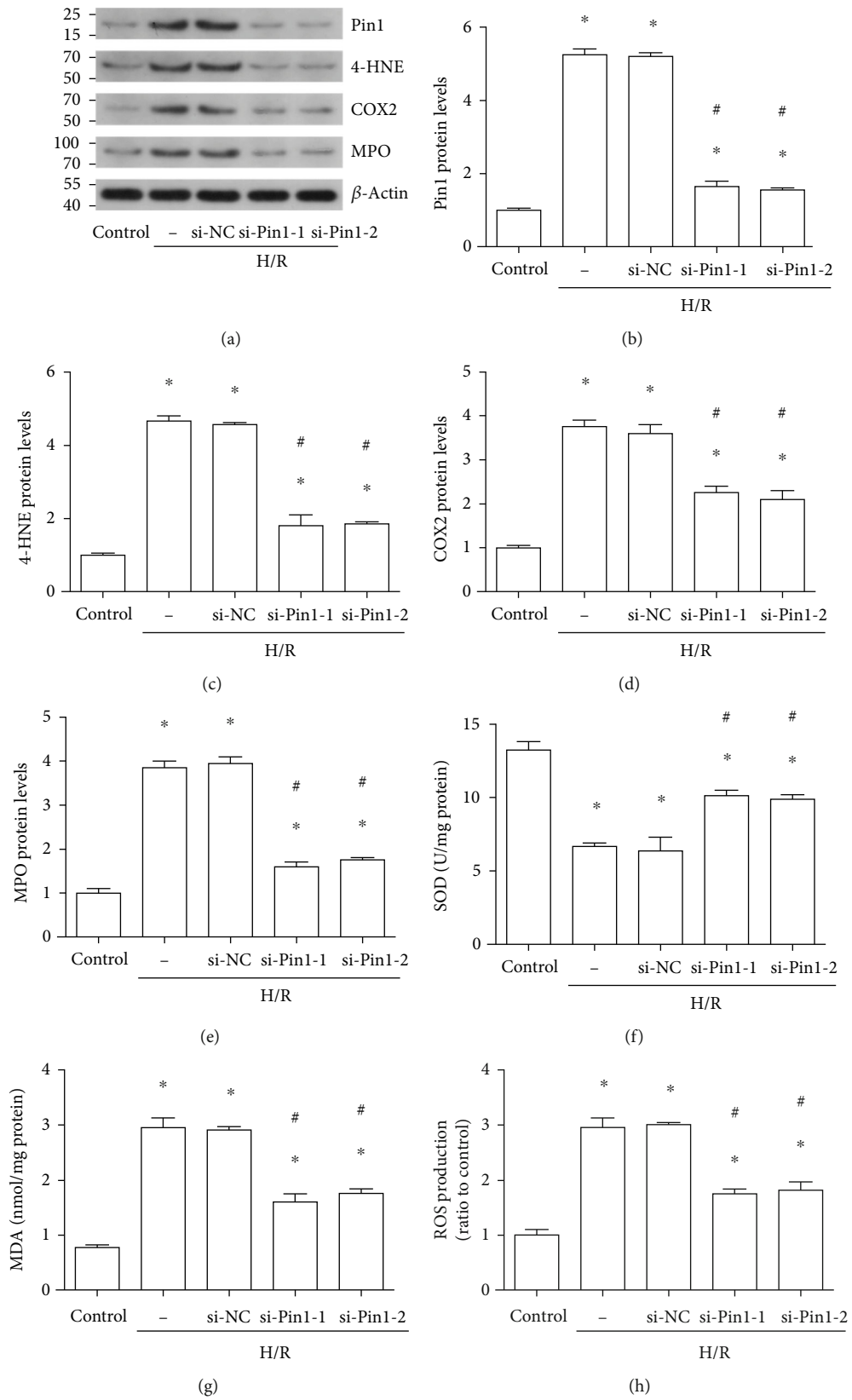

(b)

(c)

(d)

(e)

(f)
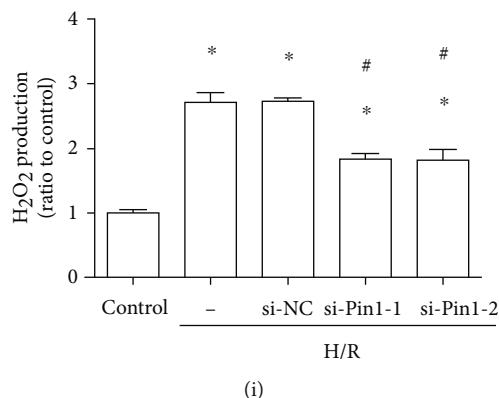

(g)

(h)

FIGURE 6: Continued.

(i)

FIGURE 6: Pin1 silence decreased oxidative stress induced by H/R in vitro. The H/R model was established with 12 h hypoxia and 6 h reoxygenation. The cells were transfected with si-NC or two different si-Pin1 for 24 h and then experienced H/R. (a–e) Western blot was used to detect the expression of Pin1, 4-HNE, COX2, and MPO and quantification was performed. (f–i) The SOD, MDA, ROS, and H_2O_2 levels were detected after H/R in vitro ($n = 5$). The values were presented as mean $\pm$ SEM. $^*P < 0.05$ vs. the control group and $^\#P < 0.05$ vs. the si-NC group.

viability had no differences between groups (Figure 5(a)). Western blot results showed that Pin1, 4-HNE, COX2, and MPO expression was increased after H/R and the different concentration of juglone could decrease their expression in HK-2 cells (Figures 5(b)–5(f)), especially at $10\,\mu M$. Next, the results indicated that the reduced SOD level (Figure 5(g)) and the elevated MDA content (Figure 5(h)), ROS (Figure 5(i)), and H_2O_2 production (Figure 5(j)) induced by H/R were reversed by inhibition of Pin1 in HK-2 cells. Therefore, we chose juglone $10\,\mu M$ in the following experiments.

3.6. Pin1 Inhibition Reduced Oxidative Stress Caused by H/R In Vitro. Two different siRNAs against Pin1 were performed to demonstrate the role of Pin1 in oxidative stress induced by H/R in vitro. The results of Western blot showed that si-RNA against Pin1 could obviously alleviate the expression of Pin1, 4-HNE, COX2, and MPO, which was elevated after H/R in HK-2 cells (Figures 6(a)–6(e)). Also, the results indicated that compared with the si-NC group, the SOD level (Figure 6(f)) was obviously increased and the MDA content (Figure 6(g)), ROS (Figure 6(h)), and H_2O_2 production (Figure 6(i)) were decreased by si-RNA against Pin1 in HK-2 cells.

3.7. p38 MAPK Involved in the Regulation of Pin1 on Oxidative Stress Caused by H/R In Vitro. It was reported that p38 MAPK was activated in renal I/R injury. In the present study, we found that phosphorylated p38 (p-p38) was largely inhibited by si-Pin1 compared with si-NC (Figures 7(a) and 7(b)). Next, we applied the p38 MAPK activator, U-46619, to investigate the association between Pin1 and p38 MAPK. Western blot results indicated that the inhibited p-p38 by two different si-Pin1 could be reversed by U-46619 (Figures 7(c) and 7(d)). Next, we found that the expression of Pin1 did not have a difference after treatment with U-46619; however, the inhibited expression of 4-HNE, COX2, and MPO by si-Pin1 was reversed by U-46619 treatment (Figures 7(e)–7(i)). Also, compared with two different si-

Pin1 groups, the changed levels of the SOD activity (Figure 7(j)), MDA content (Figure 7(k)), ROS (Figure 7(l)), and H_2O_2 production (Figure 7(m)) were reversed after U-46619 treatment. These results suggested that Pin1 regulated oxidative stress during H/R in HK-2 cells that depended on the p38 MAPK pathway.

3.8. Inhibition of Pin1 Attenuated p38 MAPK Activation Induced by Renal I/R. Western blot results showed that p-p38 MAPK was increased after renal I/R in rats; however, the expression was inhibited by treatment with juglone, a Pin1 inhibitor (Figures 8(a) and 8(b)).

4. Discussion

In this study, we investigated the role of Pin1 in renal I/R injury and the possible mechanism. The results showed that Pin1 had important effects on the regulation of renal I/R in vivo. Firstly, we found that the inhibition of Pin1 could alleviate renal injury induced by I/R *in vivo* and *in vitro*. Besides, oxidative stress induced by H/R depended on Pin1 levels in HK-2 cells and inhibition of Pin1 using siRNA or the specific inhibitor blocked oxidative stress caused by H/R in vitro. Furthermore, we also found that ROS generation was modulated by Pin1 through p38 MAPK activation. So, our study demonstrated that Pin1 might become a target for treatment of renal I/R injury.

I/R is the common pathophysiological process that leads to renal tubular epithelial cell death and subsequently rapid deterioration of renal function [17]. Experimental renal I/R models are critical for the researchers to investigate the pathogenesis and explore the development of effective therapeutics. The in vivo models of renal I/R included both renal pedicle clamping (bilateral I/R) and one renal pedicle clamping (unilateral I/R) or unilateral I/R with contralateral nephrectomy [18]. Also, the ischemic time and reperfusion period were different which depended on the species or experimental purpose. In our research, the renal I/R model on rats was established, with ischemic time ranging from 15 min to 45 min

(a)

(b)

(c)

(d)

(e)

(f)

(g)

(h)

FIGURE 7: Continued.

(i)

(j)

(k)

(l)

(m)
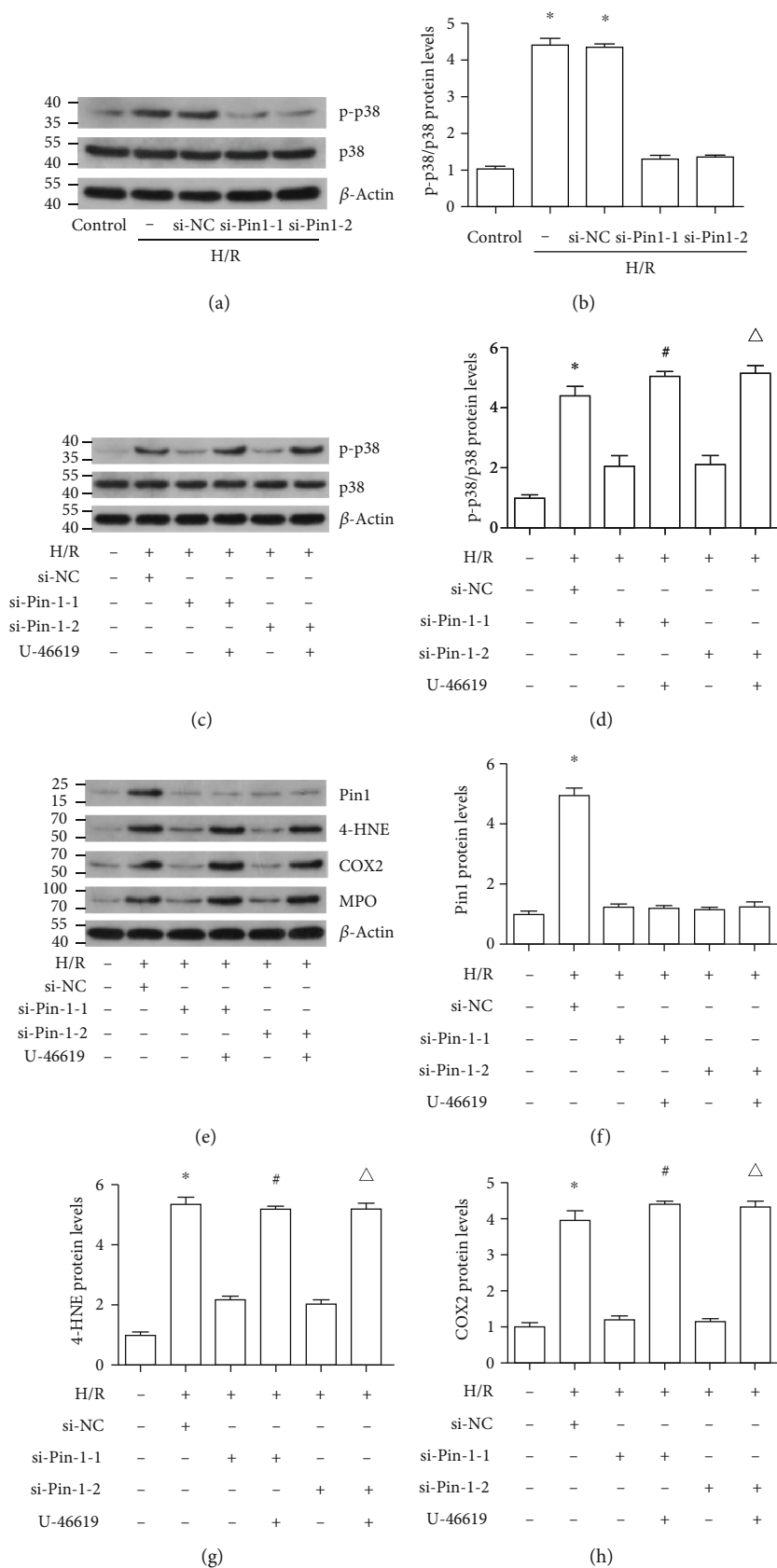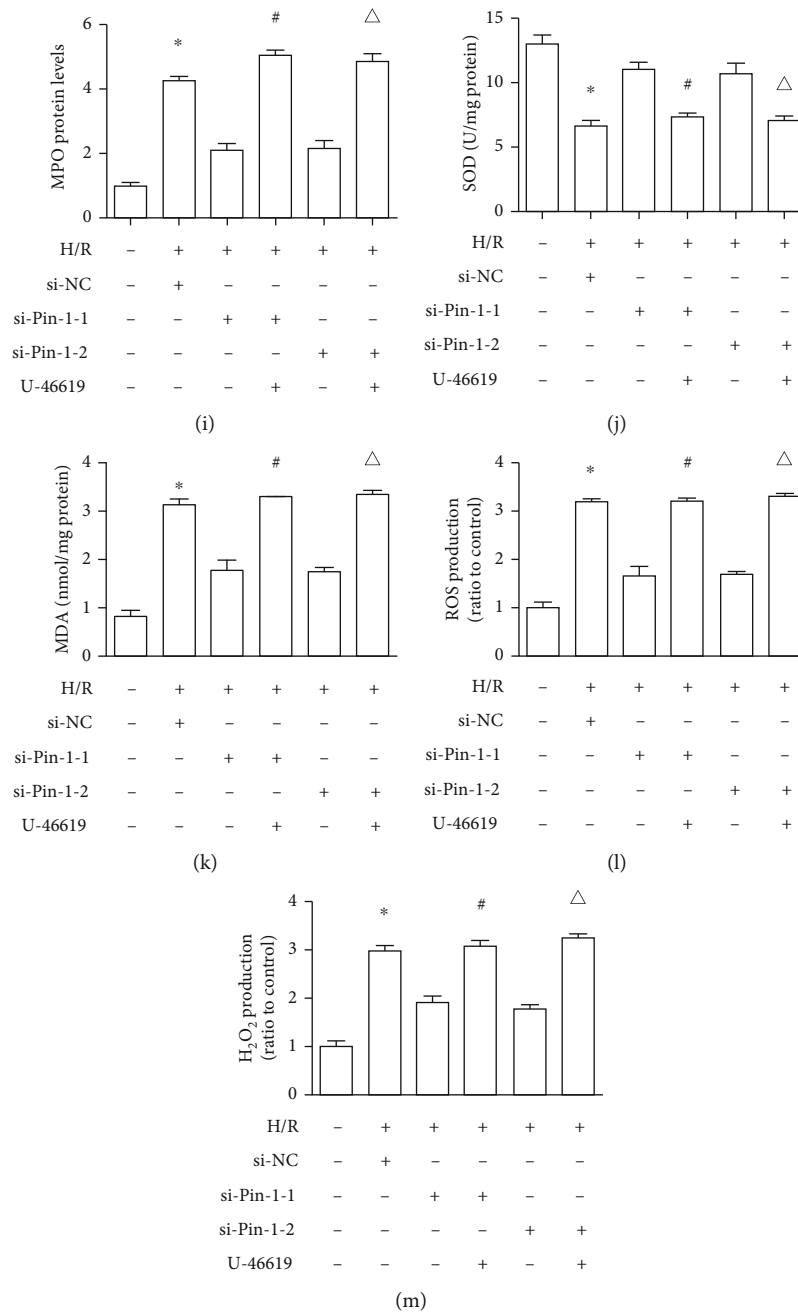
Figure 7: Pin1 aggravates oxidative stress caused by H/R injury via activation of p38 MAPK. The H/R model was established with 12 h hypoxia and 6 h reoxygenation. The cells were transfected with si-NC or two different si-Pin1 for 24 h and then experienced the H/R process, with or without treatment with the p38 MAPK activator (5 μM). (a, b) Western blot was used to detect the expression of p-p38/p38 after Pin1 silence and quantification was performed. (c, d) The expression of p-p38/p38 after Pin1 silence and its quantification, with or without treatment with the p38 MAPK activator. (e–i) Western blot was used to detect the expression of Pin1, 4-HNE, COX2, and MPO and quantification was performed. (j–m) The SOD, MDA, ROS, and H_2O_2 levels were detected ($n = 5$). The values were presented as mean $\pm$ SEM. $^*P < 0.05$ vs. the control group; $^\#P < 0.05$ vs. the si-Pin1-1 group; $^\triangle P < 0.05$ vs. the si-Pin1-2 group.

and 24 h reperfusion. The results showed that oxidative stress became more serious as the ischemic time prolonged, especially at 45 min ischemia, which was consistent with a previous study, demonstrating that oxidative stress might be important in renal I/R injury.

Pin1, a key regulatory mediator, is involved in various cellular processes through specifically recognizing pSer/pThr-Pro

motifs and inducing conformational changes to control protein function [19]. Previous studies focused more on the effect of Pin1 on tumorigenesis and progression; however, it also played an important role in organic ischemic injury, including cardiac, hepatic, cerebral, and intestinal I/R [8, 19–21]. In the present study, it indicated that Pin1 expression continued to increase as the ischemic time extended, especially at 45 min
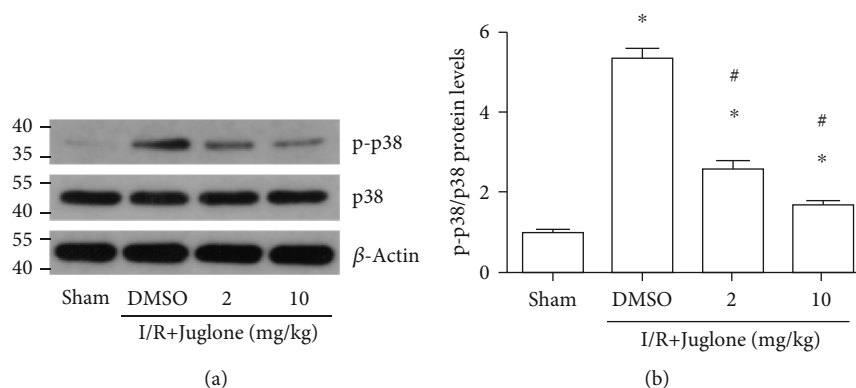
FIGURE 8: The Pin1 inhibitor, Juglone, ameliorates p38 MAPK activation induced by renal I/R in rats. The model was performed with 45 min ischemia and 24 h reperfusion. (a–b) The regulatory effect of the Pin1 inhibitor on p-p38/p38 expression after renal I/R in rats and quantification performed ($n = 5$). The values were presented as mean ± SEM. $^*P < 0.05$ vs. the sham group and $^\#P < 0.05$ vs. the I/R group.

ischemia. The H/R process was performed to mimic the in vitro model and the results indicated that Pin1 expression was elevated as hypoxia time prolonged, especially at hypoxia 12 h, which was consistent with our in vivo results. The inhibition of Pin1 could protect renal tissue and function against I/R injury.

ROS, at low concentrations, serves to regulate various cellular signaling pathways and modulate cell fate and proliferation, thus maintaining cellular and tissue homeostases. However, the high ROS level is also detrimental to physiological function. Oxidative stress results from the accumulation of high levels of ROS and plays the vital role during the organic I/R injury [22]. A previous study indicated that trehalose could protect the kidney against I/R injury through blocking oxidative stress [23]. In our research, the results indicated that inhibition of Pin1 could reverse the elevated 4-HNE, COX2, and MPO expression induced by renal I/R, as well as the reduced SOD activity and elevated MDA content. To demonstrated the results in vivo, we also used si-RNA against Pin1 and juglone, a Pin1-specific inhibitor, through the H/R model in vitro. The results in vitro were consistent with those in vivo that inhibition of Pin1 could alleviate the expression of 4-HNE, COX2, and MPO; MDA content; ROS; and H_2O_2 production and increased SOD activity after H/R in HK-2 cells. Our results indicated that Pin1 inhibition could alleviate renal I/R injury through the regulation of oxidative stress.

P38-MAP kinase, a critical component of MAPK systems, is involved in the modulation of cellular function [24]. Different stimuli could activate p38-MAPK and aggravate I/R injury [25]. A recent study indicated that p38-MAPK caused kidney I/R injury through regulation of redox stress and cell apoptosis, which suggested that it might be a potential target of AKI [26]. The relationship of Pin1 and p-p38 had already been reported and the mechanism was complex. Coimmunoprecipitation analysis showed that Pin1 could bind to p-p38, which implied that the p-p38 MAPK might be a substrate of Pin1. Then, with GST pulldown experiment, it showed that Pin1 could not directly bind to p-p38 MAPK in vitro, suggesting that Pin1 might affect p38 MAPK through kinases or other proteins [27]. In this

study, we found that the activation of p38 MAPK was induced by I/R injury and inhibition of Pin1 could suppress p38 MAPK activation in vivo and in vitro. Besides, with the p38 MAPK activator, we further demonstrated that the decreased p-p38 level was elevated in response to U-46619, compared with si-Pin1 only. In addition, the results also indicated that the changed expression of 4-HNE, COX2, and MPO induced by two different si-Pin1, as well as the changed levels of SOD activity, MDA content, ROS, and H_2O_2 production, could be reversed by U-46619, which demonstrate that Pin1 regulated oxidative stress through p38 MAPK. The mechanism of Pin1 regulating on the activation of p38 MAPK might be through modulation of protein kinases.

5. Conclusion

In summary, we found that Pin1 inhibition could protect the renal tissue against I/R injury and prevent kidney tissue through modulating p38 MAPK-mediated ROS production. Overall, the present study indicated that Pin1 might become a potential treatment for renal I/R injury.

Abbreviations

Pin1:	Peptidyl-prolyl cis/trans isomerase
SD:	Sprague-Dawley
I/R:	Ischemia and reperfusion
HK-2:	Human kidney
BUN:	Blood urea nitrogen
H/R:	Hypoxia and reoxygenation
AKI:	Acute kidney injury
4-HNE:	4-Hydroxynonenal
COX2:	Cyclooxygenase 2
MPO:	Myeloperoxidase
Cr:	Creatinine
siRNA:	Small interfering RNA
DMSO:	Dimethyl sulfoxide
ROS:	Reactive oxygen species
NC:	Negative control
H&E:	Hematoxylin and eosin
H_2O_2:	Hydrogen peroxide

MAPK: Mitogen-activated protein kinases
qRT-PCR: Real-time quantitative reverse transcription-
            polymerase chain reaction.

Data Availability

The datasets in this study are available from the correspond-
ing author.

Conflicts of Interest

The authors report no conflicts of interest in this work.

Authors' Contributions

All authors participated to conceive the idea, carry out the
work, and analyze the data. Xiaojie Zhao, Dan Wang, and
Shanshan Wan contributed equally to this work.

Acknowledgments

References

[1] L. Yang, G. Xing, L. Wang et al., "Acute kidney injury in China:
a cross-sectional survey," *Lancet*, vol. 386, no. 10002,
pp. 1465–1471, 2015.

[2] M. Zhao, Y. Wang, L. Li et al., "Mitochondrial ROS promote
mitochondrial dysfunction and inflammation in ischemic
acute kidney injury by disrupting TFAM-mediated mtDNA
maintenance," *Theranostics*, vol. 11, no. 4, pp. 1845–1863,
2021.

[3] C. Li, Z. Zheng, Y. Xie et al., "Protective effect of taraxasterol
on ischemia/reperfusion-induced acute kidney injury via inhi-
bition of oxidative stress, inflammation, and apoptosis," *Inter-
national Immunopharmacology*, vol. 89, no. Part A, article
107169, 2020.

[4] C. Diao, Z. Chen, T. Qiu et al., "Inhibition of PRMT5 Attenu-
ates Oxidative Stress-Induced Pyroptosis via Activation of the
Nrf2/HO-1 Signal Pathway in a Mouse Model of Renal Ische-
mia- Reperfusion Injury," *Oxidative Medicine and Cellular
Longevity*, vol. 2019, Article ID 2345658, 18 pages, 2019.

[5] K. P. Lu, Y. C. Liou, and X. Z. Zhou, "Pinning down proline-
directed phosphorylation signaling," *Trends in Cell Biology*,
vol. 12, no. 4, pp. 164–172, 2002.

[6] K. P. Lu and X. Z. Zhou, "The prolyl isomerase PIN1: a pivotal
new twist in phosphorylation signalling and disease," *Nature
Reviews Molecular Cell Biology*, vol. 8, no. 11, pp. 904–916,
2007.

[7] K. Takahashi, C. Uchida, R. W. Shin, K. Shimazaki, and
T. Uchida, "Prolyl isomerase, Pin1: new findings of post-
translational modifications and physiological substrates in
cancer, asthma and Alzheimer's disease," *Cellular and Molecu-
lar Life Sciences*, vol. 65, no. 3, pp. 359–375, 2008.

[8] P. Penela, J. Inserte, P. Ramos, A. Rodriguez-Sinovas,
D. Garcia-Dorado, and F. Mayor Jr., "Degradation of GRK2
and AKT is an early and detrimental event in myocardial

ischemia/reperfusion," *EBioMedicine*, vol. 48, pp. 605–618,
2019.

[9] P. Balaganapathy, S. H. Baik, K. Mallilankaraman, D. G. Jo,
T. V. Arumugam, and C. G. Sobey, "Interplay between notch
and p53 promotes neuronal cell death in ischemic stroke,"
Journal of Cerebral Blood Flow and Metabolism, vol. 38,
no. 10, pp. 1781–1795, 2018.

[10] G. Pearson, F. Robinson, T. Beers Gibson et al., "Mitogen-acti-
vated protein (MAP) kinase pathways: regulation and physio-
logical functions," *Endocrine Reviews*, vol. 22, no. 2, pp. 153–
183, 2001.

[11] Y. Terada, S. Inoshita, H. Kuwana et al., "Important role of
apoptosis signal-regulating kinase 1 in ischemic acute kidney
injury," *Biochemical and Biophysical Research Communica-
tions*, vol. 364, no. 4, pp. 1043–1049, 2007.

[12] C. Wang, Z. Hao, J. Zhou, L. Zhang, Y. Sun, and C. Liang,
"Rutaecarpine alleviates renal ischemia reperfusion injury in
rats by suppressing the JNK/p38 MAPK signaling pathway
and interfering with the oxidative stress response," *Molecular
Medicine Reports*, vol. 16, no. 1, pp. 922–928, 2017.

[13] L. Wang, Z. Chen, X. Weng, M. Wang, Y. du, and X. Liu,
"Combined ischemic postconditioning and ozone postcondi-
tioning provides synergistic protection against renal ischemia
and reperfusion injury through inhibiting pyroptosis," *Urol-
ogy*, vol. 123, pp. 296.e1–296.e8, 2019.

[14] H. Liu, L. Wang, X. Weng et al., "Inhibition of Brd4 alleviates
renal ischemia/reperfusion injury-induced apoptosis and
endoplasmic reticulum stress by blocking FoxO4-mediated
oxidative stress," *Redox Biology*, vol. 24, article 101195, 2019.

[15] P. Jablonski, B. O. Howden, D. A. Rae, C. S. Birrell, V. C. Mar-
shall, and J. Tange, "An experimental model for assessment of
renal recovery from warm ischemia," *Transplantation*, vol. 35,
no. 3, pp. 198–204, 1983.

[16] H. Liu, Z. Chen, X. Weng et al., "Enhancer of zeste homolog 2
modulates oxidative stress-mediated pyroptosis in vitro and in
a mouse kidney ischemia-reperfusion injury model," *FASEB
Journal*, vol. 34, no. 1, pp. 835–852, 2020.

[17] A. Jamadar and R. Rao, "Glycogen synthase kinase-3 signaling
in acute kidney injury," *Nephron*, vol. 144, no. 12, pp. 609–612,
2020.

[18] N. Shiva, N. Sharma, Y. A. Kulkarni, S. R. Mulay, and A. B.
Gaikwad, "Renal ischemia/reperfusion injury: an insight on
in vitro and in vivo models," *Life Sciences*, vol. 256, article
117860, 2020.

[19] S. Kuboki, N. Sakai, C. Clarke et al., "The peptidyl-prolyl isom-
erase, Pin1, facilitates NF- κ B binding in hepatocytes and pro-
tects against hepatic ischemia/reperfusion injury," *Journal of
Hepatology*, vol. 51, no. 2, pp. 296–306, 2009.

[20] D. Feng, J. Yao, G. Wang et al., "Inhibition of p66Shc-mediated
mitochondrial apoptosis via targeting prolyl-isomerase Pin1
attenuates intestinal ischemia/reperfusion injury in rats," *Clini-
cal Science*, vol. 131, no. 8, pp. 759–773, 2017.

[21] S. H. Baik, M. Fane, J. H. Park et al., "Pin1 promotes neuronal
death in stroke by stabilizing Notch intracellular domain,"
Annals of Neurology, vol. 77, no. 3, pp. 504–516, 2015.

[22] P. Malko and L. H. Jiang, "TRPM2 channel-mediated cell
death: An important mechanism linking oxidative stress-
inducing pathological factors to associated pathological condi-
tions," *Redox Biology*, vol. 37, article 101755, 2020.

[23] S. Liu, Y. Yang, H. Gao et al., "Trehalose attenuates renal
ischemia-reperfusion injury by enhancing autophagy and

inhibiting oxidative stress and inflammation," *American Journal of Physiology. Renal Physiology*, vol. 318, no. 4, pp. F994–F1005, 2020.

[24] Y. Qiu, Y. Wu, H. Zhao, H. Sun, and S. Gao, "Maresin 1 mitigates renal ischemia/reperfusion injury in mice via inhibition of the TLR4/MAPK/NF-kappaB pathways and activation of the Nrf2 pathway," *Drug Design, Development and Therapy*, vol. 13, pp. 739–745, 2019.

[25] J. M. Kyriakis and J. Avruch, "Mammalian mitogen-activated protein kinase signal transduction pathways activated by stress and inflammation," *Physiological Reviews*, vol. 81, no. 2, pp. 807–869, 2001.

[26] M. I. Ashraf, M. Ebner, C. Wallner et al., "A p38MAPK/MK2 signaling pathway leading to redox stress, cell death and ischemia/reperfusion injury," *Cell Communication and Signaling*, vol. 12, no. 1, p. 6, 2014.

[27] R. Dong, Z. Xue, G. Fan et al., "Pin1 promotes NLRP3 inflammasome activation by phosphorylation of p38 MAPK pathway in septic shock," *Frontiers in Immunology*, vol. 12, article 620238, 2021.

Research Article

miRNA-146a Mimic Inhibits NOX4/P38 Signalling to Ameliorate Mouse Myocardial Ischaemia Reperfusion (I/R) Injury

Lili Xiao [ID],[1] **Yulei Gu** [ID],[2] **Gaofei Ren** [ID],[3] **Linlin Chen** [ID],[1] **Liming Liu** [ID],[1] **Xiaofang Wang** [ID],[1] **and Lu Gao** [ID][1]

[1]*Department of Cardiology, The First Affiliated Hospital of Zhengzhou University, Zhengzhou, Henan Province, China*
[2]*Emergency Intensive Care Unit, The First Affiliated Hospital of Zhengzhou University, Zhengzhou, Henan Province, China*
[3]*Endocrinology Department, The First Affiliated Hospital of Zhengzhou University, Zhengzhou, Henan Province, China*

Correspondence should be addressed to Yulei Gu; guyulei@live.com and Lu Gao; gaomei1215@163.com

Evidence suggests that miR-146a is implicated in the pathogenesis of cardiovascular diseases; however, the role of miR-146a in myocardial ischaemia reperfusion (I/R) injury is unclear. The aim of this study was to explore the functional role of miR-146a in myocardial ischaemia reperfusion injury and the underlying mechanism. C57BL/6J mice were subjected to 45 min of ischaemia and 1 week of reperfusion to establish a myocardial I/R injury model. A miR-146a mimic (0.5 mg/kg) was administered intravenously at the beginning of the ischaemia process. Neonatal rat cardiomyocytes were also subjected to hypoxia/reperfusion (H/R). Cells were treated with the miR-146a mimic or antagonist. As a result, the miR-146a mimic attenuated H/R-induced cardiomyocyte injury, as evidenced by increased cell viability and reduced lactate dehydrogenase (LDH) levels. In addition, the miR-146a mimic inhibited oxidative stress in cells suffering from H/R injury. Moreover, the miR-146a antagonist exerted adverse effects in vitro. In mice with myocardial I/R injury, the miR-146a mimic preserved cardiac function and reduced the infarction area and fibrosis. Moreover, the miR-146a mimic decreased the inflammatory response and reactive oxygen species (ROS) accumulation in mouse hearts. Mechanistically, we found that miR-146a directly regulated the transcription of NOX4, which subsequently affected P38 signalling in cardiomyocytes. When we knocked down NOX4, the effects of the miR-146a antagonist in worsening the cell condition were counteracted in in vitro experiments. Taken together, the results suggest that miR-146a protects against myocardial ischaemia reperfusion injury by inhibiting NOX4 signalling. The miR-146a mimic may become a potential therapeutic approach for patients with myocardial ischaemia reperfusion.

1. Introduction

In clinical emergencies worldwide, the incidence of acute myocardial infarction (AMI) is particularly alarming, ranking first in the world. The most effective way to reduce early AMI injury and infarction is timely coronary revascularization via thrombolytic therapy or percutaneous coronary stent implantation (PCI) [1]. Although myocardial reperfusion is a recognized method of reducing injury, myocardial reperfusion itself can trigger a variety of pathological reactions, leading to myocardial cell death [2]. The mechanisms underlying myocardial ischemia reperfusion injury (IRI) include oxidative stress, Ca^{2+} overload, and mitochondrial permeability

transition pore (mPTP) opening [3]. It has been proven difficult to translate cardioprotective measures into clinical practice. Although ischaemic conditioning strategies are promising, their transformation effect is weak [4]. Therefore, it is very important to explore the mechanism underlying IRI and identify new cardioprotective measures.

The reactive oxygen species (ROS) burst during myocardial reperfusion is the primary cause of myocardial cell death, leading to the opening of the mPTP, which plays a critical role in reperfusion damage [5]. Oxidative stress can affect the expression level of miRNAs, and miRNAs can regulate oxidative stress by regulating the expression of redox sensor proteins [6]. Although miRNAs do not encode proteins, they

play a key role in the regulation of gene expression at the posttranscriptional level [6]. miR-146a has been widely recognized as a critical regulatory element in the cardiovascular system. miR-146a was reported to regulate mitochondrial function in a myocardial infarction mouse model [7, 8]. miR-146a also protected against myocardial fibrosis in a rat constrictive pericarditis model [8]. miR-146a protected against doxorubicin-induced cardiotoxicity by modulating autophagy [9].

All this evidence suggests a protective effect of miRNA-146a in cardiovascular disease. In this study, we aimed to explore whether a miRNA-146a mimic could protect against myocardial reperfusion injury as well as the underlying mechanism.

2. Methods

2.1. Animals. C57BL/6J male mice (8 weeks old, 24-25 g) were purchased from the Chinese Academy of Medical Sciences (Beijing, China) and raised in the SPF Laboratory Animal Center of Zhengzhou University. The mice were divided into 4 groups ($n = 12$ for each group): vehicle-sham, miR-146a mimic-sham, vehicle-I/R, and miR-146a mimic-I/R. The mice were administered with intracoronary injections of 0.5 mg/kg miR-146a mimics (mmu-miR-146a, Fermentas GmbH, Germany) formulated [10] as lipoplexes with DMAPAP/DOPE cationic liposomes at the beginning of ischaemia [11]. The control mice were injected with lipoplexes containing irrelevant miRNA mimics. All the animal experiments were approved by the Institutional Animal Care and Use Committee of Zhengzhou University (Zhengzhou, China).

2.2. Animal Model. The model of I/R injury was established by 45 min of ischaemia and 1 week of reperfusion. Left coronary artery ligation surgery (LAD) was conducted according to previously published protocols [12, 13]. In short, after anaesthetization, the mouse chest was opened on the left side between the third and fourth intercostal spaces. After opening the pericardium, the proximal descending branch of the LAD was ligated with 7~0 silk thread. After 45 min of ischaemia, the ligation was released, and the heart was reperfused for 1 week. The LAD was not ligated in the sham group.

2.3. Echocardiographic Evaluation. Transthoracic echocardiography was performed as previously described [13, 14]. Isoflurane (1.5%) was used to anaesthetize the mice, and echocardiography was performed with a 10 MHz linear array ultrasound transducer to obtain M-mode echocardiography data. The left ventricle (LV) end-diastolic dimension (LVEDd) and LV end-systolic dimension (LVESd) were obtained, and the LV ejection fraction (LVEF) and LV fractional shortening (LVFS) values were calculated. A total of 10 mice from each group were subjected to transthoracic echocardiography.

2.4. Triphenyltetrazolium Chloride, PSR Staining, and Immunofluorescence Staining. Triphenyltetrazolium chloride (TTC, 1%, Sigma, USA) staining was used to evaluate the MI area and morphological changes in the heart. The hearts were cut into 1-2 mm thick myocardial sections along the long axis

of the heart. For the infarct area calculation, Image-Pro Plus 6.0 was used to analyse 5 sections from each heart and 6 hearts from each group. PSR staining was used to show the collagen volume. For the fibrosis area calculation, Image-Pro Plus 6.0 was used to analyse 6 sections from each heart and 6 hearts from each group. Macrophages were subjected to immunofluorescence staining to assess CD68 expression. After dehydration, antigen repair was conducted at a high temperature and pressure, and the sections were sealed with 8% goat serum. The heart sections were incubated with an anti-CD68 antibody (Abcam, 1 : 100 dilution). A secondary antibody, goat anti-rabbit IRdye 800CW (LI-COR), was used. The nucleus was stained with DAPI. We counted the number of CD68-positive cells in each group (10 fields for each heart). Dihydroethidium (DHE) staining (Sigma-Aldrich) was performed to identify intracellular ROS production. Mean DHE fluorescence was calculated by subtracting the integrated density of the background signal from the integrated density of the fluorescent staining from 10 fields/heart and 5 hearts/group, and the results were normalized to the control.

2.5. Cardiomyocyte Isolation and Culture. Neonatal rat cardiomyocyte (NRCM) culture was performed as previously described [13, 14]. Briefly, the hearts of Sprague-Dawley rats (1-3 days old) were quickly removed, and ventricles were preserved and digested with 0.125% trypsin-EDTA (Gibco) 4 times for 15 min each time. Digestion was stopped with DMEM-F12 supplemented with 15% foetal bovine serum (FBS, Gibco, USA). After 5 digestion reactions, the cells were collected and incubated in a 100 mm dish with DMEM-F12 supplemented with 15% FBS. After 90 min, the cell culture medium was collected, and NRCMs in the upper layer of the cell medium were removed and seeded onto a 6-well plate to exclude the noncardiac myocytes that adhered to the bottom of the 100 mm dish. NRCMs were identified by α-actin staining.

For the H/R model, cardiomyocyte culture medium was converted into H/R buffer (4 mM HEPES, 12 mM KCl, 117 mM NaCl, 0.49 mM MgCl$_2$, 0.9 mM CaCl$_2$, 20 mM sodium lactate, and 5.6 mM 2-deoxyglucose, pH 6.2) and placed in a hypoxic chamber (95% N$_2$/5% CO$_2$, Billups-Rothenberg) at 37°C for 30 min [15]. The chamber was closed, and a normal oxygen supply was added for an additional 4 hours, followed by reperfusion with DMEM supplemented with 10% FBS. NRCMs were transfected with miR-146a mimics, miR-146a inhibitor (Exiqon, Denmark), or their corresponding negative controls at a final concentration of 50 nM for 24 h using Lipofectamine 2000 before the H/R model was established in accordance with the manufacturer's instructions. NRCMs were transfected with NOX4 siRNA (RiboBio, China) to knock down NOX4. Cell viability was detected with a CCK8 kit (Beyotime Biotechnology, Shanghai, China) with a microplate reader measuring the intensity of the light absorption at 450 nm wavelength.

2.6. ELISA Detection of Inflammatory Cytokines. The tumour necrosis factor α (TNFα) and interleukin- (IL-) 1 levels in mouse hearts and cardiomyocytes were detected with ELISA purchased from BioLegend (430901, 432604). An ELISA
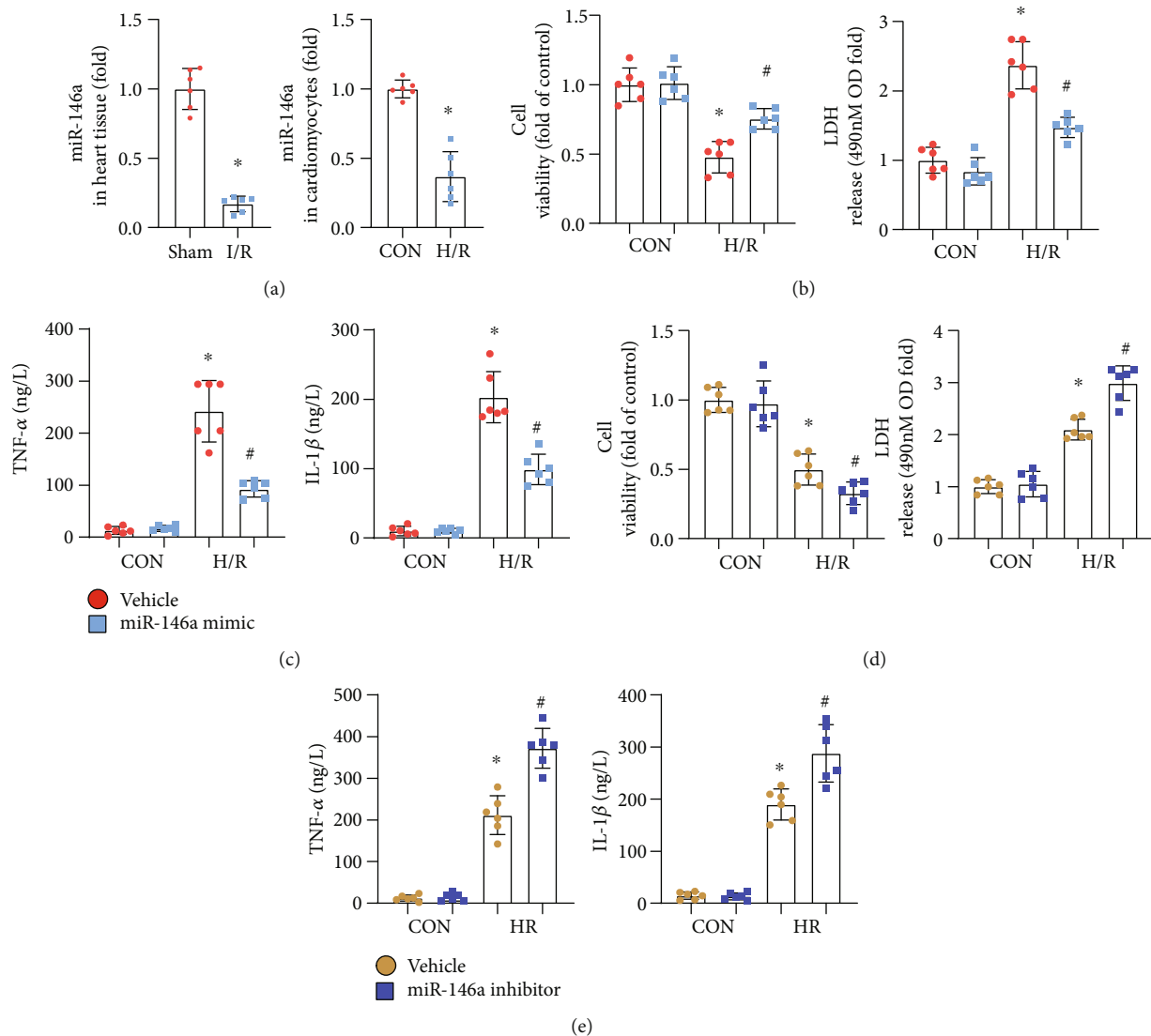
Figure 1: miR-146a protects NRCMs from H/R-induced inflammation. (a) The mRNA level of miR-146a in heart tissue after I/R injury ($n = 6$) and in cardiomyocytes after H/R injury ($n = 6$). (b, c) NRCMs were transfected with the miR-146a mimic and subjected to H/R injury. (b) Cell viability detected by the CKK8 assay and LDH release in each group ($n = 6$). (c) TNFα and IL-1β production in cells detected by the ELISA ($n = 6$). *$P < 0.05$ vs. vehicle-CON; #$P < 0.05$ vs. vehicle-H/R. (d, e) NRCMs were transfected with the miR-146a inhibitor and subjected to H/R injury. (d) Cell viability detected by the CKK8 assay and LDH release in each group ($n = 6$). (e) TNFα and IL-1β production in cells detected by ELISA ($n = 6$). *$P < 0.05$ vs. vehicle-CON; #$P < 0.05$ vs. vehicle-H/R. Cell experiments were repeated for 3 times. Unpaired Student's t-test was used in (a); two-way analysis of variance was used in (b)–(e).

instrument (Synergy HT, BioTek, United States) was used to measure the absorbance.

2.7. Oxidative Stress Assessment.

The activities of manganese superoxide dismutase, superoxide dismutase 2 (MnSOD), nicotinamide adenine dinucleotide phosphate (NADPH) oxidase, and malondialdehyde (MDA) in heart tissues and cardiomyocytes were detected by using corresponding kits purchased from Beyotime (Shanghai, China) according to the manufacturer's instructions [13]. The level of ROS was measured according to a previous study [16] using $2',7'$-dichlorofluorescin diacetate (DCFH-DA) and an ELISA plate reader (Synergy HT, BioTek, Vermont, USA).

2.8. Cardiac Troponin I (cTNI) and Lactate Dehydrogenase (LDH) Release.

After 2 hours of reperfusion, venous blood was collected and centrifuged at 4000 r/min at 4°C for 10 min, and serum was collected to detect the concentration of cTNI. All the procedures were performed in accordance with the instructions of the kit (Nanjing Jiancheng Biological Company) with an ELISA plate reader (Synergy HT, BioTek, Vermont, USA). The levels of LDH released were detected in the cell supernatant using an LDH release assay kit (Nanjing Jian) according to the manufacturer's instructions.

2.9. Western Blotting and qPCR.

Total protein was isolated from heart tissues and NRCMs and then subjected to SDS-PAGE (50 μg per sample). After transfer onto Immobilon
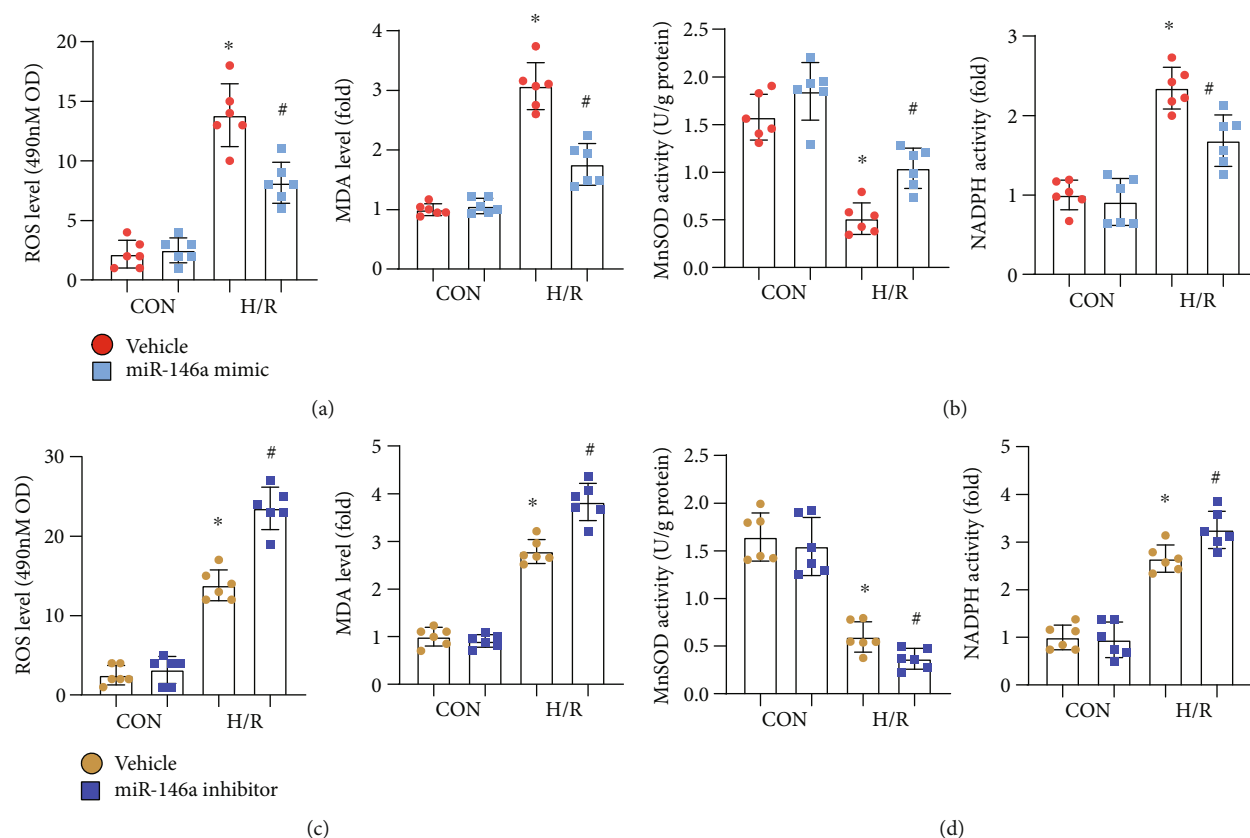
FIGURE 2: miR-146a protects NRCMs from H/R-induced oxidative stress. (a, b) NRCMs were transfected with the miR-146a mimic and subjected to H/R injury. (a) ROS level detected by the $2',7'$-dichlorofluorescin diacetate probe and MD level in each group ($n = 6$). (b) MnSOD and NADPH oxidase activity in cells ($n = 6$). $^*P < 0.05$ *vs.* vehicle-CON; $^#P < 0.05$ *vs.* vehicle-H/R. (c, d) NRCMs were transfected with the miR-146a inhibitor and subjected to H/R injury. (c) ROS level detected by the $2',7'$-dichlorofluorescin diacetate probe and MD level in each group ($n = 6$). (d) MnSOD and NADPH oxidase activity in cells ($n = 6$). $^*P < 0.05$ *vs.* vehicle-CON; $^#P < 0.05$ *vs.* vehicle-H/R. Cell experiments were repeated for 3 times. Two-way analysis of variance followed by Tukey's post hoc test was used.

membranes (Millipore, Billerica, MA, USA), proteins were incubated overnight at 4°C with primary antibodies against NOX2 (ab129068) and NOX4 (ab133303), which were purchased from Abcam (1 : 1000 dilution), and phosphorylated and total P38 (4511P/9212P) and GAPDH (2118), which were purchased from Cell Signaling Technology (1 : 1000 dilution). The blots were developed with enhanced chemiluminescence (ECL) reagents (Bio-Rad, Hercules, CA, USA), and images were captured by using a ChemiDoc MP Imaging System (Bio-Rad). GAPDH served as an internal reference protein.

Total RNA (2 μg per sample) from frozen mouse heart tissue and cardiomyocytes was reverse transcribed into cDNA using oligonucleotide (DT) primers and a transcript first-strand cDNA synthesis kit (Roche). Then, a LightCycler 480 instrument (software version 1.5, Roche) and SYBR Green PCR Master Mix (Roche) were used to perform RT-PCR. All the genes were normalized using GAPDH.

2.10. Luciferase Assay. The full-length $3'$UTR of NOX4 was amplified by PCR (forward: $5'$-CGCCTCCCGGGTTTGC ACCACTCTCCTGCCTCAGCCTCCTG-$3'$; reverse: $5'$-ATCATTTTTATTGTCTCAAGAAGAACTTAATAGCAA TTAG-$3'$). The NOX4 $3'$-UTR sequences were inserted into the pmirGLO vector (Guangzhou Boxin Biotechnology Co., Ltd.). The empty particle vector was used as control. NRCMs were cotransfected with the reporter plasmid, miR-146a mimic, inhibitor, or negative controls for 24 h. A GloMax® 20/20 Luminometer (Promega) was used to detect luciferase.

2.11. Statistical Analysis. All the data are expressed as the mean ± SD. Differences among groups were analysed by two-way analysis of variance followed by Tukey's post hoc test. Comparisons between two groups were analysed by unpaired Student's *t*-test. P values less than 0.05 indicated statistical significance.

3. Results

3.1. miR-146a Protects NRCMs from H/R-Induced Inflammation. We first evaluated the expression of miR-146a in heart tissues and cardiomyocytes after I/R injury. miR-146a expression was reduced in heart tissue after I/R injury and decreased in cardiomyocytes after H/R injury (Figure 1(a)). We then evaluated the effect of the miR-146a mimic on H/R injury in cardiomyocytes. As shown in Figure 1(b), cell viability was reduced in H/R cardiomyocytes, while the miR-146a mimic increased cell viability when cells
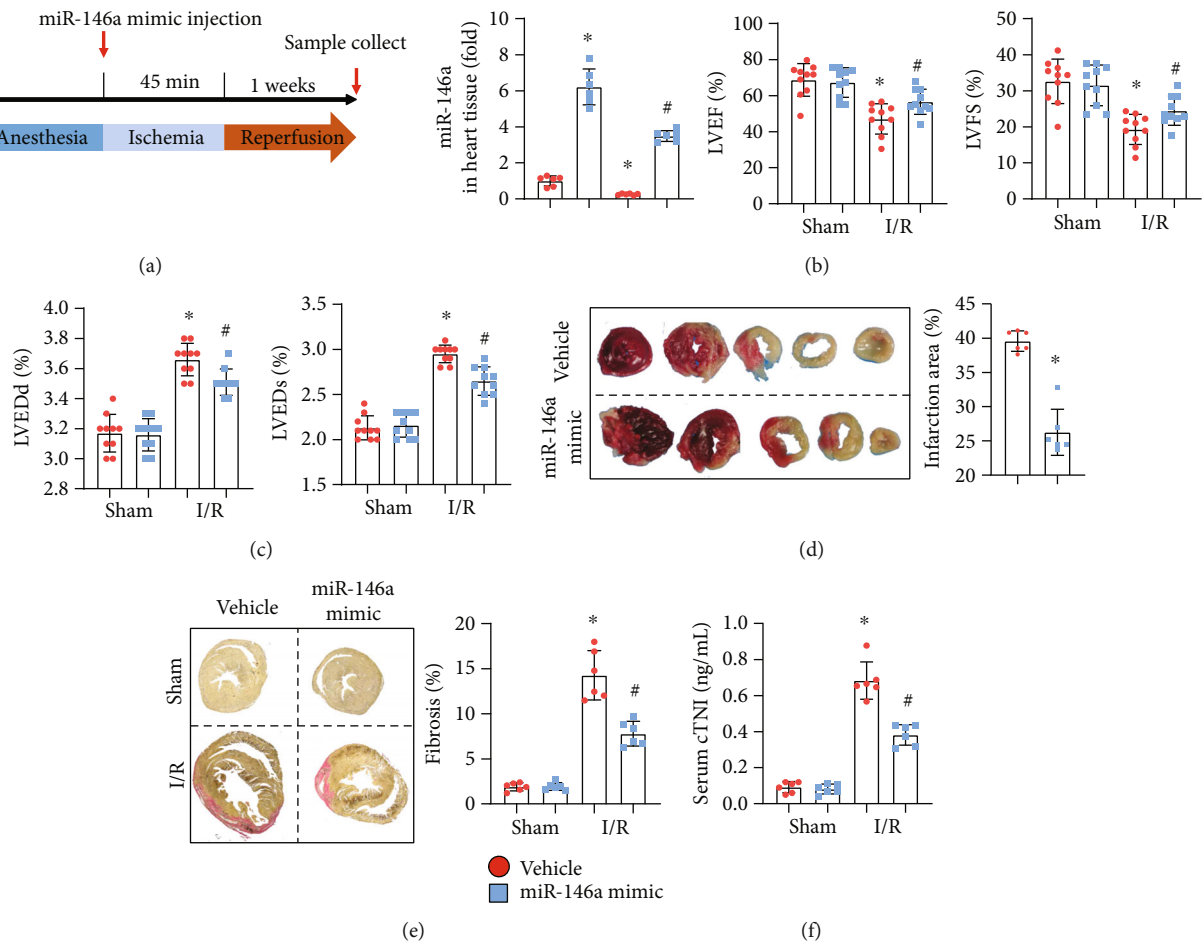
(a)

(b)

(c)

(d)

(e)

(f)

FIGURE 3: miR-146a mimic attenuates mouse I/R injury. (a) The procedure of mouse experiments. (b) The mRNA level of miR-146a in mouse heart 1 week after injection ($n = 6$). (c) Echocardiography results of LVEF, LVFS, LVEDd, and LVESd in each group ($n = 10$). (d) TTC staining image and quantitative results ($n = 6$). (e) PSR staining image and quantitative results ($n = 6$). (f) cTNI concentration in mouse serum 2 h after I/R injury. $^*P < 0.05$ vs. vehicle-sham; $^\#P < 0.05$ vs. vehicle-I/R. Two-way analysis of variance was used in (b), (c), (e), and (f). Unpaired Student's t-test was used in (d).

were treated with the miR-146a mimic before exposure to H/R injury. In addition, cells treated with the miR-146a mimic showed less LDH release and reduced TNFα and IL-1 levels (Figure 1(c)). These results suggest that the miR-146a mimic could attenuate H/R-induced cardiomyocyte injury and inflammation. Next, we explored the role of the miR-146a inhibitor. The miR-146a inhibitor exacerbated cardiomyocyte H/R injury, as assessed by lower cell viability and higher LDH release (Figure 1(d)) as well as higher TNFα and IL-1 levels (Figure 1(e)) than the vehicle-treated group. These data suggest that miR-146a protects against cardiomyocyte H/R injury.

3.2. miR-146a Protects NRCMs from H/R-Induced Oxidative Stress.
Oxidative stress is the main cause of cell death in I/R injury. We then detected whether miR-146a influences the redox balance in cardiomyocyte H/R injury. ROS levels were reduced in cells treated with the miR-146a mimic (Figure 2(a)). The levels of MDA, the intermediate metabolite of lipid peroxidation, were also lower in cells treated with the miR-146a mimic (Figure 2(a)). The antioxidant activity

and MnSOD activity were elevated, but NADPH oxidase activity was reduced in cells treated with the miR-146a mimic (Figure 2(b)). In cells treated with the miR-146a inhibitor, the ROS level was elevated (Figure 2(c)) after H/R injury. In addition, MDA levels and NADPH oxidase activity were also increased, while MnSOD activity was decreased in cells treated with the miR-146a inhibitor (Figure 2(d)). Thus, miR-146a protects against cardiomyocyte H/R injury by inhibiting oxidative stress.

3.3. miR-146a Mimic Attenuates Mouse I/R Injury.
Mice were subjected to I/R injury to confirm the protective effect of miR-146a in vivo. The miR-146a mimic was injected into mice at the beginning of ischaemia. One week postreperfusion, mice were subjected to echocardiogram to detect cardiac function (Figure 3(a)). miR-146a expression was upregulated in mouse hearts in both the sham group and the I/R group (Figure 3(b)). LVEF and LVFS were reduced in the I/R group, while LVEDd and LVEDs were elevated in the I/R group compared to the sham group. Mice in the miR-146a mimic group showed improved cardiac function,
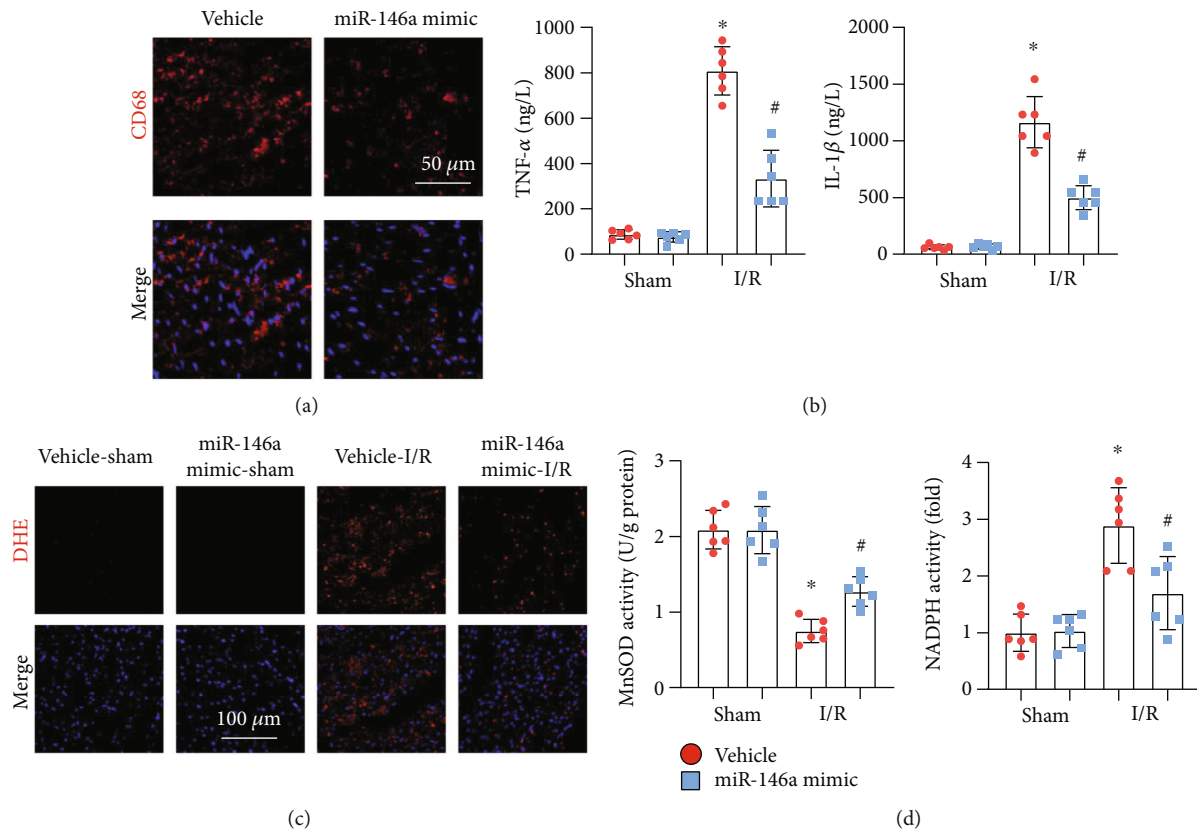
(a)

(b)

(c)

(d)

FIGURE 4: miR-146a mimic inhibits inflammation and oxidative stress in I/R mice. (a) CD68 staining in heart tissue image ($n = 6$). (b) TNFα and IL-1β production in heart tissue in mice with miR-146a mimic treatment ($n = 6$). (c) ROS level detected by DHE staining in heart tissue ($n = 6$). (d) MnSOD and NADPH oxidase activity in heart tissue ($n = 6$). $^*P < 0.05$ vs. vehicle-sham; $^\#P < 0.05$ vs. vehicle-I/R. Two-way analysis of variance was used in (b) and (d).

as assessed by increased LVEF and LVFS and reduced LVEDd and LVESd (Figure 3(c)). The infarction area was also detected by TTC staining. Mice treated with the miR-146a mimic showed diminished infarction size (Figure 3(d)). The fibrotic area was also diminished in mice treated with the miR-146a mimic, as assessed by PSR staining (Figure 3(e)). After 2 hours of reperfusion, the serum cTNI level was reduced in miR-146a mimic-treated mice compared with vehicle-treated mice (Figure 3(f)).

3.4. miR-146a Mimic Inhibits Inflammation and Oxidative Stress in I/R Mice. Inflammation and oxidative stress were also assessed in vivo. The miR-146a mimic decreased the inflammatory response, as evidenced by reduced CD68-labelled macrophage infiltration and reduced levels of TNFα and IL-1 (Figures 4(a) and 4(b)). The miR-146a mimic also decreased the ROS level in I/R-injured hearts, as assessed by DHE staining (Figure 4(c)). The miR-146a mimic increased MnSOD activity and diminished NADPH oxidase activity in mouse hearts after I/R injury (Figure 4(d)).

3.5. miR-146a Affects NOX4-P38 Signalling. To explore the mechanism by which miR-146a inhibits oxidative stress, we detected the levels of proteins associated with ROS production and found that NOX4 but not NOX2, the main subtype of NADPH oxidase expressed in hearts, was inhibited by

miR-146a (Figure 5(a)). We also observed that miR-146a reduced the NOX4 level in cardiomyocytes suffering from H/R injury (Figure 5(b)). We then detected whether miR-146a affects NOX4 at the transcriptional level. qPCR results revealed that miR-146a reduced the transcription of NOX4 but not NOX2 in cardiomyocytes (Figure 5(c)). We then hypothesized that miR-146a may directly regulate the promoter region of NOX4 to inhibit its transcription. To test our hypothesis, we performed the luciferase assay. As shown in Figure 5(d), we observed a significant decrease in NOX4-Luc transcriptional activity in miR-146a-treated cells. The use of the miR-146a inhibitor increased NOX4-Luc transcriptional activity.

3.6. NOX4 Silencing Abolishes the Effect of the miR-146a Inhibitor. To confirm the targeting role of miR-146a in NOX4, we performed reverse experiments in vitro. Cells were treated with NOX4 siRNA to knock down NOX4 and with the miR-146a inhibitor. In cells treated with NOX4 siRNA, the expression of NOX4 was decreased significantly (Figure 6(a)). NOX4 knockdown relieved cardiomyocyte H/R injury, as assessed by increased cell viability, reduced LDH release, and diminished TNFα and IL-1 levels (Figures 6(b) and 6(c)). NOX4 knockdown dramatically reduced ROS levels and increased MnSOD activity (Figure 6(d)). However, cells treated with both the miR-146a inhibitor and NOX4 siRNA
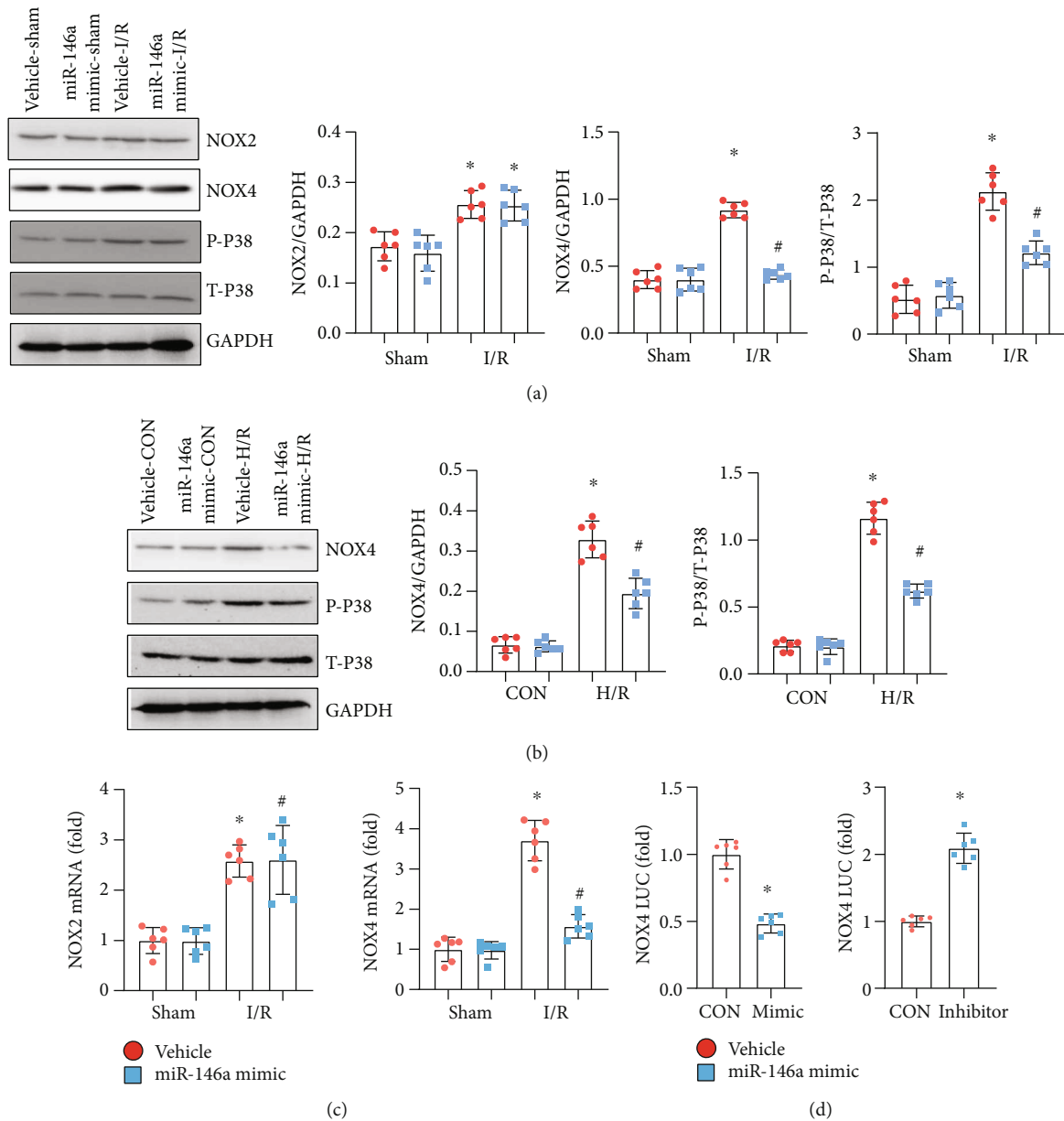
FIGURE 5: miR-146a affects NOX4-P38 signalling. (a) Protein level of NOX2, NOX4, phosphorylated- (P-) P38, and total- (T-) P38 in heart tissue in mice with miR-146a mimic treatment ($n = 6$). (b) Protein level of NOX4, P-P38, and T-P38 in NRCMs transfected with the miR-146a mimic ($n = 6$). (c) mRNA level of NOX2 and NOX4 in NRCMs transfected with the miR-146a mimic ($n = 6$). (d) Luciferase assay in NRCMs transfected with the miR-146a mimic and miR-146a inhibitor ($n = 6$). Cell experiments were repeated for 3 times. $^{*}P < 0.05$ *vs.* vehicle-sham/CON; $^{\#}P < 0.05$ *vs.* vehicle-I/R or vehicle-H/R. Two-way analysis of variance was used in (a)–(c). Unpaired Student's *t*-test was used in (d).

showed no deteriorating H/R injury, as determined by the same extent of increased cell viability and reduced LDH release, inflammation, and oxidative stress compared with cells treated merely with NOX4 siRNA (Figures 6(b)–6(d)). These data indicate that miR-146a protects against myocardial I/R injury by targeting NOX4 expression.

4. Discussion

Myocardial ischaemia-reperfusion injury is organ damage caused by reopening of the blood supply after acute myocar-

dial infarction [4]. During myocardial ischaemia, limited oxygen supply is associated with acidosis, energy consumption, and ion homeostasis changes, leading to cell death and cardiac dysfunction [2]. During reperfusion, in the presence of oxygen, ROS are produced in the myocardium [17]. Several miRNAs have been reported to regulate the redox system [6]. Among these, miR-146a is reported as a negative regulator of many cardiovascular diseases, such as myocardial infarction, doxorubicin-induced cardiotoxicity, and cardiac fibrosis in a constrictive pericarditis model [7–9]. Studies have described that miR-146a negatively regulates ROS

FIGURE 6: NOX4 silencing abolishes the effect of the miR-146a inhibitor. (a) NRCMs were transfected with NOX4 siRNA ($n = 6$). The protein level of NOX4 after 48 h of transfection ($n = 6$). $^*P < 0.05$ $vs.$ ScRNA. (b–d) NRCMs were transfected with the miR-146a inhibitor and/or NOX4 siRNA and subjected to H/R injury. (b) Cell vi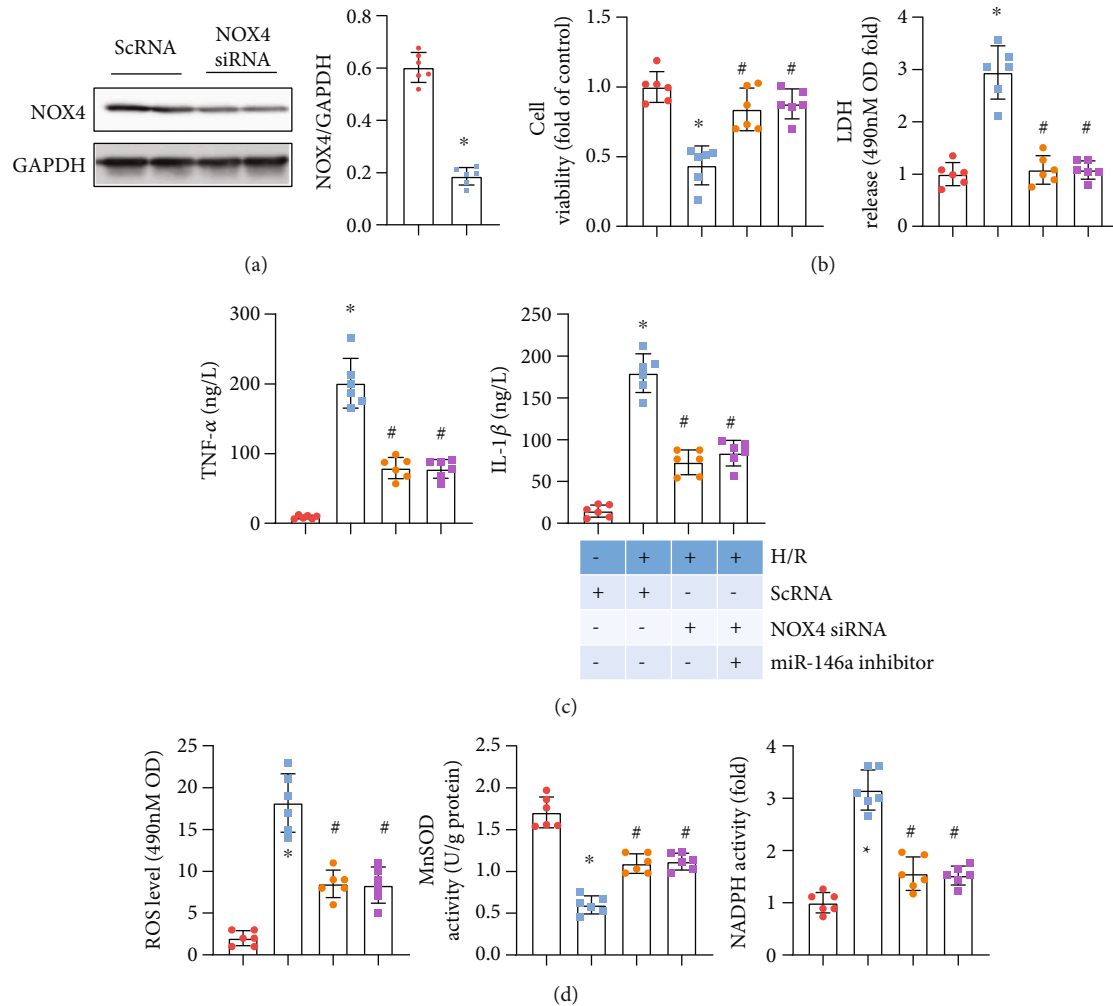ability detected by the CKK8 assay and LDH release in each group ($n = 6$). (c) TNFα and IL-1β production in cells detected by ELISA ($n = 6$). (d) ROS level and MnSOD and NADPH oxidase activity in cells ($n = 6$). $^*P < 0.05$ $vs.$ ScRNA-CON; $^\#P < 0.05$ $vs.$ ScRNA-H/R. Cell experiments were repeated for 3 times. Unpaired Student's t-test was used in (a); one-way analysis of variance was used in (b)–(d).

generation in H9c2 cardiomyocytes [18]. Here, in this study, we demonstrated that the miR-146a mimic could ameliorate cardiomyocyte H/R injury, while the miR-146a inhibitor aggravated cardiomyocyte H/R injury. We specify in vivo that the miR-146a mimic could relieve myocardial I/R injury after 45 min of ischaemia and 1 week of reperfusion, reduce the infarction area and fibrosis area, and improve cardiac function.

During IR, ROS are mainly produced by the mitochondrial respiratory chain and NOx family enzymes. Other sources of ROS include xanthine oxidase (XO) and uncoupled nitric oxide synthase (NOS) [19]. To date, seven NOx subtypes (NOX1-5 and duox1-2) have been identified, among which NOX2 and NOX4 are the most abundantly expressed in the heart [20]. NOX2- and NOX4-mediated oxidative damage is very important during reperfusion. Oxygen supply during reperfusion provides a substrate for NOX-mediated ROS production [17]. Cardiac-specific

NOX4-knockout mice showed decreased ROS and infarct size after IR, suggesting that NOX4 in cardiomyocytes plays a major role in mediating IR injury [21]. Surprisingly, mice with both NOX2 and NOX4 double knockout exhibited exacerbated myocardial injury [21]. A previous study reported that a miR-146a-5p mimic increased ROS production in SH-SY5Y cells [22]. However, An et al. reported that overexpression of miR-146a reduced ROS generation in H9c2 cardiomyocytes by increasing ErbB4 [18]. This paradox may account for different cell types as well as different miR-146 induction. In this study, we found that the miR-146a mimic decreased H/R- and I/R-induced ROS generation in cardiomyocytes and mouse hearts. Moreover, the miR-146a mimic reduced the level of MDA and diminished NADPH oxidase activity. Furthermore, we found that miR-146 directly inhibited the transcription level of NOX4 in cardiomyocytes. Recently, Wang et al. found that miRNA-146a inhibits NOX4 transcription in endothelial cells [23]. miR-146a was

also reported to regulate NOX4-ROS in the human kidney cell line HK-2 [24]. In our study, we found that miR-146a could target the promoter region of NOX4 in cardiomyocytes. The miR-146a inhibitor enhanced the transcription level of NOX4. NOX4 silencing abolished the effects of the miR-146a inhibitor. This suggests that miR-146a inhibits ROS generation by directly inhibiting the transcription of NOX4, thus exerting cardioprotective effects during myocardial IR injury. However, the baseline expression of NOX4 was not changed after miR-146a mimic treatment, and other factors may regulate the transcription and translation of NOX4 under physiological conditions.

We also observed a reduction in inflammation in miR-146a mimic-treated mice and cardiomyocytes. During the myocardial infarction phase, acute inflammation leads to endothelial dysfunction and left ventricular pathological remodelling [25]. During the reperfusion phase, ROS can directly mediate the recruitment of neutrophils to the vascular inflammatory region and increase the inflammatory cascade by releasing various cytokines, leading to the activation of resident immune cells in heart tissue [26]. The anti-inflammatory effect of the miR-146a mimic may be a secondary result of anti-ROS generation. Reduced ROS could decrease the activation of immune cells and reduce cardiomyocyte injury. We observed that the number of CD68-labelled macrophages was reduced after miR-146a mimic injection. The inflammatory response in cardiomyocytes itself was also inhibited by the miR-146a mimic. Another anti-inflammatory effect of miR-146a may occur via P38 inhibition. P38, as a family of MAPK cascades, responds to stresses, such as oxidant stress, osmotic shock, infection, and cytokine exposure. P38 is rapidly activated within a few minutes of exposure to ROS, and P38 inhibition is reported to be sufficient to achieve anti-inflammatory effects in the heart [27]. We observed reduced P38 phosphorylation in miR-146a mimic-treated cardiomyocytes and mouse hearts. P38 injection may be a second effect of miR-146a on NOX4. The reduced P38 activation in the miR-146a mimic may be mediated by ROS inhibition, subsequently leading to inflammation inhibition in the heart.

Taken together, these results show that the miR-146a mimic protects against myocardial IR injury via the NOX4-ROS pathway, and the miR-146a mimic may become a promising treatment approach for patients with AMI who are subjected to coronary revascularization.

Data Availability

Data are available on request.

Conflicts of Interest

The authors declare no conflicts of interest.

Acknowledgments

References

[1] S. M. Davidson, P. Ferdinandy, I. Andreadou et al., "Multitarget Strategies to Reduce Myocardial Ischemia/Reperfusion Injury:," *Journal of the American College of Cardiology*, vol. 73, no. 1, pp. 89–99, 2019.

[2] N. B. Liu, M. Wu, C. Chen et al., "Novel molecular targets participating in myocardial ischemia-reperfusion injury and cardioprotection," *Cardiology Research and Practice*, vol. 2019, Article ID 6935147, 16 pages, 2019.

[3] A. Bellis, C. Mauro, E. Barbato et al., "The rationale of neprilysin inhibition in prevention of myocardial ischemia-reperfusion injury during ST-elevation myocardial infarction," *Cell*, vol. 9, no. 9, p. 2134, 2020.

[4] Y. Wu, H. Liu, and X. Wang, "Cardioprotection of pharmacological postconditioning on myocardial ischemia/reperfusion injury," *Life Sciences*, vol. 264, pp. 118628–118628, 2021.

[5] K. Bugger HPfeil, "Mitochondrial ROS in myocardial ischemia reperfusion and remodeling," *Biochimica et Biophysica Acta - Molecular Basis of Disease*, vol. 1866, no. 7, article 165768, 2020.

[6] T. Carbonell and A. V. Gomes, "MicroRNAs in the regulation of cellular redox status and its implications in myocardial ischemia-reperfusion injury," *Redox Biology*, vol. 36, article 101607, 2020.

[7] Q. Su, Y. Xu, R. Cai et al., "miR-146a inhibits mitochondrial dysfunction and myocardial infarction by targeting cyclophilin D," *Molecular Therapy - Nucleic Acids*, vol. 23, pp. 1258–1271, 2021.

[8] Y. Xiao, W. Qiao, X. Wang, L. Sun, and W. Ren, "miR-146a mediates TLR-4 signaling pathway to affect myocardial fibrosis in rat constrictive pericarditis model," *Journal of Thoracic Disease*, vol. 13, no. 2, pp. 935–945, 2021.

[9] J. A. Pan, Y. Tang, J. Y. Yu et al., "miR-146a attenuates apoptosis and modulates autophagy by targeting TAF9b/P53 pathway in doxorubicin-induced cardiotoxicity," *Cell Death & Disease*, vol. 10, no. 9, p. 668, 2019.

[10] M. Ammari, J. Presumey, C. Ponsolles et al., "Delivery of miR-146a to Ly6ChighMonocytes inhibits pathogenic bone erosion in inflammatory arthritis," *Theranostics*, vol. 8, no. 21, pp. 5972–5985, 2018.

[11] H. Fang, N. C. Lai, M. H. Gao et al., "Comparison of adeno-associated virus serotypes and delivery methods for cardiac gene transfer," *Human Gene Therapy Methods*, vol. 23, no. 4, pp. 234–241, 2012.

[12] L. Zhang, X. Wang, H. Zhang et al., "Exercise-induced peptide EIP-22 protect myocardial from ischaemia/reperfusion injury via activating JAK2/STAT3 signalling pathway," *Journal of Cellular and Molecular Medicine*, vol. 25, no. 7, pp. 3560–3572, 2021.

[13] Y. Gu, X. Hu, P. B. Ge, Y. Chen, S. Wu, and X. W. Zhang, "CTRP1 aggravates cardiac dysfunction post myocardial infarction by modulating TLR4 in macrophages," *Frontiers in Immunology*, vol. 12, article 635267, 2021.

[14] J. Zong, F. F. Li, K. Liang et al., "Nuclear localization leucine-rich-repeat protein 1 deficiency protects against cardiac hypertrophy by pressure overload," *Cellular Physiology and Biochemistry*, vol. 48, no. 1, pp. 75–86, 2018.

[15] L. Jiang, X. Yin, Y. H. Chen et al., "Proteomic analysis reveals ginsenoside Rb1 attenuates myocardial ischemia/reperfusion injury through inhibiting ROS production from mitochondrial complex I," *Theranostics*, vol. 11, no. 4, pp. 1703–1720, 2021.

[16] T. M. West, Q. Wang, B. Deng et al., "Phosphodiesterase 5 associates with β2 adrenergic receptor to modulate cardiac function in type 2 diabetic hearts," *Journal of the American Heart Association*, vol. 8, no. 15, article e012273, 2019.

[17] S. Cadenas, "ROS and redox signaling in myocardial ischemia-reperfusion injury and cardioprotection," *Free Radical Biology & Medicine*, vol. 117, pp. 76–89, 2018.

[18] R. An, J. Feng, C. Xi, J. Xu, and L. Sun, "miR-146a attenuates sepsis-induced myocardial dysfunction by suppressing IRAK1 and TRAF6 via targeting ErbB4 expression," *Oxidative Medicine and Cellular Longevity*, vol. 2018, Article ID 7163057, 9 pages, 2018.

[19] Z. M. Moghadam, P. Henneke, and J. Kolter, "From flies to men: ROS and the NADPH oxidase in phagocytes," *Frontiers in Cell and Development Biology*, vol. 9, article 628991, 2021.

[20] S. Matsushima, H. Tsutsui, and J. Sadoshima, "Physiological and pathological functions of NADPH oxidases during myocardial ischemia-reperfusion," *Trends in Cardiovascular Medicine*, vol. 24, no. 5, pp. 202–205, 2014.

[21] S. Matsushima, J. Kuroda, T. Ago et al., "Broad suppression of NADPH oxidase activity exacerbates ischemia/reperfusion injury through inadvertent downregulation of hypoxia-inducible Factor-1α and upregulation of peroxisome proliferator-activated Receptor-α," *Circulation Research*, vol. 112, no. 8, pp. 1135–1149, 2013.

[22] H. Zhan-qiang, Q. Hai-hua, Z. Chi et al., "miR-146a empeora el deterioro cognitivo y la patologia tipo Alzheimer al promover el estres oxidativo a traves de la via de señalizacion MAPK," *Neurologia*, 2021.

[23] H. J. Wang, Y. L. Huang, Y. Y. Shih, H. Y. Wu, C. T. Peng, and W. Y. Lo, "MicroRNA-146a decreases high glucose/thrombin-induced endothelial inflammation by inhibiting NAPDH oxidase 4 expression," *Mediators of Inflammation*, vol. 2014, Article ID 379537, 12 pages, 2014.

[24] R. J. Wan and Y. H. Li, "MicroRNA-146a/NAPDH oxidase4 decreases reactive oxygen species generation and inflammation in a diabetic nephropathy model," *Molecular Medicine Reports*, vol. 17, no. 3, pp. 4759–4766, 2018.

[25] D. L. Mann, "Innate immunity and the failing heart: the cytokine hypothesis revisited," *Circulation Research*, vol. 116, no. 7, pp. 1254–1268, 2015.

[26] L. Pearce, S. M. Davidson, and D. M. Yellon, "Does remote ischaemic conditioning reduce inflammation? A focus on innate immunity and cytokine response," *Basic Research in Cardiology*, vol. 116, no. 1, p. 12, 2021.

[27] S. Wang, L. Ding, H. Ji, Z. Xu, Q. Liu, and Y. Zheng, "The role of p38 MAPK in the development of diabetic cardiomyopathy," *International Journal of Molecular Sciences*, vol. 17, no. 7, p. 1037, 2016.

Research Article

Association of NFE2L2 Gene Polymorphisms with Risk and Clinical Characteristics of Acute Type A Aortic Dissection in Han Chinese Population

Yiran Zhang [iD],[1] **Qi Zheng** [iD],[1] **Ruoshi Chen** [iD],[1] **Xiaoyi Dai** [iD],[1] **Yimin Zhu** [iD],[2] **and Liang Ma** [iD][1]

[1]*Department of Cardiovascular Surgery, First Affiliated Hospital, School of Medicine, Zhejiang University, Hangzhou 310003, China*
[2]*Department of Epidemiology & Biostatistics, School of Public Health, Zhejiang University, Hangzhou 310058, China*

Correspondence should be addressed to Yimin Zhu; zhuym@zju.edu.cn and Liang Ma; ml1402@zju.edu.cn

The present study is aimed at investigating the association of NFE2L2 gene polymorphisms with risk and clinical characteristics of acute type A aortic dissection (AAAD) in a Han Chinese population. Six SNPs (rs1806649, rs13001694, rs2364723, rs35652124, rs6721961, and rs2706110) in NFE2L2 were genotyped using SNaPshot Multiplex Kit in 94 adult patients diagnosed with AAAD at our hospital, and 208 healthy Han Chinese subjects from the 1000 Genomes Project were served as the control group. The CC genotype of rs2364723 (CC versus (GC+GG), OR = 2.069, 95% CI: 1.222-3.502, $p = 0.006$) and CC genotype of rs35652124 (CC versus (CT+TT), OR = 1.889, 95% CI: 1.112-3.210, $p = 0.018$) were identified as risk factors for AAAD. Multivariable linear regression analysis revealed that the CC genotype of rs2364723 ($\beta = 5.031$, 95% CI: 1.878-8.183, $p = 0.002$) and CC genotype of rs35652124 ($\beta = 4.751$, 95% CI: 1.544-7.958, $p = 0.004$) were associated with increased maximum ascending aorta diameter of AAAD. Patients carrying rs2364723 CC genotype had a higher incidence of coronary artery involvement (31% vs. 12%, $p = 0.027$), while patients carrying rs35652124 CC genotype had a higher incidence of brain ischemia (9% vs. 0%, $p = 0.045$). In conclusion, NFE2L2 gene polymorphisms were correlated with risk and severity of AAAD in Han Chinese population.

1. Introduction

Acute type A aortic dissection (AAAD) is a medical emergency with 48.6% of the patients died before hospital admission [1] and in-hospital mortality rate as high as 32.5% [2]. Therefore, it is important to identify the pathogenesis and risk factors of AAAD, which could help prevention and early intervention of the disease.

Genetic susceptibility is an important risk factor for AAAD. It has been shown that nearly 20% AAAD patients also had hereditary disorders such as Marfan syndrome, Loeys-Dietz syndrome, and Turner syndrome [3]. Several recent studies reported that polymorphisms in genes such as TLR4 [4], ALDH2 [5], and Mfn2 [6] were associated with risk of sporadic aortic dissection. However, the genetic determinants of AAAD remained largely undiscovered.

It has been indicated that oxidative stress participated in degeneration and necrosis of aortic media, which played an essential role in the development of aortic dissection. A proteomic study showed that the expression and activity of superoxide dismutase were decreased in the aortic media of patients with thoracic aortic dissection, while the level of lipid peroxidation was increased [7]. It has been shown that increased fluid shear stress on aorta wall led to accumulation of reactive oxygen species (ROS), inducing phenotype switch of vascular smooth muscle cells, which played a vital role in formation of aortic aneurysm and dissection [8, 9].

Nuclear factor erythroid 2 like 2 (NFE2L2) is a gene localized on chromosome 2q31.2, which encodes a transcription factor Nrf2. Nrf2 regulates a number of antioxidative genes by binding to antioxidant response elements (ARE) in their promoters, and the Nrf2-ARE signaling played a protective

role in various kinds of oxidative stress injury [10]. A number of studies suggested that activating Nrf2-ARE signaling could alleviate apoptosis [11], calcification [12], and phenotype switch [13] of vascular smooth muscle cells. Moreover, several single-nucleotide polymorphisms (SNPs) in NFE2L2 gene have been reported to be associated with coronary artery disease [14], vascular stiffness [15], and cardiovascular mortality [16] in different populations. Thus, we inferred that NFE2L2 gene polymorphisms may be associated with AAAD, while no study has examined this relationship. The present study investigated the association of NFE2L2 gene polymorphisms with risk and clinical characteristics of AAAD in a Han Chinese population.

2. Materials and Methods

2.1. Study Population. This study was approved by the ethics committee of the First Affiliated Hospital, School of Medicine, Zhejiang University in China (reference number: IIT2020-277). All participants gave informed consents before inclusion in the study. The inclusion criteria were as follows: (1) Han Chinese patients older than 18 years, (2) aortic dissection diagnosed according to computed tomography angiography (CTA) and echocardiography, and (3) the time from the onset of the symptom to admission within 14 days. The exclusion criteria were as follows: (1) patients with familial aortic dissection or other types of acute aortic syndrome (i.e., intramural hematoma, penetrating ulcer, and iatrogenic/traumatic dissection) and (2) patients who did not sign the informed consents. A total of 94 adult patients diagnosed with AAAD were enrolled in this study between September 2018 and November 2020 at our hospital (Figure 1).

5 mL of the peripheral blood was collected from each participant and stored at -80°C for further examination. All blood samples were handled anonymously. Clinical variables of each patient were obtained through review of medical records, which included demographics (age and gender), medical histories (hypertension, diabetes, chronic kidney disease, prior aortic stent implant, prior cardiac surgery, smoking, and bicuspid aortic valve), blood pressure on admission (systolic and diastolic), maximum diameter of ascending aorta (measured by echocardiography preoperatively), severity of aortic valve regurgitation, the site and number of primary/secondary entry tears (according to the operation note), DeBakey classification of the dissection, organ ischemia (brain, coronary artery involvement, and lower limber), and laboratory tests on admission (white blood cell count, platelet count, hemoglobin, high sensitivity C-reactive protein, fibrinogen, D-dimer, serum uric acid, creatine, and urea nitrogen).

The control group consisted of 208 healthy Han Chinese subjects from the publicly available population-based database of the 1000 Genomes Project, which included 103 Han Chinese in Beijing, China (CHB) and 105 Southern Han Chinese, China (CHS) (Figure 1).

2.2. SNP Selection and Genotyping. Six SNPs (rs1806649 [17], rs13001694 [16], rs2364723 [16], rs35652124 [18], rs6721961 [14, 15], and rs2706110 [19]) located in NFE2L2 previously

reported to be associated with cardiovascular risk were selected for genotyping.

Genomic DNA was extracted from venous blood samples using Trelief Animal Genomic DNA Kit (Beijing TsingKe Biotech Co., Ltd., Beijing, China) according to the manufacturer's instruction. Genotyping of the six SNPs was performed using the SNaPshot Multiplex Kit (Thermo Fisher Scientific, Waltham, MA, USA). Amplification primers and extension primers are listed in Table 1. Briefly, multiplex polymerase chain reaction was performed followed by a single-nucleotide primer extension assay test. The SNPs were detected by capillary electrophoresis using ABI 3730xl DNA Analyzer (Thermo Fisher Scientific, Waltham, MA, USA). The data was analyzed using GeneMapper 4.1 software (Applied Biosystems, Foster City, CA, USA).

2.3. Statistical Analysis. The Hardy-Weinberg equilibrium (HWE) was evaluated using Genetics package in R software to determine the representativeness of the study population. Categorical variables were presented as numbers and proportions and were compared between different groups using Pearson's chi-square or Fisher's exact test, as appropriate. Normally distributed continuous data were presented as the mean $\pm$ SD and were compared using unpaired Student t-test. Nonnormally distributed continuous data were presented as median with interquartile range (IQR) and were compared by the Mann-Whitney U test. Dominant, recessive, and homozygote genetic models of inheritance were chosen to evaluate the association between each SNP and AAAD risk with odds ratio (OR) and 95% confidence interval (95% CI). Multivariable linear regression model was used to adjust the effect of potential confounders on the association between NFE2L2 gene polymorphisms and maximum ascending aorta diameter. All statistical analyses were processed using SPSS 25.0 software (SPSS Inc., Chicago, IL, USA) and R programming language (version 4.0.0). All p values of <0.05 were considered statistically significant.

3. Results

3.1. Genotype and Allele Frequencies of NFE2L2 Gene Polymorphisms. The genotype frequencies for all 6 SNPs were in line with HWE in the control group (rs1806649, $p = 0.379$; rs13001694, $p = 0.741$; rs2364723, $p = 1.000$; rs35652124, $p = 1.000$; rs6721961, $p = 0.600$; and rs2706110, $p = 0.450$) and the AAAD group (rs1806649, $p = 1.000$; rs13001694, $p = 1.000$; rs2364723, $p = 0.292$; rs35652124, $p = 0.285$; rs6721961, $p = 0.205$; and rs2706110, $p = 0.754$), indicating that the results of the present study have a representative genetic group. The genotype distribution and allele frequency of each SNP are shown in Tables 2 and 3. The genotype distribution of rs2364723 differed significantly between the AAAD group and control group ($p = 0.021$). The allele frequencies of rs2364723 ($p = 0.009$) and rs35652124 ($p = 0.021$) were significantly linked to AAAD risk.

3.2. Association between NFE2L2 Gene Polymorphisms and AAAD Risk. The association between NFE2L2 gene polymorphisms and AAAD risk in different genetic models is shown
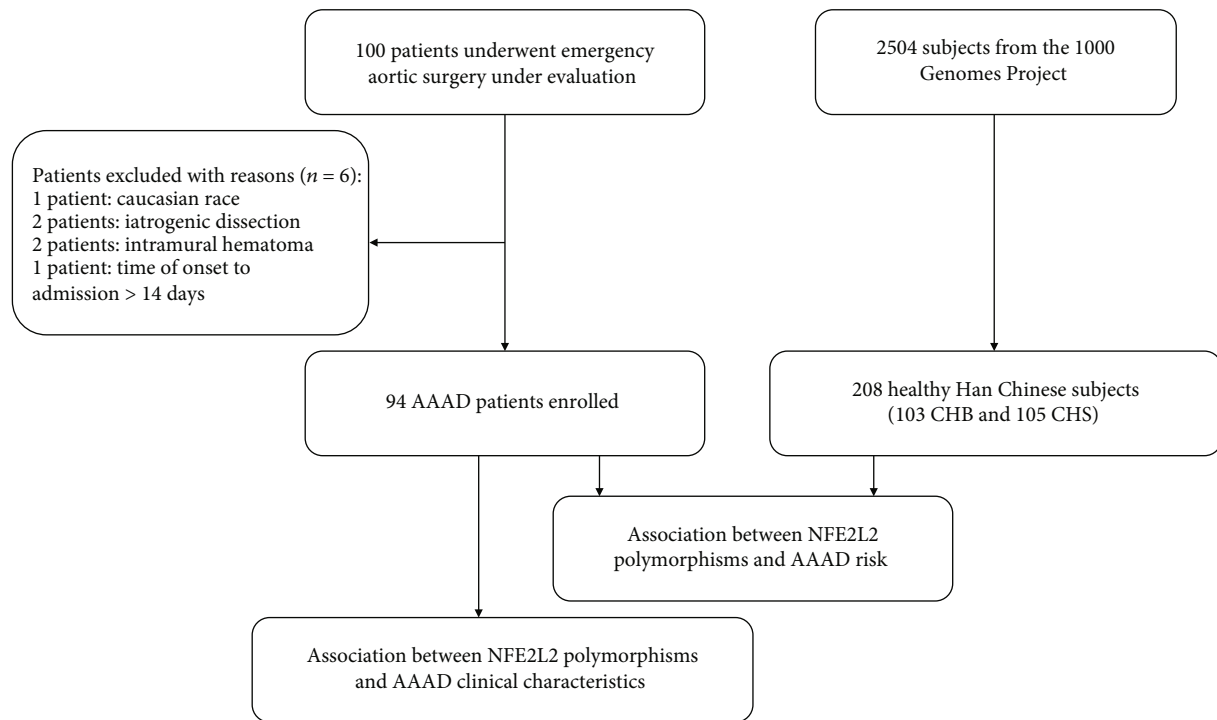
FIGURE 1: Flow chart of the study design. AAAD: acute type A aortic dissection; CHB: Han Chinese in Beijing, China; CHS: southern Han Chinese, China.

TABLE 1: Amplification primers and extension primers of selected SNPs.

SNPs	Amplification primers	Extension primers
rs1806649	Forward: ACTGTCACAGCATTGTCATGTATCA Reverse: TAGGAATCTTTCAGGGCATGAAG	TTTTTTTTTTTTTTTAGTCTTAGAGGAACTCATATCCTAAG
rs13001694	Forward: TTGCAGCTGTAGGTCCGAGA Reverse: TTTTGTAGGGAAGCCTGCCA	TTTTTTTTTTTTTCTGGACAAGTCACTCTACCTGC
rs2364723	Forward: AGCAATTATGTCTGGCACCC Reverse: CCAGGAAAAGTTGAAAGCCAAATG	TTTTTTTTTTTTTTTTTTTTTTTGGTTTTGTGTCAATATTTCCTC
rs35652124	Forward: CTCACTTTACCGCCCGAGAA Reverse: GTTCTCTTGGGGTTCCCGTT	TTTTTTTTTTTTTTTTTTTTTTTTTTTTTACACGTGGGAGTTCAGAGG
rs6721961	Forward: CTCACTTTACCGCCCGAGAA Reverse: GTTCTCTTGGGGTTCCCGTT	TTTTTTTTTTTTTTTTTTTTTTTTTTTTTTTTCTAGGGGAGATGTGGACAGC
rs2706110	Forward: GCTCCCCTCAAAAACAGGAAC Reverse: ACGAGGGAACTGGCCATAGAA	TTTTTTTTTTTTTTTTTTTTTTTTTTTTTTTTTTTTATTAGTCATGGCATAGTTGAGA

in Table 4. rs2364723 was strongly correlated with the risk of AAAD in the recessive genetic model (CC versus (GC+GG), OR = 2.069, 95% CI: 1.222-3.502, $p = 0.006$) and the homozygous model (CC versus GG, OR = 2.333, 95% CI: 1.177-4.627, $p = 0.014$), which indicated that the CC genotype of rs2364723 was a risk factor for AAAD. rs35652124 was strongly correlated with the risk of AAAD in the recessive genetic model (CC versus (CT+TT), OR = 1.889, 95% CI: 1.112-3.210, $p = 0.018$) and the homozygous model (CC versus TT, OR = 2.125, 95% CI: 1.076-4.195, $p = 0.029$), which indicated that the CC genotype of rs35652124 was a risk factor for AAAD.

3.3. Association between rs2364723 and rs35652124 Polymorphisms with AAAD Clinical Characteristics. Table 5 summarizes the clinical characteristics of the 94 AAAD

patients in different genotype groups. Compared with patients carrying rs2364723 GC+GG genotypes, patients with rs2364723 CC genotype had increased maximum diameter of ascending aorta (median diameter, 49 vs. 42 mm, $p = 0.002$, Table 5 and Figure 2(a)) and higher incidence of coronary artery involvement (31% vs. 12%, $p = 0.027$, Table 5). Compared with patients carrying rs35652124 CT+TT genotypes, patients with rs35652124 CC genotype had increased maximum diameter of ascending aorta (median diameter, 49 vs. 43 mm, $p = 0.011$, Table 5 and Figure 2(b)) and higher incidence of brain ischemia (9% vs. 0%, $p = 0.045$, Table 5).

3.4. Multivariable Linear Regression Analysis for Maximum Ascending Aorta Diameter. After adjusting for potential confounders including demographics (age and gender) and

TABLE 2: Genotype distribution of NFE2L2.

SNP		Genotype (frequency, %)			χ^2	p value
		TT	CT	CC		
rs1806649	Case	1 (1.1)	17 (18.1)	76 (80.9)	0.289	0.865
	Control	3 (1.4)	33 (15.9)	172 (82.7)		
		GG	GA	AA		
rs13001694	Case	2 (2.1)	22 (23.4)	70 (74.5)	0.311	0.856
	Control	4 (1.9)	43 (20.7)	161 (77.4)		
		CC	GC	GG		
rs2364723	Case	36 (38.3)	40 (42.6)	18 (19.1)	7.742	0.021
	Control	48 (23.1)	104 (50.0)	56 (26.9)		
		CC	CT	TT		
rs35652124	Case	34 (36.2)	41 (43.6)	19 (20.2)	5.891	0.053
	Control	48 (23.1)	103 (49.5)	57 (27.4)		
		TT	GT	GG		
rs6721961	Case	2 (2.1)	35 (37.2)	57 (60.6)	4.434	0.109
	Control	15 (7.2)	87 (41.8)	106 (51.0)		
		TT	CT	CC		
rs2706110	Case	3 (3.2)	32 (34.0)	59 (62.8)	1.005	0.605
	Control	10 (4.8)	79 (38.0)	119 (57.2)		

TABLE 3: Allele frequency of NFE2L2.

SNP		Allele (frequency, %)		χ^2	p value
		T	C		
rs1806649	Case	19 (10.1)	169 (89.9)	0.080	0.778
	Control	39 (9.4)	377 (90.6)		
		G	A		
rs13001694	Case	26 (13.8)	162 (86.2)	0.287	0.592
	Control	51 (12.3)	365 (87.7)		
		C	G		
rs2364723	Case	112 (59.6)	76 (40.4)	6.854	0.009
	Control	200 (48.1)	216 (51.9)		
		C	T		
rs35652124	Case	109 (58.0)	79 (42.0)	5.330	0.021
	Control	199 (47.8)	217 (52.2)		
		T	G		
rs6721961	Case	39 (20.7)	149 (79.3)	3.682	0.055
	Control	117 (28.1)	299 (71.9)		
		T	C		
rs2706110	Case	38 (20.2)	150 (79.8)	0.949	0.330
	Control	99 (23.8)	317 (76.2)		

medical histories (hypertension, diabetes, chronic kidney disease, prior aortic stent implant, prior cardiac surgery, smoking, and bicuspid aortic valve) using multivariable linear regression model, we found that rs2364723 (Model 1, $\beta = 5.031$, 95% CI: 1.878-8.183, $p = 0.002$, Table 6) and rs35652124 (Model 2, $\beta = 4.751$, 95% CI: 1.544-7.958, $p = 0.004$, Table 6) were still significantly associated with maximum ascending aorta diameter. Besides, prior cardiac surgery was also found to be significantly associated with maximum ascending aorta diameter (Model 1, $\beta = 9.652$, 95% CI: 2.142-17.162, $p = 0.012$; Model 2, $\beta = 10.228$, 95% CI: 2.646-17.810, $p = 0.009$, Table 6).

TABLE 4: Association of NFE2L2 gene polymorphisms with risk of AAAD.

SNP	Genetic model	Genotype	OR (95% CI)	p value
	Dominant	(TT+CT) vs. CC	1.132 (0.605-2.118)	0.699
rs1806649	Recessive	TT vs. (CT+CC)	0.735 (0.075-7.158)	1.000
	Homozygote	TT vs. CC	0.754 (0.077-7.370)	1.000
	Dominant	(GG+GA) vs. AA	1.174 (0.667-2.069)	0.578
rs13001694	Recessive	GG vs. (GA+AA)	1.109 (0.199-6.161)	1.000
	Homozygote	GG vs. AA	1.150 (0.206-6.425)	1.000
	Dominant	(CC+GC) vs. GG	1.556 (0.855-2.829)	0.146
rs2364723	Recessive	CC vs. (GC+GG)	2.069 (1.222-3.502)	0.006
	Homozygote	CC vs. GG	2.333 (1.177-4.627)	0.014
	Dominant	(CC+CT) vs. TT	1.490 (0.827-2.684)	0.182
rs35652124	Recessive	CC vs. (CT+TT)	1.889 (1.112-3.210)	0.018
	Homozygote	CC vs. TT	2.125 (1.076-4.195)	0.029
	Dominant	(TT+GT) vs. GG	0.675 (0.411-1.107)	0.118
rs6721961	Recessive	TT vs. (GT+GG)	0.280 (0.063-1.249)	0.076
	Homozygote	TT vs. GG	0.248 (0.055-1.123)	0.052
	Dominant	(TT+CT) vs. CC	0.793 (0.481-1.308)	0.364
rs2706110	Recessive	TT vs. (CT+CC)	0.653 (0.175-2.429)	0.738
	Homozygote	TT vs. CC	0.605 (0.160-2.282)	0.659

4. Discussion

The present study was the first to evaluate the association of NFE2L2 gene polymorphisms with risk and clinical characteristics of AAAD. Our data indicated that the CC genotype of rs2364723 and CC genotype of rs35652124 were risk factors for AAAD. Multivariable linear regression analysis revealed that the CC genotype of rs2364723 and CC genotype of rs35652124 were associated with increased maximum ascending aorta diameter. Besides, patients carrying rs2364723 CC genotype had a higher incidence of coronary artery involvement, while patients carrying rs35652124 CC genotype had a higher incidence of brain ischemia.

The protective role of Nrf2 on aortic dissection and aneurysm has been indicated by several studies. It has been shown that the Nrf2 expression in the thoracic aortic aneurysm tissue from patients with Loeys-Dietz Syndrome was decreased, compared with nondamaged aortic tissue from control subjects [20]. Animal experiments using angiotensin II-induced aortic aneurysm model in mice showed that NFE2L2 gene deficiency increased the risk of development and rupture of aortic aneurysm [21, 22]. The potential mechanisms underlying the protective role of Nrf2 on aortic dissection and aneurysm may be multifactorial. It has been suggested that activating the Nrf2-ARE pathway suppressed the angiotensin II-induced phenotype switch and proliferation [13], apoptosis [11], calcification [12], and fibrotic [23] of vascular smooth muscle cells. It has also been found that activating the Nrf2-ARE pathway promoted endothelial repair during vascular injury [24].

In the present study, we found that CC genotype of rs2364723 and CC genotype of rs35652124 were linked to an increased risk of AAAD. The rs35652124 polymorphism

locates in the promoter region of the NFE2L2 gene, which might regulate Nrf2 expression by influencing the NFE2L2 promoter activity [25]. In vitro transient transfection reporter gene assays showed that rs35652124 C allele reduced the NFE2L2 promoter activity in human microvascular endothelial cells [18]. It has been found that, in healthy African American population, rs35652124 C allele carriers had lower forearm blood flow (FBF) and higher forearm vascular resistance (FVR) under basal condition as well as in response to vasodilators [18]. The maximum FBF response to endothelium-dependent vasodilator in patients with Marfan syndrome has been found to be significantly reduced [26]. These evidences indicate that NFE2L2 gene polymorphisms were associated with vasomotion abnormality, which might play a role in aortic enlargement and dissection. The rs2364723 polymorphism locates in the intron 1 region of the NFE2L2 gene. In a general population-based cohort of Caucasian, it was found that rs2364723 GG carriers had lower cardiovascular mortality and triglyceride levels compared with GC+CC carriers [16]. While abnormal serum lipid composition has been indicated to play a key role in development of aortic dissection [27], it should be noted that the rs2364723 polymorphism was in high linkage disequilibrium (LD) with rs35652124 ($r^2 = 0.99$) [28]; thus, the association of rs2364723 with AAAD risk might also represent the effect of rs35652124 due to almost complete LD.

We further investigated the correlation of rs2364723 and rs35652124 polymorphisms with clinical characteristics of AAAD patients and found that rs2364723 CC carriers and rs35652124 CC carriers had increased maximum ascending aorta diameter. Increased ascending aorta diameter is associated with reduced elastin density and increased collagen density, which has a profound impact on aortic dissection [29]. A study on 230 patients with thoracic aortic aneurysm from

TABLE 5: Association of rs2364723 and rs35652124 polymorphisms with AAAD clinical characteristics.

Variables	Overall	rs2364723			rs35652124		
		CC	GC or GG	p	CC	CT or TT	p
Number of patients	94	36	58		34	60	
Demographics							
Age (years)	52 ± 13	52 ± 13	52 ± 13	0.865	51 ± 13	52 ± 13	0.762
Male, n (%)	75 (80)	30 (83)	45 (78)	0.500	28 (82)	47 (78)	0.641
Medical histories, n (%)							
Hypertension	63 (67)	25 (69)	38 (66)	0.694	24 (71)	39 (65)	0.580
Diabetes	3 (3)	2 (6)	1 (2)	0.556	1 (3)	2 (3)	1.000
CKD	3 (3)	1 (3)	2 (3)	1.000	1 (3)	2 (3)	1.000
Prior aortic stent implant	3 (3)	1 (3)	2 (3)	1.000	1 (3)	2 (3)	1.000
Prior cardiac surgery	5 (5)	2 (6)	3 (5)	1.000	1 (3)	4 (7)	0.650
Smoking	38 (40)	16 (44)	22 (38)	0.532	15 (44)	23 (38)	0.583
Bicuspid aortic valve	7 (7)	5 (14)	2 (3)	0.102	5 (15)	2 (3)	0.094
Clinical presentation							
Systolic blood pressure (mmHg)	151 ± 27	152 ± 23	151 ± 30	0.817	151 ± 22	152 ± 30	0.870
Diastolic blood pressure (mmHg)	82 ± 19	78 ± 17	84 ± 20	0.127	77 ± 17	84 ± 20	0.075
AoD_{max} (mm)	45 (41-52)	49 (42-57)	42 (39-51)	0.002	49 (42-56)	43 (39-52)	0.011
Organ ischemia, n (%)							
Brain	3 (3)	3 (8)	0 (0)	0.053	3 (9)	0 (0)	0.045
Lower limb	15 (16)	8 (22)	7 (12)	0.191	6 (18)	9 (15)	0.736
Coronary artery involvement	18 (19)	11 (31)	7 (12)	0.027	10 (29)	8 (13)	0.057
Dissection characteristics							
DeBakey classification, n (%)							
Type I	84 (89)	32 (89)	52 (90)	1.000	30 (88)	54 (90)	1.000
Type II	10 (11)	4 (11)	6 (10)		4 (12)	6 (10)	
Primary entry site, n (%)							
Ascending aorta	62 (66)	26 (72)	36 (62)		25 (74)	37 (62)	
Aortic arch	19 (20)	6 (17)	13 (22)	0.600	5 (15)	14 (23)	0.490
Descending aorta or unknown	13 (14)	4 (11)	9 (16)		4 (12)	9 (15)	
Secondary entry site, n (%)							
None	76 (81)	29 (81)	47 (81)		28 (82)	48 (80)	
Ascending aorta	2 (2)	1 (3)	1 (2)	1.000	1 (3)	1 (2)	0.948
Aortic arch	14 (15)	5 (14)	9 (16)		4 (12)	10 (17)	
Descending aorta	2 (2)	1 (3)	1 (2)		1 (3)	1 (2)	
Entry tears≥2, n (%)	18 (19)	7 (19)	11 (19)	0.954	6 (18)	12 (20)	0.781
Aortic valve regurgitation, n (%)							
None	14 (15)	4 (11)	10 (17)		3 (9)	11 (18)	
Mild	36 (38)	14 (39)	22 (38)		13 (38)	23 (38)	
Mild-moderate	11 (12)	3 (8)	8 (14)	0.298	3 (9)	8 (13)	0.205
Moderate	14 (15)	7 (19)	7 (12)		7 (21)	7 (12)	
Moderate-severe	10 (11)	2 (6)	8 (14)		2 (6)	8 (13)	
Severe	9 (10)	6 (17)	3 (5)		6 (18)	3 (5)	

TABLE 5: Continued.

| Variables | Overall | rs2364723 | | | rs35652124 | | |
		CC	GC or GG	p	CC	CT or TT	p
		Laboratory tests on admission					
WBC (10^9/L)	13.2 ± 4.0	13.1 ± 4.1	13.3 ± 4.9	0.904	13.1 ± 4.3	13.3 ± 3.8	0.878
PLT (10^9/L)	156 (124-192)	155 (137-184)	157 (122-208)	0.800	154 (137-183)	157 (122-211)	0.620
Hb (g/L)	134 ± 22	133 ± 24	134 ± 20	0.957	134 ± 24	133 ± 20	0.831
CRP (mg/L)	6.8 (2.4-20.3)	8.7 (2.7-19.2)	5.3 (2.3-22.1)	0.602	8.7 (2.7-21.3)	5.6 (2.3-20.9)	0.698
Fibrinogen (g/L)	2.13 (1.52-2.79)	2.36 (1.47-3.03)	1.95 (1.52-2.64)	0.621	2.31 (1.45-3.00)	1.96 (1.53-2.74)	0.953
D-dimer (μg/mL FEU)	10.9 (4.8-28.6)	8.9 (4.2-27.2)	12.0 (5.8-29.8)	0.283	9.6 (4.2-29.9)	11.4 (5.7-27.5)	0.544
UA (μmol/L)	405 ± 110	397 ± 115	411 ± 107	0.574	402 ± 116	407 ± 107	0.831
Creatinine (μmol/L)	98 (76-127)	98 (78-129)	97 (74-127)	0.876	96 (77-124)	98 (75-128)	0.642
BUN (mmol/L)	6.78 (5.39-7.98)	6.56 (5.36-7.87)	6.91 (5.49-8.07)	0.735	6.56 (5.38-7.68)	6.91 (5.41-8.12)	0.645

Data are represented as the median (interquartile range), n(%), or mean ± SD. CKD: chronic kidney disease; AoD$_{max}$: maximum diameter of ascending aorta; WBC: white blood cell count; PLT: platelet; Hb: hemoglobin; UA: uric acid; BUN: blood urea nitrogen.
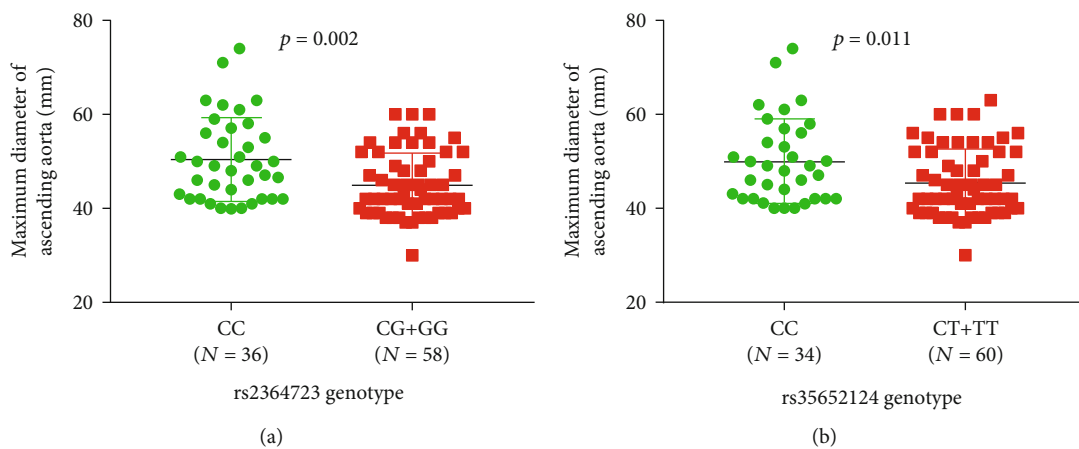

FIGURE 2: Maximum diameter of ascending aorta in AAAD patients grouped by rs2364723 and rs35652124 genotypes.

TABLE 6: Multiple linear regression of maximum ascending aorta diameter.

| Variables | Model 1 | | | Variables | Model 2 | | |
	β (95% CI)	p value	Tolerance		β (95% CI)	p value	Tolerance
rs2364723 (CC: 1, GC+GG: 0)	5.031 (1.878-8.183)	0.002	0.943	rs35652124 (CC: 1, CT+TT: 0)	4.751 (1.544-7.958)	0.004	0.946
Age	0.126 (-0.21-0.274)	0.093	0.624	Age	0.139 (-0.10-0.287)	0.068	0.625
Male	0.710 (-4.117-5.537)	0.771	0.589	Male	1.054 (-3.806-5.913)	0.667	0.590
Hypertension	-2.945 (-6.213-0.323)	0.077	0.938	Hypertension	-3.149 (-6.447-0.149)	0.061	0.935
Diabetes	2.338 (-6.946-11.622)	0.618	0.831	Diabetes	4.093 (-5.196-13.382)	0.383	0.843
CKD	1.383 (-7.946-10.712)	0.769	0.823	CKD	0.632 (-8.762-10.027)	0.894	0.824
Prior aortic stent implant	6.274 (-2.376-14.925)	0.153	0.957	Prior aortic stent implant	6.379 (-2.337-15.096)	0.149	0.957
Prior cardiac surgery	9.652 (2.142-17.162)	0.012	0.779	Prior cardiac surgery	10.228 (2.646-17.810)	0.009	0.776
Smoking	-0.497 (-3.929-2.934)	0.774	0.780	Smoking	-0.553 (-3.992-2.926)	0.760	0.780
Bicuspid aortic valve	4.633 (-1.274-10.540)	0.123	0.920	Bicuspid aortic valve	4.620 (-1.348-10.588)	0.127	0.915

CKD: chronic kidney disease.

1985 to 1996 showed that the median diameter of ascending aorta was 6.0 cm at time of aorta rupture or dissection [30]. More recent data on nature history of ascending aortic aneu- rysm between 5 and 6 cm found two hinge points for aorta rupture or dissection—one at 5.25 cm and the other at 5.75 cm [31]. Recent studies also indicated that aortic

diameter ≥ 40 mm was an independent risk factor for in-hospital mortality of acute aortic dissection [32], and increased ascending aortic diameter was found to be negatively correlated with total survival time in patients with ascending aortic dissection [33]. Our study also found the correlation of rs2364723 and rs35652124 polymorphisms with incidence of organ ischemia such as brain ischemia and coronary artery involvement. Recent data showed that vital organ ischemia was a risk factor for early mortality after AAAD repair [34]. These evidences suggested that NFE2L2 gene polymorphisms not only correlated with onset risk but also severity of AAAD.

There are several limitations in the present study. Firstly, it is a pilot, single-center research with relatively small sample size, and our findings cannot be generalized to the general population since we included only Han Chinese subjects. Secondly, this study only focused on 6 SNPs previously reported to be associated with cardiovascular risk, while other SNPs with potential influence were not examined. Moreover, we had not collected the aortic tissue of the AAAD patients, which made us unable to measure the oxidative stress condition in dissected aorta of the patients. Thus, further multicenter studies with different ethnicities and larger sample size were needed, and additional studies should determine the mechanisms underlying the effects of gene polymorphisms on functions of NFE2L2, and its role in the pathogenesis of AAAD.

5. Conclusions

The present study showed that rs2364723 and rs35652124 polymorphisms in NFE2L2 gene were correlated with risk of AAAD in a Han Chinese population. These two SNPs were also related to maximum ascending aorta diameter and vital organ ischemia in AAAD patients.

Data Availability

The data used to support the findings of this study are available from the corresponding authors upon request.

Conflicts of Interest

The authors declare that there is no conflict of interest regarding the publication of this paper.

Acknowledgments

References

[1] D. P. Howard, A. Banerjee, J. F. Fairhead et al., "Population-based study of incidence and outcome of acute aortic dissection and premorbid risk factor control: 10-year results from the Oxford Vascular Study," *Circulation*, vol. 127, no. 20, pp. 2031–2037, 2013.

[2] R. H. Mehta, T. Suzuki, P. G. Hagan et al., "Predicting death in patients with acute type A aortic dissection," *Circulation*, vol. 105, no. 2, pp. 200–206, 2002.

[3] E. M. Isselbacher, C. L. Lino Cardenas, and M. E. Lindsay, "Hereditary influence in thoracic aortic aneurysm and dissection," *Circulation*, vol. 133, no. 24, pp. 2516–2528, 2016.

[4] T. Li, X. Liu, H. Ning, X. Li, J. Yang, and C. Ma, "Association of Toll-like receptor 4 gene polymorphisms with acute aortic dissection in a Chinese Han population," *BioMed Research International*, vol. 2020, Article ID 8306903, 11 pages, 2020.

[5] K. Yang, J. Ren, X. Li et al., "Prevention of aortic dissection and aneurysm via an ALDH2-mediated switch in vascular smooth muscle cell phenotype," *European Heart Journal*, vol. 41, no. 26, pp. 2442–2453, 2020.

[6] J. Han, J. Liu, Q. Zhou, S. Nie, J. Liu, and S. Wen, "Single nucleotide polymorphisms (SNPs) genotyping reveals that Mfn2 polymorphisms are associated with thoracic aortic dissection in Han Chinese population," *Medical Science Monitor*, vol. 25, pp. 2419–2428, 2019.

[7] M. Liao, Z. Liu, J. Bao et al., "A proteomic study of the aortic media in human thoracic aortic dissection: implication for oxidative stress," *The Journal of Thoracic and Cardiovascular Surgery*, vol. 136, no. 1, pp. 65–72.e3, 2008, e1-3.

[8] L. M. Fan, G. Douglas, J. K. Bendall et al., "Endothelial cell-specific reactive oxygen species production increases susceptibility to aortic dissection," *Circulation*, vol. 129, no. 25, pp. 2661–2672, 2014.

[9] L. Xia, C. Sun, H. Zhu et al., "Melatonin protects against thoracic aortic aneurysm and dissection through SIRT1-dependent regulation of oxidative stress and vascular smooth muscle cell loss," *Journal of Pineal Research*, vol. 69, no. 1, p. e12661, 2020.

[10] P. Shaw and A. Chattopadhyay, "Nrf2–ARE signaling in cellular protection: mechanism of action and the regulatory mechanisms," *Journal of Cellular Physiology*, vol. 235, no. 4, pp. 3119–3130, 2020.

[11] T. Xiao, L. Zhang, Y. Huang et al., "Sestrin2 increases in aortas and plasma from aortic dissection patients and alleviates angiotensin II-induced smooth muscle cell apoptosis via the Nrf2 pathway," *Life Sciences*, vol. 218, pp. 132–138, 2019.

[12] R. Wei, M. Enaka, and Y. Muragaki, "Activation of KEAP1/NRF2/P62 signaling alleviates high phosphate-induced calcification of vascular smooth muscle cells by suppressing reactive oxygen species production," *Scientific Reports*, vol. 9, no. 1, p. 10366, 2019.

[13] X. He, J. Deng, X. J. Yu, S. Yang, Y. Yang, and W. J. Zang, "Activation of M3AChR (type 3 muscarinic acetylcholine receptor) and Nrf2 (nuclear factor erythroid 2-related factor 2) signaling by choline alleviates vascular smooth muscle cell phenotypic switching and vascular remodeling," *Arteriosclerosis, Thrombosis, and Vascular Biology*, vol. 40, no. 11, pp. 2649–2664, 2020.

[14] I. Sarutipaiboon, N. Settasatian, N. Komanasin et al., "Association of genetic variations in NRF2, NQO1, HMOX1, and MT with severity of coronary artery disease and related risk factors," *Cardiovascular Toxicology*, vol. 20, no. 2, pp. 176–189, 2020.

[15] S. Shimizu, J. Mimura, T. Hasegawa et al., "Association of single nucleotide polymorphisms in the NRF2 promoter with vascular stiffness with aging," *PLoS One*, vol. 15, no. 8, article e0236834, 2020.

[16] S. M. Figarska, J. M. Vonk, and H. M. Boezen, "NFE2L2 polymorphisms, mortality, and metabolism in the general

population," *Physiological Genomics*, vol. 46, no. 12, pp. 411–417, 2014.

[17] B. Wang, M. Liu, W. Yan et al., "Association of SNPs in genes involved in folate metabolism with the risk of congenital heart disease," *The Journal of Maternal-Fetal & Neonatal Medicine*, vol. 26, no. 18, pp. 1768–1777, 2013.

[18] E. D. Marczak, J. Marzec, D. C. Zeldin et al., "Polymorphisms in the transcription factor NRF2 and forearm vasodilator responses in humans," *Pharmacogenetics and Genomics*, vol. 22, no. 8, pp. 620–628, 2012.

[19] T. Kunnas, K. Maatta, and S. T. Nikkari, "Genetic polymorphisms of transcription factor NRF2 and of its host gene sulfiredoxin (SRXN1) are associated with cerebrovascular disease in a Finnish cohort, the TAMRISK study," *International Journal of Medical Sciences*, vol. 13, no. 5, pp. 325–329, 2016.

[20] M. E. Soto, L. G. Manzano-Pech, V. Guarner-Lans et al., "Oxidant/antioxidant profile in the thoracic aneurysm of patients with the Loeys-Dietz syndrome," *Oxidative Medicine and Cellular Longevity*, vol. 2020, Article ID 5392454, 17 pages, 2020.

[21] A. Kopacz, E. Werner, A. Grochot-Przeczek et al., "Simvastatin attenuates abdominal aortic aneurysm formation favoured by lack of Nrf2 transcriptional activity," *Oxidative Medicine and Cellular Longevity*, vol. 2020, Article ID 6340190, 16 pages, 2020.

[22] H. Song, T. Xu, X. Feng et al., "Itaconate prevents abdominal aortic aneurysm formation through inhibiting inflammation via activation of Nrf2," *eBioMedicine*, vol. 57, p. 102832, 2020.

[23] Y. C. Hseu, T. Y. Yang, M. L. Li et al., "Chalcone flavokawain A attenuates TGF-β1-induced fibrotic pathology via inhibition of ROS/Smad3 signaling pathways and induction of Nrf2/ARE-mediated antioxidant genes in vascular smooth muscle cells," *Journal of Cellular and Molecular Medicine*, vol. 23, no. 2, pp. 775–788, 2019.

[24] J. Zhang, W. Cai, Z. Fan et al., "MicroRNA-24 inhibits the oxidative stress induced by vascular injury by activating the Nrf2/Ho-1 signaling pathway," *Atherosclerosis*, vol. 290, pp. 9–18, 2019.

[25] J. M. Marzec, J. D. Christie, S. P. Reddy et al., "Functional polymorphisms in the transcription factor NRF2 in humans increase the risk of acute lung injury," *The FASEB Journal*, vol. 21, no. 9, pp. 2237–2246, 2007.

[26] M. Nakamura, S. Itoh, S. Makita, A. Ohira, N. Arakawa, and K. Hiramori, "Peripheral resistance vessel dysfunction in Marfan syndrome," *American Heart Journal*, vol. 139, no. 4, pp. 661–666, 2000.

[27] H. Tanaka, Y. Iida, T. Iwaki et al., "Elevated plasma levels of LDL cholesterol promote dissecting thoracic aortic aneurysms in angiotensin II-induced mice," *Annals of Vascular Surgery*, vol. 48, pp. 204–213, 2018.

[28] M. Siedlinski, D. S. Postma, J. M. Boer et al., "Level and course of FEV1 in relation to polymorphisms in NFE2L2 and KEAP1 in the general population," *Respiratory Research*, vol. 10, no. 1, 2009.

[29] V. Deplano, M. Boufi, V. Gariboldi et al., "Mechanical characterisation of human ascending aorta dissection," *Journal of Biomechanics*, vol. 94, pp. 138–146, 2019.

[30] M. A. Coady, J. A. Rizzo, G. L. Hammond et al., "What is the appropriate size criterion for resection of thoracic aortic aneurysms?," *The Journal of Thoracic and Cardiovascular Surgery*, vol. 113, no. 3, pp. 476–491, 1997, discussion 89-91.

[31] B. A. Ziganshin, M. A. Zafar, and J. A. Elefteriades, "Descending threshold for ascending aortic aneurysmectomy: is it time for a "left-shift" in guidelines?," *The Journal of Thoracic and Cardiovascular Surgery*, vol. 157, no. 1, pp. 37–42, 2019.

[32] D. Wen, P. Jia, X. Du, J. Z. Dong, and C. S. Ma, "Value of N-terminal pro-brain natriuretic peptide and aortic diameter in predicting in-hospital mortality in acute aortic dissection," *Cytokine*, vol. 119, pp. 90–94, 2019.

[33] Y. Wu, M. Gong, R. Fan, T. Gu, X. Qian, and H. Zhang, "Analysis of ascending aortic diameter and long-term prognosis in patients with ascending aortic dissection," *Echocardiography*, vol. 38, no. 4, pp. 531–539, 2021.

[34] M. Yamasaki, H. Yoshino, T. Kunihara et al., "Risk analysis for early mortality in emergency acute type A aortic dissection surgery: experience of Tokyo acute aortic super-network," *European Journal of Cardio-Thoracic Surgery*, 2021.

Research Article

New Markers of Platelet Activation and Reactivity and Oxidative Stress Parameters in Patients Undergoing Coronary Artery Bypass Grafting

Petar Vukicevic [1,2] Aleksandra Klisic [3] Vojislava Neskovic [2,4] Luka Babic [1]
Aleksandar Mikic [5,6] Natasa Bogavac-Stanojevic [7] Milos Matkovic [6,8]
Svetozar Putnik [6,8] Nemanja Aleksic [6,8] and Jelena Kotur-Stevuljevic [7]

[1]*Clinic for Cardiac Surgery, Military Medical Academy, Belgrade, Serbia*
[2]*University of Defense, Medical Faculty of the Military Medical Academy, Belgrade, Serbia*
[3]*Primary Health Care Center, University of Montenegro-Faculty of Medicine, Podgorica, Montenegro*
[4]*Clinic for Anesthesiology and Critical Care, Military Medical Academy, Belgrade, Serbia*
[5]*Clinic for Cardiac Surgery, UC Clinical Centre, Belgrade, Serbia*
[6]*University of Belgrade-Faculty of Medicine, Belgrade, Serbia*
[7]*Department for Medical Biochemistry, University of Belgrade-Faculty of Pharmacy, Belgrade, Serbia*
[8]*Department for Cardiac Surgery, Clinical Center of Serbia, Belgrade, Serbia*

Correspondence should be addressed to Aleksandra Klisic; aleksandranklisic@gmail.com

Objective. Recent studies have shown that the red cell distribution width- (RDW-) to-platelet (PLT) count ratio (i.e., RPR) and the mean platelet volume (MPV)/PLT ratio (i.e. MPR) are more sensitive markers of atherosclerosis-connected risk than RDW and PLT alone. The present study is aimed at investigating the oxidative stress status and these two new markers of platelet activation in two different heart surgery modalities: cardiopulmonary bypass (CPB) and off-pump coronary artery bypass (OPCAB). We also aimed to test the possible relationship between RPR and MPR, respectively, and the severity and complexity of atherosclerotic plaque, measured as Syntax Score. *Patients and Methods*. A total of 107 patients encompassed this prospective study (i.e., 60 patients in CPB group and 47 patients in OPCAB). Blood samples were drawn at several time intervals: before skin incision (t1), immediately after intervention (t2), 6 h (t3), 24 h (t4), 48 h (t5), and 96 h after cessation of the operation (t6). *Results*. The values of RPR and MPR were similar in CPB and OPCAB before surgery and started to rise in t2 (i.e., immediately after the intervention). This increase lasted to t5 (i.e., 48 hours after the intervention), when it became the highest. After that, both markers started to regress about the 96th hour after the beginning of surgery. Nominal values of both indices were higher in CPB than in OPCAB in all study points after the surgery. Furthermore, a significantly higher level of antioxidative parameters (i.e., total sulfhydryl groups and paraoxonase 1) in the OPCAB group compared to the CPB group was noted at t5 study point (i.e., 48 hours after the surgery), whereas no significant difference was noted in prooxidant levels (i.e., lipid hydroperoxides and advanced oxidation protein products) between these groups at this study point. MPR and RPR correlated positively with Syntax Score at several study points after the surgery completion. Syntax Score, MPR, and RPR showed good clinical accuracy in surgery-related complication prediction ((AUC = 0.736), 95th CI (0.616-0.856), $P = 0.003$)). *Conclusion*. When combined, MPV, RDW, and platelet count, such as MPR and RPR, could be good predictors of coronary artery disease status, regarding the aspect of joint inflammation, oxidative stress, and thrombosis.

1. Introduction

Oxidative stress, inflammation, and thrombosis are mutually involved in the atherosclerosis development, and progression of this features is evident as disease becomes irreversible [1, 2]. Oxidative stress and chronic systemic low-level inflammation and neurohumoral activation could cause increase in heterogeneity of erythrocytes in circulation and influence platelet reactivity [3, 4]. Previous studies have investigated the relationship between several simple and routine hematological parameters and atherosclerotic plaque gravity and complexity prediction of unwanted acute cardiovascular events, and acute myocardial infarction outcome [3–6]. Decreased platelet (PLT) count connected with increased mean platelet volume (MPV) could predict changes in platelet reactivity and aggregability [6, 7]. On the other hand, red cell distribution width (RDW) per se is related with adverse outcome in acute coronary syndrome [8–10].

Platelet response in any particular situation depends on the current balance between proaggregatory stimuli and anti-aggregatory substances and is additionally governed by many traditional atherosclerosis risk factors: dyslipidemia, hypertension, and smoking [7]. Anisocytosis, measured as RDW is a well-recognized predictor of unwanted clinical outcomes in different diseases, including coronary artery disease [11]. Increased RDW is in fact connected with several different aspects of red blood cells metabolic specificities. Namely, there are data about the influence of anemia, iron concentration and status, so as cholesterol membrane content on cells' deformability, shorter lifespan, and faster turnover, so all of these increase RDW, as a measure of erythrocyte activation upon united oxidative stress and inflammation conditions [8].

Also, erythrocytes may become a part of advanced atherosclerotic plaque, which on one side lowers these blood cells' count in systemic circulation and on the other side increases cholesterol content in the lipid core of the plaque, and thus directly influence its stability. Otherwise, lower red blood cells' count pushes immature cells into the bloodstream [9–11].

We have recently shown increased oxidative stress in patients before and after coronary artery bypass grafting (CABG) [12]. In order to get deeper insight into the complex pathophysiological mechanisms of coronary artery disease, we continued the quest for more sensitive markers connected with erythrocytes and platelets activation which is presumably governed by oxidative stress, inflammation, and advanced atherosclerosis condition. Recent studies have shown that the RDW-to-PLT count ratio (i.e. RPR) and the MPV/PLT ratio (i.e., MPR) are even more sensitive markers of atherosclerosis-connected risk [5, 6], than RDW and PLT alone. Also, previous studies have shown an inflammatory and thrombotic predictive role of MPV, RDW, MPR, and RPR in many other diseases, such as obesity, type 2 diabetes, and hepatosteatosis [13–16].

The present study was designed to estimate oxidative stress status and the two new markers of platelet activation and reactivity in the two different heart surgery modalities (cardiopulmonary bypass (CPB) and off-pump coronary artery bypass (OPCAB)). We also aimed to test the possible connection between these two hematological indices and severity and complexity of atherosclerotic plaque, measured as Syntax Score [17].

To the best of our knowledge, RPR and MPR have not been examined regarding CPB and OPCAB surgical procedures. We hypothesize that these two indices of platelet and erythrocyte activation in atherosclerotic setting could be increased as a consequence of long-term oxidative stress and inflammation influence.

This is an important issue, because larger disturbance in reductive balance during and after the cardiac surgery leads to poorer outcomes and increased mortality in operated patients.

2. Materials and Methods

2.1. Study Design and Patients.
The study was planned as a prospective, interventional study at the Department for Cardiac Surgery, Medical Military Academy, Belgrade, Serbia. The whole study was planned according the ethical standards following the Declaration of Helsinki, as revised in 1983; the study protocol was approved by the institutional Ethics Committee, and all patients involved in the study signed an informed consent.

The study involved a total of 107 patients scheduled for an elective operation with one to four CABG. The patients were divided according to the number of bypass graft received during the CABG surgery, and also according to surgery modality, i.e., CPB ($n = 60$) and OPCAB ($n = 47$) subgroups. In the CPB group, the patients underwent surgery using CPB on the potassium-arrested heart, whereas in the OPCAB group, the patients underwent surgery on the beating-heart without a CPB machine.

Exclusion criteria for the current study patients were as follows: redo surgery or emergency surgery, concomitant valvular disease, ventricular aneurysms, myocardial infarction within the past 3 months or perioperative myocardial infarction, cerebral insult within the past 3 months, usage of systems for intraoperative blood salvage—Cell Saver machine and tubing system—systemic inflammatory or malignant disease, immunosuppressive drugs usage, massive postoperative mediastinal bleeding, heart failure, and presence of an infection.

Aspirin and clopidogrel were excluded from the therapy 7-10 days before the surgery. In both groups, all patients received low-molecular weight heparin (50-70 IU/kg), preoperatively.

2.2. Anesthesia.
The anesthetic technique was standardized for all patients and consisted of balanced anesthesia. General anesthesia was induced by etomidate (0.1–0.2 mg/kg), and sufentanil (0.5–1 μg/kg) and maintained with sevoflurane (0.6–1.0%) and sufentanil (0.5–1 μg/kg/h).

2.3. Surgical Procedure.
In both groups, midline sternotomy and harvesting of left internal mammary artery as a pedicle and saphenous vein grafts were followed by full exposure of the coronary artery branches to be revascularised.

TABLE 1: General characteristics of the study groups.

Variable	CPB group $N = 60$	OPCAB $N = 47$	P
Age, years	63.6 ± 9.3	64.7 ± 9.3	ns
Gender (males/females), n (%)*	48/12 (81/19)	32/15 (68/32)	ns
BMI (kg/m^2)	28.9 ± 3.8	27.0 ± 3.3	0.006
Obesity*	9/28/23	13/25/9	
Normal weight/overweight/obese, n (%)	(15/47/37)	(28/53/19)	ns
Hypertension, n (%)*	52 (88)	41 (87)	ns
Diabetes mellitus, n (%)*	23 (39)	11 (23)	ns
Hyperlipidemia, n (%)*	40 (68)	30 (64)	ns
Chronic obstructive pulmonary disease, n (%)*	9 (15)	3 (6)	ns
Smoking, n (%)*	42 (71)	33 (70)	ns
Myocardial infarction, n (%)	33 (56)	28 (60)	ns
Peripheral arterial disease, n (%)	22 (37)	24 (51)	ns
Family history, n (%)∗	45 (76)	35 (74)	ns
Clinical characteristics			
EuroSCORE Logistic	6 (3-8)	6 (4-9)	ns
Left ventricular ejection fraction, %	50.9 ± 9.2	48.8 ± 10.8	ns
Syntax Score	32.2 ± 9.29	20.7 ± 7.9	<0.001
Previous medications			
β-Blockers, n (%)∗	57 (97)	44 (94)	ns
Angiotensin-converting enzyme inhibitors, n (%)*	51 (86)	42 (89)	ns
Calcium antagonists, n (%)*	18 (30)	18 (38)	ns
Nitrates, n (%)*	54 (92)	40 (85)	ns
Statins, n (%)*	42 (71)	33 (70)	ns
Oral antidiabetics, n (%)*	13 (22)	9 (19)	ns
Insulin, n (%)*	10 (17)	2 (4)	0.040
Diuretics, n (%)*	19 (32)	17 (36)	ns

*Comparison performed by the χ^2 test.

2.4. Syntax Score Calculation. The Syntax Score [17] which is a broadly used tool for prediction events following percutaneous coronary intervention was obtained for each patient that underwent CABG.

2.5. Sample Collection and Analyses. Blood samples were collected at different time points according to the study protocol. Samples were obtained before skin incision (t1), immediately after protamine-sulfate administration (t2), 6 hours (t3), 24 hours (t4), 48 hours (t5), and 96 hours after cessation of operation and surgical trauma (t6). In all patients, the samples of venous blood were obtained from the central venous line from jugular internal vein. The venous blood collection was drawn into test tubes (Vaccuette® Blood Collection Tubes, Greiner Bio-One Diagnostics GmbH, Rainbach, Austria), and the sera were separated by centrifugation (Multifuge 3L, Heraeus, Kendro Laboratory Products, Osterode, Germany) and kept in 2 mL plastic tubes at −80°C until analysis.

Complete blood count results were obtained from the Cell-Dyn®3700 System, Abbott (Abbott Laboratories, IL, USA).

2.6. Oxidative Stress Status Markers. Parameters of oxidative stress were determined as described previously on an ILAB 650 analyzer (Instrumentation Laboratory, Milan, Italy). In brief, paraoxonase 1 (PON1) activity was determined kinetically with a substrate-paraoxon (Chem Service Inc., West Chester, Pennsylvania, USA) using the method of Richter and Furlong [18]. The total sulfhydryl groups' (tSHG) levels were determined using dinitrodithiobenzoic acid as a reagent in alkaline buffer referred to Ellman's method [19]. Advanced oxidation protein products (AOPP) were measured according to the method of Witko-Sarsat, by a reaction with potassium iodide and glacial acetic acid [20]. Lipid hydroperoxides (LOOH) were determined by the method of Gay and Gebicki, using the ferric-xylenol orange method, following the precipitation in perchloric acid [21].
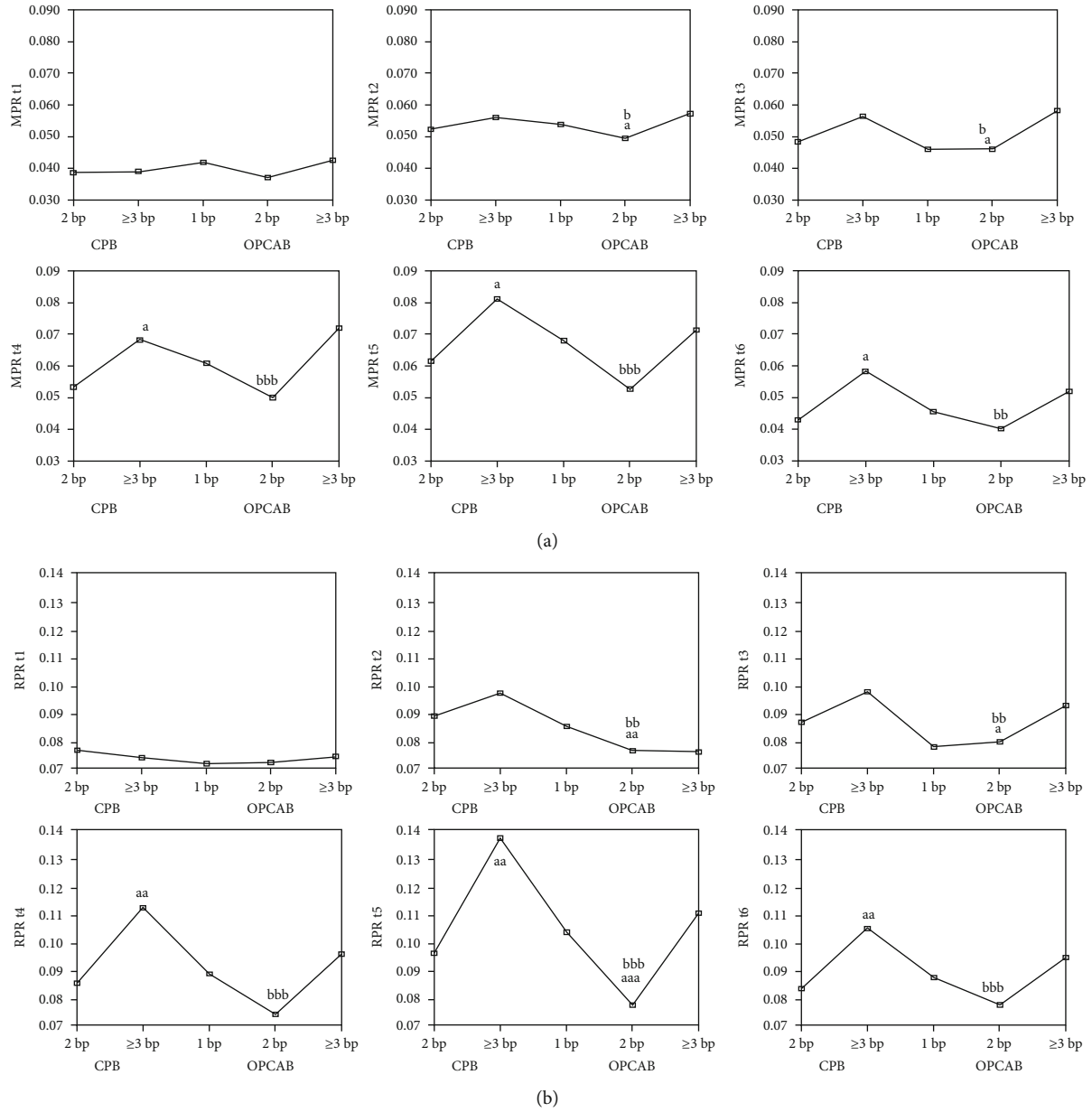
(a)

(b)

FIGURE 1: MPR (a) and RPR (b) according to bypass number and surgery modality during different study points. $^aP < 0.05$, $^{aa}P < 0.01$, and $^{aaa}P < 0.001$ vs. the 2 bp CPB group, $^bP < 0.05$, $^{bb}P < 0.01$, and $^{bbb}P < 0.001$ vs. the 3 bp CPB group. The Kruskal-Wallis test and then the Mann-Whitney U test.

2.7. RPR and MPR Indices Calculation.
RPR is calculated as the ratio of RDW and PLT number, and MPR as MPV and PLT number.

2.8. Statistical Analysis.
Parameters' distribution was estimated by the Shapiro-Wilk test and Kruskall-Wallis nonparametric analysis of variance, followed by the Mann-Whitney U test in order to assess intergroup differences. The comparison between categorical variables was performed by the Chi-square test. The correlation between variables was checked with using Spearman's nonparametric correlation method. Binary logistic regression analysis was used to investigate the association of Syntax Score values with RPR and MPR concentration increment 48 hours after the

TABLE 2: Correlation between platelet activity indices, MPR and RPR with Syntax Score in coronary artery bypass grafting patients.

Parameter	Syntax Score ρ	Parameter	ρ
MPR t1	–	RPR t1	–
MPR t2	–	RPR t2	0.229*
MPR t3	0.350***	RPR t3	0.374***
MPR t4	0.321**	RPR t4	0.340***
MPR t5	0.329**	RPR t5	0.374***
MPR t6	0.282**	RPR t6	0.316**

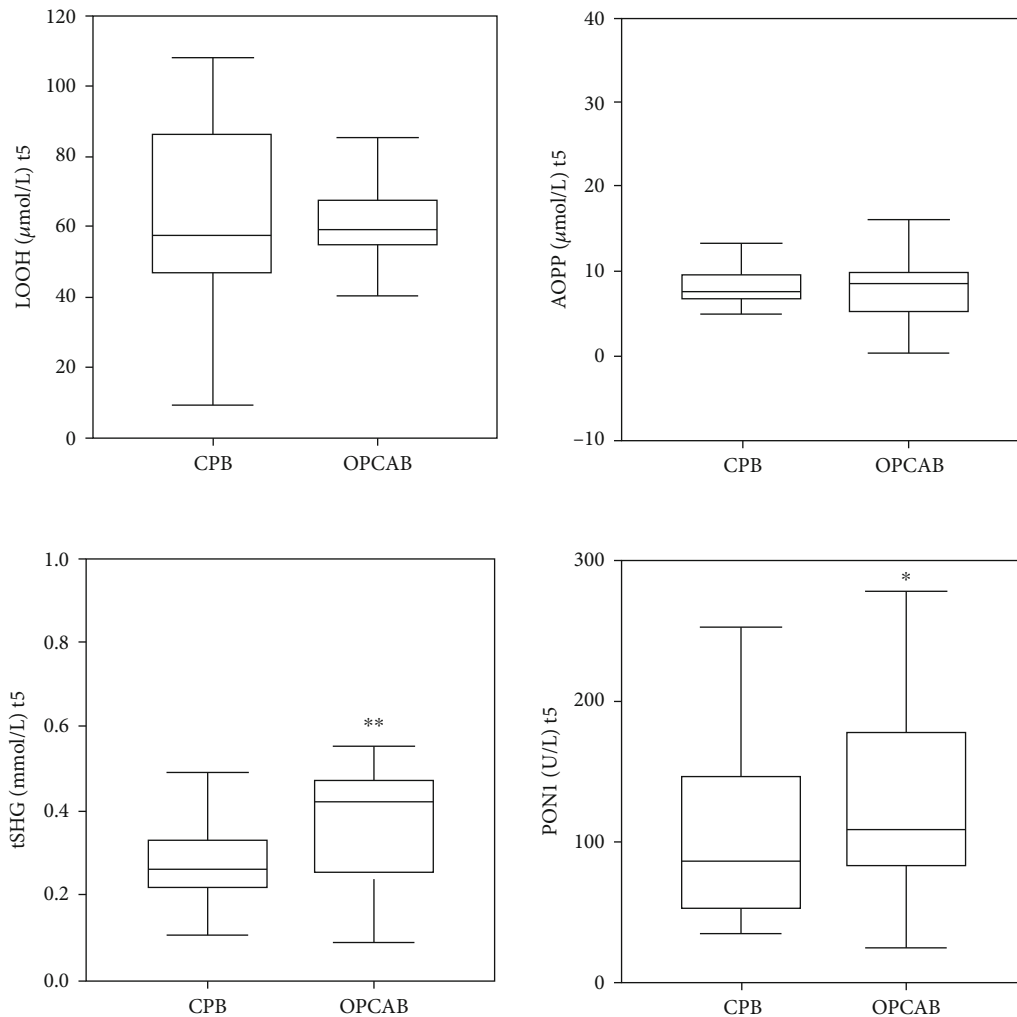ρ: Spearman's rho. $^*P < 0.05$, $^{**}P < 0.01$, $^{***}P < 0.001$.

FIGURE 2: Oxidative stress status parameters at t5 (48 h after surgery), when platelet and erythrocyte indices showed the peak increment.

surgery (unadjusted and after the adjustment for starting values of the parameter of interest).

Clinical accuracy of the examined parameters was assessed by using the receiver operating characteristic (ROC) curve analysis towards postoperative complications presence.

Statistical analysis was performed with SPSS version 18.0 (IBM, Chicago, IL, USA). In all analyses P value < 0.05 was considered statistically significant.

3. Results

A total number of 60 patients were included in the CPB group, whereas 47 patients encompassed the OPCAB group. There were no difference in age and gender distribution between groups ($P > 0.05$).

Comparing the general and clinical characteristics of the two subgroups, we noticed a significantly higher body mass index (BMI) in the CPB group, higher percent of diabetic patients who used insulin, and also higher Syntax Score (Table 1). Other clinical variables were comparable in both study subgroups related to the surgery modality.

In order to get a more precise insight into the surgical condition influence on selected hematological parameters, the patients were categorized according to the surgical modality (CBP vs. OPCAB), and then in each of the two main groups, further division was performed according to the number of bypass grafts patients received during the surgical revascularisation procedure.

Results of this part of analysis are presented in Figure 1.

Analysing this part of results, we could notice that both platelet markers (i.e., MPR and RPR) were increased during the surgery, but increment was always higher in the CPB compared to the OPCAB group, and also regarding the bypass graft number of subgroups (augmentation was increasing with the number of implemented bypass grafts). If we look at patients' division this way, it is obvious that the peak values for both indices are reached in t5 study point, i.e., 48 hours after the surgery.

The results of potential correlation between the MPR and RPR parameters and Syntax Score are presented in Table 2.

Our results revealed a significant positive correlation between the levels of atherosclerotic plaque complexity, estimated through the Syntax Score value and platelet activity

TABLE 3: Binary logistic regression analysis for the association of Syntax Score with RPR and MPR increase above the 75th percentile value 48 hours after the surgery.

Syntax Score	Wald	Odds ratio	95th CI	P
RPR 48 h,				
Unadjusted Syntax Score	7.38	1.068	1.018-1.120	0.007
Adjusted Syntax Score for RPR b.s.	6.64	1.068	1.016-1.122	0.010
Adjusted Syntax Score for oxidative stress parameter model	9.76	1.084	1.028-1.140	0.002
MPR 48 h,				
Unadjusted Syntax Score	8.83	1.079	1.026-1.135	0.003
Adjusted Syntax Score for MPR b.s.	9.38	1.093	1.032-1.156	0.002
Adjusted Syntax Score for oxidative stress parameter model	10.80	1.094	1.037-1.153	0.001

b.s.: before surgery.

indices, i.e., MPR and RPR in several study points after the completion of surgical procedure.

We have also measured several oxidative stress status markers, and here, we presented their values at t5 study point, since MPR and RPR reached the peak increment values at this study point.

Figure 2 shows the concentration of LOOH, AOPP, and tSHG and the activity of PON1 at t5 (i.e., 48 hours after the surgery), when platelet and erythrocyte indices showed the peak increment.

Results showed significantly higher antioxidative parameters (i.e., tSHG and PON1) in the OPCAB group compared to the CPB group. Other oxidative stress status markers did not differ regarding implemented surgical technique 48 hours after the surgery completion.

Binary logistic regression analysis was performed in order to estimate the coronary vessel wall stenosis complexity influence (as Syntax Score value) on RPR and MPR amplification 48 hours after the surgery (study point when these indices reached the peak increment) (Table 3).

This analysis confirmed the significant influence of Syntax Score as a measure of plaque complexity on platelet activation indices, unadjusted, and even after the adjustment for basal RPR and/or MPR values, respectively. We also estimated the adjustment for oxidative stress parameter model (LOOH t5, AOPP t5, PON1 t5, and tSHG t5). Values of these parameters were measured in the same study point when platelet indices reached maximal increment (48 hours after the surgery). Oxidative stress parameters could not abrogate the Syntax Score influence at platelet activation indices increment, which further confirmed its independent influence of two calculated measures of platelet and erythrocyte activity and functionality.

We further performed ROC analysis to estimate possible clinical accuracy of these two new indices of platelet and erythrocyte function and activity, so as preoperative Syntax Score value in the prolonged time after the specific surgical treatment to predict clinical complication evolution in a group of CABG patients. It is important to note that complications were developed in 15 patients (i.e., 14% of all patients), mainly pulmonary thromboembolism, pleural effusion, shallow sternal wound infection, and leg wound infection.

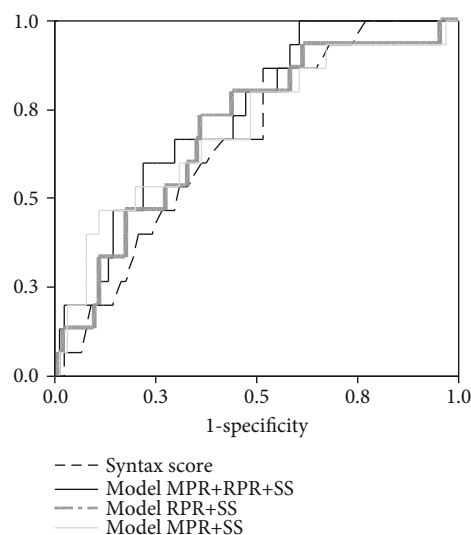Results are presented in Figure 3 and Table 4.

FIGURE 3: ROC curve for the postoperative complication prediction accuracy.

We constructed logistic regression models in order to get more accurate complication prediction, and the results of ROC analysis showed that the combination of Syntax Score, MPR, and RPR (integrated values of all study times) showed the best accuracy, compared to other parameter combination (Table 4).

4. Discussion

Several important findings of the current study need to be mentioned. The values of both markers of platelet and erythrocyte-platelet-joined activation were similar in the two main patients' groups, CPB and OPCAB, and also in subgroups according to bypass number, before surgery. MPR and RPR started to rise in t2 (i.e., immediately after the intervention), and this increase lasted to t5 (i.e., 48 hours after the intervention), when it became the highest. After that, both markers started to regress about the 96th hour after the beginning of surgery. It is important to note that nominal values of both indices were higher in CPB than in OPCAB in all study points after the surgery (Figure 1). Furthermore, it should be emphasized that a significantly higher level of antioxidative parameters (i.e., tSHG and PON1) in OPCAB

TABLE 4: ROC curve parameters for postoperative complication prediction.

Test result variable(s)	AUC (SE)	95th CI	P
Syntax Score	0.668 (0.065)	0.540-0.796	0.038
Model MPR+Syntax Score	0.700 (0.077)	0.550-0.851	0.013
Model RPR+Syntax Score	0.692 (0.071)	0.552-0.832	0.017
Model MPR+RPR+Syntax Score	0.736 (0.061)	0.616-0.856	0.003

ROC parameters: area under the curve (AUC), standard error (SE), 95th confidence interval, and P for Syntax Score. Models: SS in combination with MPR, RPR, and all three parameters.

group compared to CPB group was noted at t5 study point (i.e., 48 hours after the surgery), when platelet and erythrocyte indices showed peak increment.

Unal et al. [22] considered MPV a main marker of platelet production rate and activation, better than the platelet count alone. We assumed that MPR is even a more sensitive indicator of an eventual thrombotic event. This ratio takes into account not only the platelet enlargement but also their number which, if started to fall, could serve as a warning sign that platelets are actually wasting at thrombus formation.

The most convincing results of our current study which could explain the blood cells' involvement in atherosclerosis development is the significant correlation between MPR and RPR, respectively, with Syntax Score (Table 2). Syntax Score is a measure of atherosclerotic lesion severity and complexity [17], and here, we found positive correlation with platelet and erythrocyte-platelet activation indices at several study points after the surgery completion. To our knowledge, this is the first study which documented the direct relationship between the two platelet activity indices (i.e., MPR and RPR) and Syntax Score values. Several studies have already reported the relationship between MPV and RDW with different markers of atherosclerotic plaque severity, calculated as scores [23–25]. The work of Ekici et al. presented a positive correlation between MPV and two plaque related scores, i.e., Gensini and Syntax Score [23]. Willoughby et al. [7] explained the way of platelet activation upon atherosclerotic pathological events. In such conditions, where plaque exists in different phases of formation, maturation, and rupture, endothelial damage exposes subendothelial structures, and then, platelets respond promptly by attaching at vulnerable places.

A few studies reported a significant positive correlation between RDW and plaque severity and complexity measured with Syntax Score [24, 25]. Bujak et al. [11] proposed in its review article the possible mechanisms of RDW relationship with atherosclerotic lesion complexity and thus negative prognostic effects of higher RDW through its connection with inflammation, oxidative stress, vitamin D, and iron deficiency on bone marrow function.

In our current study, we have noticed a higher increase in platelet activation indices in CPB than in the OPCAB group. This could be explained by the results from the study of Koning and associates [26].

They found that CPB causes changes in human plasma which further jeopardizes endothelial barrier function, especially cell-cell integrity. At the same time, CPB usage causes increase in endothelial activation markers (P-selectin, vascular cell adhesion molecule-1, von Willebrand factor plasma concentrations, and an increase in the angiopoietin-2-to-angiopoietin-1 ratio). It is expectable that increase in platelet consumption at the site of plaque formation leads to larger platelets release from the bone marrow [21].

In line with this, although oxidative stress status markers (i.e., LOOH and AOPP) did not differ regarding the implemented surgery modality 48 hours after the intervention, diminished antioxidative protection, in terms of lower activity of PON1 and lower levels of tSHG [12, 27], was found in the CPB than in the OPCAB group 48 hours after the intervention. This could be attributed to the decreased ability of patients who underwent CPB to respond to the oxidative stress, as well as more severe conditions of the CPB intervention than OPCAB [12].

We performed binary logistic regression analysis to estimate coronary vessel wall stenosis complexity influence (as Syntax Score value) on RPR and MPR amplification 48 hours after the surgery, i.e., the study point when these indices reached the peak increment (Table 3). Syntax Score remained a significant predictor of MPR and RPR values even after adjustment for its starting values, before surgery, and for oxidative stress indices. This leads us to conclude that the relationship between stenosis level and gravity and blood cells' activation indices are independent and involve some basic mechanisms of atherosclerotic disease progression, and certainly conditions during the surgery setting.

ROC analysis enabled us to test the clinical accuracy of these two new indices of platelet and erythrocyte function and activity and Syntax Score value in the time after the specific surgical treatment. ROC enabled to predict the clinical complication evolution in the group of CABG patients (in 15 patients, i.e., in 14% of them, we have noticed complications). The most important clinical complications in our group of patients were as follows: shallow sternal wound infection, pulmonary thromboembolism, leg wound infection, and pleural effusion.

Our analysis confirmed that integrated model of Syntax Score, MPR, and RPR had good [28] clinical accuracy in surgery-related complication prediction which additionally established their mutual connection in advanced atherosclerosis patients.

This research was conducted as a single-center which is one of the limitations of the study. Another drawback is a relatively small number of patients who underwent CABG. Taking this into account, a new larger sample size and multicenter studies are necessary to validate the obtained results.

5. Conclusion

The results of the current study imply conclusion that it is worthy to calculate this simple and inexpensive platelet functionality indices as an auxiliary tool for possible unwanted coronary artery disease event prediction. MPV, RDW, and platelet count are readily available as routine parameters and, when combined, such as MPR and RPR, could be good predictors of coronary artery disease status, regarding the joint inflammation, oxidative stress, and thrombosis aspect.

Data Availability

The data will be available upon reasonable request (contact person: aleksandranklisic@gmail.com).

Conflicts of Interest

All authors declare no conflicts of interest.

Acknowledgments

References

[1] R. D'Oria, R. Schipani, A. Leonardini et al., "The role of oxidative stress in cardiac disease: from physiological response to injury factor," *Oxidative Medicine and Cellular Longevity*, vol. 2020, Article ID 5732956, 29 pages, 2020.

[2] A. Klisic, N. Kavaric, S. Vujcic, V. Spasojevic-Kalimanovska, J. Kotur-Stevuljevic, and A. Ninic, "Factorial analysis of the cardiometabolic risk influence on redox status components in adult population," *Oxidative Medicine and Cellular Longevity*, vol. 2021, Article ID 6661940, 9 pages, 2021.

[3] G. F. Veraldi, L. Mezzetto, L. Scorsone, M. Macrì, F. Simoncini, and G. Lippi, "Red blood cell distribution width predicts 1-month complications after percutaneous transluminal angioplasty," *Journal of Medical Biochemistry*, vol. 38, no. 4, pp. 468–474, 2019.

[4] I. Vogiatzis, A. Samaras, S. Grigoriadis, E. Sdogkos, K. Koutsampasopoulos, and I. Bostanitis, "The mean platelet volume in the prognosis of coronary artery disease severity and risk stratification of acute coronary syndromes," *Medieval Archaeology*, vol. 73, no. 2, pp. 76–80, 2019.

[5] X. Zhu, G. Li, S. Li, Z. Gong, J. Liu, and S. Song, "Neutrophil-to-lymphocyte ratio and red blood cell distribution width-to-platelet ratio predict cardiovascular events in hemodialysis patients," *Experimental and Therapeutic Medicine*, vol. 20, no. 2, pp. 1105–1114, 2020.

[6] I. Sincer, Y. Gunes, A. K. Mansiroglu, M. Cosgun, and G. Aktas, "Association of mean platelet volume and red blood cell distribution width with coronary collateral development in stable coronary artery disease," *Postepy Kardiol Interwencyjnej*, vol. 14, no. 3, pp. 263–269, 2018.

[7] S. Willoughby, A. Holmes, and J. Loscalzo, "Platelets and cardiovascular disease," *European Journal of Cardiovascular Nursing*, vol. 1, no. 4, pp. 273–288, 2002.

[8] N. Li, H. Zhou, and Q. Tang, "Red blood cell distribution width: a novel predictive indicator for cardiovascular and cerebrovascular diseases," *Disease Markers*, vol. 2017, Article ID 7089493, 23 pages, 2017.

[9] A. C. Valenti, M. Vitolo, J. F. Imberti, V. L. Malavasi, and G. Boriani, "Red cell distribution width: a routinely available biomarker with important clinical implications in patients with atrial fibrillation," *Current Pharmaceutical Design*, vol. 27, 2021.

[10] G. Lippi, G. Cervellin, and F. Sanchis-Gomar, "Red blood cell distribution width: a marker of anisocytosis potentially associated with atrial fibrillation," *World Journal of Cardiology*, vol. 11, no. 12, pp. 292–304, 2019.

[11] K. Bujak, J. Wasilewski, T. Osadnik et al., "The prognostic role of red blood cell distribution width in coronary artery disease: a review of the pathophysiology," *Disease Markers*, vol. 2015, Article ID 824624, 12 pages, 2015.

[12] P. Vukicevic, A. Klisic, J. Kotur-Stevuljevic et al., "Paraoxonase 1 low activity and Syntax Score may predict postoperative complications after coronary artery surgery," *European Review for Medical and Pharmacological Sciences*, vol. 25, no. 3, pp. 1511–1521, 2021.

[13] G. Aktas, M. Z. Kocak, T. Taslamacioglu Duman et al., "Mean platelet volume (MPV) as an inflammatory marker in type 2 diabetes mellitus and obesity," *Bali Medical Journal*, vol. 7, no. 3, pp. 650–653, 2018.

[14] S. Bilgin, G. Aktas, M. Zahid Kocak et al., "Association between novel inflammatory markers derived from hemogram indices and metabolic parameters in type 2 diabetic men," *The Aging Male*, vol. 23, no. 5, pp. 923–927, 2020.

[15] T. T. Duman, G. Aktas, B. Atak, and M. Z. Kocak, "Is mean platelet volume to platelet ratio a promising indicator of diabetic regulation in type 2 diabetes mellitus?," *Journal of Medical Research*, vol. 4, no. 3, pp. 137–139, 2018.

[16] E. Erkus, M. Z. Kocak, and M. A. Kosekli, "Mean platelet volume to platelet ratio as a promising marker of hepatosteatosis," *Experimental Biomedical Research*, vol. 1, no. 2, pp. 55–59, 2018.

[17] P. W. Serruys, Y. Onuma, S. Garg et al., "Assessment of the Syntax Score in the syntax study," *EuroIntervention*, vol. 5, no. 1, pp. 50–56, 2009.

[18] R. J. Richter and C. E. Furlong, "Determination of paraoxonase (PON1) status requires more than genotyping," *Pharmacogenetics*, vol. 9, no. 6, pp. 745–753, 1999.

[19] G. L. Ellman, "Tissue sulfhydryl groups," *Archives of Biochemistry and Biophysics*, vol. 82, no. 1, pp. 70–77, 1959.

[20] V. Witko-Sarsat, M. Friedlander, C. Capeillere-Blandin et al., "Advanced oxidation protein products as a novel marker of oxidative stress in uremia," *Kidney International*, vol. 49, no. 5, pp. 1304–1313, 1996.

[21] C. A. Gay and J. M. Gebicki, "Measurement of protein and lipid hydroperoxides in biological systems by the ferric-xylenol orange method," *Analytical Biochemistry*, vol. 315, no. 1, pp. 29–35, 2003.

[22] E. U. Unal, A. Ozen, S. Kocabeyoglu et al., "Mean platelet volume may predict early clinical outcome after coronary artery bypass grafting," *Journal of Cardiothoracic Surgery*, vol. 8, no. 1, p. 91, 2013.

[23] B. Ekici, A. F. Erkan, A. Alhan, I. Sayin, M. Ayli, and H. F. Töre, "Is mean platelet volume associated with the angiographic severity of coronary artery disease?," *Kardiologia Polska*, vol. 71, no. 8, pp. 832–838, 2013.

[24] F. Akin, N. Köse, B. Ayça et al., "Relation between red cell distribution width and severity of coronary artery disease in patients with acute myocardial infarction," *Angiology*, vol. 64, no. 8, pp. 592–596, 2013.

[25] O. Sahin, M. Akpek, B. Sarli et al., "Association of red blood cell distribution width levels with severity of coronary artery disease in patients with non-ST elevation myocardial infarction," *Medical Principles and Practice*, vol. 24, no. 2, pp. 178–183, 2015.

[26] N. J. Koning, M. A. Overmars, C. E. van den Brom et al., "Endothelial hyperpermeability after cardiac surgery with cardiopulmonary bypass as assessed using an _in vitro_ bioassay for endothelial barrier function," *British Journal of Anaesthesia*, vol. 116, no. 2, pp. 223–232, 2016.

[27] A. J. Lepedda and M. Formato, "Oxidative modifications in advanced atherosclerotic plaques: a focus on in situ protein sulfhydryl group oxidation," *Oxidative Medicine and Cellular Longevity*, vol. 2020, Article ID 6169825, 7 pages, 2020.

[28] A. M. Šimundić, "Measures of diagnostic accuracy: basic definitions," *EJIFCC.*, vol. 19, no. 4, pp. 203–211, 2009.